STUDIES OF ELECTROSTATIC SPACE FOCUSING OF MOLECULAR BEAMS

A thesis presented for the Degree of Doctor of Philosophy

at the University of Keele

by

DHIA HAMDI HAKIEM AL AMIEDY B.Sc.

Department of Physics
University of Keele
Staffordshire U.K.

1979

The following has been redacted from this digital copy of the original thesis, at the request of the awarding university:

Appendix 1, pages 115-117

Appendix 2, pages 118-120

بِسْمِ اللّٰهِ الرَّحْمٰنِ الرَّحِيْمِ

اَلْحَمْدُ لِلّٰهِ رَبِّ الْعَالَمِيْنَ ۝ الرَّحْمٰنِ الرَّحِيْمِ ۝ مَالِكِ يَوْمِ الدِّيْنِ ۝ اِيَّاكَ نَعْبُدُ وَ
اِيَّاكَ نَسْتَعِيْنُ ۝ اِهْدِنَا الصِّرَاطَ الْمُسْتَقِيْمَ ۝ صِرَاطَ الَّذِيْنَ اَنْعَمْتَ عَلَيْهِمْ
غَيْرِ الْمَغْضُوْبِ عَلَيْهِمْ وَلَا الضَّآلِّيْنَ ۝

صدق الله العلي العظيم

سورة الفاتحه
القرآن الكريم

In the name of Allah, the Beneficent, the Merciful

Praise be to Allah, Lord of the Worlds, ۝ The Beneficent, the Merciful. ۝ Owner of the Day of Judgment, ۝ Thee (alone) we worship; Thee (alone) we ask for help. ۝ Show us the straight path, ۝ The path of those whom Thou hast favoured; ۝ Not (the path) of those who earn Thine anger nor of those who go astray.

This is word by word translation of the opening verse of the Holy Koran, and it is not correspondendent to the original scrip.

ACKNOWLEDGEMENTS

The author would like to express his thanks to:

Dr. D.C. Laine for his continuous encouragement, constructive guidance, and useful discussions.

Dr. D.E. Dugdale for his continuous help especially in setting the computing programme and many useful discussions.

His colleagues, Mr. A.M. Al-Jumaily, Mrs. S. Hope, Dr. A.K.H. Maroof, Mr. M.J. Truman, and Mr. A.I.Corb for many useful discussions.

Mr. G. Dudley and the Workshop staff of the Physics Department, Mr. E.J.T. Greasly, Mr. G. Marsh, Mr. M. Wallace and Mr. H. Wardell and his Staff of the University Workshop.

Mr. M.G. Davies, Mr. B.J. Minshull and the Electronic Staff of the Department.

Mr. F. Rowerth, Mr. C.B. Harrison for their assistance.

Mr. M. Daniels for the preparation of the photographs of this thesis.

The Computer Center in the University, especially Dr. P. Collies, and the computer operators, Mr. and Mrs. N. Carter, Mr. R. Lindop, Mr. R. Harvey, Mr. P. Redfern, Mr. T. Rhodes, Mr. T. Smith, Mrs. C. Booth and Mrs. E. Lister for their invaluable assistance.

Professor Fuller for the provision of the laboratory facilities.

Mrs. S. Cooper and Mrs. J. Gill for typing this thesis.

The Ministry of Education - Baghdad, Iraq for provision of study leave.

The Cultural Department in the Iraqi Embassy, London for their assistance.

Especial thanks to my family for their continuous encouragement.

Especial thanks to my wife for her patient support.

ABSTRACT

In this thesis a study has been made of various schemes of space focusing of molecules in a molecular beam. Molecules, for which the effective dipole moment is either $\mu_{eff} > 1$ or $\mu_{eff} < 1$, may be focused by using state selector electrode geometries where the electric field gradient with respect to the beam axis is of the appropriate sign. Whilst systems for focusing molecules with $\mu_{eff} < 1$ are readily made, a more difficult problem is the focusing of molecules with $\mu_{eff} > 1$. A special study of this latter problem has been made both theoretically and experimentally for the following types of state-selector: ring, crossed-wire and single straight wire. Further studies have also been made with state selectors of molecules with $\mu_{eff} > 1$, including the ring, octopole and especially with a new single wire helix electrode system. It is shown that focusing of a molecular beam with either sing of μ_{eff} is often accompanied by an unexpectedly strong beam of molecules state selected into an annular region around the focused beam. Hitherto, these molecules have been as "rejected" and lost. Realization of their presence is relevant in optimising state selection efficiency.

These studies, which have been carried out with ammonia as the test molecule, used one of two detection techniques. The first was the normal molecular beam spectroscopy method to detect absorption or emission; the other used the change in the amplitude of maser oscillation to detect emissive or absorptive molecules entering the maser cavity, head on to the beam sustaining maser oscillation. This latter method is particularly useful for detection of weakly state selected beams. The focusing schemes studied here have been examined both experimentally and theoretically, and the trajectories computed for the ring, single straight wire and single helical wire electrode geometries, and the results compared with the experimental data.

Studies of the operation of two state selectors in series have also been made, and an anomalous behaviour attributed to spatial reorientation of the molecules has been discovered.

CHAPTER ONE

INTRODUCTORY REVIEW OF FOCUSING SCHEMES

The deflection and focusing of molecular beams by inhomogenous electric field has been the subject of intense investigations by various research workers over many years, and several different types of deflecting and focusing fields have been investigated experimentally. A recent review of these has been given by Zorn and English (1973).

Electric field deflection and focusing schemes have found important applications in the following areas of study: a) spectroscopy (and determination of dipole moments) using MBER, b) molecular beam scattering, (beam-target, beam-beam) for basic studies of physical and chemical processes, and c) molecular beam masers

Note b) and often a) require rather precise focusing, whereas c) can be operated with less well defined beams. Thus for investigations of type (c), a wider range of possibilities exist for state selection and focusing, as will be shown in this introduction.

In this section, the various deflecting schemes are briefly discussed. For convenience, these may be divided into three groups based on the direction of the deflecting field with respect to the molecular beam. These are (i) schemes where the focusing or deflecting field is essentially perpendicular to the beam axis, (ii) systems where the focusing field is approximately parallel to the beam axis, (iii) schemes where the focusing field possesses transverse and parallel components relative to the beam axis.

The earliest molecular beam deflection scheme was used by Stern and Gerlach in 1924, by using a magnetic field, to deflect atomic beams. Townes and co-workers (1953) proposed that the electrostatic analogue of the Stern-Gerlach field could be used to make a molecular beam maser. However, a quadrupole type of state selector was used instead which possessed the property of focusing, thus leading to stronger emission

signals than would be possible with beam deflection alone as with the Stern-Gerlach type of field. Up to this present year molecular beam masers have relied upon some form of focusing in association with state selection. However, Hope (1979) has succeeded in using a Stern-Gerlach type of beam deflector for state selecting J = 1, K = 1 inversion state ammonia molecules. It was found that the device produced both a strongly absorptive and a strongly emissive molecular beam with deflections in opposite senses. Although the emissive beam was strong, it was found to be insufficient to produce maser oscillation with this particular transition. However it appears that an oscillation may be possible with the stronger J = K = 3 inversion line. The strength of the absorption line is probably the strongest yet to be produced with any type of electrostatic state selector.

To improve the intensity of the state selected beam, two-wire fields are often used. The theory of the two-wire field and its application to molecular beam spectroscopy has been discussed by Ramsey (1956), Kusch and Hughes (1959), McColm (1966), and Auerbach et al. (1966).

From the analysis of the two-wire field, a multipole theory was developed by Friedburg and Paul (1951) for the case of a hexapole magnet which state selects and focuses paramagnetic atoms. The electrostatic analogue was used by Bennewitz, Paul and Schlier (1955) to state select and focus polar diatomic molecules.

In 1954, Gordon et al., used an electrostatic quadrupole focuser in conjunction with the first operational molecular beam maser. The ideal quadrupole field focuser requires electrodes with hyperbolic rather than circular cross-sections, although in practice circular cylinders are usually quite adequate for molecular beam electric resonance work.

Theoretical analyses of multipole electrode focusers have been given by Shimoda (1957), Vonbun (1958), Hirono (1959) and van Mierlo (1974).

Shimoda (1957) found that the relative number of molecules in each M state changes in a complex way with increasing focuser voltage, and in addition the number of focused molecules with a large M value saturated faster than with a smaller M value, because the number of focused molecules is proportional to M^2, where M is the magnetic quantum number.

Vonbun (1958), who analysed the focusing action of a multipole rod focuser, pointed out that the entrance position, entrance velocity and angle has a considerable influence upon the separation action.

The characteristics of the eight pole rod focuser of the maser oscillator were examined by Hirono (1958), and compared with those of four pole rod and square-well focusers, taking into account the Maxwellian velocity distribution of the effusive molecular beam source. The variation of focusing action against the focusing length and the incident angle of the particles passing through the focuser was discussed. Van Mierlo (1974) discussed the theoretical performance of an electrostatic n-pole rod state selector using hyperbolically shaped electrodes for focusing HDO molecules.

A comparison was made by Helmer (1956), between the characteristics of the harmonic focuser ($n = 4$), with the multipole rod focuser ($n \geq 4$), where n is the number of the poles. It was suggested that the harmonic focuser offers the greatest advantage since precise calculations of trajectory can be made, and it possesses one of the greatest possible solid angles of acceptance of multipole state selectors. Even greater solid angles are possible by the use of combination of quadrupole and hexapole or by twisted quadrupole fields.

Most beam maser spectrometers (Dymanus 1976)* are operated with

---

*In Dymanus' paper page 139 the effective dipole moment μ_{eff} was defined as $\frac{\partial W}{\partial E}$, where W is the energy of molecules in an external electric field E, whereas in the paper by Zorn and English (1973) p. 256 the effective dipole moment was defined as $-\frac{\partial W}{\partial E}$. Here μ_{eff} follows the latter definition.

octopole and dode capole focusers for molecules with a second-order Stark effect and with hexapole focusers for molecules with a first order Stark effect. At low microwave frequency, the intensity gain of the focuser is quite significant for broad beams.

A tapered quadrupole rod focuser was also used by Helmer 1960, 1961, in order to have a better focusing action compared with the uniform quadrupole rod focuser. In addition it was suggested that the tapered quadrupole focuser has the best performance with a long cylindrical cavity, because of better defocusing of the lower energy state molecules which initially travel close to the focuser axis.

So far, consideration has been given to multipole fields to focus molecules in quantum states whose Stark energy increase in an applied electric field ($\mu_{eff} < 0$) (Helmer et al., 1960; Lainé, 1970). Less well known is the use of multipole fields to focus molecules whose Stark energy decreases in an applied electric field ($\mu_{eff} > 0$). Several attempts have been made to develop suitable devices for this purpose. However the number of molecules state selected by such multipole fields is usually low when $\mu_{eff} > 0$.

The co-axial wire focuser (scheme i) was first operated with an ammonia molecular beam by Helmer et al. (1960), then by Lainé and Sweeting (1971). It was found that the vacuum chamber (Lainé and Sweeting, 1971), could act as the outer earthed "cylinder", and the focuser in practice is simply a single straight wire. This device is thus called the single straight wire focuser.

The use of the single straight wire system to focus linear Stark slope molecules was investigated theoretically by ter Meulen (1974)*.

---

*It was claimed by ter Meulen that this type of focuser cannot focus molecules with a quadratic Stark effect. However, this conclusion is in error, because of a wrong sign in equation (29)) of ter Meulen's theory. The correct expression for equation (29) is

$$\frac{d^2\mu}{d\phi^2}\left[\frac{c'v^2}{(\ln r_2/r_1)^2}\frac{m}{J^2} + 1\right](-u) = 0$$

The theory of the single straight wire focuser is discussed in (2.5.2.1).

The use of a ten-pole field (with a 2-pole symmetry) to focus CsF molecules whose Stark energy decreases in an applied electric field $\mu_{eff} > 0$ has been reported by Waech et al. (1968). This focuser is a one dimensional one where molecules are focused to a line rather than a single point.

A method of two dimensional focusing of molecules with $\mu_{eff} > 0$ has been described by Kakati and Laine (1967), by the use of a succession of eight dipole fields, to achieve alternate-gradient (AG) focusing in conjunction with an ammonia molecular beam. The principle of this scheme applied to molecular beams was first discussed by Auerbach et al. (1966). Reuss and Nelissen (1967) has also reported a similar focusing system for a molecular beam which consisted of four identical pairs of two-wire (magnetic) type of deflecting fields. Gunther and Schugerl (1972) have also discussed an AG focuser which selects rotational states of potassium fluoride KF for which $\mu_{eff} > 0$. Molecules with a positive Stark effect ($\mu_{eff} < 0$) are also focused in the AG focusing system. It should be noticed however, that the intensity of the focused beam is rather small with the AG scheme on account of a rather limited acceptance angle.

Al-Amiedy and Laine (1978) have suggested the use of an AG focuser consisting of rings of small diameter (first element of AG lens), spatially separated from a ring focuser of larger diameter (second element of AG lens). This type of focuser falls into the scheme type (ii). The use of a ring focuser of small diameter for focusing molecules with $\mu_{eff} > 0$ will be considered in detail in section (5.2).

Becker (1963) investigated in detail the theory of focusing action for both schemes (i) and (ii) employing a double ladder type of focusing system. These systems are used to produce flat beams of

molecules, and their focusing property is essentially one dimensional, i.e. molecules are focused to a line rather than to a single point. Becker (1963) made detailed comparisons between the double ladder focuser type (i) and a 4-pole rod electrode such as used by Barnes (1959). In the measurements by Barnes (1959) using a long 4-pole rod electrode focuser operated at 37 kV, an increase of only 11% of the total flux was observed. In Barnes' measurement, the total flux was measured by an ion gauge whose aperture size and position corresponded to the resonator entrance. The flux was then measured as a function of the electrode voltages. It was concluded from this comparison, that a double ladder focuser had a relatively good focusing action for ribbon-beams, even when comparatively short (Becker, 1963). An arrangement of transverse electrodes, has the advantage from the constructional point of view that the wire lengths are shorter, which permits fabrication with smaller wire diameters.

A focuser of the tapered double ladder type with the separation between the ladder electrodes increasing linearly with the axial distance in an attempt to increase the acceptance solid angle was devised (Laine and Smart, 1971). This type of focuser produced a line of upper energy state ammonia molecules.

Another electrode configuration makes use of ring electrodes and falls under scheme (ii). It was proposed by Krupnov (1959) and was subsequently investigated by many authors. Basov, Zuev and Suidzinskii (1964), and Shcheglov (1961) carried out calculations of the potential of the inside a ring capacitor which is used as a ring focuser for molecular beam work*.

Kazachok (1965) suggested an electrodynamic method of slowing

---

*The constant k in equation (31) in Shcheglov's paper is incorrect, and should read:

$$k = 3.196 \frac{d_o M_J K}{J(J+1)} \cdot \frac{V_o}{\zeta^3} \cdot m$$

the velocity of molecules by applying a time varying field to a ring focuser having a parabolic dependence of ring radius on axial distance. However, no successful report of such an operating device has yet been made.

Strakhovskii and Tatarenkov (1965) proposed a curved ring focuser which played a double rôle. It sorted out the molecules according to their energy states and also acted as a velocity selector. Only upper energy state molecules with a velocity equal or less than a critical value were focused into the resonant cavity. The molecules with a high velocity as well as lower energy state left the focusing system and did not enter the resonant cavity. They obtained a weak stimulated emission with ammonia molecules (J = K = 3)inversion transition) of signal to noise of 3 with such a device, curved at angle of 30^{o}.

Becker (1961, 1963) used different types of ring and bifilar helix systems of very short length. It was shown that their operation can be well described by an optical lens of known focal length.

A focuser of type (iii) comprising a single wire helix has been used in conjunction with a molecular beam maser operated with a cylindrical cavity. This type of device produced a focusing action sufficient to sustain molecular beam maser oscillation with the J = K = 3 inversion line of ammonia. This new type of device has been studied in some detail and is discussed in section (5.3).

Other types of helical electrode focuser schemes have also been investigated experimentally and theoretically. These are the bifilar helix and multipole helical electrode systems. Krupnov (1959) was the first to propose the use of the bifilar helix. Mednikov and Parygin (1963), investigated this device theoretically and experimentally. They use it to operate an ammonia maser based on the J = K = 3 inversion line of ammonia. It was found that the maser signal produced by the

bifilar helix was approximately five times greater than could be obtained by the use of a quadrupole rod focuser with the same focusing voltage and same geometrical dimensions.

Igritskii (1961) presented a theoretical method for the calculation of the tape helical electrode system designed for the electrostatic periodic focusing of rod-like and tubular-like electron beams in backward-oscillators and travelling-wave tubes.

Recently, it was suggested that a four-pass winding may be used as an electrostatic focusing system (Koshel'kov and Krochik, 1972). A theoretical treatment of such a system was given earlier by Koshel'kov (1973). It was claimed to have the efficiency of a bifilar helix focuser with the same length of device for the reason that the time that the molecules spend in the four-pass winding will be double the time due to their spiral motion, to that the molecules spend in the bifilar helix. A four-pass winding could prove to be particularly valuable in a molecular oscillator using open cavities in which saturation is usually reached at higher molecular beam intensities than with a closed cylindrical cavity.

Trostsyuk (1969) has given a general discussion of the focusing properties of electrode systems with helical symmetry. The relationship between the pitch and radius of the helical system, and optimum length for the focusing device have been obtained.

Strashkevich (1965) investigated in detail the potential distribution and the trajectories of molecules with multipole helical electrode strips. No report has yet been given of the successful operation of such a scheme in the context of molecular beams.

Koshel'kov (1975) proposed the use of a selective molecular pumping method for improving the efficiency of state selection. The principle of this scheme is based on the fact that molecules with $\mu_{eff} > 0$ are defocused towards the annular or helical electrode

focusing system and are then subjected to microwave radiation before they reach the maximum value of the electrostatic field of the focusing system. Consequently, some molecules with $\mu_{eff} > 0$ make transitions to a molecular state with $\mu_{eff} < 0$ after absorption of a quantum of high frequency field energy. Thus molecules which enter the focuser system with $\mu_{eff} > 0$ will be "sucked out" of the axial region of the system, to refocus down the focuser axis as molecules with $\mu_{eff} < 0$. It was speculated that if this method were to be used in a four-pass winding with CH_2O molecules, a 30% improvement in the maser oscillator stability could be expected, and about a 70% increase in the power compared to an annular focusing system of the same size.

Hill and Gallagher (1975) described the use of an inhomogenous microwave field as a molecular beam deflector. The theory of the technique as well as potential applications were also discussed. The microwave cavity possessed a high electric field gradient in the beam region, in order to produce a sizable deflection, and at the same time the field was low enough to satisfy the criterion $\mu E << B$ to avoid mixing rotational states. Here B is the rotational constant. It was found that a convenient length of the cavity was 20 cm for 11 GHz radiation for the J = 0 and 1 transition of CsF molecules. It was observed that deflection of J = 1 and 1 molecules could be detected as a decrease in the undeflected on-axis beam or as an increase in the off-axis beam.

The deflecting and focusing of electron beams by the use of an electron gun has been the subject of intense investigation by various research workers over many years.

Pierce (1949) discussed in detail the theory and design of the electron beam. The electron beam produced by the electron gun which accelerates the electrons from an emitting cathode to "shoot" them out in the form of a beam having the sharpest possible lateral

boundaries, and frequently of a very high current density. Muller (1956) added new points of view in the design of electron guns for cylindrical beams of high space charge.

Zinchenko and Saeko. (1963) calculated the potential difference in a cylindrical electron beam in a fixed electrostatic field. The result indicated that in choosing the variation of magnetic field along the axis of magnetic focusing it was necessary to take account of the sag in the axial potential.

Zinchenko (1967) investigated theoretically and experimentally some applications of high-perveance three electrode electron guns. This device produced electron beams with current densities exceeding that in conventional electrostatic guns by a factor of ten or so for the same electron energies. It was concluded that the future of high-perveance guns would also include ion sources with electron impact ionization and injectors of high current accelerators.

The angular divergence of molecular beams of several species (Bobbio et al., 1975) are reduced substantially if the species move coaxially within an electron beam. The flux of molecules observed arriving at a detector set on the molecular beam axis is increased by factor up to 10^3 for a beam of KCl and 10^2 for a beam of K. The increase in the flux of molecules becomes smaller as the intensity of the beam increases in the field of the device. Molecules in energy states which decrease in energy with increasing field ($\mu_{eff} > 0$) are subjected to a radial force directed toward the common axis of the beam.

State selection and focusing with space charge devices appear to be a fruitful area for further investigation in the future but on the experimental evidence to date these are much more complicated to construct and operate than the electrostatic systems discussed in this introduction. In this thesis only electrostatic devices are considered.

CHAPTER TWO

GENERAL PRINCIPLES OF ELECTROSTATIC STATE SELECTION OF MOLECULES

2.1 Stark Effect in molecules

Whether space focusing of molecules in a given quantum state is possible depends on the precise form of the Stark energy interaction of molecules over a wide range of electric field values (Laine, 1970). Two basic forms of Stark interaction are those of the linear rotor and molecules with close spaced (repulsive) levels.

The form of the Stark interaction in the former case is given by the following equation in the case of weak fields

$$\Delta W_E = \frac{\mu^2 E^2 [J(J+1) - 3M^2]}{2 h B_0 J(J+1)(2J-1)(2J+3)} \quad (J \neq 0) \qquad (2.1)$$

$$\Delta W_E = - \frac{\mu^2 E^2}{6 h B_0} \quad (J = 0) \qquad (2.2)$$

where μ is the permanent dipole moment of molecules

E is the magnitude of the inhomogeneous electric field

J is the total angular momentum excluding nuclear spin

M is the projection of J on the direction of the field

h is Planck's constant

and B_0 is the rotation constant

In the case of high values of E field, higher order terms need to be considered. This has been done by Hughes (1947), Peter and Strandberg (1957) and Shirley (1963). Fig (2.1) shows the Stark effect of linear molecules and symmetric top molecules with K = 0.

The energy of symmetric-top molecules is given by the following approximate formula for the case of $K \neq 0$

$$\Delta W = - \frac{\mu_0 EMK}{J(J+1)} \qquad (2.3)$$

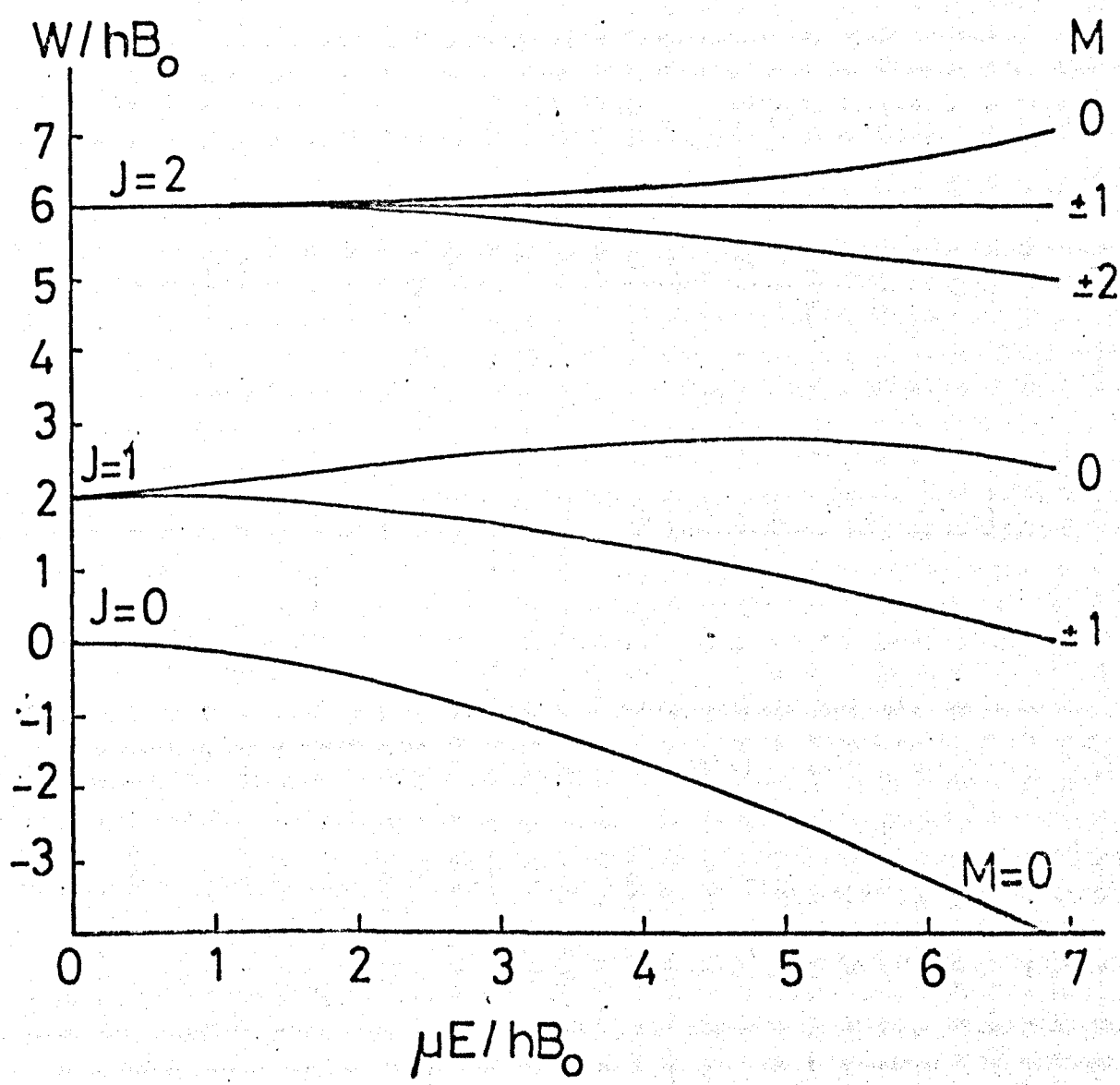

FIGURE (2.1) SHOWS THE STARK EFFECT OF LINEAR MOLECULES AND SYMMETRIC TOP MOLECULES WITH K=0.

The expression for the case K = 0 for symmetric top molecules is identical with that for linear molecules, and is given by equation (2.1).

The full equation for the energy of molecules of the symmetric top type that interact with an electric field for beam maser work can be expressed as (Townes and Schawlow, 1955)

$$W_{JKM} = -\frac{KM}{J(J+1)}\,\mu_0 E + \frac{(\mu_0 E)^2}{2hB}\left[\frac{[2K^2 - J(J+1)][3M^2 - J(J+1)]}{J^2(J+1)^2\,(2J-1)(2J+3)} - \frac{M^2K^2}{J^3(J+1)^3}\right] + \ldots \qquad (2.4)$$

The effect of an inhomogenous electric field on ammonia molecules

The inhomogenous electric field of the focuser produces a force on ammonia molecules due to an induced dipole moment. In zero electric field ammonia molecules have no average dipole moment, as a result of the inversion. By increasing the electric field, the inversion is slowly quenched and an average dipole moment appears. By neglecting the hyperfine structure effects, the Stark energies of the inversion state of NH_3 may be written for all field strengths as follows (Gordon et al., 1955)

$$W = W_0 \pm \left[\left(\frac{h\nu_0}{2}\right)^2 + \left(\mu_0 E \frac{M_J K}{J(J+1)}\right)^2\right]^{\frac{1}{2}} \qquad (2.5)$$

where W is the Stark energy of the inversion state of NH_3 molecules,

$W_0 = \frac{W_1 + W_2}{2}$ is the average energy of the upper and lower inversion levels and

$\pm$ corresponds to the upper and lower inversion state respectively,

h is Planck's constant,

ν_0 is the inversion frequency in zero electric field,

μ is the permanent dipole moment of the molecules (which can be taken as the effective dipole moment) for the case of no inversion $\mu = \mu_0 \frac{M_J K}{J(J+1)}$

E is the magnitude of the electric field

J is the quantum number specifying the total angular momentum excluding nuclear spins, $J = \sqrt{J(J+1)}\ \hbar$,

K is the projection of J on the direction of the electric field,

M is the projection of J on the direction of the electric field

The electric interaction energy (or the Stark energy) W_E is given by the following expression

$$\Delta W_E = \pm \left[\left(\frac{h\nu_0}{2} \right)^2 + \left(\frac{\mu_0 K M_J E}{J(J+1)} \right)^2 \right]^{\frac{1}{2}} \mp \frac{h\nu_0}{2} \qquad (2.6)$$

where minus and plus signs refer to upper and lower energy states ammonia molecules respectively.

Fig (2.2) shows the diagram of the Stark energy levels of $J = K = 3$ inversion line of NH_3. From the figure it is seen that the energy of molecules in the $M = 0$ level is not affected by electric field. However the energy of upper inversion energy state molecules ($M \neq 0$) increases with electric field, whereas molecules in the lower inversion state ($M \neq 0$) decrease in energy with increasing electric field.

While the molecules travel through the focuser, the change in magnitude and direction of the electric field E varies slowly compared to the rate of precession of J around E. For that reason M may be considered to be a constant of the motion.

The radial force exerted by the focuser on molecules is given by the negative gradient of W. From equation (2.5) this is given

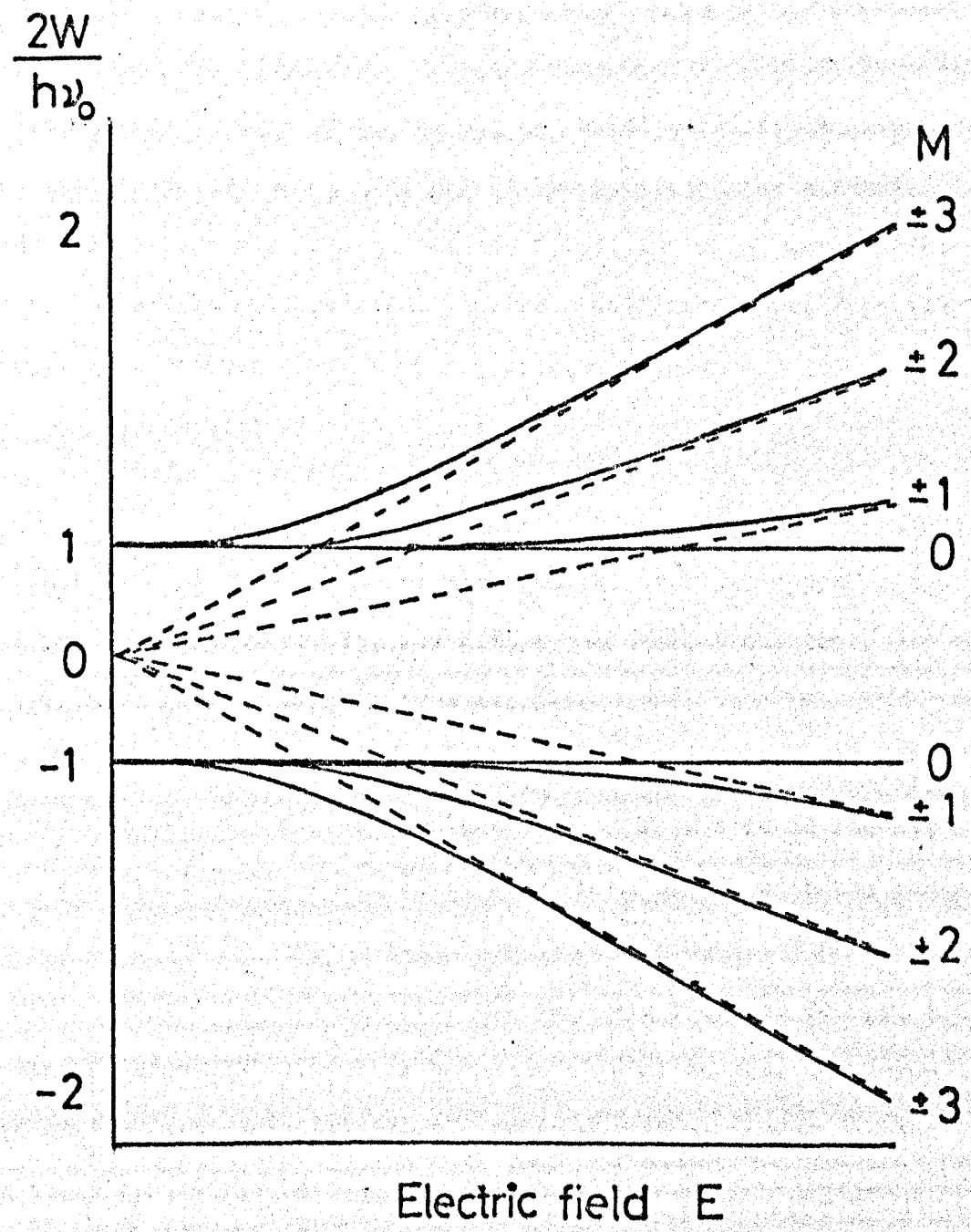

FIGURE (2.2) DIAGRAM OF THE STARK ENERGY LEVELS OF J=K=3 INVERSION LINE OF NH_3.

by

$$f_r = - \nabla W$$

$$f_r = - \frac{W}{r} = \mp \frac{\mu^2 E \frac{\partial E}{\partial r}}{\left[\left(\frac{h\nu_0}{2} \right)^2 + (\mu E)^2 \right]^{\frac{1}{2}}} \qquad (2.7)$$

For the same value of K, and M_J the radial force f_r is proportional to the radial gradient of the square of the electric field. As an example of the focusing force, two cases were taken:

a) For simple multipole rod electrode configurations, Higa (1957) showed that the force exerted by the focuser is given by the following expression:

$$f_r = \pm K r^n$$

where the plus and minus sign refers to lower and upper energy state molecules respectively, and K is a geometrical constant. The following special simple cases were discussed:

1) $n > 1$: as an example of this case was the multipole rod focuser, n increasing with the number of electrodes. This type of focuser has a zero field on the axis, increasing in magnitude with the radial distance from the focuser axis.

2) $0 < n < 1$: as an example for this case was the a.c. focuser proposed by Higa (1957). This proposed type of focuser was comprised of low frequency cylindrical cavity operating in such a mode that the field configuration provided the necessary inhomogeneous electric field gradients for focusing action.

3) $n < 0$: This is the case for focusing systems such as the single straight wire in which the field has a maximum value at focuser axis, and diminishes with increasing radius.

b) For other electrode configurations such as the ring, single wire helix and multipole helix focusing systems, the form of the

radial force is more complicated, and it is hard to generalize. Specific systems are discussed in detail in Chapter 5.

Inversion spectra of ammonia molecules

The ammonia inversion spectrum was first observed in the microwave region by Cleeton and Williams (1934). It has been studied in detail by many investigators (see Townes & Schawlow, 1955; Ingram, 1955).

Ammonia molecules which have a molecular structure of the pyramidal type, possess four atoms. Three of them are hydrogen atoms situated in one plane, and the other is a nitrogen atom, which has two equally probable position on either side of the plane formed by three hydrogen atoms. The structure of ammonia molecules offers the possibility of the nitrogen atom moving from one equilibrium position on one side to the other by overcoming the potential hill formed by the close proximity of the hydrogen atoms.

The frequency of the inversion spectrum is dependent on the rotational energy of molecules (Straughan & Walker, 1976). Molecules with higher rotational quantum number values possess a higher angular velocity and are therefore subject to greater centrifugal forces which distorts the molecular structure.

The separation (0.79 cm^{-1}) between the ammonia ground state doublet vibration level was employed to produce the maser action. The ground state doublet vibration levels of ammonia molecules have different signs of induced electric dipole moments, and as a consequence, they are deflected differently by a strong inhomogenous electric field. Thus higher energy state ammonia molecules may be separated from those in the lower state.

2.2 General principles of state selection and space focusing of molecules

State selection and space focusing of molecules may be achieved

using a device called a focuser or state selector. A focuser is a device capable of capturing and focusing molecules in certain quantum states and defocusing those in the other quantum states.

Whilst the focuser may be employed as a state selector, a state selector does not always act as a focuser (Lainé, 1975).

It should be pointed out that the term "focuser" used in this thesis in conjunction with molecular beam, does not apply with the strict optical meaning, on account of the velocity distribution and range of entrance angles which leads to poor focusing properties. But these features do not prevent the use of the optical analogue of the focuser as an aid to analysis.

Condition for focusing a molecular beam

The necessary condition for the molecules passing through a focuser to be focused is that the maximum Stark energy of molecules ($\Delta W_{E_{max}}$) must be greater than the radial or transverse component of the kinetic energy of molecules.

The maximum Stark energy of molecules in the case of ammonia equation (2.4) is given by the following expression

$$\Delta W_{E_{max}} = \left[\left(\frac{h\nu_0}{2} \right)^2 + (\mu_{12} E)^2 \right]^{\frac{1}{2}} - \frac{h\nu_0}{2} \qquad (2.8)$$

The radial or transverse component of kinetic energy of molecules is given by the following formula

$$\text{K. E.} = \tfrac{1}{2} m V_t^2$$

where m is the mass of molecules

and V_t is the transverse component of velocity of molecules

Focusing follows when

$$\tfrac{1}{2} m V_t^2 < \Delta W_{E_{max}} = \tfrac{1}{2} m V_c^2 \qquad (2.9)$$

If $\Delta W_E << h\nu_0$, then the critical radial velocity, V_c is

proportional to the focuser voltage since

$$V_c = \mu_{12} E_m \left(\frac{2}{m h\nu_0} \right)^{\frac{1}{2}} \qquad (2.10)$$

Shimoda (1957) used the approach that the focuser could be treated as an optical lens to a good approximation. However, throughout the calculations carried out in this thesis, a different approach has been taken in which all the force components were taken into account. For example, in calculations with the ring focuser, the radial and the axial components of the force were calculated; with the single wire helix the radial, axial and angular components of the force were taken into account. Details of these calculations are presented in Chapter 5.

2.3 Basic types of state selection schemes

2.3.1. Single straight wire focuser

An introduction to the single straight wire focuser has been given in section (3.4). Here, the theory is presented in detail.

Theory of the single straight wire focuser

To develop the theory of the single straight wire focuser, molecules are assumed to move in a cylindrical symmetric electric field $\vec{E}$ at a distance r from the wire axis. The force acting on the molecules is designated as $\vec{F}$, the electric field $\vec{E}$, and Stark energy W.

The position of a given molecule is specified by a radial distance r, from the wire axis. The following differential equation then represents the molecular orbit

$$m \vec{r} = |F(r)| \vec{r} \qquad (2.11)$$

where m is the mass of molecules

$\vec{r}$ is the acceleration of molecules

$\vec{r}$ is the unit vector.

The wire lies along the z-direction. Assume the force F is always zero along the z-axis, and acts in a transverse direction.

It is possible to express $\ddot{\vec{r}}$ in the polar co-ordinates r and ϕ as follows:

$$\ddot{\vec{r}} = (\ddot{r} - r\dot{\phi}^2)\,\vec{r} + (2\dot{r}\dot{\phi} + r\ddot{\phi})\,\vec{\phi} \tag{2.12}$$

The substitution of equation (2.12) in equation (2.11) yields two equations:

$$m(\ddot{r} - r\dot{\phi}^2) = |\vec{F}(r)| \tag{2.13}$$

$$(2\dot{r}\dot{\phi} - r\ddot{\phi}) = 0 \tag{2.14}$$

equation (2.14) represents the conservation of the angular momentum, then

$$J = mr^2\dot{\phi} \tag{2.15}$$

where J represents the angular momentum of a molecule along the z-axis. Equation (2.13) can be solved by using

$$\dot{r} = \frac{1}{u} \tag{2.16}$$

together with the derivative of r with respect to t.

$$\dot{r} = \frac{dr}{dt} = \frac{dr}{d\phi} \cdot \frac{d\phi}{dt} \tag{2.17}$$

and by taking the derivative of r in equation (2.16) with respect to ϕ .

$$\frac{dr}{d\phi} = \frac{d(1/u)}{d\phi} = -\frac{1}{u^2}\frac{du}{d\phi} \tag{2.18}$$

Substituting equation (2.18) in (2.17) and from equation (2.15), equation (2.17) is given by:

$$\dot{r} = -\frac{J}{m}\frac{du}{d\phi} \tag{2.19}$$

from which it follows that

$$\ddot{r} = -\frac{J^2}{m^2}u^2\frac{d^2u}{d\phi^2} \tag{2.20}$$

substitution of equation (2.20) in (2.13) yields

$$- m \frac{J^2 u^2}{m^2} \frac{d^2 u}{d\phi^2} - mr\dot{\phi}^2 = F \qquad (2.21)$$

and by substituting $F = - c/r^3$ for molecules with a quadratic Stark effect, the polar form of equation (2.11) becomes

$$\frac{d^2 u}{d\phi^2} = (\frac{cm}{J^2} - 1)\, u \qquad (2.21a)$$

The above equation (2.21) describes the motion of molecules in the electrostatic field of single straight wire focuser. The general solution of equation (2.21) is given by

$$u = A\, e^{\lambda\phi} + B\, e^{-\lambda\phi} \qquad (2.22)$$

thus

$$r = \frac{1}{A\, e^{\lambda\phi} + B\, e^{-\lambda\phi}} \qquad (2.23)$$

where

$$\lambda^2 = \left| \frac{cm}{J^2} - 1 \right| \qquad (2.24)$$

The initial conditions, at $t = 0$ are $e^{\lambda\phi} = 1$, $\dot{u} = u_0$, then

$$A = \tfrac{1}{2}(u_0 + \frac{m\dot{u}(0)}{\lambda J u^2_0}) \qquad (2.25)$$

and

$$B = \tfrac{1}{2}\,(u_0 - \frac{m\dot{u}(0)}{\lambda J u^2_0}) \qquad (2.26)$$

From the initial condition at $t = 0$, $u_0 = A + B$, thus $\dot{u}(0) = 0$

$$\therefore \quad A = B = \frac{u_0}{2}$$

The force acting on the ammonia molecules in the potential field is determined by the following equation

$$f = - \text{grad } W$$

The component of the force f acting on the molecules in the field of the single straight wire focuser is written in the form

$$f_r(U,L) = \mp q(E)\, E \frac{\partial E}{\partial r} \qquad (2.27)$$

where $$q(E) = \frac{\mu_{12}^2}{\left[\left(\frac{h\nu_0}{2}\right)^2 + (\mu_{12}E)^2\right]^{\frac{1}{2}}}$$

The positive and negative signs refer to the lower and upper inversion state of ammonia molecules respectively.

The equation of the electric field for the cylindrical capacitor focuser shows that the electric field as a function of the radial distance from the wire is given by

$$E = \frac{U}{\ln(r_2/r_1)} \frac{1}{r} \qquad (2.28)$$

where U is the voltage applied between wire and cylinder

r_2 is the radius of the earthed cylinder (or the distance between the wire and the chamber in the experiment described in this thesis)

r_1 is the radius of the wire.

$$f_r(U, L) = \mp \frac{\mu_{12}^2}{\left[\left(\frac{h\nu_0}{2}\right)^2 + (\mu_{12}E)^2\right]^{\frac{1}{2}}} \frac{U^2}{\ln(r_2/r_1))^2} \frac{1}{r^3} \qquad (2.29)$$

or $$f_r(U, L) = \mp \acute{c} \frac{1}{r^3}$$

where $$\acute{c} = \frac{1}{\left[\left(\frac{h\nu_0}{2}\right)^2 + (\mu_{12}E)^2\right]^{\frac{1}{2}}} \left[\frac{\mu_{12}^2 U}{\ln(r_2/r_1)}\right]^2$$

By substituting the following quantity in equation (2.29) $\acute{c}$ may be calculated $\mu_0 = 1.47 \times 10^{-18}$ e.s.u., $h = 6.6 \times 10^{-27}$ erg.sec., $\nu_0 = 2.4 \times 10^{10}$ Hz, $J = 3$, $K = 3$, $M_J = \sqrt{7}$ (Shimoda, 1960), $\mu_{12} = 9.723 \times 10^{-19}$ e.s.u., $U = 1$ kV $= 10/3$ e.s.u., $r_1 = 0.029$ cm, $r_2 = 5$ cm, then $\acute{c} = 2 \times 10^{-18}$ erg.cm^3. The value of r is calculated by substituting the value of $\acute{c}$ in equations (2.24) and (2.23).

Fig (2.3) represents the spiral motion of J = 3, K = 3 ammonia molecules around the single straight wire focuser , for a transverse component of velocity equal to 7×10^4. $\tan\theta$ where $\theta = 1/85$ radian.

When the transverse component of velocity on entering the focuser field is zero, the radial component changes from zero to a finite value, but ϕ is constant, i.e. the molecules do not have a spiral motion. The component of velocity which is parallel to the single straight wire focuser will be constant in this case.

Trajectory of ammonia molecules effected by the field of the single straight wire focuser with

a) on-axis nozzle source

Now assume that the molecules emerge from an on-axis nozzle (single hole nozzle). For simplicity of the calculation, assume that the ammonia molecules have a velocity V at the entrance of the focuser. The radial velocity component is then V sin θ, where θ is the angle at which the molecule emerges from the source with respect to the focuser axis. The other (constant) component parallel to the wire is V cos θ, and the molecules lie at a distance R from the wire. The maximum angle that the molecules possess at the entrance of the focuser is equal to 0.033 radian. The minimum angle is restricted to the diameter of the wire and the dimension of the diaphragm as shown in fig (2.4). While the molecules pass in the vicinity of the focuser, they interact with the electric field produced by the wire. The electric field is transverse with respect to the beam and thus focuser axis. The radial component of velocity of molecules decreases while molecules pass in the vicinity of the focuser. The equations of motion are as follows:

$$\frac{dr}{dt} = V \qquad (2.30)$$

$$\frac{dV}{dt} = -\epsilon/mr^3 \qquad (2.31a)$$

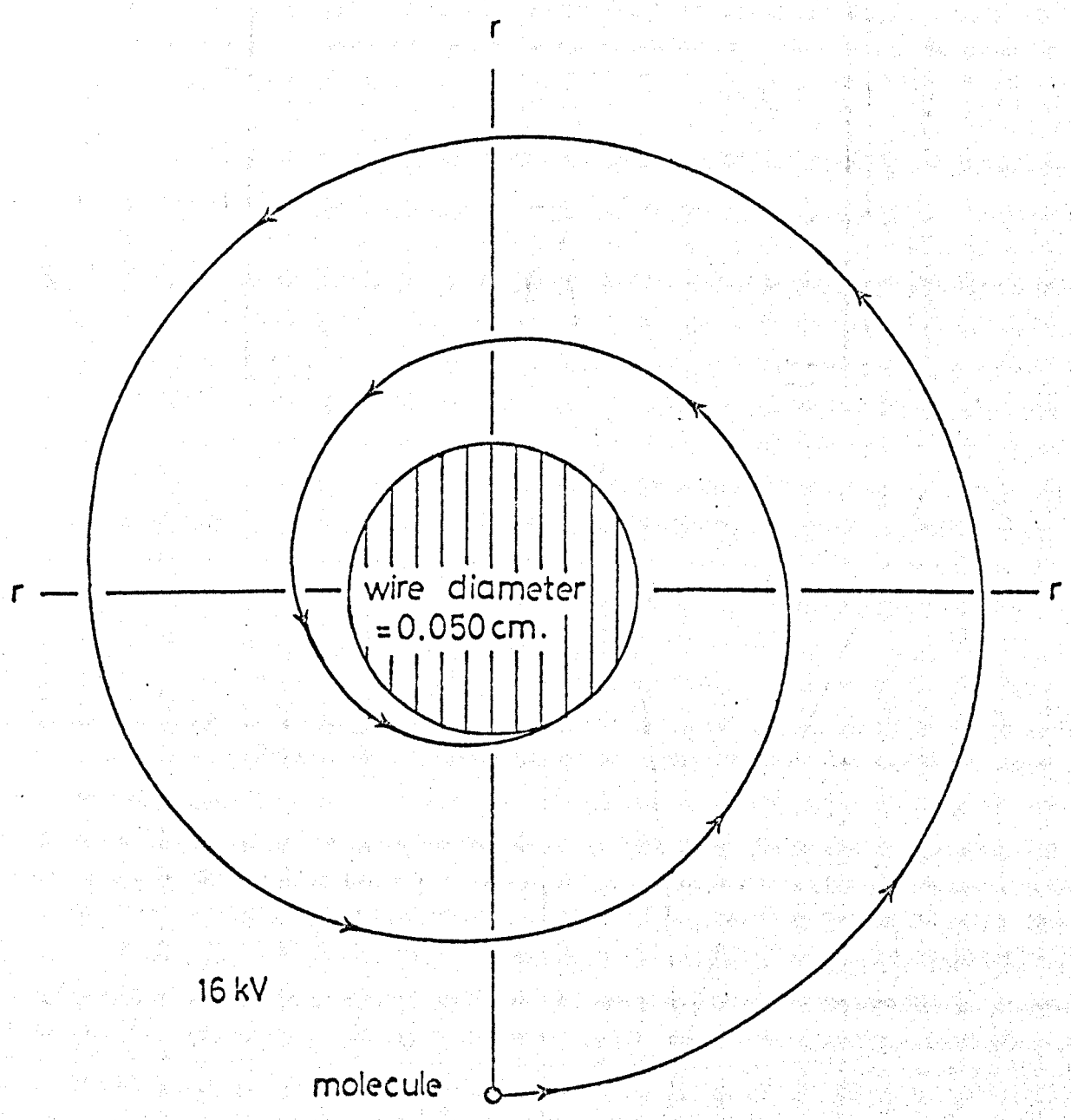

FIGURE(2.3) REPRESENTS THE SPIRAL MOTION OF J=3 K=3 AMMONIA MOLECULES AROUND THE SINGLE STRAIGHT WIRE FOCUSER.

FIGURE (2.4A) REPRESENTS THE TRAJECTORY OF J=K=3 AMMONIA MOLECULES INTERACTING WITH THE FIELD OF A SINGLE STRAIGHT WIRE FOCUSER.

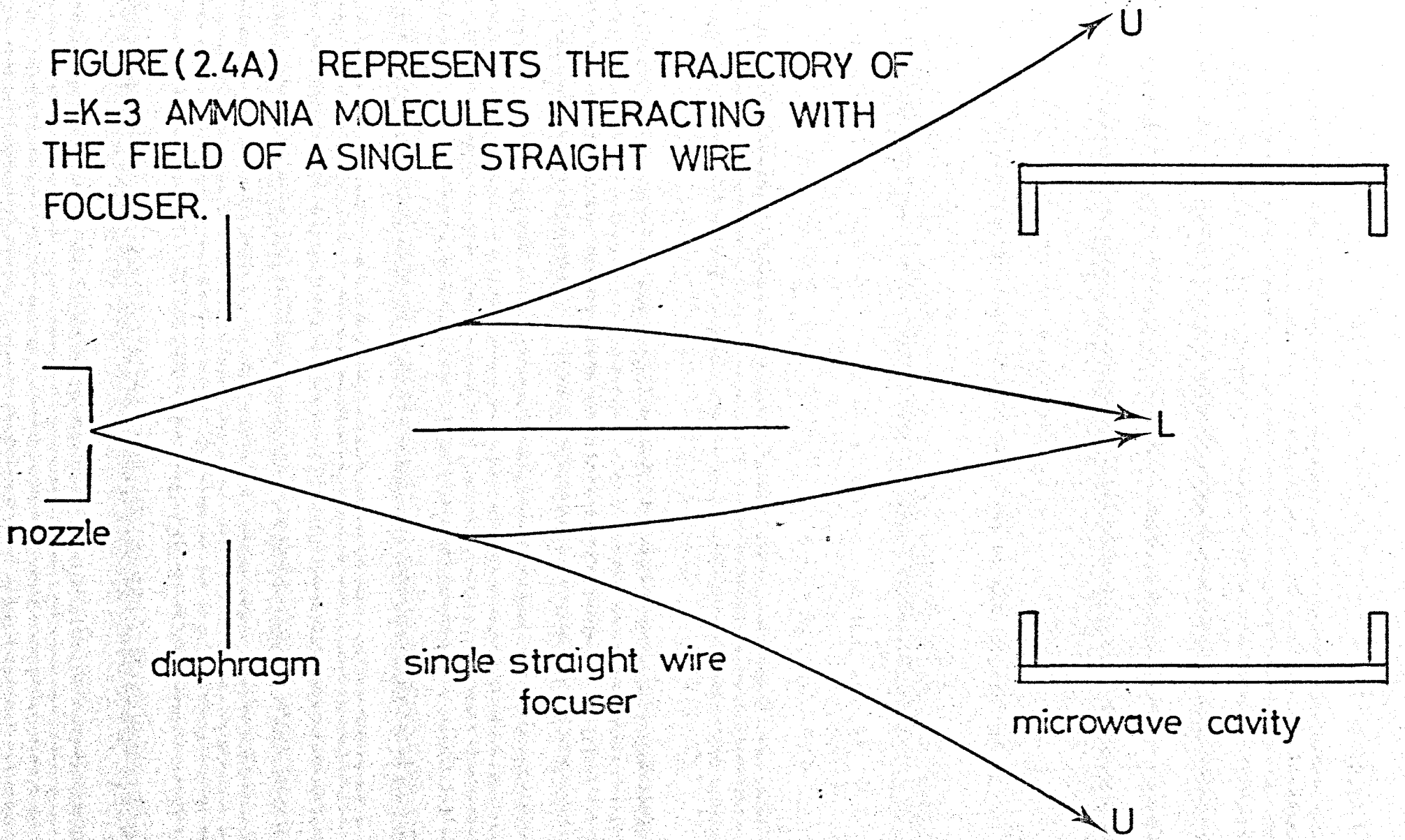

To solve these two equations, the initial conditions are

$$r_0 = L \tan \theta \tag{2.32a}$$

$$V_0 = V \sin \theta \tag{2.33a}$$

where r_0 is the initial radial distance of molecules at the entrance of the focuser

V_0 is the initial radial velocity of ammonia molecules at the entrance of the focuser

L is the nozzle-focuser separation

V is the speed of ammonia molecules at the temperature of the nozzle chamber.

In order to know the trajectory and the final values of r and V of the molecules in the vicinity of the wire, two equations are set; the first is the prediction equation and the second is the correction equation (McCracken & Dorn, 1964).

$$r_{n+1} = r_n + V_n . H \tag{2.34}$$

$$V_{n+1} = V_n - (\vec{c}/m\, r_n^3) \cdot H \tag{2.35a}$$

Then in order to correct these equations the following equations were used

$$r_{n+1} = r_n + \left(\frac{V_n + V_{n+1}}{2} \right) \cdot \frac{H}{2} \tag{2.36}$$

$$V_{n+1} = V_n + \left(\frac{\vec{c}}{m\, r_n^3} + \frac{c_1}{m\, r_{n+1}^3} \right) \cdot \frac{H}{2} \tag{2.37a}$$

where the variable

$$c_1 = \left[\frac{1}{\left(\frac{h\nu_0}{2}\right)^2 + (\mu_{12} E)^2} \right]^{\frac{1}{2}} \cdot \left[\frac{\mu_{12} \cdot U}{\ln (r_2/r_1)} \right]^2$$

and $E_1 = \frac{U}{\ell n(r_2/r_1)} \cdot \frac{1}{r_{n+1}}$

where r_{n+1} is the final radial distance at the end of the focuser

V_{n+1} is the final radial velocity at the end of the single straight wire focuser

n is the number of the integration step, which is 20 steps in the programme used

H is the integration step and is given by the following equation

$H = F_\ell / Z_a \cdot V \cos\theta$

where F_ℓ is the focuser length

Z_a is the number of elemental lengths of the focuser, in this case 40.

b) off-axis nozzle source

When off-axis sources are used, then with respect to the axis of the focuser there is a tangential component of velocity V_{TO} as well as a radial component, as in the case of an on-axis source, fig (2.4b). The molecules are under the influence of the electrical force due to the Stark effect as a result of voltage applied to the focuser. This latter force acts inwards or outwards for molecules with $\mu_{eff} > 0$ or $\mu_{eff} < 0$ respectively. Besides the variation of the angle θ at which the molecules emerge from the off-axis nozzle source, there is another angle θ_2 which is defined by the diagram, fig (2.4b) for which the molecules rotate around the off-axis source.

The equations of motion are as follows

$$\frac{dr}{dt} = V \qquad (2.30)$$

$$\frac{dv}{dt} = -\mathcal{C}/mr^3 + \frac{J^2}{m^2 r^3} \qquad (2.31b)$$

FIGURE (2.4B) REPRESENTS THE TRAJECTORY OF J=K=3 AMMONIA MOLECULES INTERACTING WITH THE FIELD OF A SINGLE STRAIGHT WIRE FOCUSER.

w denotes the wire axis.

s denotes the off axis source.

a is the perpendicular distance between the nozzle (off axis) and the wire axis.

L nozzle-focuser separation.

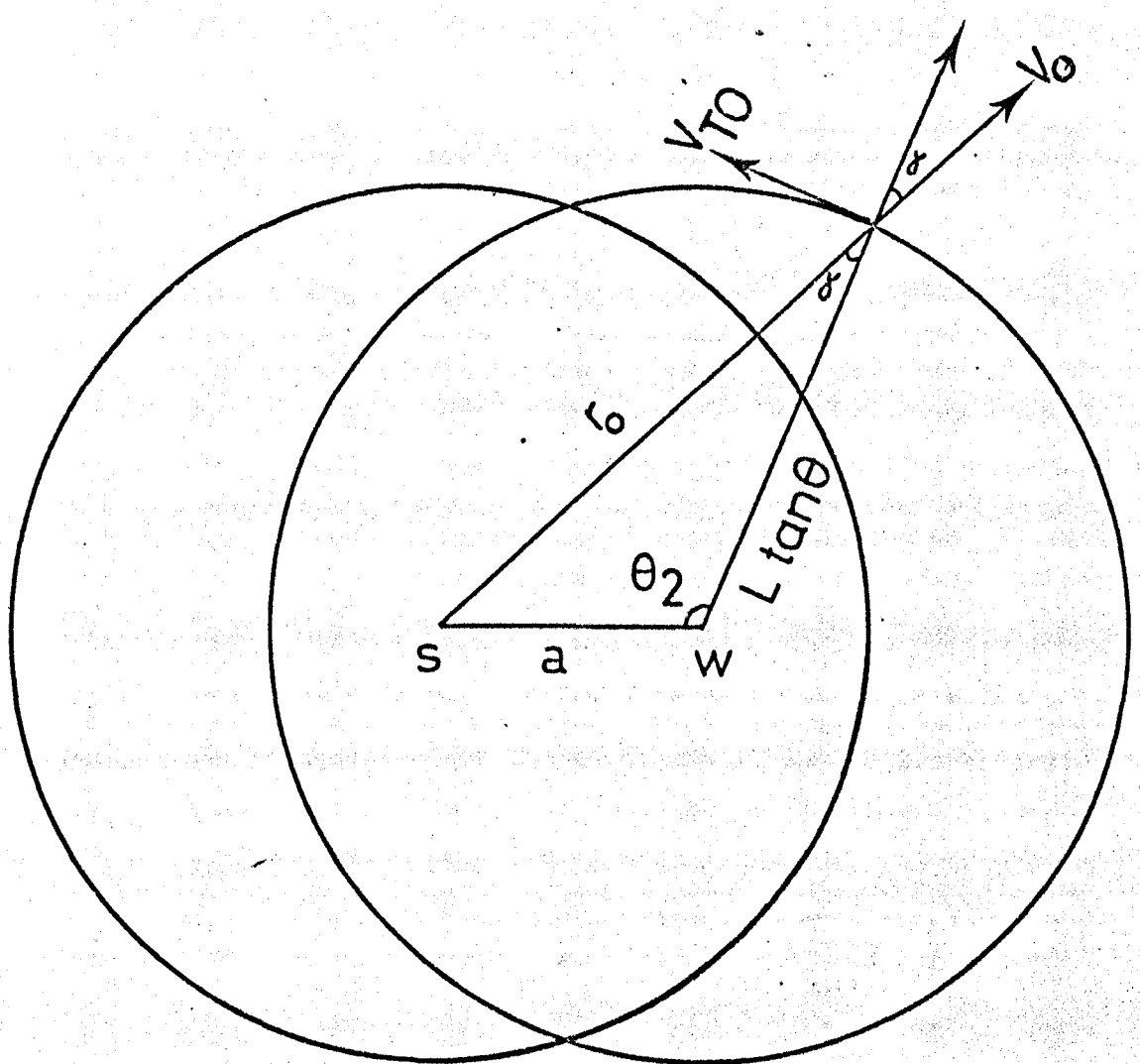

In order to solve the two equations (2.30) and (2.31b) for an off-axis nozzle source; the initial conditions are:

$$r_0 = \left[a^2 + (L \tan\theta)^2 - 2.a.L \tan\theta.\cos\alpha\right]^{\frac{1}{2}} \qquad (2.32b)$$

$$V_0 = V.\sin\theta\,(1 - B^2)^{\frac{1}{2}} \qquad (2.33b)$$

where $B = \cos\alpha = \dfrac{r_0^2 + (L\tan\theta)^2 - a^2}{2\, r_0\, L \tan\theta}$

or V_0 can be written as $V_0 = V \sin\theta \cos\alpha$.

In order to know the trajectory and the final r_f and V_f of $J = 3$, $K = 3$ ammonia molecules (both upper and lower energy state) for an off-axis nozzle source in the vicinity of the wire, two equations were set, the first was the prediction equation and the second was the correction equation.

$$r_{n+1} = r_n + V_n \cdot H \qquad (2.34)$$

$$V_{n+1} = V_n - (\mathcal{E}/mr_n^3) \cdot H + \frac{J^2}{m^2 r_n^3} \cdot H \qquad (2.35b)$$

where the variable $\mathcal{E} = \left[\dfrac{\mu_{12} U}{\ell_n (r_2/r_1)}\right]^2 \left[\dfrac{1}{\left(\frac{h\nu_0}{2}\right)^2 + (\mu_{12}E)^2}\right]^{\frac{1}{2}}$

$$E = \frac{VOL}{\ell n(r_2/r_1)} \frac{1}{r_n}$$

and $J = m\, r_0\, V_{TO}$

The initial tangential component velocity is given by $V_{TO} = S \sin\theta \sin\alpha$

The correction equation for the equations (2.34 and 2.35b) are:

$$r_{n+1} = r_n + (V_n + V_{n+1}) \cdot \frac{H}{2} \qquad (2.36)$$

$$V_{n+1} = V_n - \frac{\mathcal{E}}{mr_n^3} + \frac{c_1}{mr_{n+1}^3} \cdot \frac{H}{2} + \frac{J^2}{m^2 r_n^3} + \frac{J^2}{m^2 r_{n+1}^3} \cdot \frac{H}{2} \qquad (2.37b)$$

where the variable C_1

$$C_1 = \left[\frac{\mu_{12}U}{\ln(r_2/r_1)}\right]^2 \left[\frac{1}{\left(\frac{h\nu_0}{2}\right)^2 + (\mu_{12}E_1)^2}\right]^{\frac{1}{2}}$$

$$E_1 = \frac{U}{\ln(r_2/r_1)} \frac{1}{r_{n+1}}$$

when the ammonia molecules leave the single straight wire focuser, it is assumed that no further focusing forces due to fringe fields are operative.

The following equation shows the radial position of the molecules at the entrance of the resonant cavity x cm away from the single straight wire focuser:

$$D = r_f + V_f \cdot t$$

where $t = (x/V \cdot \cos\theta)$

where x is the distance between the focuser and the cavity.

The computer programme was adjusted to account only for those molecules that emerge from the focuser and pass through the cavity without hitting or colliding with the walls.

For the calculation of the intensity of the state selected beam by the use of the single straight wire focuser, the maxwellian distribution of the molecules emerging from the nozzle was taken into consideration. For details see appendix (7). The computed results of the variation of the absorption signal intensity as a function of the voltage applied to the single straight wire focuser is illustrated in fig (2.5). Experimental results with the single wire focuser will be discussed in section (4.2).

2.3.2 Crossed-wire focuser

This focuser was devised by Laine and Sweeting (1971) to focus lower energy state ammonia molecules.

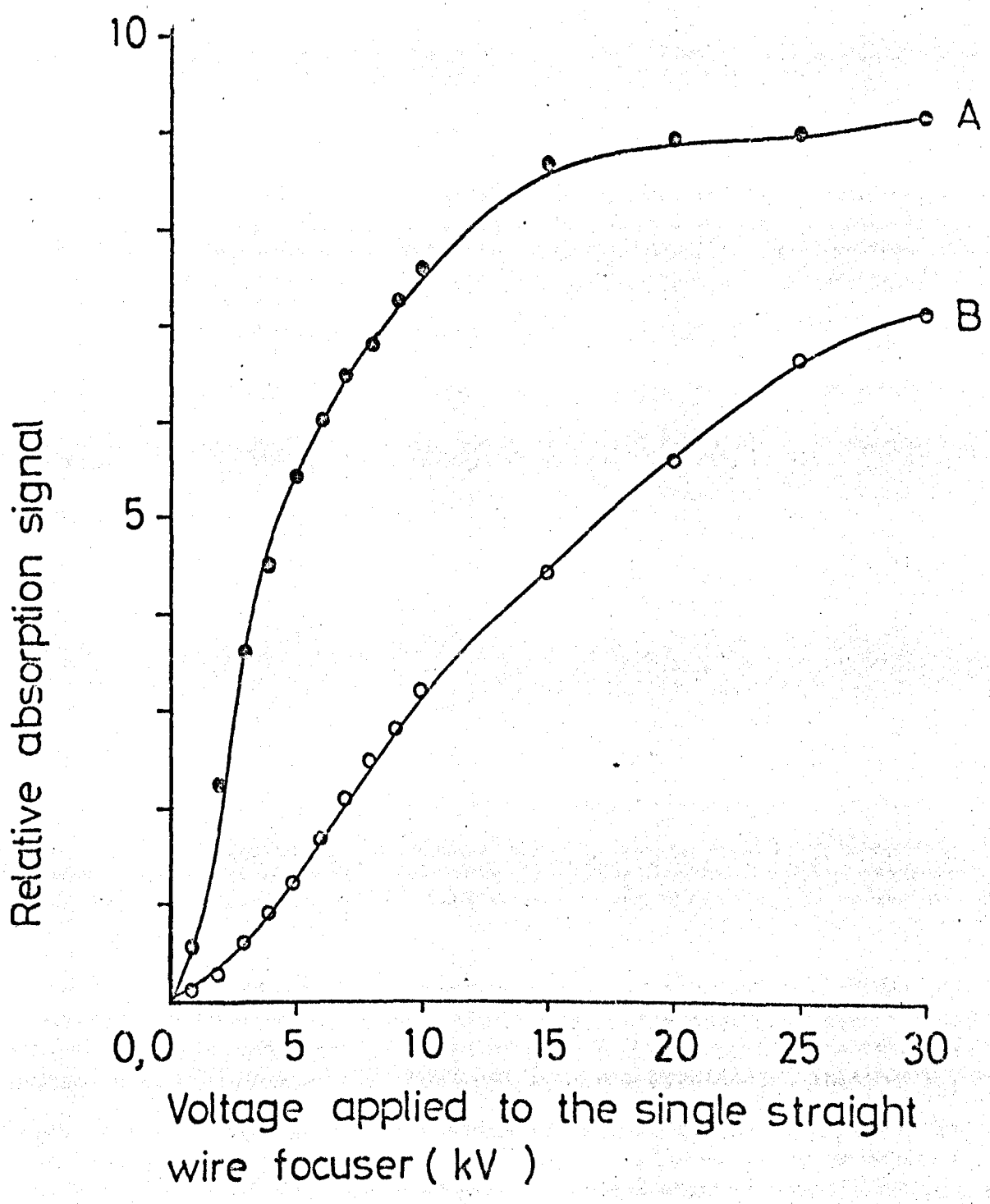

FIGURE (2.5) COMPUTER RESULTS REPRESENTING THE VARIATION OF THE ABSORPTION SIGNAL INTENSITY AS A FUNCTION OF THE VOLTAGE APPLIED TO THE SINGLE STRAIGHT WIRE FOCUSER FOR R1=0.028 CM, R2=5 CM. A) REPRESENS THE RESULTS FOR AN ON-AXIS SOURCE B) REPRESENTS THE RESULTS FOR AN OFF-AXIS SOURCE.

Sweeting (1971) assumed that each single insulated wire had a uniform charge density on its surface even when another wire was brought close to it. This assumption is incorrect. In fact the distribution of the electrical charge will have a maximum magnitude at the focuser axis, and will decrease gradually outwards from the axis until it reaches a constant value.

In fact it would be better to take successive wire electrodes of the crossed-wire focuser as a single element. Experimental results obtained with the crossed wire focuser are discussed in section (4.2).

2.3.3 The eight pole rod focuser

Introduction

This focuser selects ammonia molecules that are in the upper inversion energy state and focuses them into the cylindrical maser cavity. It defocuses the molecules in the lower energy state and deflects them away from the beam axis.

The focuser consists of eight parallel rods positioned symmetrically about the axis of the beam. Four alternate rods are connected to the EHT supply and the other four are grounded. This arrangement forms an electric field which is zero along the beam axis and whose magnitude increases rapidly in any radial direction.

If the electrodes of the focuser are cooled to a low temperature with liquid nitrogen, lower energy state molecules may be frozen out. This leads to a stronger maser signal and reduces the threshold voltage for oscillation. In practice the build-up of solid ammonia is to be avoided since the electric field is gradually reduced in time. Thus it is more usual to surround the focuser with a liquid nitrogen jacket and molecules are frozen on the inner surface of that rather on the focuser itself.

Theory of the eight pole rod focuser

The magnitude of the electric field of a general 2n-pole multipole focuser is given by Hirono (1959) as

$$E = \left(\frac{n\, r^{n-1}}{2\, a^{n}} \right) U \qquad (2.38)$$

where n is an even number of alternately charged parallel rods located symmetrically about the axis of the molecular beam (or n = half of the number of electrodes)

r is the distance from the beam axis of the focuser

a is the distance of the surface of the electrode from the beam axis

U is the potential difference between the neighbouring electrodes.

The electrostatic field at a distance r from the axis for the eight pole focuser is

$$E = \left(\frac{2\, r^{3}}{a^{4}} \right) U_{8} \qquad (2.39)$$

The inner maximum electric field of the eight pole focuser is obtained when r = a

$$E_{m} = \left(\frac{2}{a} \right) U_{8} \qquad (2.39a)$$

Motion of the ammonia molecules in the focuser

The total internal energy of the ammonia molecules (when hyperfine structure effects are neglected) is given by equation (2.5). For strong electric field, $\left(\frac{h\nu_0}{2} \right)^2 >> (\mu_{12}E)^2$, and the energy of the molecules is given by

$$W = W_0(J, K) \pm \left[\left(\frac{h\nu_0}{2} \right) + U(r) \right]^{\frac{1}{2}} \qquad (2.40)$$

$$\text{where } U(r) = \frac{1}{h\nu_0} \left[\mu_{12} E \right]^2$$

The radial force exerted by the focuser on the ammonia molecules is given by the negative gradient of W

$$f_r = - \frac{\partial W}{\partial r} \simeq \mp \frac{\partial U}{\partial r}$$

$$f_r = \mp \frac{1}{h\nu_0} 2 \mu_{12} E_r \frac{\partial E}{\partial r} \qquad (2.41)$$

where the negative and positive signs refer to the upper and lower energy state molecules respectively.

Fig (2.6) shows the computed values of the radial gradient of the square of the electric field $\frac{\partial E^2}{\partial r}$ as a function of the radial distance r away from the octopole rod focuser axis. It is clear that the radial gradient has a zero value at the focuser axis. As the radial distance increases the gradient gradually increases, first slowly, and then when r = 0.8 R, where R is the radius of the octopole rod focuser, the gradient increases then more rapidly, reaching its maximum value at the surface of the rod electrode.

The condition for focusing upper energy state molecules requires the radial energy to be less than the height of the potential well U(a) of an octopole rod focuser of radius a

$$\tfrac{1}{2} m V_r^2 < U(a) \qquad (2.42)$$

Therefore the radial velocity V_r of the molecules, is equal to or less than V_c ($V_r \leq V_c$), where V_c is the critical radial velocity given by

$$V_c = \left(\frac{2}{m h\nu_0} \right)^{\frac{1}{2}} \mu_{12} E_m \qquad (2.43)$$

The focusing length (for upper energy state molecules) or the skip distance for the eight pole rod focuser is given by the following equation

$$L = 2.43 \left(\frac{a}{V_c}\right) V_z \qquad (2.44)$$

INSIDE THE OCTOPOLE ROD ELECTRODE SYSTEM

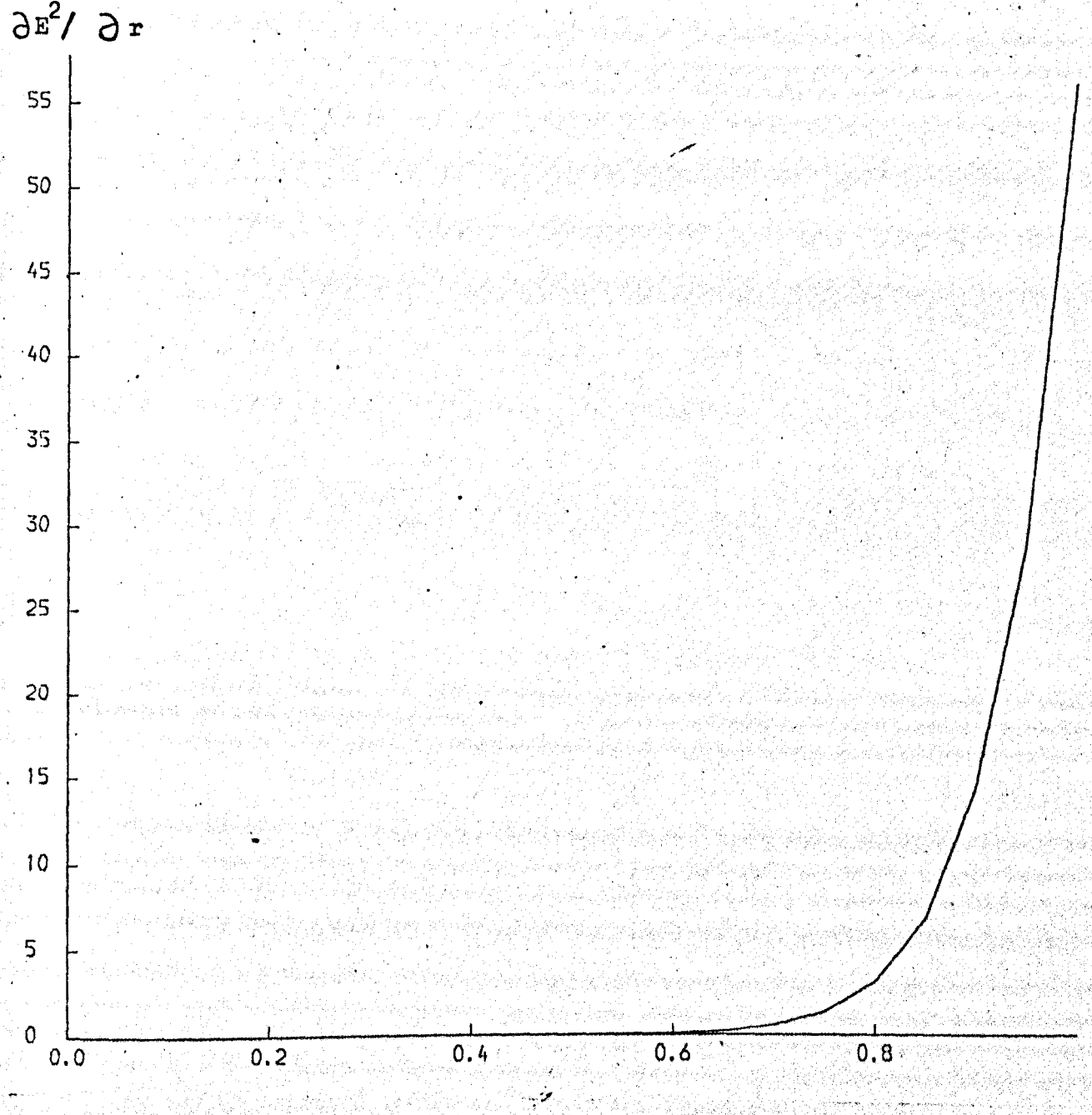

FIGURE (2.6) COMPUTED RESULTS GIVING THE RADIAL GRADIENT OF THE SQUARE OF THE ELECTRIC FIELD $\partial E^2 / \partial r$ INSIDE THE OCTOPOLE ROD FOCUSER AS A FUNCTION OF THE RADIAL DISTANCE r AWAY FROM THE FOCUSER AXIS .

where V_z is the axial velocity of the molecules.

From the above equation, it is evident that the focusing length decreases with an increase of the voltage applied to the focuser electrodes. This is shown in fig (2.7) by setting d = 0.6 cm (radius of the octopole rod focuser). V_c is calculated from equation (2.44) by substituting $m = 28.22 \times 10^{-24}$ gm, $h = 6.6 \times 10^{-27}$ erg.sec, $\nu_0 = 2.4 \times 10^{10}$ Hz, $\mu_0 = 1.47 \times 10^{-18}$ e.s.u, J = 3, K = 3, $M_J = \sqrt{7}$, $\mu_{12} = 9.723 \times 10^{-19}$ e.s.u, E_m is calculated from equation (2.39a), and $V_z = 7 \times 10^4$ cm/sec, and using different values of voltage varying from 2 to 30 kV (using e.s.u. of voltage).

In order to find the equation of the molecules in the focuser, by using polar coordinates:

$$m\ddot{r} = F(r) \tag{2.45}$$

from equation (2.45) the motion of molecules is described by the following equation:

$$\ddot{r} = \mp Cr^5 = \mp \frac{3V_c^2}{a^6} \tag{2.46}$$

by substituting the value of V_c from equation (2.43)

$$\ddot{r} = \mp \frac{6.\mu_{12}^2 E^2}{m\, h\nu_0\, a^6} \tag{2.46a}$$

Vonbun (1958) calculated the trajectory for ammonia using (2.46a).

It may be expected that a multipole rod focuser of a small diameter such as described in this section, but sheathed with a molecular beam, may also be used for focusing lower energy state molecules ($\mu_{eff} > 0$) in a similar way to the single straight wire focuser. Thus by using a spectrometer cavity as a beam detector which can be moved transversely across the beam axis, it is expected that when the molecular beam is of greater diameter than that of the focuser, there will be an absorption signal on axis flanked on both

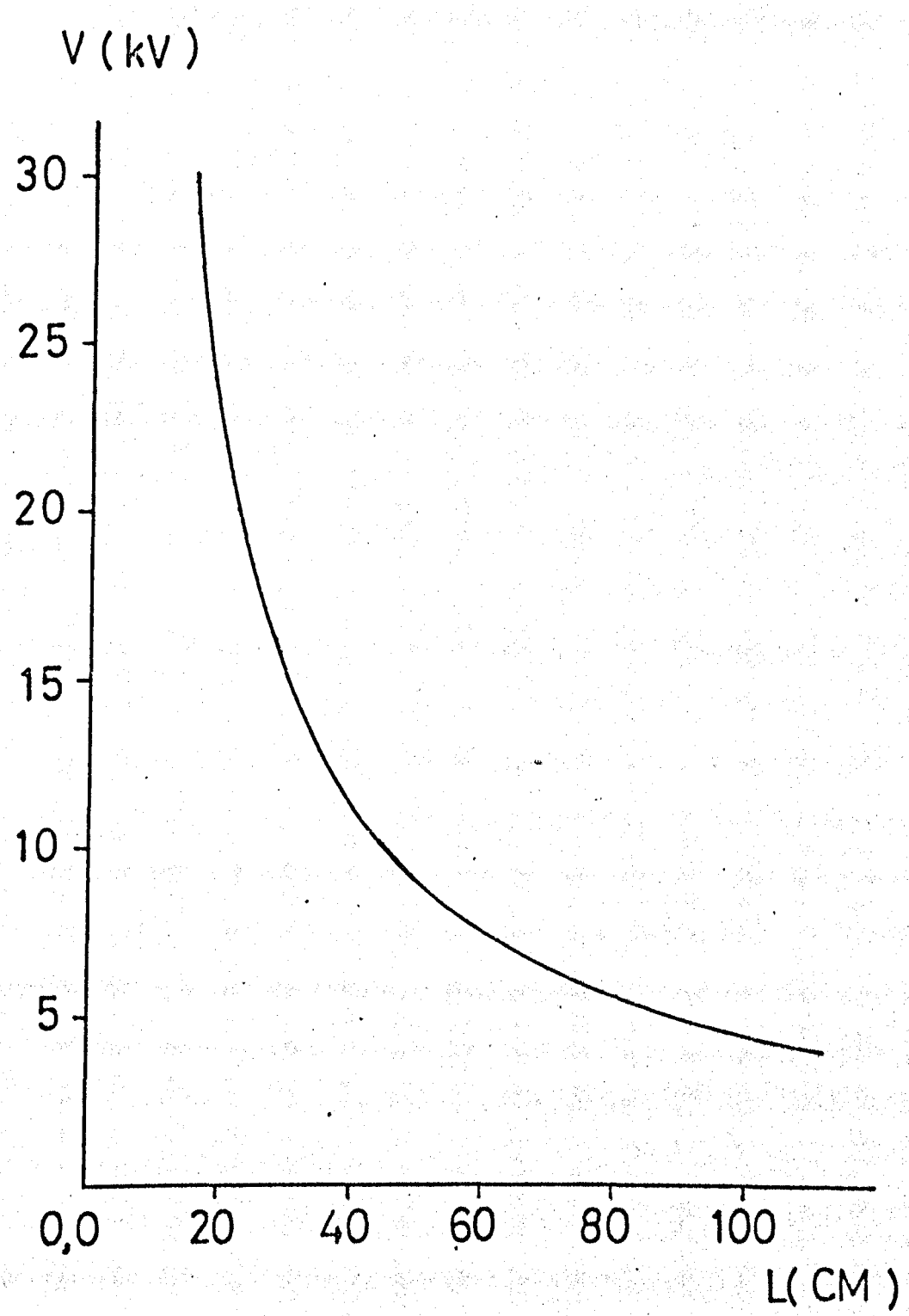

FIGURE (2.7) THE VARIATION OF THE FOCUSING LENGTH (SKIP DISTANCE) (L) WITH THE VOLTAGE APPLIED TO THE EIGHT POLE ROD FOCUSER (V).

sides by an emission signal, when an axial beam stop is used. Conversely maser action (stimulated emission) on axis flanked on both sides by an absorption signal should be obtained when no molecules are allowed to pass outside the focuser, the axial beam stop having been replaced by a beam aperture. Evidence for this latter case will be presented in section (4.1).

2.3.4 Ring focuser

The ring focuser was first proposed by Krupnov (1959). It was used successfully by Becker (1963), Basov et al. (1966), and Bardo and Laine (1971).

According to Shecheglov (1961) the electrostatic potential in the ring focuser can be expressed approximately by

$$\phi(P, Z) = \frac{0.5\ U_0}{I_0(\pi P_0/l)}\ I_0\left(\frac{\pi P}{l}\right) \sin\left(\frac{\pi Z}{l}\right) + \frac{0.1\ U_0}{I_0(\pi P_0/l)}\ I_0\left(\frac{3\pi P}{l}\right) \sin\left(3\pi Z/l\right) \tag{2.47}$$

where Z = the focuser axis

P_0 = radial distance from the focuser axis to the ring

P = radial distance from the focuser axis

l = ring separation

I_0 = is the Bessel function of zero order of pure imaginary argument

U_0 = the focuser potential with respect to earth

The electric field in the ring system is given by:

$$E = \left\{\left(\frac{\partial\phi}{\partial P}\right)^2 + \left(\frac{\partial\phi}{\partial Z}\right)^2\right\}^{\frac{1}{2}}$$

$$E = 0.3\pi\ \frac{U_0}{l}\left\{\left[2\ \frac{I_0(\pi P/l)}{I_0(\pi P_1/l)} \sin\frac{\pi Z}{l} + \frac{I_0(3\pi P/l)}{I_0(3\pi P_1/l)} \sin\frac{3\pi Z}{l}\right]^2 + \left[2\ \frac{I_0(\pi P/l)}{I_0(\pi P_1/l)} \cos\frac{\pi Z}{l} + \frac{I_0(3\pi P/l)}{I_0(3\pi P_1/l)} \cos\frac{3\pi Z}{l}\right]^2\right\}^{\frac{1}{2}} \tag{2.48}$$

where $I_1(x)$ is the Bessel function of first order and imaginary argument.

Fig (2.8) illustrates the computed results and shows the dependence of the modulus of the electric field intensity on the variation of the Z-coordinate (multiplied by the factor $8/l$) in the range $(-\ l/2 \leq Z \leq l/2)$, for a fixed value of P and for the case when $P_0 = l$. It is seen from the graph that the magnitude of the modulus drops to 1/3 maximum value just when $P = 0.8\ P_0$.

Fig (2.9) shows the computed plot of the dependence of the modulus of the intensity E on the distance from the focuser axis at fixed values of Z. It is seen that the magnitude of the modulus E increases to 1/3 of its maximum value just when $P = 0.6\ P_0$.

The value of the electric field E at $P = P_0 = l$, averaged over the period Z calculated from fig (2.8), is equal to

$$\bar{E}_m = \tfrac{1}{2}\left[E_{max}\ (P_0, Z) + E_{min}\ (P_0, Z)\right]$$

where $E_{min} = 0.66\ U_0/l$ and $E_{max} = 2.82\ U_0/l$ and therefore

$$\bar{E}_m = 1.74\ U_0/l \qquad (2.49)$$

Within the ring diameter, the electric field increases radially outwards from the beam axis, thus providing the necessary field gradient fro state selection of molecules for conventional beam maser action.

From the electric field equation, the conclusion could be drawn that on the periphery of the focuser, the transverse electric field is approximately 1.7 times as great as the longitudinal electric field. A sufficiently long ring focuser should be used in order to obtain the maximum number of upper energy state molecules.

Fig (2.10) shows the computed values of the radial gradient of the square of the electric field $\frac{\partial E^2}{\partial r}$ at fixed values of Z. It is clear that the radial gradient has a zero value at the focuser axis.

INSIDE THE RING ELECTRODE SYSTEM

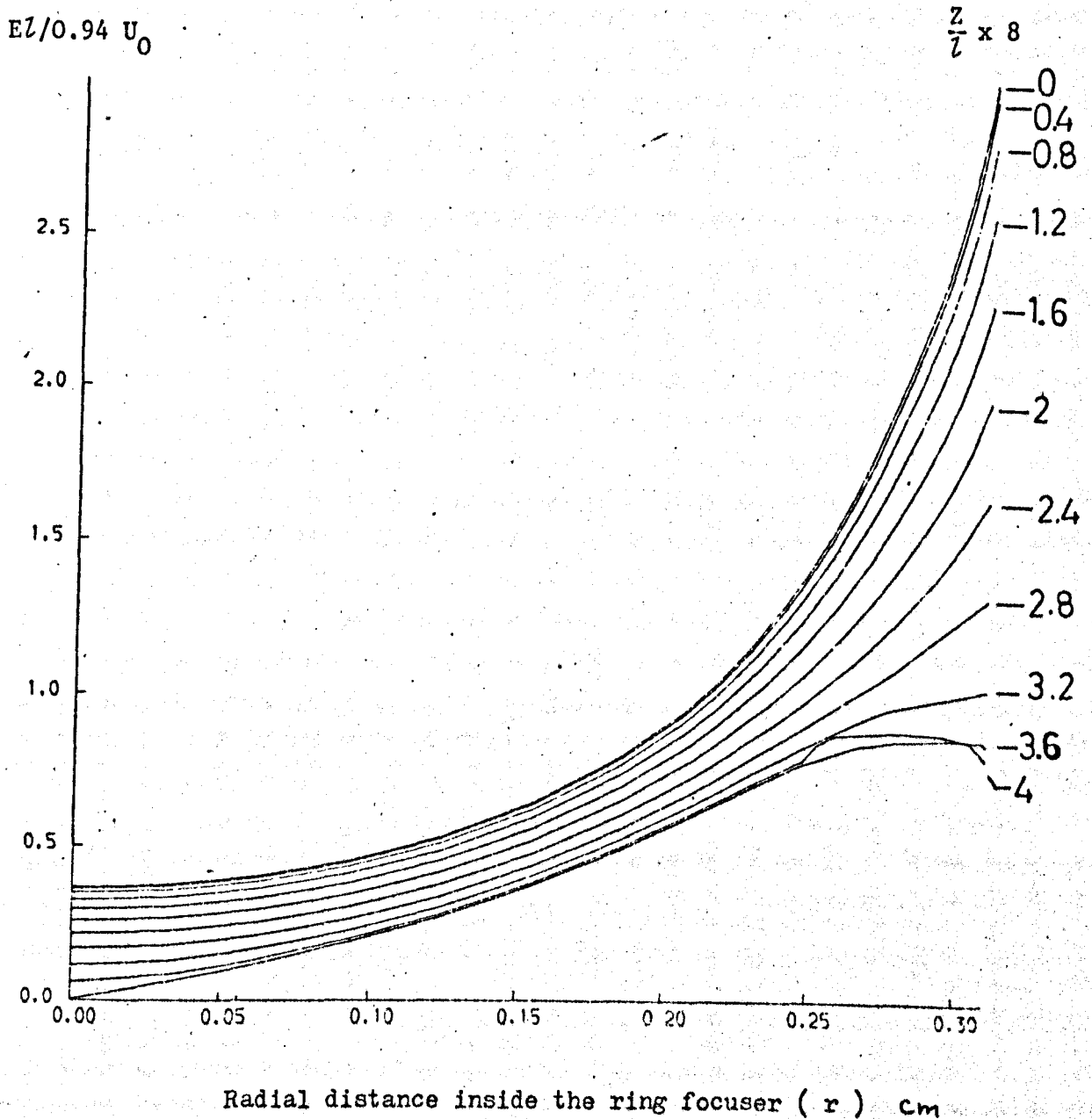

FIGURE (2.8) COMPUTED RESULTS GIVING THE DEPENDENCE OF THE MODULUS OF THE ELECTRIC FIELD INTENSITY E INSIDE THE RING FOCUSER ON THE DISTANCE TO THE AXIS AT FIXED VALUE OF Z ($P \leq P_0 = \ell$)

INSIDE THE RING ELECTRODE SYSTEM

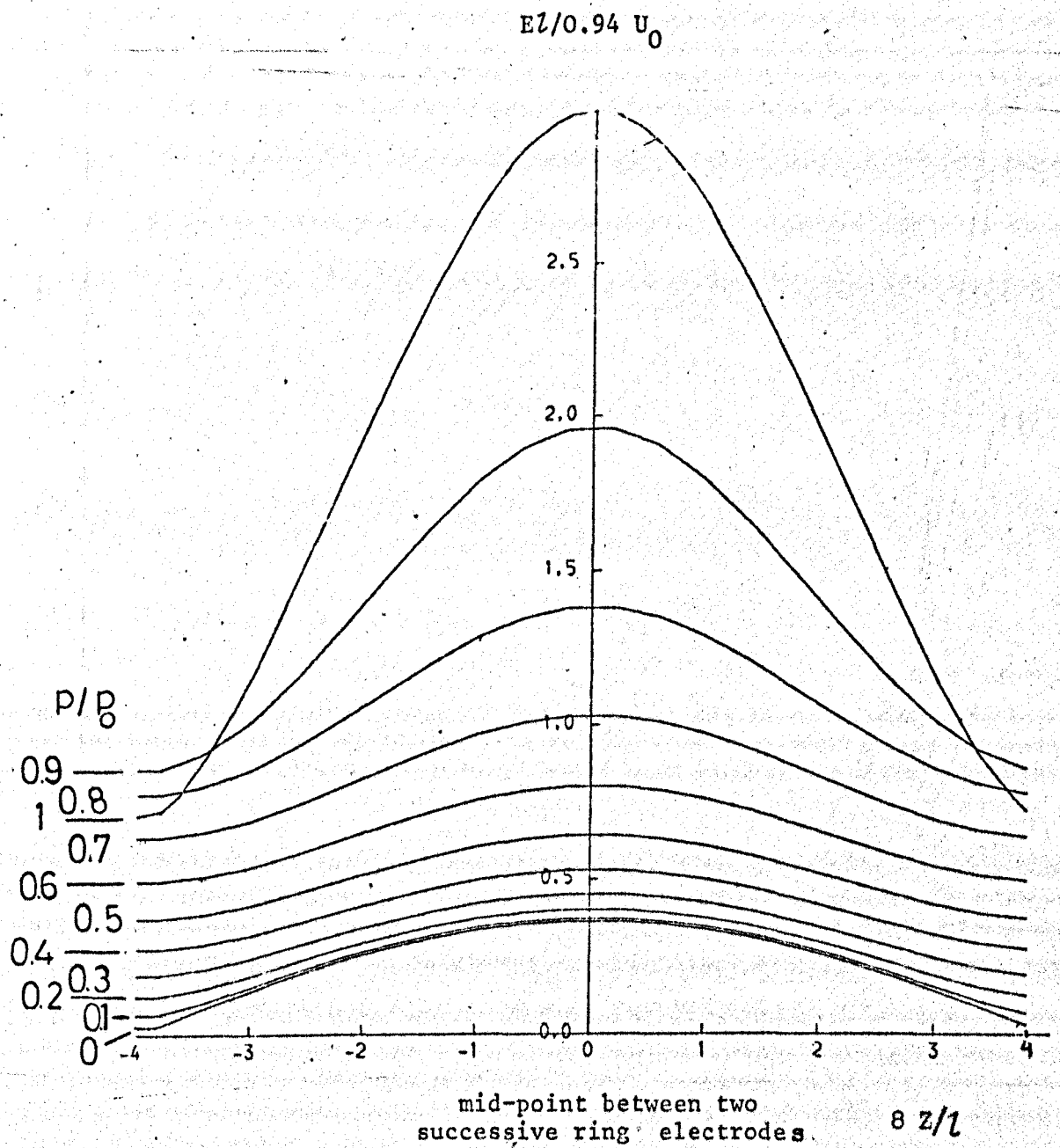

FIGURE (2.9) COMPUTED PLOT SHOWING THE DEPENDENCE OF THE MODULUS OF THE INTENSITY OF THE ELECTRIC FIELD E INSIDE A RING FOCUSER ON Z ($-\ell/2 \leq Z \leq \ell/2$) FOR FIXED VALUES OF P ($|z| \leq \ell/2$, $P_0 = \ell$). ZERO ON THE Z AXIS REPRESENTS THE MID-POINT BETWEEN TWO SUCCESSIVE RING ELECTRODES

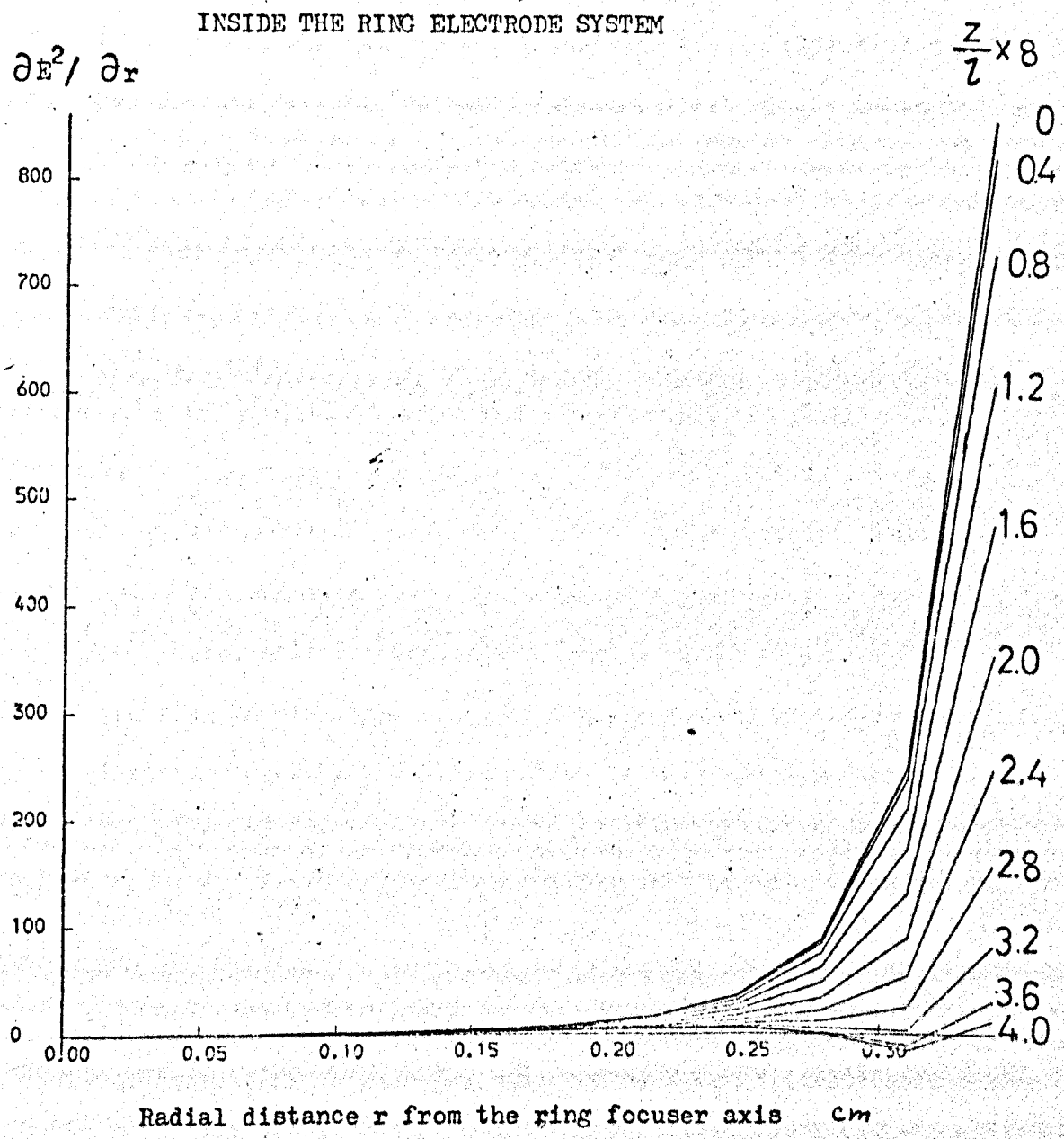

FIGURE (2.10) COMPUTED RESULTS GIVING THE RADIAL GRADIENT OF THE SQUARE OF THE ELECTRIC FIELD $\partial E^2 / \partial r$ INSIDE THE RING FOCUSER AS A FUNCTION OF THE RADIAL DISTANCE r FOR A FIXED VALUE OF Z ($p \leq p_0 = l$). THE SUDDEN STEP IN THE GRAPH IS DUE TO THE QUANTIZATION OF THE RADIAL DISTANCE INTO 10 INCREMENT STEPS.

As the radial distance increases the gradient gradually increases, first slowly, and then when r = 0.8 R, where R is the radius of the ring focuser, the gradient increases rapidly, reaching its maximum value at the surface of the ring electrode.

Trajectory of the ammonia molecules passing through the ring focuser

The trajectory calculation for the J = K = 3 ammonia molecules passing originally within the focuser then through it (without scattering) was carried out as follows. For molecules that pass into the ring focuser the computer programme was adjusted to calculate the molecular trajectories point by point using the inside form of E, F_r, F_2 ... etc. If the computed molecular trajectory went outside the ring focuser, the computer was programmed to switch to the outside formula of E, F_r, F_2 ... etc. For details see appendix (6). The computed results of the variation of the emission signal intensity as a function of the voltage applied to the ring focuser is illustrated in fig (2.11).

2.3.5 The bifilar helix focuser

The bifilar helix focuser was proposed by Krupnov (1959) and used by Becker (1963) and Mednikov and Parygin (1963) in molecular beam masers to focus upper energy state and defocus lower energy state molecules of the J = 3, K = 3 inversion transition of ammonia. The threshold voltage of the focuser to sustain maser oscillation was 9 kV (Mednikov and Parygin, 1963).

The experimental advantage of the bifilar helix is that the electrodes are smooth along the focuser length, which leads to a reduction of the possibility of electrical breakdown. This focuser is considered to be one of the most efficient types from the point of view of wide capture angle and large magnitude of the mean value of the electric field strength. However these focusers are inclined

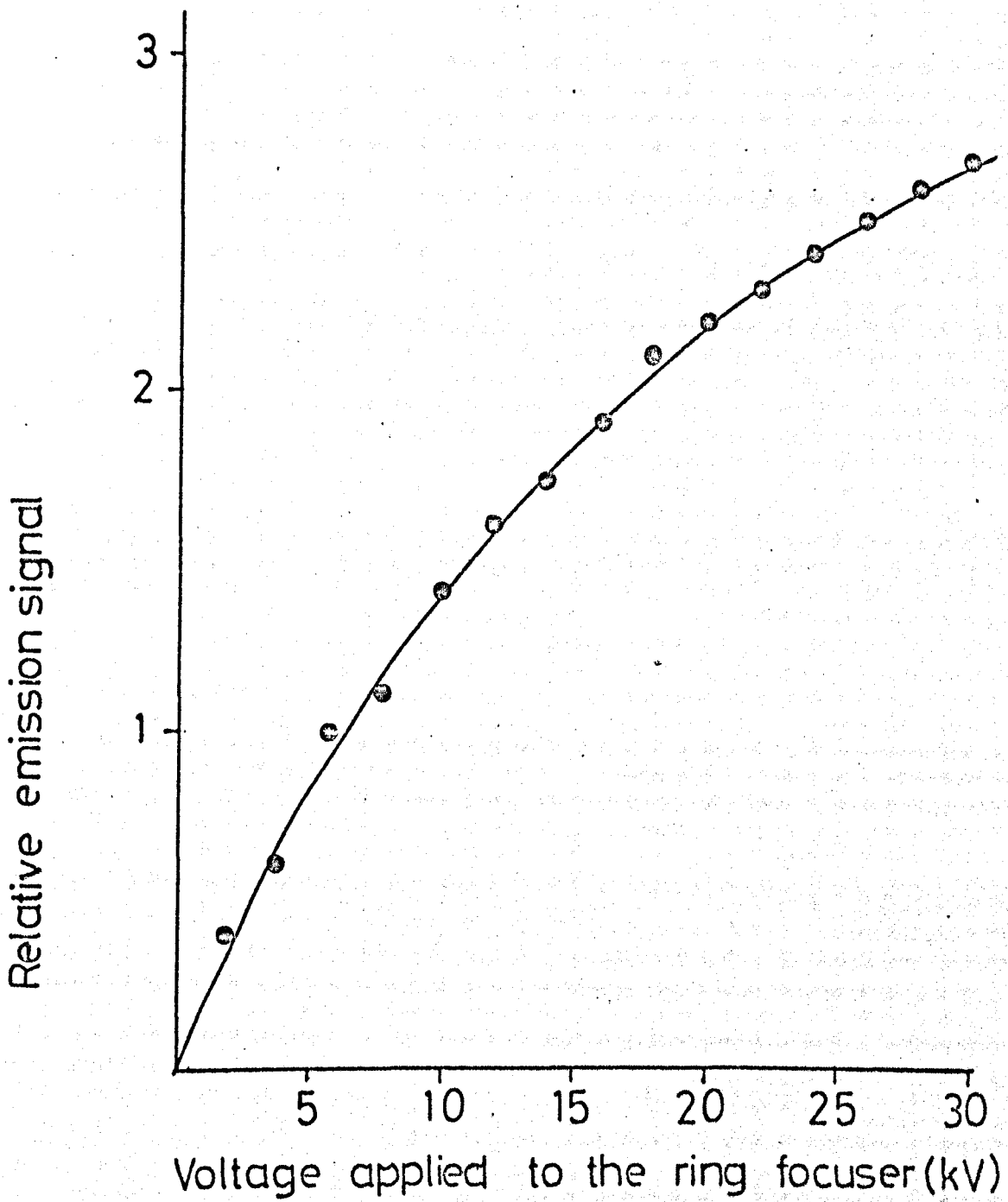

FIGURE (2.11) COMPUTED RESULTS FOR THE RELATIVE EMISSION SIGNAL AS A FUNCTION OF THE VOLTAGE APPLIED TO THE RING FOCUSER.

to be microphonic except when the helix is supported at many points along their length or alternatively made from several sections arranged in series

The theory of the bifilar helix focuser

The potential ϕ_C of the field of the bifilar helix is given in the form (A. I. Igritskiy, 1961):

$$\phi_C = 0.13\ UI_1\left(\frac{\pi r}{d}\right)\sin\left(\frac{\pi Z}{d} - \phi\right) + 10^{-4}\ UI_3\left(\frac{3\pi r}{d}\right)\sin\left(\frac{3\pi Z}{d} - 3\phi\right) \tag{2.50}$$

where U = the focuser voltage,

I_1 = Bessel function of the first kind,

Z = the focuser axis,

r = radial distance from the focuser axis,

d = neighbouring ring windings,

I_3 = Bessel function of the third kind,

ϕ = the angle between r and the winding as shown in fig (2.12)

The average value for E for $r = a = d$ is given by

$$E_m = 1.9\ \frac{U}{d} \tag{2.51}$$

For simplicity, the field will assume to be dependent on the radial distance r. The equation of the field can then be written as:

$$E = 1.41\ \frac{U}{a^2}\,r^2 + 0.09\ \frac{U}{a} \tag{2.52}$$

Within the helix diameter, the electric field increases radially outwards from the beam axis (focuser axis), thus providing the necessary field gradient for state selection of molecules for a conventional beam maser.

Fig (2.13) shows the computed plot for different angles of the magnitude of the electric field inside the focuser as a function of the radial distance r away from the focuser axis. It is clear that

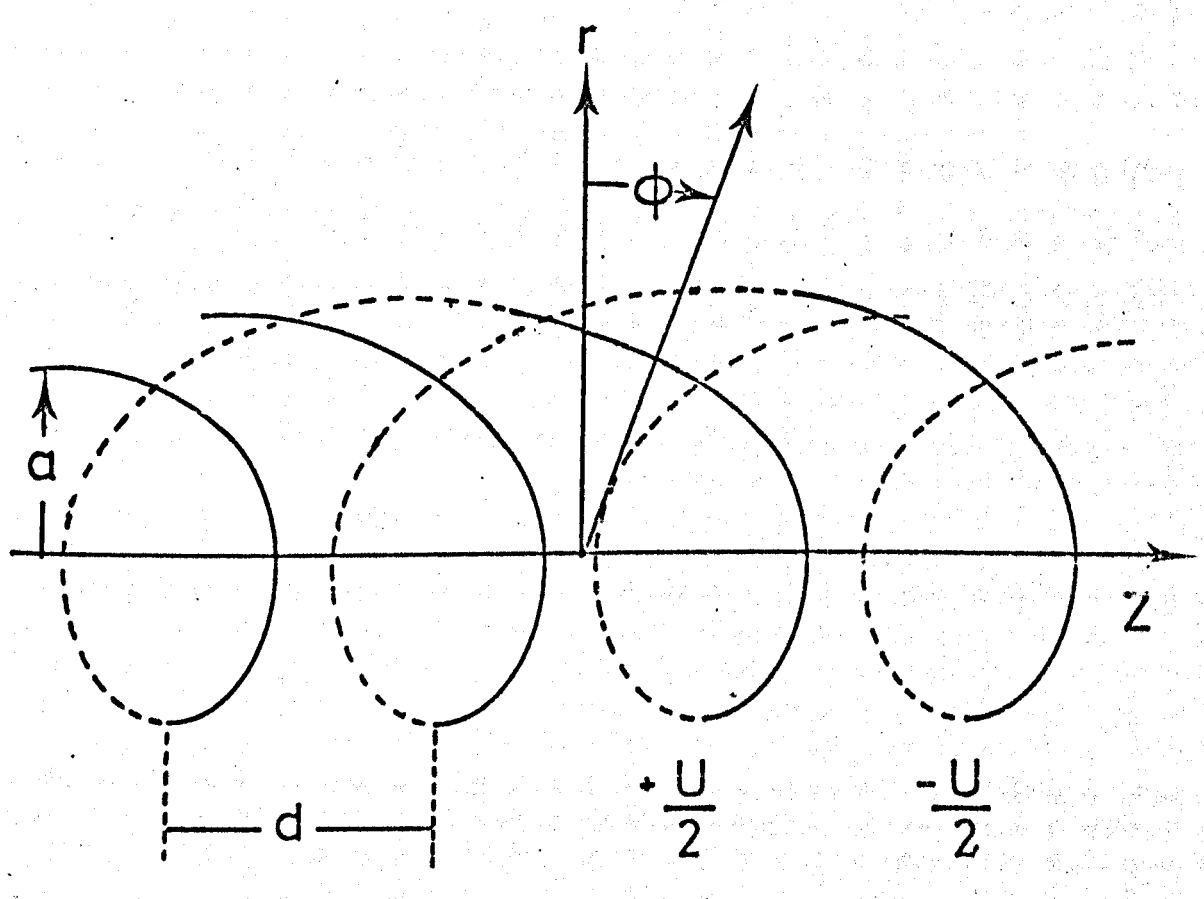

FIGURE (2.12) DIAGRAM OF THE BIFILAR HELIX FOCUSER GIVING THE KEY PARAMETERS.

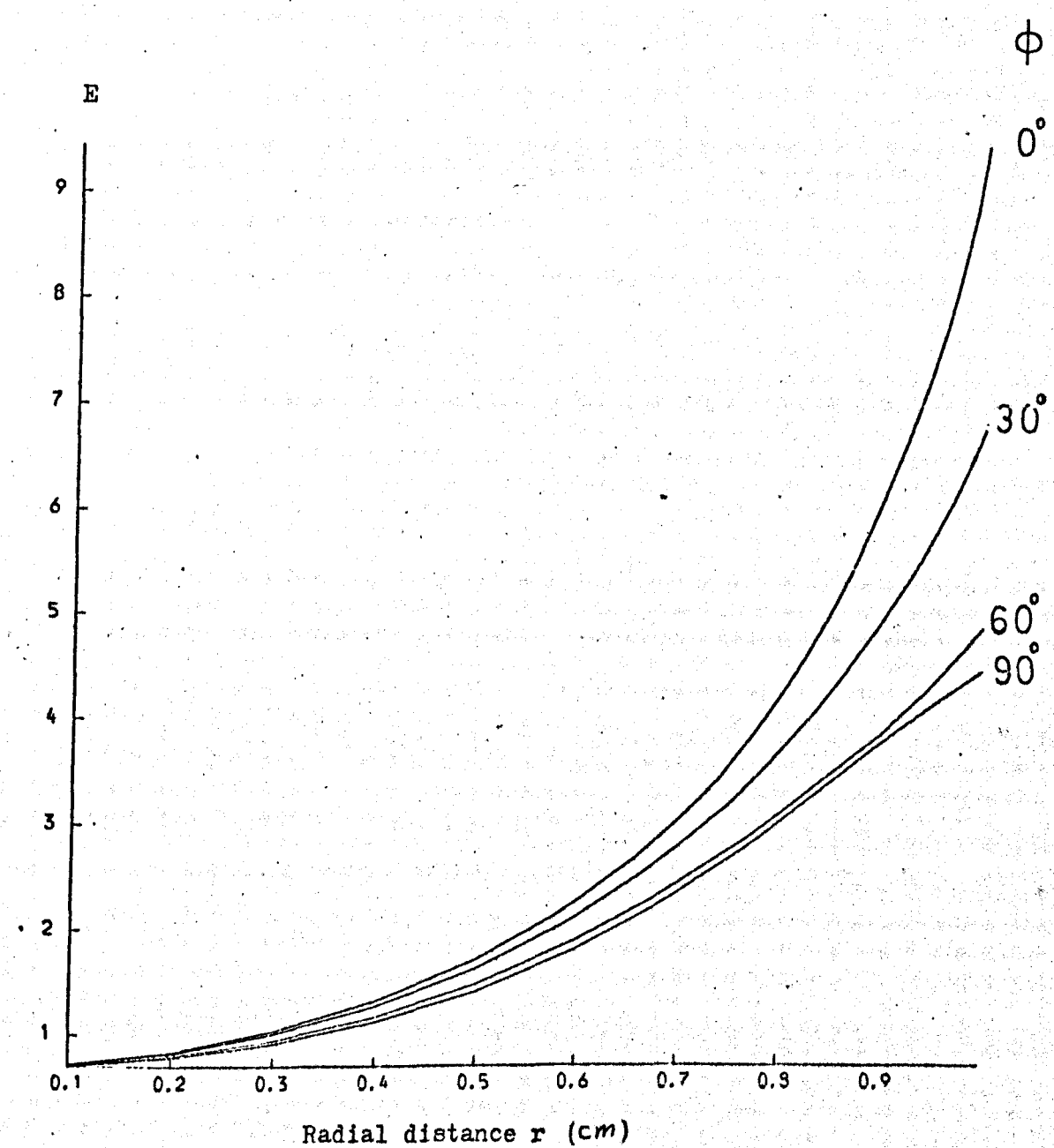

FIGURE(2.13) COMPUTED RESULTS THAT SHOW THE MAGNITUDE OF THE ELECTRIC FIELD INSIDE THE THE BIFILAR HELIX AS A FUNCTION OF THE RADIAL DISTANCE r.ϕ REPRESENTS THE ANGLE BETWEEN A VERTICAL AXIS AT THE ORIGIN OF THE COORDINATE SYSTEM CHOSEN, AND THE RADIAL VECTOR.

the electric field has an angular dependence and has also angular symmetry. Fig (2.14) shows the radial gradient of the square of the electric field $\frac{\partial E^2}{\partial r}$ as a function of the radial distance r away from the focuser axis. It is obvious that the radial gradient has a zero value at the focuser axis. As the radial distance increases the gradient gradually rises, and then when $r \approx 0.8$ R, where R is the radius of the bifilar helix, the radial gradient of the square of electric field increase rapidly, reaching its maximum value at the surface of the bifilar helix electrode.

From the electric field equation, the conclusion may be drawn that on the periphery of the focuser the transverse electric field is approximately 1.5 times as great as the longitudinal electric field. A sufficiently long bifilar helix focuser should be used in order to obtain the maximum number of upper energy state molecules.

Mednikov and Parygin (1963) pointed out in their paper that the bifilar helix type of state selector with a longitudinal field should be more efficient than a longitudinal rod type focuser with a transverse field. Experimentally, they found the maser signal obtained by the bifilar helix was approximately five times greater than can be obtained by use of a quadrupole focuser (transverse field) with the same focusing voltage and the same geometric dimensions.

Negative Stark slope bifilar helix focuser

The equation of the potential outside the helix is obtained from equation (2.50); by multiplying the first term by a factor of $\frac{I_1(\pi)}{K_1(\pi)}$ and the second term by a factor of $\frac{I_1(3\pi)}{K_1(3\pi)}$. The reason for that is, because the constants 0.13 and 10^{-4} in equation (2.50) are absorbed in a Bessel function, i.e. 0.13 is in fact $= \frac{\text{constant}}{I_1(\pi)}$, and 10^{-4} is equal to $\frac{\text{constant}}{I_1(3\pi)}$.

Now the equation of the potential of negative Stark slope bifilar

INSIDE THE BIFILAR HELIX FOCUSER

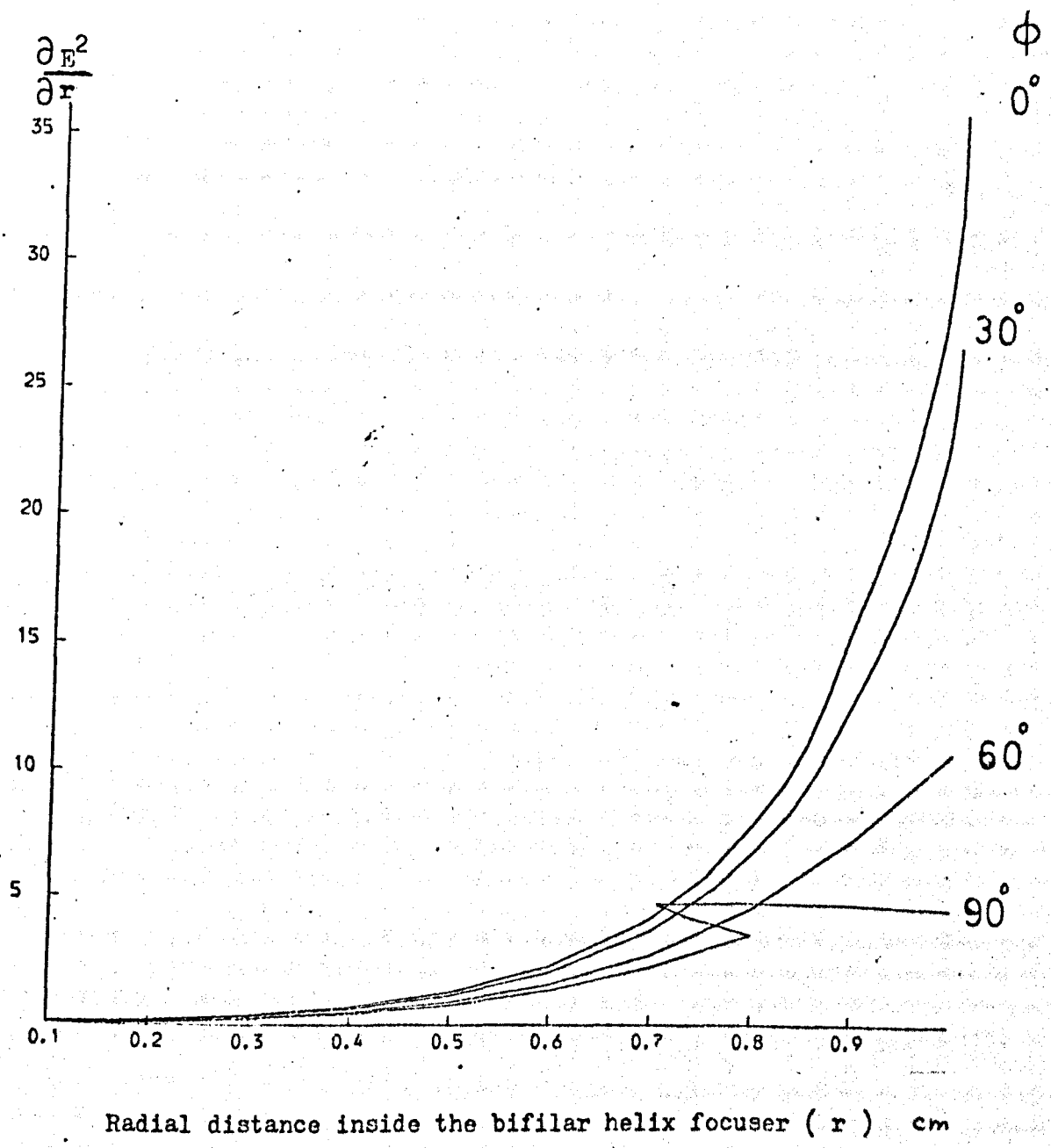

FIGURE (2.14) COMPUTED VALUES OF THE RADIAL GRADIENT OF THE SQUARE OF THE ELECTRIC FIELD $\partial E^2 / \partial r$ INSIDE THE BIFILAR HELIX FOCUSER AT FIXED VALUE OF Z. ϕ REPRESENTS THE ANGLE BETWEEN A VERTICAL AXIS AT THE ORIGIN OF THE COORDINATE SYSTEM CHOSEN, AND THE RADIAL VECTOR.

helix is given by the following expression

$$\phi = 0.13\ U \frac{I_1(\frac{\pi r_1}{d})}{K_1(\frac{\pi r_1}{d})} \cdot K_1(\frac{\pi r}{d}) \sin(\frac{\pi Z}{d}) - \phi)$$

$$+ 10^{-4}\ U \frac{I_3(\frac{3\pi r_1}{d})}{K_3(\frac{3\pi r_1}{d})} K_3(\frac{3\pi r}{d}) \sin(\frac{3\pi Z}{d}) - 3\phi) \qquad (2.53)$$

where r_1 is the radius of the focuser

$K_1(x)$ is the Bessel function of the first kind

$K_3(x)$ is the Bessel function of the third kind

Fig (2.15) shows the computed plot of the magnitude of the electric field outside the focuser as a function of the radial distance. The electric field has a maximum value at the surface of the electrode and when r = 1.4 R, where R is the radius of the bifilar helix focuser E drops to 1/5th of the maximum value.

Fig (2.16) shows the radial gradient of the square of the electric field as a function of the radial distance r. $\frac{\partial E^2}{\partial r}$ has a maximum value at the surface of the electrode. As the radial distance increases $\frac{\partial E^2}{\partial r}$ decreases. When r = 1.2 R, where R is the radius of the focuser, $\frac{\partial E^2}{\partial r}$ drops to 1/3rd of its maximum value.

It will be expected that the bifilar helix focuser of a small diameter (with or without a beam stop) may also be used successfully for focusing lower energy state molecules ($\mu_{eff} > 0$) in a similar way to the ring focuser.

The external electric field of the bifilar helix focuser has both longitudinal and transverse components and will therefore state select molecules with either a transverse or longitudinal orientation of dipole moment which should lead to efficient sorting, just as in the case where the internal field is employed. By the use of the external field of the bifilar helix focuser a ring of upper state ammonia molecules will be produced in a similar way to that demonstrated

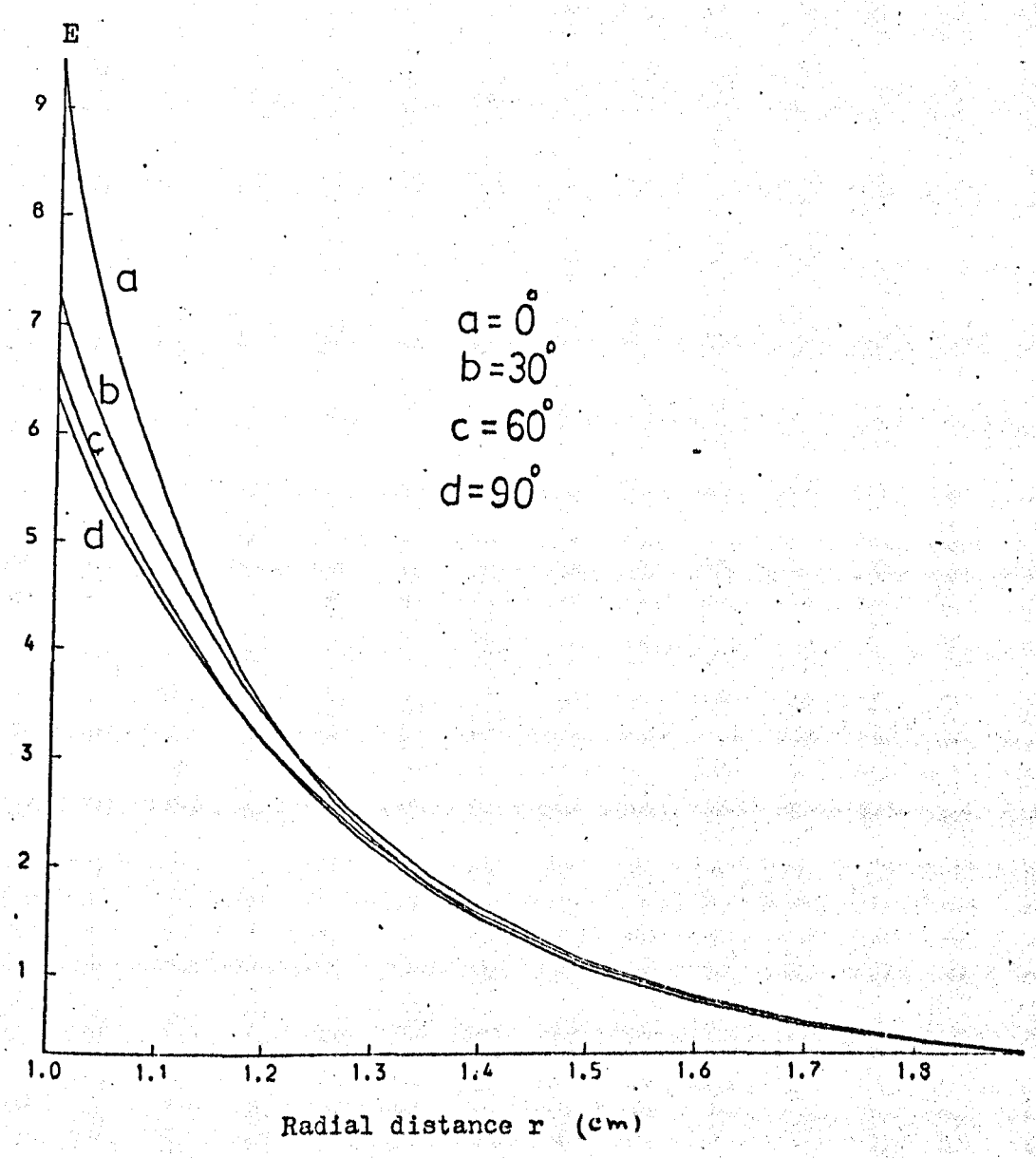

FIGURE (2.15) COMPUTED RESULTS THAT SHOW THE MAGNITUDE OF THE ELECTRIC FIELD OUTSIDE THE BIFILAR HELIX AS A FUNCTION OF THE RADIAL DISTANCE r. ϕ REPRESENTS THE ANGLE BETWEEN A VERTICAL AXIS AT THE ORIGIN OF THE COORDINATE SYSTEM CHOSEN, AND THE RADIAL VECTOR.

OUTSIDE THE BIFILAR HELIX FOCUSER

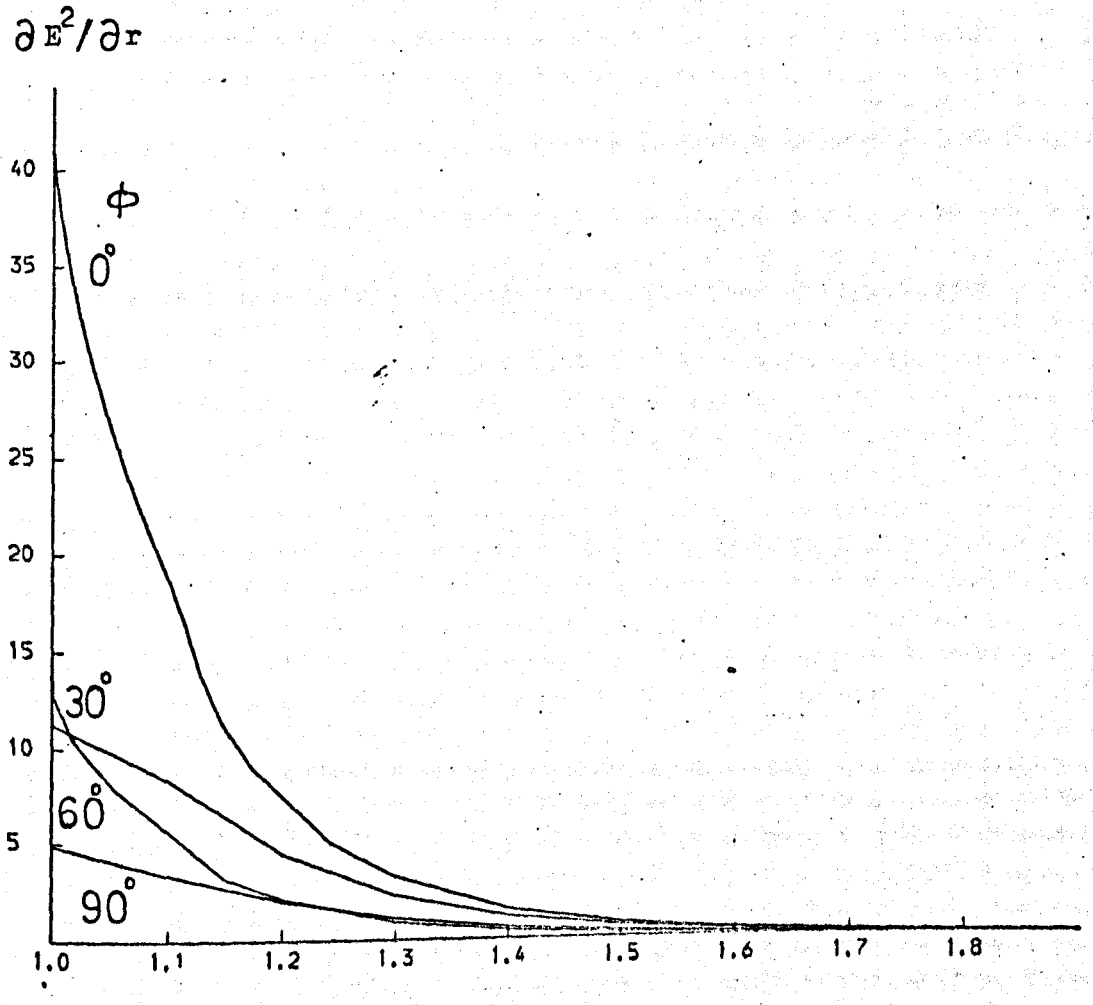

FIGURE (2.16) COMPUTED VALUES OF THE RADIAL GRADIENT OF THE SQUARE OF THE ELECTRIC FIELD $\partial E^2/\partial r$ OUTSIDE THE BIFILAR HELIX FOCUSER AT FIXED VALUE OF Z. Φ REPRESENTS THE ANGLE BETWEEN A VERTICAL AXIS AT THE ORIGIN OF THE COORDINATE SYSTEM CHOSEN, AND THE RADIAL VECTOR.

with the ring focuser (Al-Amiedy and Laine, 1978). Thus by the use of a spectrometer cavity as a beam detector and moving it transversely across the beam axis, it is expected that when the molecular beam is of greater diameter than the focuser, there will be an absorption signal on axis, flanked on both sides by an emission signal, when a beam stop is used.

It is concluded from the calculation of the efficiency of various schemes discussed in this section that the bifilar helix focuser has a better efficiency for focusing molecules by its external field than other types of focuser.

CHAPTER 3

EXPERIMENTAL APPARATUS

3.1 Introduction

The ammonia beam maser consists of four basic components: a) a gas source (effuser or nozzle), b) a focuser (state selector), and c) a microwave cavity, housed in d) a vacuum chamber which is continuously pumped to below a pressure of about 2×10^{-6} torr in order to allow a mean free path of the order of the dimensions of the apparatus. Ammonia gas emerges from the nozzle either through a variable diameter diaphragm or a fixed diameter conical skimmer set in the dividing wall of the source and main chamber. The main chamber contains one, or on occasions two, of the state selectors and a single cavity, arranged so that the molecular beam passes through each in succession. Part of the ammonia gas is captured by the state selector which focuses and defocuses the upper and lower energy state molecules respectively. The focused beam then passes into a high Q microwave cavity (cylindrical type, E_{010} mode). The resonant cavity is used to concentrate the radiation field coming from the sideband of a K-band klystron along the trajectory of the ammonia molecules. A stimulating microwave signal within the maser emission linewidth leads to amplification when cavity wall and the coupling losses are small.

3.2 Maser vacuum system

3.2.1 General

The vacuum system consists of three chambers as shown in fig (3.1). The first chamber is made of brass, 24.5 cm long and contains the ammonia source (single or multiple hole nozzle). This chamber is pumped by an oil diffusion pump Edwards type 403A backed by a Metrovac type GDR1 two-stage rotary pump. Without cryopumping, the pumping speed of the oil diffusion pump is 0.3 $m^3\ s^{-1}$. The first part of the second chamber is made of an aluminium-bronze casting 45.7 cm long. It contains the

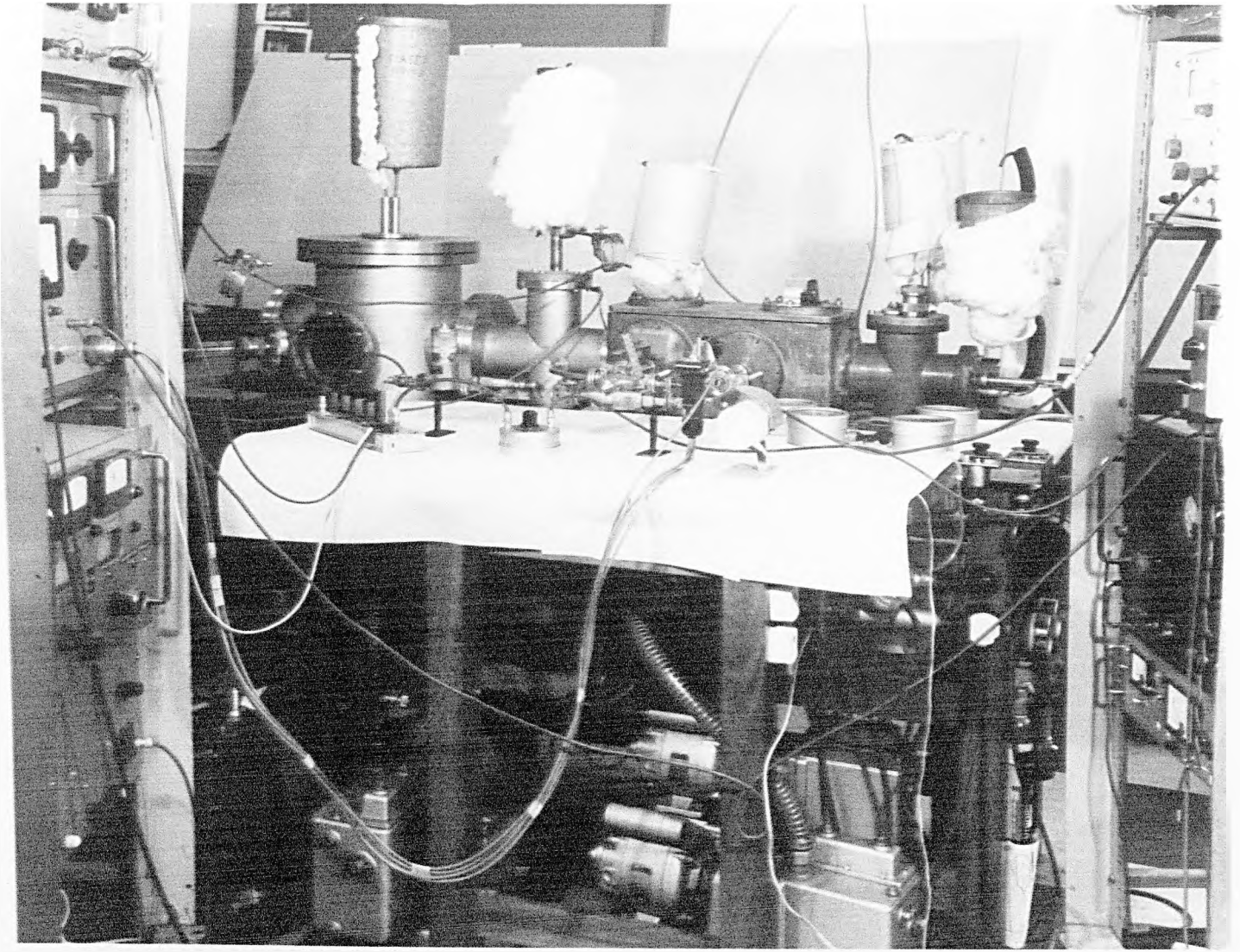

FIGURE (3.1) GENERAL VIEW OF THE MASER SYSTEM

focusing system and a single cavity, and is pumped by two 7.62 cm Metrovac type A033G oil diffusion pumps backed by a Metrovac type GDR1 two-stage rotary pump. The second part of this chamber is made from a stainless steel chamber 93.2 cm long containing a second state selector for the use of the second beam (beam 2), and pumped by 0.35 $m^3\ s^{-1}$, NGN type CP350 oil diffusion pump backed by a Metrovac type GDR1 two-stage rotary pump. The third chamber is also made of stainless steel and is pumped by a 0.6 $m^3\ s^{-1}$ oil diffusion pump Edwards type 603, backed by an Edwards type ED660 two-stage rotary pump. A skimmer is set in the dividing wall between the second and third chambers. The third chamber is used as a nozzle chamber for the second beam head-on to the first.

During the operation of the ammonia maser the pressure in the three consecutive chambers are typically of the order 10^{-6}, 10^{-7}, 10^{-6} torr respectively.

3.2.2 The first nozzle chamber

This is shown in fig (3.1) and is made of rolled brass tubes of 10.16 cm and 7.62 cm internal diameter. It is fitted with two flanges: one carries a liquid nitrogen trap, the other carries the supply line of ammonia gas to the nozzle and also a liquid nitrogen trap. This latter trap surrounds the nozzle gas supply and is used to cool the nozzle, as well as cryopumping the ammonia gas, thus increasing the overall pumping speed. The pressures with and without the use of the liquid nitrogen traps are 4×10^{-7} torr and 2×10^{-6} torr respectively. The dividing wall between the first and the second chamber contains the skimmer with its apex on the nozzle side and a variable iris diaphragm on the other. The diameter of the diaphragm could be controlled from outside the vacuum chamber by using an Edwards rotary drive lead-through which is coupled to a screw driven carriage inside the chamber by a flexible nylon tube. Rotating the external control results in a translational motion of the carriage which is used to effect a change in the diameter

of the aperture of the diaphragm iris.

3.2.3 Main chamber

The first part of the main chamber is an aluminium-bronze casting approximately 45.7 cm x 20.3 cm x 21 cm, fig (3.2), which has been sealed with Araldite on the outside surface, and with a silicone varnish on the inside, and cured at 200°C, to avoid leak problems through pores in the casting. It is fitted with a brass lid carrying a liquid nitrogen trap, and with two brass flanges, each of which carries a single K-band waveguide which simultaneously couples to and supports the waveguide cavity. One panel of the first part of the main chamber is machined flat to carry electrical lead throughs.(EHT, heater coil), and mechanical lead-throughs (ionization gauge head, pirani gauge head, rotary drive lead through). All connections are sealed with rubber "o" rings. This part of the main chamber contains (i) the state selectors which are mounted in a brass holder, (ii) the microwave cavity which is electrically earthed to the vaccum box and, is connected via one K-band waveguide, which contains an impedance matching stub. Upon adjustment of the stub tuner it is possible to find the optimum cavity coupling. This piece of waveguide is connected flange to flange to other pieces via a plastic coupler in order to minimize the thermal conduction between the cavity and the chamber walls. A mica disc mounted between the flanges and the "o" rings of the waveguide coupling, provides a vacuum seal. The waveguide is mounted in a tube and this assembly passes through an "o" ring seal in the wall of the chamber, which allows rotation and translation motion of the cavity in order to make possible the alignment of the cavity with the nozzle and the state selector. A long brass tube for the waveguide as shown in fig (3.3), allows horizontal movement of the cavity for the purpose of the experiment explained in chapter 4 section 1.

The second part of this chamber is made of two stainless steel tubes of 10.16 cm internal diameter fixed at right angles to one another

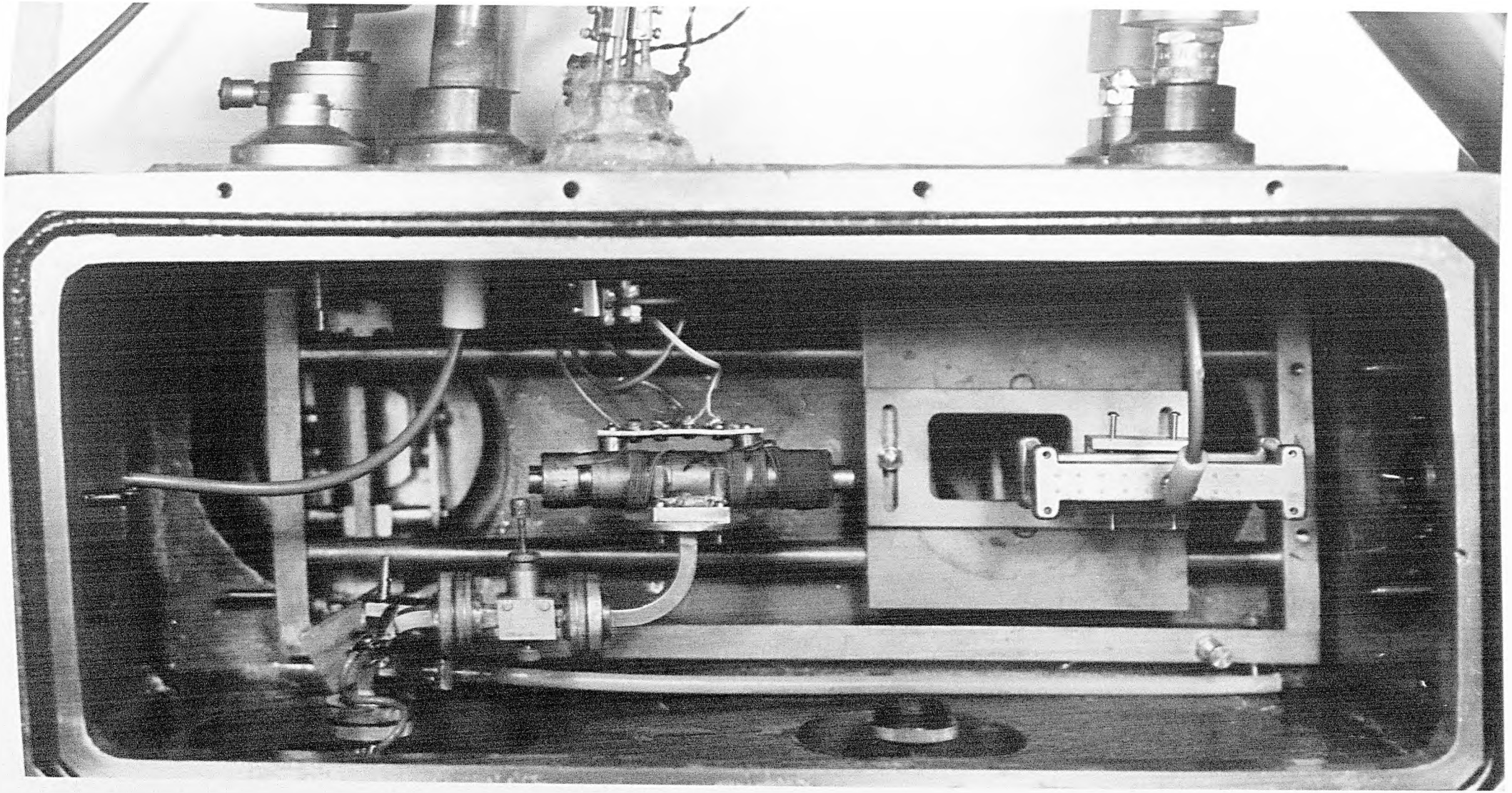

FIGURE (3.2) THE MAIN VACUUM CHAMBER

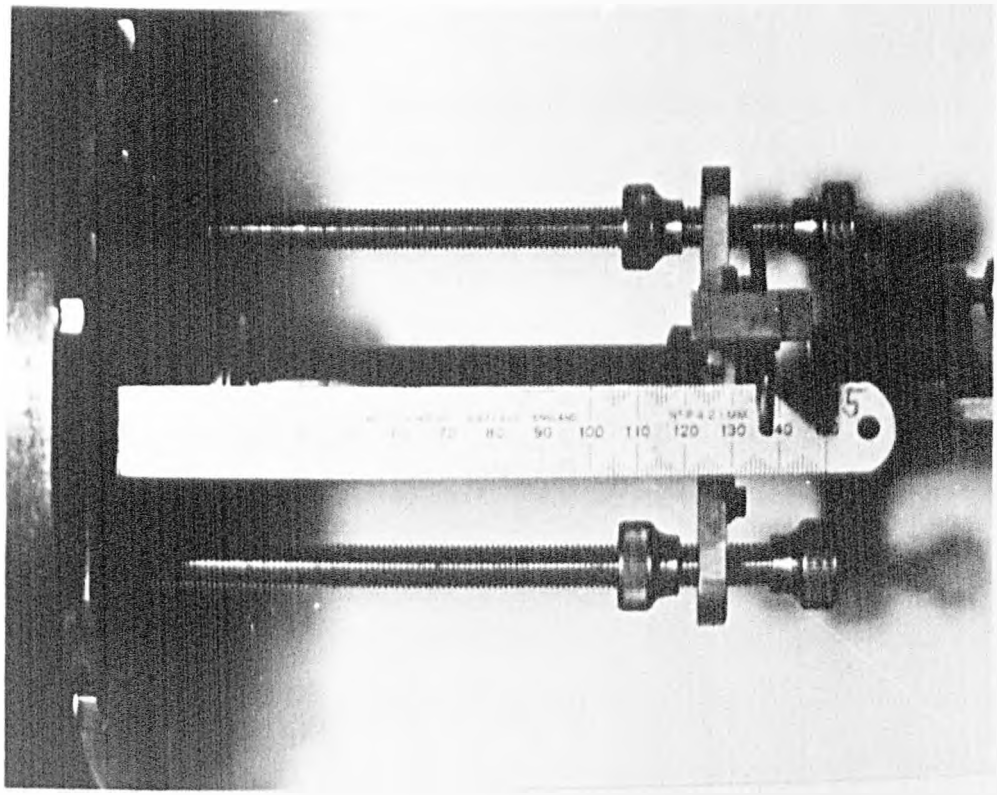

FIGURE (3.3) THE LONG BRASS WAVEGUIDE

FOR THE TRANSVERSE MOVEMENT OF THE CAVITY

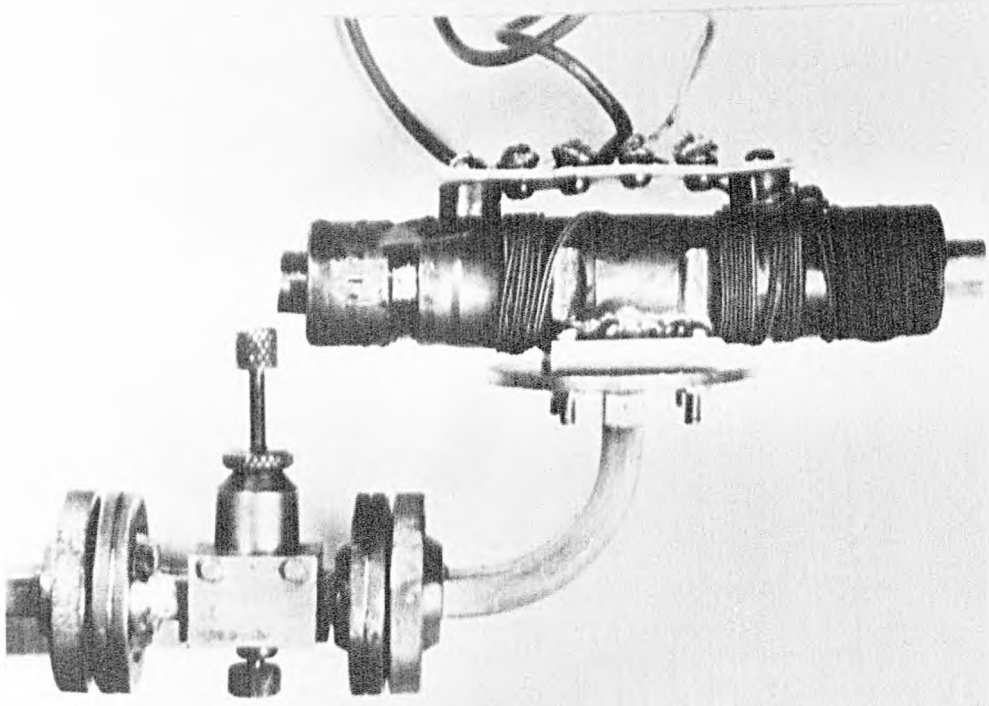

FIGURE (3.4) THE MICROWAVE CAVITY

(see fig (3.1)). It is fitted with a stainless steel flange which carries a liquid nitrogen trap. An extension to this part of the main chamber was made of stainless steel tube of 10.16 cm internal diameter 18 cm long situated inside the third chamber making the length of the main chamber 93.5 cm. The reason for this construction is to ensure that the position of the skimmer within the third chamber (i.e. second nozzle chamber) is an optimum one to gain the maximum possible pumping speed of the ammonia molecules scattered from the skimmer. It contains the second state selector which is held at one end by the stainless steel dividing wall between the second and the third chambers and the other end by a three-armed metal "spider" which fits inside the chamber. The dividing wall contains a brass skimmer holder mounted such that it faces the second nozzle and is mounted with an "o" ring to the stainless steel wall.

3.2.4 The third chamber

This chamber consists of 31.75 cm high 38.10 cm internal diameter (i.d.) rolled stainless steel cylinder, fig (3.5). It is fitted with 7 stainless steel flange windows, 2 of 10.16 cm i.d., 3 with 6.35 cm i.d., 2 of 16.51 cm i.d. The base holds a stainless steel disc, 38.10 cm outer diameter (o.d.), 22.86 cm i.d., supporting a 15.24 cm oil diffusion pump. The top flange holds a 38.10 cm o.d., stainless steel lid 2.54 cm thick through which the liquid nitrogen trap is mounted. All nine openings are sealed by rubber "o" rings and stainless steel flanges.

The ammonia gas supply passes through a 1.59 cm o.d. seamless stainless steel tube of wall thickness 10 SWG holding a multiple hole nozzle. This tube material is found to be preferable to copper which bends rather easily and causes misalignment problems which reduces the maser signal intensity.

3.2.5 Ammonia gas source and supply line

The ammonia gas source is a lecture size cylinder of anhydrous

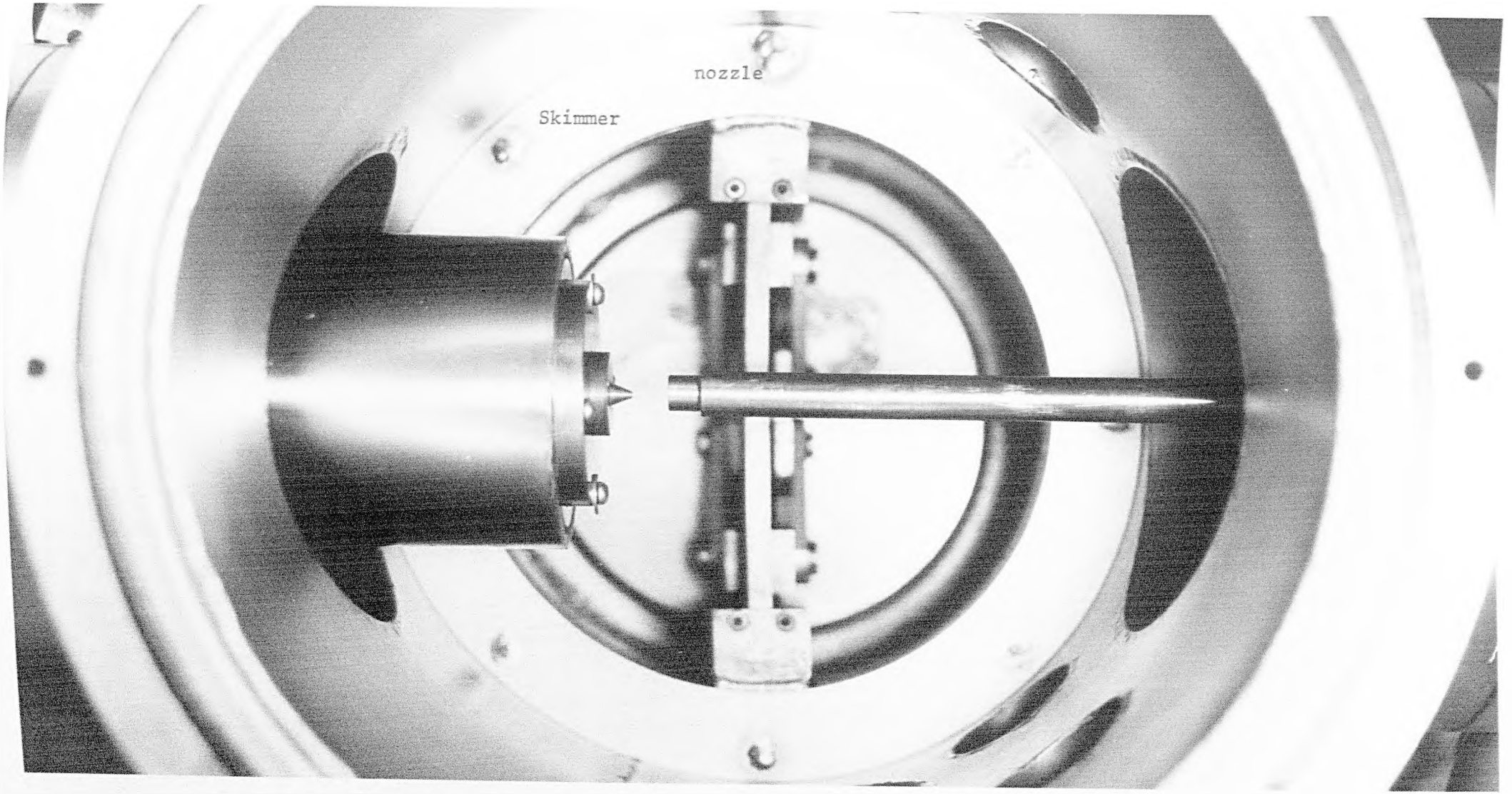

FIGURE (3.5) THE THIRD VACUUM CHAMBER

liquid ammonia. A pressure reducing valve is used to control the ammonia gas flow; it is adjusted for about 2 atmospheres output pressure (see fig (3.1). Purification of the ammonia is achieved by freezing it in a trap cooled with liquid nitrogen. During the period that the ammonia is frozen, the trap is evacuated by a rotary pump to remove gaseous impurities. Water vapour is frozen out by maintaining the trap below 0°C during the gas transfer. The ammonia gas is then stored in a 15.5 litre pressure cylinder. A hand valve and a fine needle valve (Edwards model LB2B) are used to control the gas flow from the reservoir to the gas nozzle. The needle valves are connected to the first and second nozzle flanges by 0.635 cm diameter thick walled flexible P.V.C. tubes. Two Bourdon gauges (Edwards, model CC3), with overlapping ranges 0-760 torr and 0-100 torr are used in parallel to monitor the ammonia gas pressure behind each of the nozzles. This arrangement permits greater accuracy of measurement over the full pressure range used than if the 0-760 torr Bourdon gauge alone were to be used.

3.3 Nozzle and Skimmer

3.3.1 Nozzle

To produce molecular beams a wide range of techniques have been used in recent years. These methods have been discussed in a number of general reviews (H. Pauly and J. P. Toennies, 1965; N. F. Ramsey, 1956) as well as some more specialised reports (J. B. Fenn and J. Deckers, 1963; J. B. Anderson *et al.*, 1965, 1966; J.B. Anderson, 1968).

The major requirements of the vacuum technique (Fluendy and Laweley, 1973) in any molecular beam experiment are:

1) very long mean free path provided in comparison with the length of the molecular beam, thus avoiding significant attenuation and broadening of the beam.

2) to minimize background density in the beam detector chamber.

The use of supersonic jet source was proposed by Kantrowitz and Grey 1951, and successfully operated in practice by Becker and Bier (1954).

The extremely small size and high pressure ratio behind the nozzle source provide convenient facilities to investigate a number of rate processes including rotational, vibrational and even translational relaxation, nucleation and condensation, and probably some chemical reactions (Anderson, 1966). On the other hand, condensation problems may be introduced by using high source pressures. Moreover, small size nozzles means the ratio of mean free path to Mach number in the jet has a small value.

In order to produce the supersonic jet, a nearly static gas in a stagnation chamber must be allowed to pass through a small orifice having a diameter of several tenths of a millimeter, then undergo a free expansion into a vacuum. The shape of the orifice can take the form of a converging - diverging nozzle (laval nozzle), a converging nozzle, or just a circular hole drilled in a thin flat plate.

The molecules emerging from the nozzle source to form a molecular beam are more uniform in velocity and have in general higher average velocity for the same gas source temperature compared with an effusive source.

An appropriately designed supersonic nozzle beam (Dymanus, 1976) is capable of yielding a very high intensity molecular beam of the order of two or three times higher in magnitude than a simple orifice which has the same geometry (or the same orifice area).

Decreasing the nozzle diameter will yield an increase in the intensity of the molecular beam (Bier and Schmidt, 1961), and the resulting molecular density from the nozzle flow is inversely proportional to the square of the distance from the nozzle exit (Parker et al., 1960).

The nozzle employed in the present maser system is made from brass 0.64 mm thickness with a hole of 0.1 mm diameter. The maser is operated at threshold oscillation with a voltage of 8.8 kV on the ring focuser, and an ammonia pressure of 28 torr behind the nozzle, as discussed in section (4.3).

Stronger beams can be obtained with multiple hole effuser (Dymanus, 1976) producing either a number of parallel beams (De Lucia and Gordy, 1969; Laine and Smart, 1971); or a number of radially oriented beams intersecting in the central part of the resonant region (Marcuse, 1962).

Experiments carried out with an NH_3 beam have shown that a multiple hole nozzle may be used as a beam source, the diameter of the holes (0.09 mm) being appreciably greater than the mean free path of molecules. The beam from the multiple hole nozzle source is sufficiently intense for maintaining self oscillation of the maser.

In this thesis, a multiple hole nozzle is discussed, which has been used for the first time in conjunction with the molecular beam maser and enhanced absorption spectrometer. Section (4.3) gives details of a number of multiple hole nozzles which have been used in the work described in this thesis. Fig (3.5) shows the nozzle-skimmer assembly in situ.

3.3.2 Skimmer

A skimmer is a device used to form the molecular beam by removing the outer portion of the freely expanding jet. The location of the skimmer is on the centreline of the jet, downstream from the nozzle. It is appropriate to establish that the first defining element in a nozzle beam system is the skimmer and that it plays a role analogous to the effusive slit in the oven of a conventional beam apparatus (Anderson et al., 1966).

In general the skimmer takes the form of a hollow, truncated,

circular cone. High-quality skimmers may be fabricated in a variety of shapes by a method which involve both electroforming and machining operations (Gentry and Glese, 1975).

By choosing a suitable distance between the nozzle and the skimmer it might be expected to be possible to produce a molecular beam of any desired Mach number (Fluendy and Laweley, 1973). The mean free path of the molecular beam at the skimmer is several times bigger than the skimmer aperture, and, the relation between the shape of the nozzle and the skimmer is relatively unimportant (Bier and Hagena, 1963).

The thought that the catastrophic events leading to degradation of the nozzle beam occur inside the skimmer just downstream of the aperture, has first been mentioned by Zapata et al. (1961), and under a near continuum condition studied by Bier and Hagena (1963). McMichael and French (1966, 1967) later investigated the problem in the low density range by means of electron beam visualization and densiometry.

Bossel (1969) proposed the use of the "shock beam" which models the events inside the cone of the skimmer by means of normal shock transition from the isentropic to the corresponding subsonic state.

Bier and Hagena (1966) prepared a recommendation for the optimum skimmer design, that is by the use of a skimmer of large internal divergence (internal angle), but little external acuteness (external angle). On the other hand Bossel's (1968) investigation showed that skimmers should be designed for minimum interference with the external hypersonic flow field.

The skimmer geometric parameters are: the skimmer diameter, lip radius, and skimmer length as well as the internal and external cone angle.

1) Skimmer lip geometry

The information about the influence of the lip geometry on the skimming process was rather sparse. By increasing the lip width the

beam generation process deteriorates (Zapata et al., 1961), but their beam was initially of poor quality.

The supersonic beam can be produced skimming with a flat washer (Moran, 1970), but the beams that were used also lack the near-isentropic quality. As far as the beam generation process of a near isentropic nozzle beam is concerned, it is still necessary to use sharp edge skimmers.

2) External skimmer angle

The aerodynamic performance of the skimmer depends to a great extent on the angle of the conical region adjacent to the aperture (Bossel, 1971). In the vicinity of the skimmer opening, the conditions are more complicated by the presence of the molecules reflected from the chamber end wall.

Experiments done by Bier and Hagena (1966), Campargue (1969) and Bossel (1968, 1969) show that increases of the external skimmer angle are associated with losses of beam intensity.

And finally a conclusion could be drawn for all the attainment of near isentropic beams of maximum intensity that the external half angle of skimmers should be made as small as the internal divergence and within the fabrication technique limit.

3) Skimmer length

Near the skimmer mouth, the conditions may be affected by particles diffusely reflecting from the chamber end wall, beside the effect of the molecules reflecting from the dull lip or a stubby cone. This phenomenon was first uncovered by Bossel (1968, 1969), and experimentally was confirmed by Campargue (1969).

The skimmer length must exceed the stand-off distance, in order to enhance a near-isentropic beam of maximum intensity, where the stand-off distance is the distance between the end wall chamber and end wall reflected shock.

To maintain well defined aerodynamic conditions at the skimmer, it is necessary to use an excellent collimation of the intense beam. At the skimmer tip, the need for minimizing aerodynamic interference appears to become more necessary with decreasing ambient pressure inside the nozzle exhaust chamber.

4) Internal skimmer angles

It is profitable for designing the internal skimmer geometry to determine the internal angle of the skimmer which contains the fraction of the total molecular beam flow into the beam chamber. The remaining molecules must be pumped away because it is necessary to leave the conical boundary of the ficticious system, otherwise the molecules suffer a collision with the interior skimmer wall. In some experiments done by Bier and Hagena (1966), Campargue (1969), it was found that the large internal clearance necessary to optimize the beam intensity, reflect the amount of the external skimmer interference.

5) Skimmer diameter

For efficient generation of collimated nozzle beams, the skimmer diameter must be matched to the pumping capacity of the molecular beam system. Intermolecular collision between the beam and background gas or between beam molecules may alter the quality of the beam emerging from the region of severe scattering (Valleau and Deckers, 1964; 1965).

If the dimension of the skimmer mouth is much larger than the nozzle orifice, then effects of flow divergence Hagena (1967) must be considered in the prediction of the beam intensity as well as in the design of the angular skimmer geometry.

It is recommended for utilization of nozzle beams for flow-diagnostic purposes to use smaller skimmers to ensure a near ideal performance under a wide range of operational conditions.

The skimmer used in the work described in this thesis, shown in fig (3.5) has the following parameters: inner cone angle 35^{o}, outer

cone angle 45°, skimmer diameter 1.6 mm, and used for skimming the ammonia molecules emerging from the second nozzle (beam 2) into the main chamber (second chamber).

3.4 The Focuser or State Selector

The state selector is a device used to capture and focus molecules (ammonia molecules in the present work) in certain quantum states and to defocus them in other states. It is sited between the source, after the diaphragm (or the skimmer), and the maser cavity.

Several different types of focuser are used in this work either singly, or in various combinations of two at a time. Individual types may take the form of ring, octopole rod, or a single wire helix, for upper energy state ammonia molecules, and single straight wire, or crossed wire for lower energy state ammonia molecules. Combinations of two focusers in series for lower and upper energy state, lower-lower, or upper-upper are also possible.

3.4.1 Negative Stark slope focusers

Space focusing of molecules whose stark energy decrease in an applied electric field is more difficult than for those that increase in energy, but can be achieved by using any of the following focusing schemes: ring, single wire helix, single straight wire, crossed-wire, and alternate-gradient. Of these it is shown experimentally that the ring focuser can have good focusing properties in practice, when used in a particular way. Hitherto, the ring focuser has only used for focusing and state selection of molecules whose stark energy increases in an applied electric field.

3.4.1.1 Negative Stark slope ring focuser

In this thesis, a ring focuser is discussed which has hitherto not been recognised to be capable of state selection of molecules with $\mu_{eff} > 0$.

This type of focuser can be used to focus lower and defocus upper

energy state ammonia molecules respectively (Al-Amiedy and Laine, 1978). Such a system is shown in fig (3. 6).

Generally the ring focuser has been investigated in considerable detail both experimentally and theoretically, in particular in the context of molecular beam masers (Oraevskii, 1964; Shcheglov, 1961). The molecular beam in this type of focuser passes through a succession of annular electrodes, equally spaced along the focuser axis. A potential of $\sim$ 30 kV is maintained between adjacent rings.

Inside the focuser, as explained in (5.2), the magnitude of the electric field up to the diameter of the rings increases radially outwards from the molecular beam axis, thus providing the necessary field gradient for state selection of molecules with $\mu_{eff} < 0$.

Outside the rings, however, the magnitude of the electric field decreases radially outward, and provides a radial field gradient suitable for state selection of molecules for which $\mu_{eff} > 0$. It is this external field that is used in this type of state selector.

In practice, it is found convenient to use rings formed from spring ends of stainless steel domestic safety pins. The focuser for molecules with $\mu_{eff} > 0$ was fabricated from such pins by clipping off their ends. Such rings have a smooth profile which leads to a decrease of the possibility of electrical breakdown. The alignment of the device was done by using a metal rod passed through one set of rings, and the ends of the rings placed in holes drilled to receive them in a brass strip. After alignment, the ring pins were soldered into position. The two brass strips with their assembled rings were separated by four insulated sintox tubes which were araldited in position into holes drilled into the brass strip. The lower set of rings were fastened to a brass sliding carriage which was electrically connected to earth. The upper set of rings was connected to the EHT power supply. A detail theoretical analysis of the ring focuser has been given in (5.2).

The focuser used in the present work has the constructional parameters listed in table (3.2). The upper 11 rings are connected to the EHT supply and the lower 11 rings interleave. The ratio of the outside ring diameter to ring separation was unity. Voltages in excess of 30 kV could be applied between the two sets of rings without electrical breakdown, thus providing an electric field in excess of 200 kV cm^{-1}.

3.4.1.2 Single straight wire focuser

This device focuses and defocuses lower and upper energy inversion state ammonia molecules respectively, thus enhancing microwave absorption. The use of the single straight wire was first operated with an ammonia molecular beam by Helmer et al. (1960).

In the present work, three different focusers of the same type were constructed, each of length 80 mm. The focuser electrodes were made of nickel wire 0.57 mm, 0.50 mm and 0.28 mm diameter in the three cases. The wire electrode was suspended axially by two thin nickel rods soldered to two supporting rods mounted at their ends into insulating rings of PTFE. Each PTFE ring was made with an aperture of 19 mm diameter to allow the molecular beam free passage. The focuser is illustrated in fig (3. 7).

Voltages in excess of 30 kV could be applied to the focuser without electrical breakdown, producing a field of 200 kV cm^{-1}. The single straight wire focuser provides a transverse radial electric field with respect to the molecular beam axis.

The gas source used in conjunction with the single straight wire focuser, was a four hole nozzle arranged on a circle to give a rough approximation of annular beam coaxial with the single straight wire electrode.

Such an annular beam produced a larger enhanced microwave absorption signal than with a single hole nozzle on account of the large degree of scattering by the wire electrode in the latter case.

The possibility existed that the single straight wire supporting system might itself possess significant focusing properties. Thus a check was made to establish whether or not this was the case.

When the axially active wire was removed, and the transverse wire and supporting rods connected to the EHT power supply no focusing action was found. A further check was carried out by removing the transverse wire in addition to the active wire leaving the supporting rods alone. Again no focusing of any kind was observed. From these results it was concluded that any residual focusing effects of the axial wire support structure may be disregarded.

3.4.1.3 Crossed-wire focuser

This focuser was first used by Laine and Sweeting (1971). The lower energy state molecules which decrease in energy in an applied electric field were focused by using the crossed-wire focuser, and conversely upper energy state molecules were defocused. By operating the focuser with an ammonia molecular beam in conjunction with a molecular beam spectrometer of conventional design, a strong absorption signal was observed.

The advantage of the crossed-wire focuser is the existence of an intense inhomogenous electric field surrounding the thin electrode wire. The focuser posses a good overall transparency to the ammonia molecular beam. This transparency clearly depends upon the wire diameter and the thinner the wire, the better the transparency.

The efficiency of the crossed-wire focuser depends on three principal parameters: a) effective length of the focuser, b) the smaller the diameter of the wire electrode the less the scattering of ammonia molecules which leads to greater focuser efficiency, c) the angle between the two planes of the adjacent electrodes, which is equal to 90^{o}.

The construction of the focuser was from a linear array of wires, such that the adjacent wires lay in mutually perpendicular planes. The

ammonia molecular beam passed along the axis of the focuser formed by the intersection of the two wire planes. Opposite polarity charges were carried by adjacent wire electrodes. A convenient electric field configuration was obtained when the ratio of the wire diameter to the wire separation was approximately 25:1 (Laine and Sweeting, 1971). The crossed-wire focuser has a longitudinal electric field on its axis. Voltage in excess of 30 kV can be applied to the focuser without electrical breakdown, thus providing a strong electric field of 200 kV cm^{-1} along the focuser axis.

Two focusers have been used in the present work, with the parameters given in table (3.1). The focuser has the constructional feature that the crossed-wire electrodes were supported between four equispaced brass rods 4.5 mm in diameter. The supporting rods were fitted into two PTFE insulating ring 1.2 cm thick with a 1.1 cm diameter which allowed the passage of the molecular beam. Fig (3. 8) shows the crossed-wire focuser with the parameters given in table (3.1).

The supporting rods form an enlarged quadrupole type of focuser for upper energy state molecules. Experiments were done to make sure whether or not this supporting rod system possessed significant focusing properties.

The crossed-wire electrodes were removed from the supports, and the system was connected to the EHT supply, such that adjacent electrodes carried opposite charge. No signal of any kind, emissive or absorptive was detected from the spectrometer cavity, except at the highest pressures behind the multiple hole nozzle when beam absorption was observed, but this signal was independent of focuser potentials. Thus it was concluded that the influence of the supporting rods on the operation of the crossed-wire state selector could be safely disregarded.

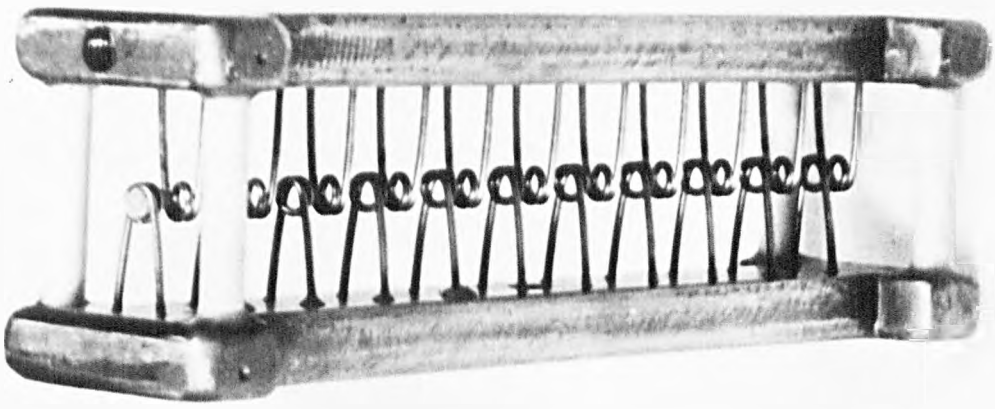

FIGURE (3.6) THE NEGATIVE STARK SLOPE RING FOCUSER

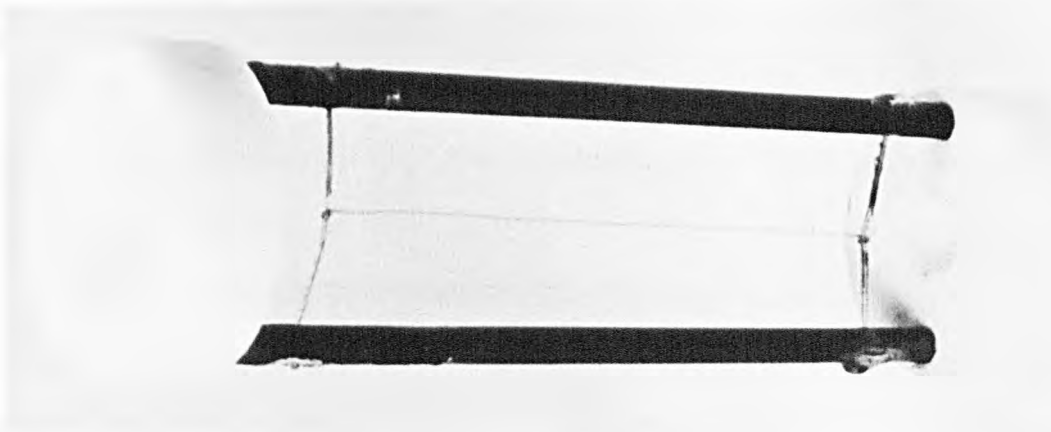

FIGURE (3.7) THE SINGLE STRAIGHT WIRE FOCUSER

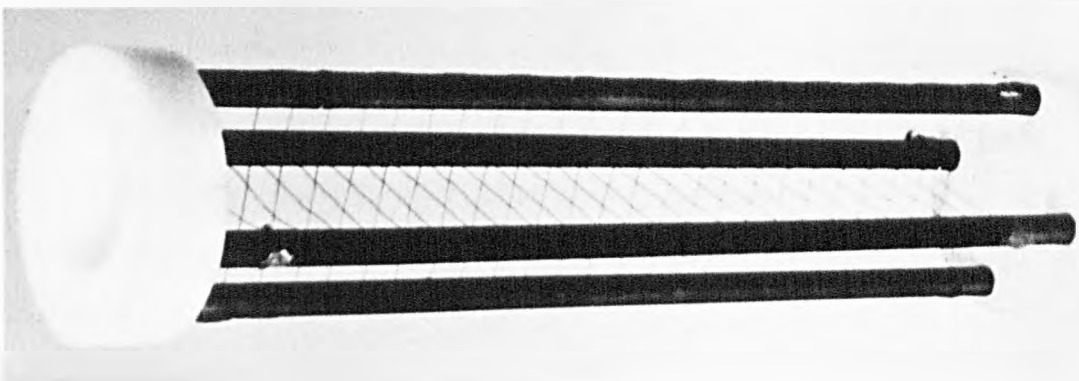

FIGURE (3.8) THE CROSSED-WIRE FOCUSER

TABLE (3.1)

	a (long focuser)	b (short focuser)
wire electrode diameter (mm)	0.13	0.13
adjacent electrode separation (mm)	2.51	2.51
wire diameter to wire separation ratio	25:1	25:1
number of wires (or electrodes)	50	34
number of pairs of focusing elements (or crossed-wire electrode)	25	17
effective focuser length (mm)	125	95

3.4.2 Positive Stark slope focusers

Space focusing of molecules whose Stark energy increase in an applied electric field is well known and may be achieved by the use of non-uniform fields. For many years, these systems have been studied in detail both theoretically and experimentally, and have been applied extensively to molecular beam work.

The main types of electrode configuration for molecules that increase in energy in an applied electric field may be divided into three groups, based on the direction of the electric field with respect to the beam axis: (i) schemes where the electric field is essentially perpendicular to the beam axis, e.g. multipole rod focusers which employ four or more rod electrodes arranged on a circle with axial symmetry with respect to the focuser axis. A modification of this type of focuser for flat beams has resulted in a double parallel ladder type of focuser with electrodes placed parallel to the beam axis, (ii) systems where the electric field is approximately parallel to the beam axis, e.g. ring, multipole helical electrode (bifilar helix, quadrupole helix, .. etc.). A modification of the ring focuser for flat beams is the double parallel ladder focuser where the electrodes are perpendicular to the beam axis. (iii) schemes which have features of both categories (i) and (ii) where the electric field is more complicated, and possesses transverse and parallel components to the beam axis. An example of a focuser of this

type is the single wire helix.

The following types of focusing systems are used in the work described in this section of the thesis; octopole rod, ring and single wire helix. Each of these three electrode systems represent examples of the categories (i), (ii) and (iii) respectively.

3.4.2.1 Single wire helix focuser

A single wire helix focuser, which utilizes a completely new electrode configuration, has been discovered and developed. Results indicate that it has experimental characteristics similar to multipole helical electrode systems used to state select and focus molecules.

The helix illustrated in fig (3. 9), was constructed from a piece of 0.58 mm diameter nickel wire wound around a 6.35mm screw rod after which it is extended to the pitch required. The helix was attached at each end to one of the four supporting brass rods 4 mm diameter, the other three supporting rods were earthed to the metal vacuum box. The supporting rods were inserted into two PTFE insulating rings, each with a hole of 4 mm diameter to allow the beam free passage along the device axis.

The wire diameter and helix length were chosen to permit a rigid construction to avoid problems of microphonics. The focusers used in the present work had the constructional parameters detailed in section (5.3). Voltages greater than 30 kV were applied to the focuser without electrical breakdown, thus providing an electric field in excess of 200 kV cm^{-1}. This focuser was used to produce an emission signal leading to oscillation. The precise value of focuser voltage for oscillation threshold depends upon two principal parameters of the helical focuser system: (i) diameter of the wire (ii) pitch of the helix.

In an attempt to increase the electric field, a 10 cm long, 10 cm diameter gauze cylinder was mounted coaxially with the single wire helix, and connected to earth. Although a strong emission signal was observed,

no oscillation could be obtained. This reduced strength of emission was attributed to the reduction in the pumping in the region of the focuser caused by scattering of the defocused portion of the molecular beam.

The supporting brass rods were set on a 55 mm pitch diameter circle by rings of PTFE. These rods formed a four electrode array, and care was taken to ensure that upper or lower energy state molecules were not focused by it. Thus a subsidiary experiment was done to make sure whether or not the supporting rods had significant focusing properties when EHT was applied. To this end the helix was removed from its supporting rod and one rod was connected to the EHT power supply and the other three rods earthed. No detectable signal was observed in the spectrometer cavity under these experimental conditions.

3.4.2.2 Ring focuser

The use of a ring focuser was first proposed by Krupnov (1959) and has been successfully by many investigators.

The ring focuser used in the present investigation is made of domestic stainless steel safety pins with their fastener ends clipped off (Bardo and Lainé, 1971). The section of the ring has a smooth profile which decreases the possibility of any electrical breakdown between adjacent electrodes. Fig (3.10) shows a photograph of the focuser. The ring focusers used for the present work have the constructional parameters given in table (3.2). In the focuser employed there are 22 rings mounted in two rows of which one linear set of 11 rings are on one side connected to the EHT supply, and a further linear set of 11 rings on the other side connected to earth such that the two sets of rings interleave. The two sets of electrodes are separated by four sintox ceramic tubes. The ratio of ring diameter to ring separation is equal to unity. Voltages in excess of 30 kV could be applied to the focuser without electrical breakdown, thus providing an electric

field well in excess of 200 kV cm^{-1}. The focusers with the parameters in table (3.2a and b) are used to produce an emission signal.

TABLE (3.2)

	a Ring focuser	b Ring focuser	c Ring focuser
Internal diameter of focuser ring (mm)	6.25	2.95	1.70
Outer diameter of focuser ring (mm)	8.15	2.57	3.15
Diameter of the wire (mm)	0.91	0.81	0.70
The ring thickness at the widest part of the spiral (mm)	1.98	1.70	1.50
The effective length of the focuser (mm)	82	80	77
Number of rings connected to the EHT supply	11	11	11
Number of rings connected to earth	11	11	11
Total number of rings	22	22	22

3.4.2.3 The eight pole rod focuser

The focuser has been discussed by many authors Helmer (1957), Shimoda (1957), Vonbun (1958), Hirono (1959), and Van Mierlo (1974). The theory of the eight pole focuser has already been given in section (2.3.3).

In the research group in which this thesis work was carried out, this type of focuser was operated by Smith (1966), and Sweeting (1971), in conjunction with a molecular beam maser.

The beam intensities provided by using multipole fields can be more than two orders of magnitude greater than those obtained by using ordinary deflecting type fields (English and Zorn, 1974). The increase in the beam intensity is due to the focusing action of the multipole electric field, a characteristic which an ordinary deflecting-type field does not possess. The other characteristic of the multipole field is that it has axial symmetry.

The eight pole rod focuser selects ammonia molecules in the upper energy state of the J = 3, K = 3 transition and focuses them into the

cylindrical cavity. It defocuses the lower inversion state molecules, and deflects them away from the molecular beam axis. The lower energy state molecules can be detected by moving the spectrometer cavity perpendicularly across the beam axis.

The focusing electrodes provide an electric field which is zero along the beam axis and whose magnitude increases in the radial direction.

The focuser used in the present work (illustrated in fig (3.11)) comprised a cylindrical cage of 8 rods of 16 SWG bright nickel plated silver steel 28 cm long. The inside diameter of the cage was 1.2 cm. Alternate electrodes were connected to a silver plated brass ring at the outside ends of the focuser and taken to earth. The remaining electrodes were connected by the inside rings of the focuser and connected to an EHT power supply. The inside and outside rings were insulated from one another with PTFE rods each 2.5 cm long. The length of the focuser was large compared with its diameter.

The focusing electrodes provided an inhomogeneous electric field, transverse with respect to the axis of both focuser and molecular beam. Voltages up to 24 kV could be applied to the focuser, and the threshold voltage to sustain oscillation was 12 kV.

The variation of the potential of the multipole focuser (Helmer, 1957) is proportional to the nth power of the radius of the focuser, where n is equal to half the number of poles. It may be shown that a large number of poles produce a potential well which is essentially square. The variation of focusing voltages changes the ratio between the number of upper and lower energy state molecules emerging from the end of the focuser which subsequently enter the cavity.

3.4.3 Positive and negative Stark slope focusers

Positive and negative Stark slope focusers can be used to focus and separate out molecules with energy statesthat either gain or lose energy in an applied electric field respectively. But an alternate

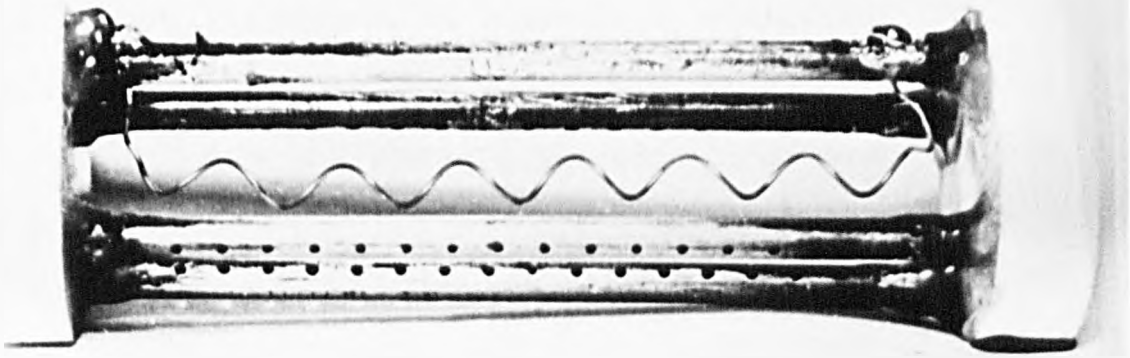

FIGURE (3.9) THE SINGLE WIRE HELIX FOCUSER

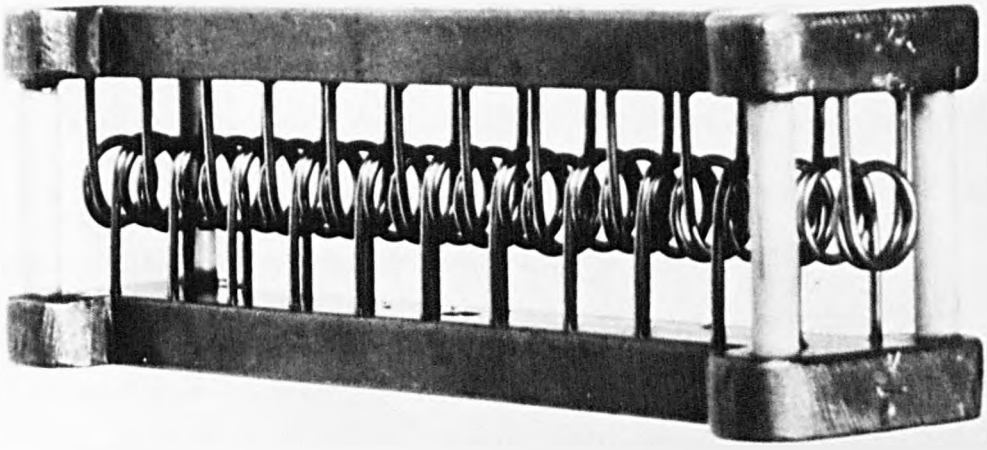

FIGURE (3.10) THE RING FOCUSER

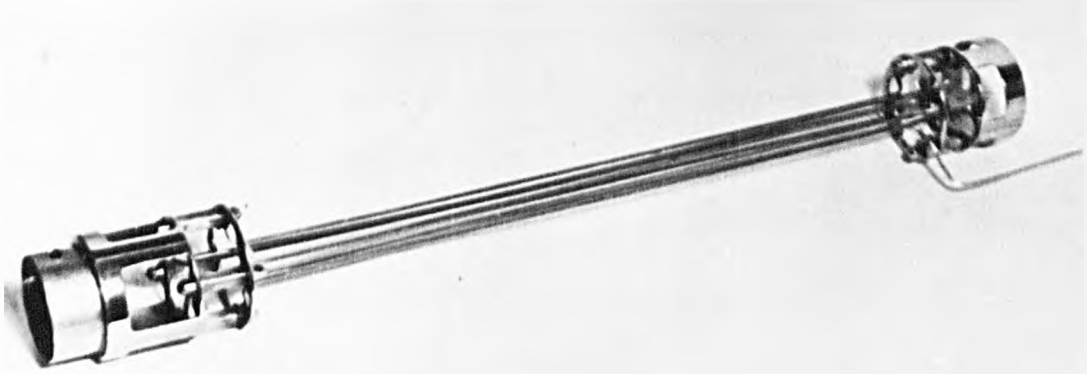

FIGURE (3.11) THE EIGHT POLE ROD FOCUSER

gradient focusing system can be used to focus molecules with either sign of Stark slope. An application of alternate gradient (AG) focusing in charged particle accelerators was discussed by Livingood (1961), Livingood and Blewett (1962). The theory of the AG focuser for neutral molecules was summarized by Auerbach et al. (1966). Reuss and Nelissen (1967) reported experimental results of an AG focusing system. Some experiment measurements were made by Kakati and Laine (1971) for ammonia molecules. Gunther and Schugerl (1972) developed the theory of an AG focusing system which was used to state select the rotational quantum state of polar diatomic molecules and showed that good experimental results could be obtained with this method even for molecules whose Stark energy decreased in an applied electric field.

In the work described in this section, two focusers in series were operated, one of them (the first element) was used to state select upper energy state ammonia molecules, whereas the other was used to state select lower energy state molecules, such as ring-crossed-wire focusers or ring-ring focusers in series. For details see (6.3).

3.5 Resonant cavity

Molecular beam masers have been operated with different types of cavity resonator. These include closed resonators of both cylindrical and rectangular types and open resonators of the laser type. The cylindrical type cavity was used in the first molecular beam maser by Gordon et al. (1955). In the investigation reported here, the cylindrical cavity has again been employed. The two types of mode for this type of cavity are characterised as transverse magnetic or transverse electric. These are 1) transverse magnetic (TM or E) where the electric field is roughly parallel to the axis of the resonator; 2) transverse electric (TE or M) where the magnetic field is roughly parallel to the axis of the resonator. The resonant condition for E modes of a cylindrical cavity is given by Montgomery (1947);

$$\lambda_o = 4 \left| \left(\frac{P}{Z_o}\right)^2 + \left(\frac{2Um,n}{\pi a}\right)^2 \right|^{-\frac{1}{2}} \qquad (3.1)$$

where

λ_o = resonant wavelength,

P = an integer equivalent to the number of half wavelengths of radiation field along the resonator axis,

$2Z_o$ = length of the resonator,

a = radius of the resonator,

$U_{m,n}$ = nth root of the mth order Bessel function $J_m(U) = 0$.

The notation $E_{m,n}$ P is used; where m is the number of the whole variations of either magnetic or electric field along a path concentric with the resonator axis, n is one or more than the number of reversals of sign of a field component along a radius of the cavity. When P = 0, the condition for E modes in the resonator is given by

$$\lambda_o = \frac{2\pi a}{U_{m,n}} \qquad (3.2)$$

If the E_{010} mode is used, the value changes so that m = 0, n = 1 and P = 0, for the ammonia inversion frequency ν = 23.87 GHz, the cavity diameter obtained for this mode is 2a = 0.9614 cm.

Shimoda, Wang and Townes (1951) have defined a "figure of merit" M of the cavity resonator resonance for producing induced transitions.

$$M = \frac{LQ_o}{A} \left(\frac{8}{\pi^2}\right)^P \qquad (3.3)$$

for P, the axial mode number, having the value 0 or 1. The factor $\left(\frac{8}{\pi^2}\right)^P$ takes into account the broadening of the resonance line due to the variation of field along the cavity axis, Q_oL/A is a measure of the sensitivity of the maser which depends on L and A the length, and cross-sectional area A of the cavity respectively. The higher the value of M, the smaller the number of molecules needed for maser oscillation, as follows from table (3.3).

The Q factor of the resonant cavity can be determined using the

relation between the frequency ν and half-width $\Delta\nu$.

$$Q = \frac{\nu}{\Delta\nu} \tag{3.4}$$

In the case of the E_{010} mode, the cavity Q is increased by inserting metal rings (end caps) into each end of the cavity so that the internal diameter of the end cap is below cut off. (The cut off wavelength of the E_{010} mode 2.61a, where a is the cavity (guide) radius for the propagation of electromagnetic radiation), with negligible leakage of microwave power. The two end caps are used to ensure that the cavity resonator is effectively closed to the microwave radiation, yet allow the molecular beam free passage. A high Q value ($\gtrsim$ 5000) is necessary to establish the oscillation condition in the molecular beam maser.

If V_0 is the mean molecular velocity of a parallel beam of molecules passing through a cavity of length L, then the total linewidth of maser signal between half-maximum power points is given by $\frac{0.9V_0}{L}$. This equation assumes that the microwave electric field is uniform along the cavity axis. This is so to a good approximation in the case of E_{010} mode which is used in the experiments discussed in this thesis.

This spectral width of emission increases under saturation conditions where the molecules make a transition from one energy state level to another several times during the time of flight through the cavity. In this case the lifetime in any one energy state level is shorter than the time of flight of the molecules inside the cavity.

Selection of the appropriate cavity mode for maser operation requires a knowledge of the position of the maximum microwave electric field strength. In the use of the E_{010} mode, the maximum microwave field lies on the cavity axis.

The cavity is constructed by depositing copper electrolytically onto a stainless steel (S80) mandrel while the mandrel is rotated

slowly. The direction of the current supplied to the electrodes is reversed periodically for about one third of the time in order to minimize the degree of uneven deposition. The solution level is kept constant during plating. When the electroform is about 2.54 cm in diameter, the plating is stopped and the electroform machined. The mandrel is removed by immersing it in a hot oil bath at which temperature the differential expansion is sufficient to permit easy removal of the mandrel from its electroform. The cavity is made slightly undersized so that it may be temperature stabilized electrically at the resonance frequency. Though undersized at room temperature, the cavity is made from mandrels 0.0005 cm greater in diameter than the calculated value for J = 3, K = 3 (0.9619 cm compared with 0.9614 cm) in order to allow for frequency shifts due to effects of the semi-open ends of the cavity. The theoretical calculated coefficient of variation of frequency with the cavity diameter is about 6 MHz per 0.0001 inch (0.000254 cm); experimentally the observed variation of the resonance frequency with the cavity temperature is approximately 0.4 MHz per degree ^{o}C.

The cavity used in the present investigation fig (3.4), has a physical length of 11.4 cm, reduced to 10.2 cm by inserting end caps 0.6 cm into each end. The cavity coupling hole is placed centrally. The cavity is undercoupled and has a loaded Q of 6050 $\pm$ 300.

To tune the cavity, and to avoid drift of its resonance frequency due to ambient temperature variations, an Airmec N.299 electronic temperature control unit is used. The cavity is thermally heated to be stabilized between 25 to 30^{o}C in order to stabilize satisfactorily. The heater coil (glass covered Eureka wire) has a resistance of 20 ohms, and the temperature sensor coil (insulated copper) has a resistance within the range 9.45 to 9.47 ohm. A bifilar winding for both the heater and the sensor is essential in order to prevent any

possibility of Zeeman splitting of the maser line. All the connecting leads between the cavity and Airmec heater control unit type N.299 and power supply unit are made of heavy gauge wire to minimize resistance changes due to variations of ambient temperature.

TABLE (3.3)

Calculated values of parameters for cylindrical cavity resonator L = 12 cm (after Shimoda, Wang and Townes, 1956)

Mode	Radius a in cm	Area A in cm^2	Q_0	Q_0L	Q_0L/A
TE_{111}	0.37	0.34	6100	73200	170233
TM_{010}	0.48	0.72	10800	129600	180000
TM_{011}	0.48	0.72	10400	124800	173333
TE_{211}	0.61	1.17	8100	97200	83076
TE_{011}	0.76	1.41	17800	213600	151489

3.6 Microwave system

Sensitivity

The signal-to-noise ratio is defined as the ratio between the change in the reflected power ΔP_r and the change in the noise power ΔP_n (Thaddeus and Krisher, 1961)

$$S/N = \frac{\Delta P_r}{\Delta P_n} \tag{3.5}$$

The maximum signal-to-noise ratio for greatest sensitivity for a resonant cavity type of molecular beam spectrometer is given by (Thaddeus and Krisher, 1961)

$$(S/N)_{max} = 3.36 \left| \frac{(L/A)\ \omega_o\ Q_L}{kTF\ \Delta\nu} \right|^{\frac{1}{2}} \frac{\mu_{12}^n}{\bar{v}} \tag{3.6}$$

where

L is the length of the stimulating field,

μ_{12} is the matrix element of the component of the dipole moment operator along E,

A is an effective area of the resonator "seen" by the beams,

Q_L is the loaded quality factor of the cavity,

ω_o is the frequency of the inversion transition,

k Boltzmann's constant,

T is the absolute temperature of the detector,

$\bar{v}$ is the average molecular velocity,

F is the noise figure of the receiver of the bandwidth $\Delta\nu$,

and n is taken as the population difference between initial and terminal state of the transition.

The (S/N) ratio depends on the quantity $(L^2 Q_L/V)$; the latter can be considered as a figure of merit M of the resonator.

The minimum detectable beam flux n_{min} for a univelocity beam (by setting $(S/N)_{max} = 1$)

$$n_{min} \simeq \frac{\bar{v}}{3.36\ \mu_{12}} \left| \frac{kTF\ \Delta\nu}{(L/A)\ \omega_o\ Q_L} \right|^{\frac{1}{2}} \qquad (3.6a)$$

by using

$\bar{v}$ $= 7 \times 10^4$ cm/sec velocity of the molecules emerging from the nozzle source,

μ_o $= 1.47 \times 10^{-18}$ e.s.u.,

M_J $= \sqrt{7}$ (Shimoda, 1957),

J $= 3$,

K $= 3$,

μ_{12} $= \mu_o \frac{M_J K}{J(J+1)} = 9.723 \times 10^{-19}$ e.s.u.,

Q_L $= 6050$,

L $= 10.8$ cm ,

A $= (0.45)^2 \times \pi = 0.636$ cm^2 where 0.45 cm is the radius of the cavity used in the work reported in this thesis,

F $= 100$ (Gordon et al., 1955),

$\Delta\nu \simeq 1$ kHz,

Boltzmann's constant $k = 1.38 \times 10^{-16}$ erg/deg.,

$\omega_o = 2.4 \times 10^{10}$ Hz, $T = 240^{o}K$.

Typical values for n_{min}, for J = 3, K = 3 line NH_3 molecules is 2.48×10^{12} molecules per second.

The crystal detector used in the work reported in this thesis (Torrey and Whitmer, 1948), consists of a fine wire in contact with a block of semiconducting material (Silicon IN26 crystal type).

The detection system is used to detect the interaction of the molecular beam with the radiation field. The microwave emission within the cavity must be as large as possible in order to obtain the highest signal-to-noise ratio. A large amount of microwave absorption power absorbed by the crystal produces too much noise which reduces the overall sensitivity. In contrast a small amount of power leads to a poorer signal-to-noise ratio. Thus an optimum power level is sought for maximum signal-to-noise ratio.

There are three properties for the detecting crystal (Ingram, 1955) that need to be considered for low noise operation: 1) Conversion loss. 2) The excess noise generated by the crystal. 3) Impedance.

1) The conversion loss measures the efficiency of the crystal in converting the microwave radiation to d.c. or low frequency modulation. For low input power and rectified current, the conversion loss is high, but its values falls asymptotically to about 6 dB for crystal currents in excess of 0.5 mA.

2) The excess noise generated by the crystal.

The overall sensitivity depends on the noise generated in the crystal. This varies with the variation of both the magnitude of the rectified current and the intermediate frequency of the output.

For a given type of intermediate frequency amplifier, the noise increases with the frequency. Also the losses of the crystal depends

on the rectified current. This leads to the result that there is a broad optimum of intermediate frequency of about 30 MHz.

3) Impedance.

In order to achieve a maximum sensitivty, the matching of the crystal is important, and both the radiofrequency and intermediate frequency impedance of the crystal varies somewhat with the strength of the input signal. The intermediate frequency impedance for rectified current above 0.5 mA remains reasonably constant and does not vary much with the frequency. A typical value of the impedance is of the order of 400 ohms.

Microwave bridge

Fig (3.12) shows the microwave bridge (Herrmann and Bonanomi (1956)) which is used for the work described in this thesis. The figure shows also the electronic detection scheme. A single klystron (OKI-24V 10A) is used to produce microwave power in the range 23 - 24 GHz. This power passes through the attenuator to the magic tee (arm no. 1). Then the microwave power is divided equally into two parts. In one of them, in the detection arm (arm no. 3), the power was fed, via a waveguide, through the matching unit M to a semiconductor microwave mixer diode (crystal detector). The power is reflected back down the arm no. 2 through the magic tee and passes through the cavity arm (arm no. 4) or the detection arm, entering the resonant cavity via a matching unit (outside the chamber) and a matching stub close to the cavity (inside the chamber). The microwave power excited the cylindrical cavity E_{010} mode which was tuned to have a uniform electric field in the direction of propagation of the molecular beam. Arms no. 2 and no. 3 are the comparison arms of the bridge, which have the characteristic that the power fed into the first arm will be transmitted equally to the second and third arms and there is no power transmitted

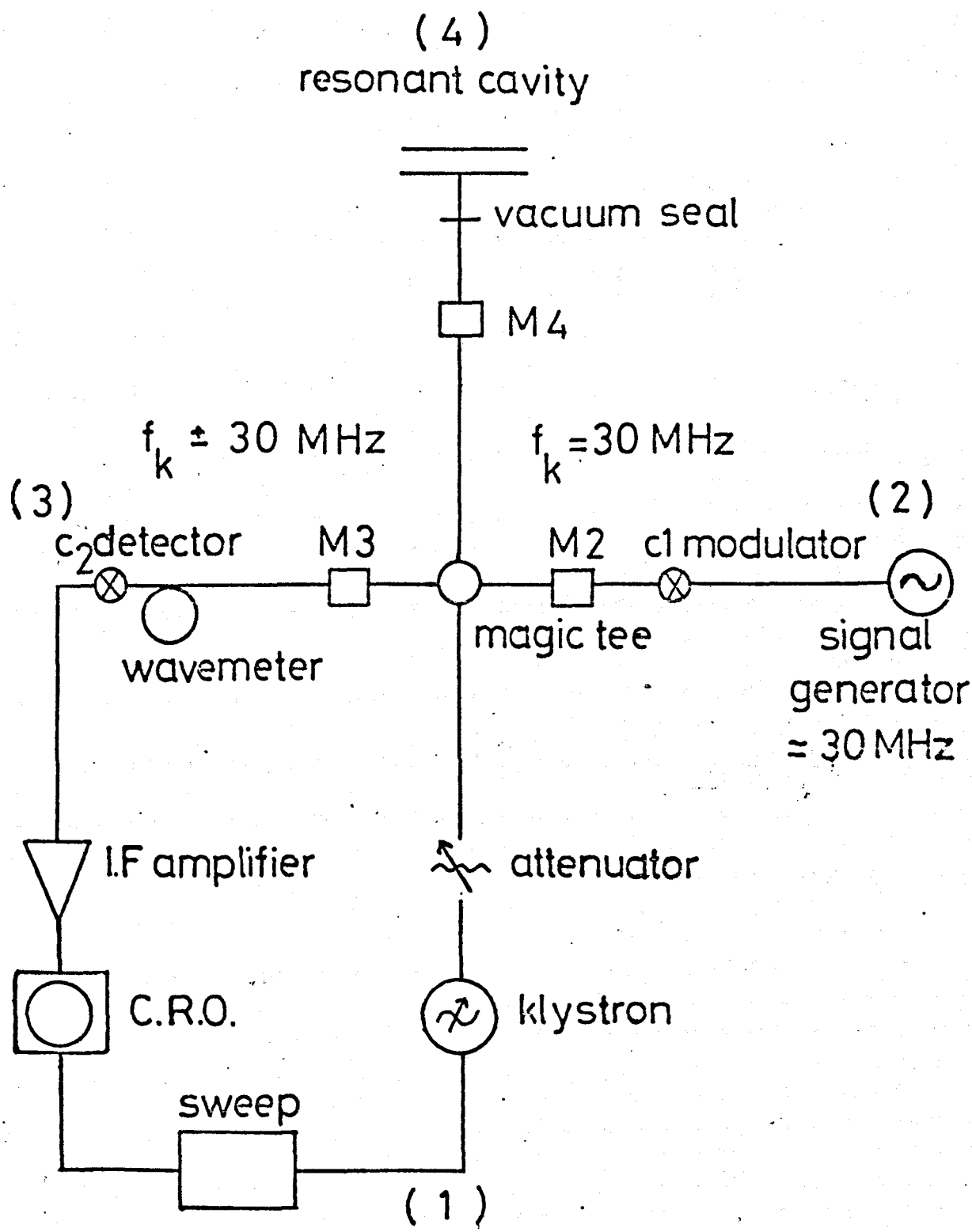

FIGURE (3.12) MICROWAVE BRIDGE AND DETECTOR COMPONENTS.

to the fourth arm.

Crystal video system

The initial use of the crystal video system is for tuning up the maser system. The microwave power produced by the klystron type (Mfg 24V10A OKI Electronic Inc.) passes through the attenuator to the magic tee (arm no. 1). The microwave bridge is shown in fig (3.12). In the magic tee, the microwave power is divided between arm 2 and arm 3. Power is reflected back down arm 2 and passes into arm 4, entering the resonant cavity E_{010} mode via a matching unit. Some power is reflected from the cavity and passes down arm 3 to detector crystal C2 (Sylvania IN26A). If the ammonia gas molecules within the resonant cavity have a resonant transition at frequency f_K, the associated signal is reflected out of the cavity to the magic tee and along arm 3 to the crystal detector IN26A which detects the resonance signal. This signal passes directly to the audio frequency vertical amplifier of a Telequipment Type D65 oscilloscope. By using the wavemeter it is possible to find the correct klystron frequency to operate the microwave cavity tuned to the J = 3, K = 3 ammonia inversion line frequency. The cavity produces an absorption resonance signal which is displayed on the oscilloscope. By using the heater control unit, the cavity resonance is made to coincide exactly with the ammonia molecular resonance corresponding to the J = 3, K = 3 frequency.

The OKI single klystron is swept over its full electronic frequency tuning range (klystron power supply Type EE4) by means of 100 V saw tooth peak-to-peak potential applied to the reflector voltage of the klystron. The frequency varies at 50 Hz about the J = 3, K = 3 frequency of 23,870 MHz.

Frequency swept superheterodyne

The microwave cavity is tuned to the ammonia molecular resonance

transition J = 3, K = 3 in the present work. This mode of operation is effected by inserting the 30 MHz amplifier and the second detector between the crystal C2 and the oscilloscope. A small fraction of the output of the klystron frequency f_K is taken to a IN26A crystal mixer which is modulated by a 30 MHz sideband generator. The power reflected from the crystal then contains the frequency components (f_K , $f_K \pm 30$) MHz. One of the sidebands (f - 30) MHz excites ammonia molecules inside the resonant cavity and the associated signal is reflected back via the fourth arm to the magic tee and through the third arm to detector crystal C2. The 30 MHz beat signal which results from frequency mixing is passed into the intermediate frequency amplifier and a spectroscopic signal is displayed on the oscilloscope. The frequencies on the local oscillator and stimulating source of power are separated so that the beat frequency after mixing falls within the passband of the IF amplifier.

In the superheterodyne receiver (Laine, 1975), noise originating in the crystal detector and receiver itself is important if the maximum signal-to-noise is to be obtained. The noise bandwidth of a superheterodyne spectrometer such as used for this work is typically 10-100 kHz. For maximum sensitivity, it is important that the bandwidth is reduced.

3.7 Electronic equipment

The klystron power supply was a Mid-Century Microwavegear type EE/4 which was used to operate an OKI high voltage klystron, type 24V 10A. The klystron frequency sweep unit was integral with the power supply unit.

The 30 MHz intermediate frequency amplifier had a gain of 66 dB and a bandwidth of 2 MHz, and was operated with a stabilized D.C. power supply unit type R1095.

A signal generator Advance type E model 2 was used to provide

modulating power to generate two 30 MHz side bands from a portion of the klystron power.

An oscilloscope Telequipment type D65 was used for visual display and experimental measurements. An Airmec N.299 temperature control unit was used to tune the cavity by electrical heating and stabilize its temperature to a predetermined value.

Three 30 kV high voltage generator units were used to operate the state selectors; two supplies were Brandenburg model S.0530/10 giving a positive polarity, the other, was a Brandenburg model 800 with a reversible polarity. Each of these three units had a voltage stability better than 0.25%. These EHT power supplies employed were radiofrequency units (S.0530/10: 100 KHz; 800: 12MHz). A 375 MΩ high resistance in series with the power supply unit was used in order to reduce current surges in case of electrical breakdown in the state selector, thereby minimizing possible damage due to arcing.

The electrical lead-throughs to the focuser were long-reach spark plugs, mounted in a machined araldite casting. An Edwards type Ion 7 ion gauge unit was used in conjunction with the Edwards gauge type IG6G and IG5G. A mass spectrometer, Centronic type AIG 50 was used for leak detection in the vacuum system.

CHAPTER FOUR

THE BASIC AMMONIA MASER

4.1 General schemes of focusing a ring of ammonia molecules

The technique of focusing a ring of ammonia molecules was first used in conjunction with an ammonia molecular beam (Al-Amiedy and Lainé, 1978). The defocused molecules deflected away from the axis of the state selector as well as the focused beam were detected by a spectrometer cavity. This was achieved by moving the cavity transversely across the beam axis, and as a consequence either an emissive or absorptive beam could be detected.

During the course of measurements, both the focuser voltage and the ammonia gas pressure behind the nozzle source were kept constant. The only variables were the position of the spectrometer cavity with respect to the focuser and beam axis, and consequently the amplitude of the molecular resonance signal detected was also variable.

This technique has been applied to the following focusing systems: single wire helix, ring, octopole rod, crossed-wire and single straight wire.

It is expected that this technique may also be used similarly for other types of focusing systems such as the bifilar helix and quadrupole helix not investigated experimentally in this thesis.

4.1.1. Focusing a ring of ammonia molecules by using a single wire helix

a) Narrow axial beam case

Within the single wire helix focuser, the computed graph illustrated in fig (5.14) shows the radial gradient of the square of electric field as a function of the radial distance r away from the focuser axis. It is clear that the radial gradient has a small but finite value at the focuser axis. As the radial distance

increases the gradient gradually rises, and then when r ≈ 0.7 R where R is the radius of the single wire helix, the radial gradient of the square of electric field increase rapidly, reaching its maximum value at the surface of the helix electrode.

The single wire helix captures upper energy ammonia molecules bringing them to a rough focus at a remote point on the focuser axis, and deflects the lower energy state molecules outwards towards the helix electrodes. Thus the state selected molecules downstream from the focuser will have a central circular region rich in emissive ammonia molecules with a maximum value on the axis of the focuser, surrounded by an outer concentric ring of absorptive molecules.

This was established experimentally as shown in fig (4.1). This graph shows an off-axis absorptive signal of approximately 0.1 of the amplitude of stimulated emission with the cavity on-axis.

b) Broad beam case

Immediately outside the single wire helix focusing system, the electric field and the radial gradient of the square of electric field have maximum values as shown from the computed graph illustrated in fig (5.15). Here the radial gradient of the square of electric field is shown as a function of the radial distance r away from the helix focuser axis. The magnitude of the radial gradient drops sharply to 1/7th of its maximum value just at a distance 1.3 R, where R is the radius of the single wire helix focuser. This means that in the vicinity of the outer region of the helix electrode, upper energy state molecules are defocused radially outwards from the helix state selector, whereas the lower energy state molecules converge towards the electrodes. Therefore at a remote point on the molecular beam axis, the lower energy state molecules converge to a circular area with a maximum value roughly at the diameter of the helix electrode, with an outer concentric ring of emissive molecules as shown in fig (4.2).

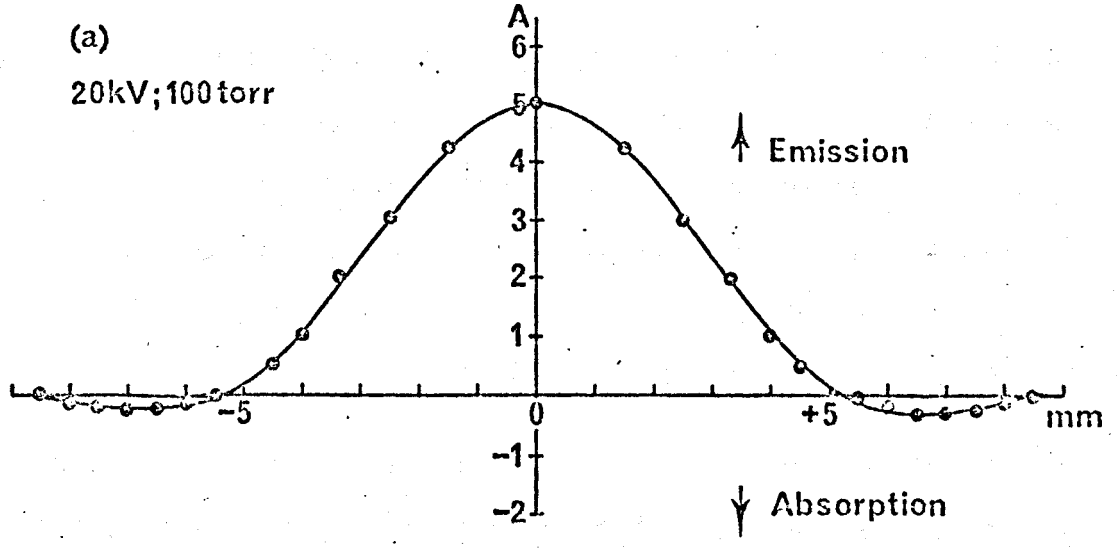

FIGURE (4.1) THE AMPLITUDE OF EMISSION AND ABSORPTION SIGNALS VERSUS TRANSVERSE POSITION OF THE SPECTROMETER CAVITY DISPLACED FROM THE BEAM AXIS (X-AXIS) USING A SINGLE WIRE HELIX (NARROW BEAM).

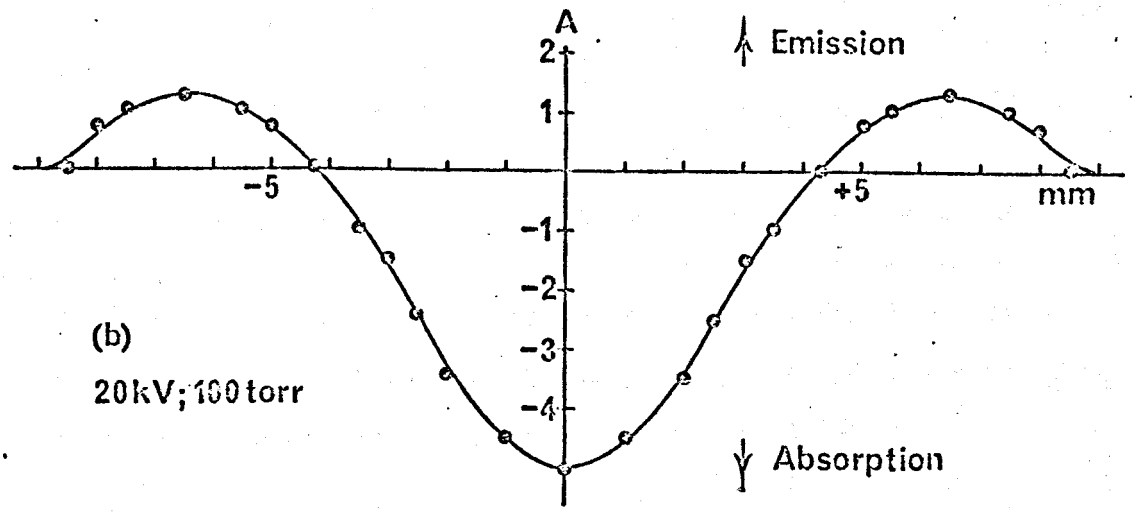

FIGURE(4.2) THE AMPLITUDE OF EMISSION AND ABSORPTION SIGNALS VERSUS TRANSVERSE POSITION OF THE SPECTROMETER CAVITY DISPLACED FROM THE BEAM AXIS (X-AXIS) USING A SINGLE WIRE HELIX (BROAD BEAM).

4.1.2 Focusing a ring of ammonia molecules by using ring electrodes

As far as the focusing action of the ring focuser is concerned, the important factor is the radial gradient of the square of electric field since the focusing force for ammonia molecules is proportional to this quantity.

Within the ring system, the computed graph illustrated in fig (2.10) gives the radial gradient of the square of electric field as a function of the radial distance r away from the focuser axis. It is clear that the radial gradient has a zero value at the focuser axis. As the radial distance increases the gradient gradually increases, first slowly, and then when $r = 0.8\,R$, where R is the radius of the ring focuser, the gradient increases rapidly, reaching its maximum value at the surface of the ring electrode. The ring focuser captures upper energy state ammonia molecules and guides them to a rough focus at a remote point on the focuser axis. The lower energy state molecules are deflected outwards towards the ring electrodes. Therefore the state selected molecular beam downstream from the focuser will have an inner circular region rich in emissive ammonia molecules with a maximum value on the axis of the focuser, surrounded by an outer concentric ring of absorptive molecules.

This was confirmed experimentally for a molecular beam constrained to pass inside the state selector and the results are shown in fig (4.3). From this graph it is clear that an absorption signal of approximately 0.45 of the amplitude of the stimulated emission with the cavity on -axis is obtained on either side of the maximum stimulated emission position.

When a beam stop filled the first ring electrode, as shown in fig (3.8), and a portion of the molecular beam allowed to pass on the outside of the ring electrode, reversed focusing occurred. From the computed graph illustrated in fig (5.4) which shows the

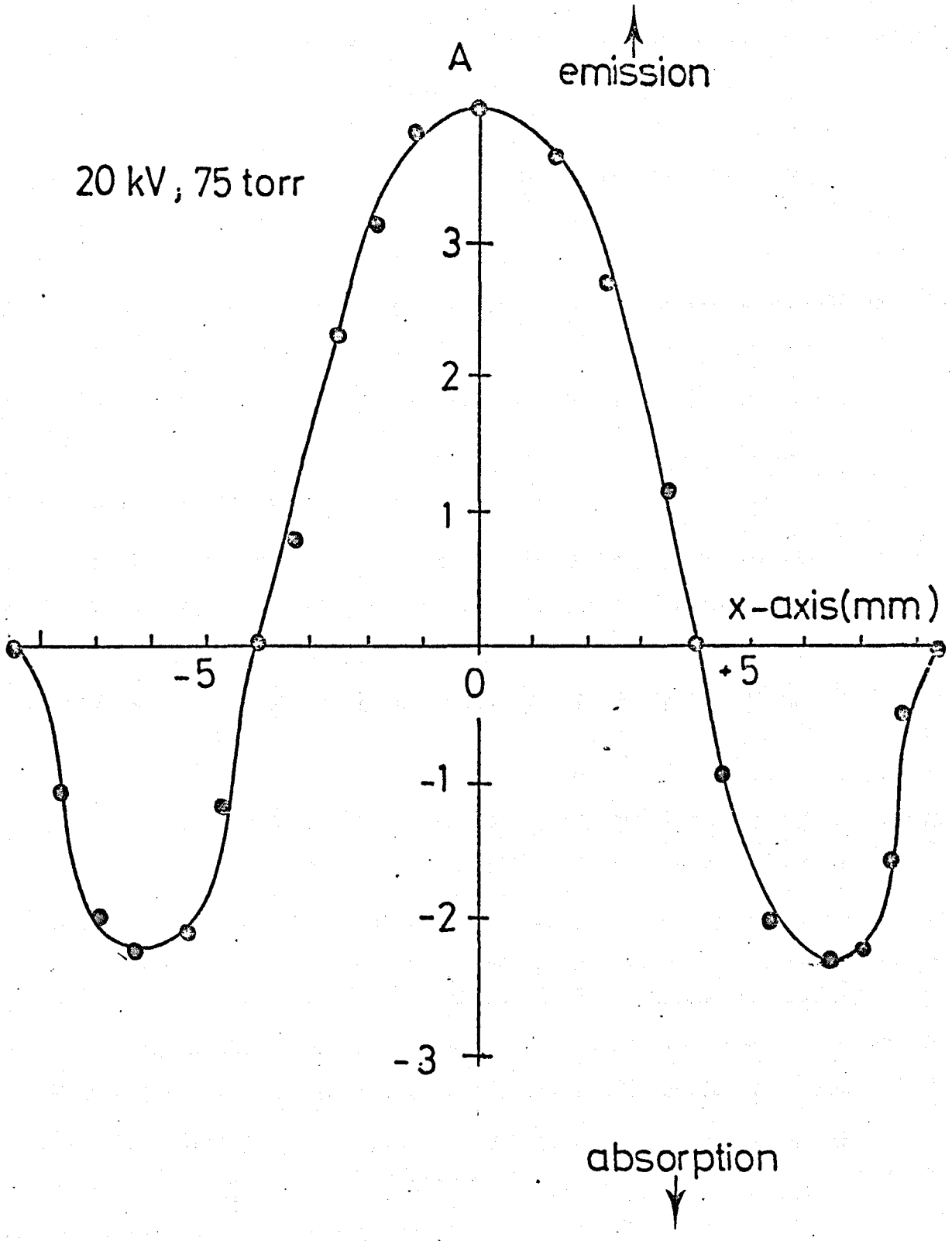

FIGURE(4.3) THE AMPLITUDE OF EMISSION AND ABSORPTION SIGNALS VERSUS TRANSVERSE POSITION OF SPECTROMETER CAVITY DISPLACED FROM THE BEAM AXIS (X-AXIS) USING RING FOCUSER (NARROW BEAM).

radial gradient of the square of electric field as a function of the radial distance r away from the focuser axis, it is obvious that the radial component has a maximum value at the ring electrode, and its magnitude drops rapidly to 0.1 of its maximum value after a distance 1.2 R from the outside ring. Thus outside the ring system, especially in the vicinity of the ring electrodes, upper energy state molecules are deflected radially outwards from the state selector, whereas the lower energy state molecules converge towards the ring electrodes. Therefore at a remote point on the molecular beam axis, the lower energy state molecules converge to a circular area with a maximum value roughly at the diameter of the ring electrodes, with an outer concentric ring of emissive molecules.

This is in agreement with the experimental results shown in fig (4.4). It is seen from the graph, that a stimulated emission signal of approximately 0.4 of the amplitude of enhanced absorption with the cavity on-axis is obtained on either side of the maximum absorption position.

4.1.3 Focusing a ring of ammonia molecules by using an octopole rod focuser

Within the octopole rod focusing system, the electric field and the radial gradient of the square of electric field has a zero value at the focuser axis, which increases slowly at first, then rapidly with the radial distance, until it reaches its maximum value at the rod electrodes. Therefore at a remote point on the focuser axis, the state selected beam downstream from the focuser will have an inner circular region rich in emissive molecules with a maximum value on the focuser axis, with an outer concentric ring of absorptive molecules.

Outside the system of electrodes the molecular deflection

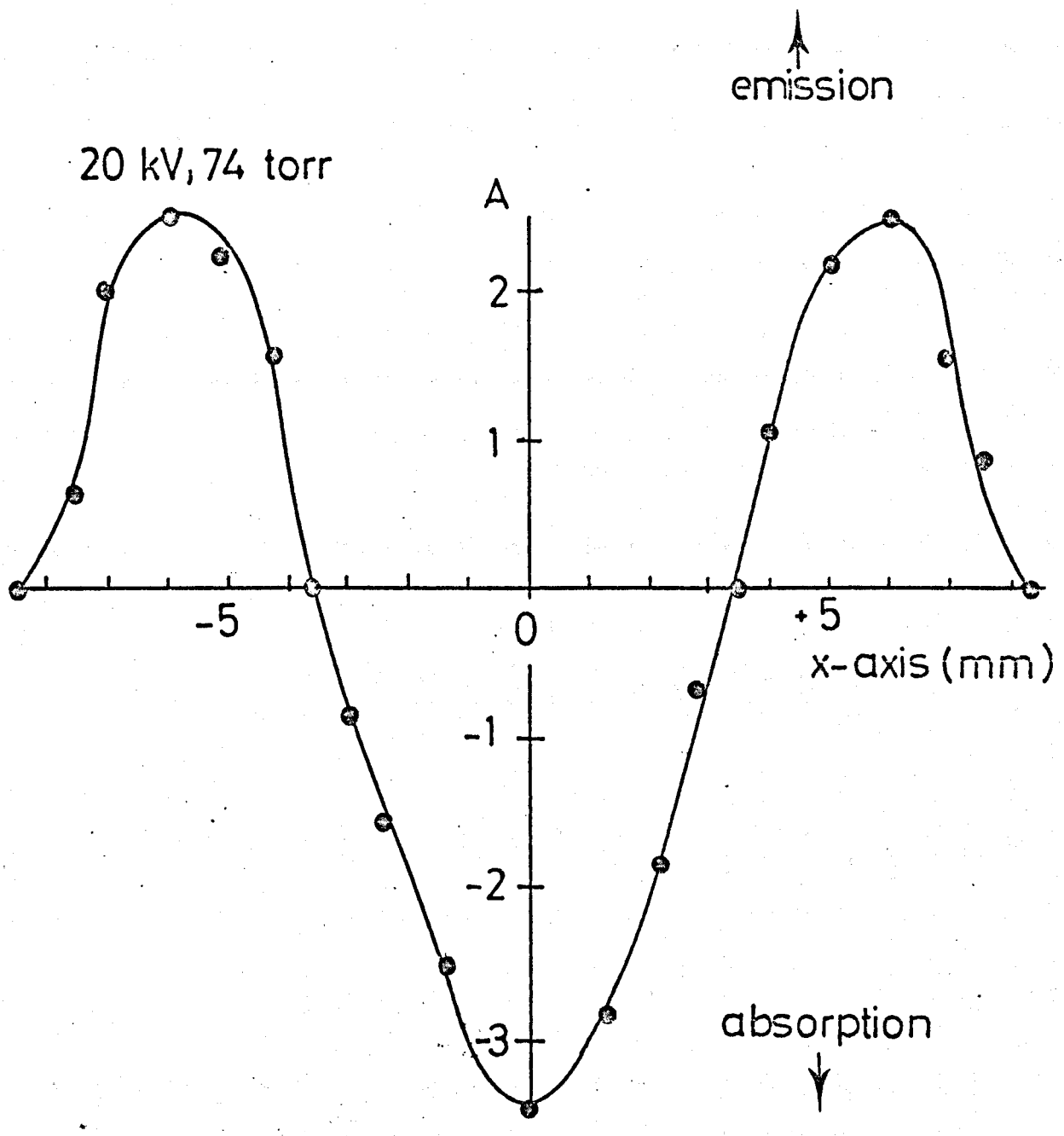

FIGURE(4.4) THE AMPLITUDE OF EMISSION AND ABSORPTION SIGNALS VERSUS TRANSVERSE POSITION OF SPECTROMETER CAVITY DISPLACED FROM THE BEAM AXIS(X AXIS) USING RING FOCUSER (BROAD BEAM).

directions reverse, where in the vicinity of the electrodes, upper energy state molecules are defocused radially outwards from the state selector, whereas the lower state molecules converge towards the electrodes. Thus at a remote point on the molecular beam axis, the lower state molecules converge to a circular area with a maximum value roughly at the diameter of the rod electrodes, with an outer concentric ring of emission signal as shown in fig (4.5). When a broad beam floods the state selector both inside and outside, a stimulated emission signal was obtained on the molecular beam axis, and was surrounded by two successive concentric rings. The first ring was a region of absorption, and second a region of stimulated emission.

4.1.4 Focusing a ring of ammonia molecules by using a crossed-wire focuser

By employing the technique of focusing a ring of ammonia molecules, as discussed in (4.1), using the crossed-wire focuser, the absorption signal detected by the spectrometer cavity becomes progressively weaker with increasing radial distance from the crossed-wire focuser axis, until its amplitude drops to zero. This follows because state selection is most efficient in the region of maximum electric field which lies along the beam axis. However, if the spectrometer cavity is slowly moved transversely across the beam axis (x-axis), then an emission signal appears which becomes progressively stronger until it reaches a maximum amplitude after which it falls to zero as shown in fig (4.6). The amplitude of the two emission signal maxima is 0.5 of the amplitude of the enhanced absorption signal with the cavity on-axis.

4.1.5 Focusing a ring of ammonia molecules using a single straight wire focuser

When the spectrometer cavity was adjusted in position by a mechanical link from outside the chamber, in a direction perpendicular

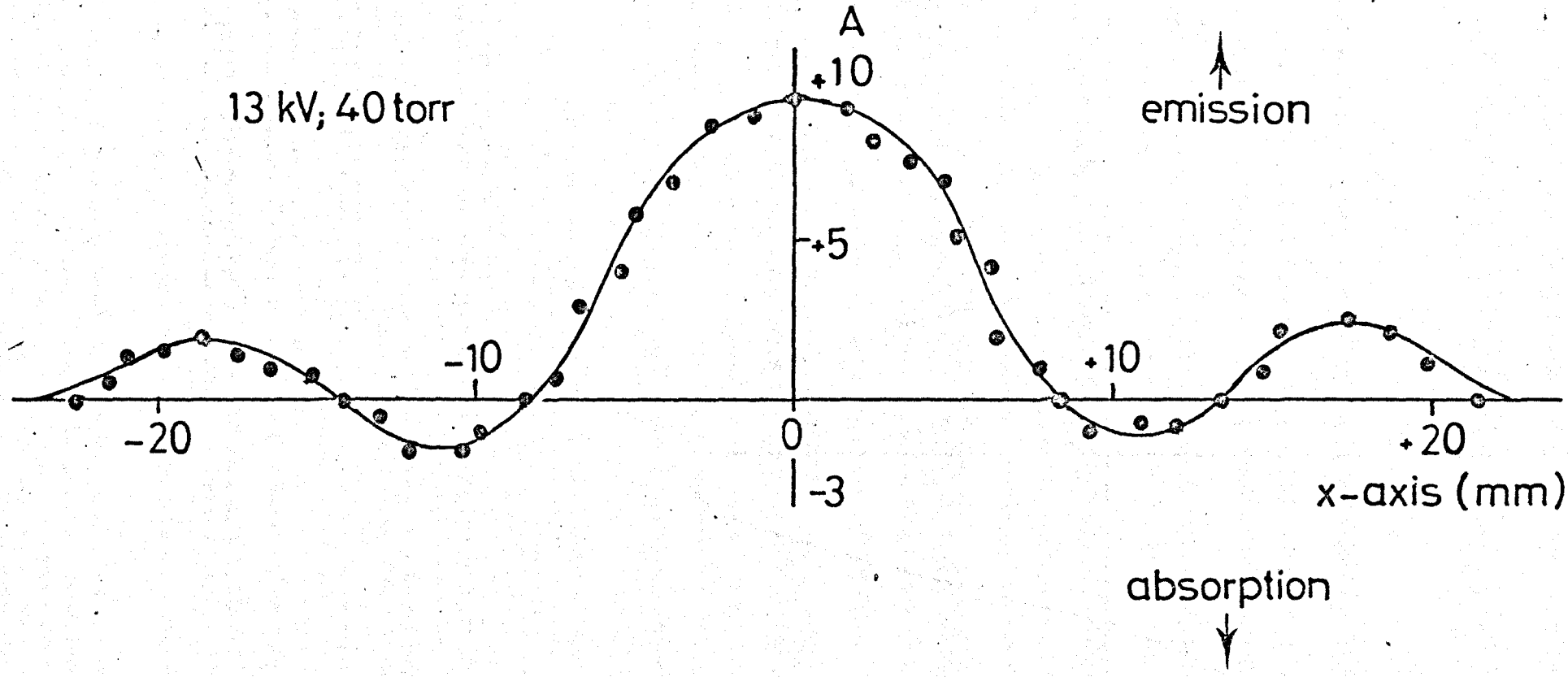

FIGURE(4.5) THE AMPLITUDE OF EMISSION AND ABSORPTION SIGNALS VERSUS TRANSVERSE POSITION OF SPECTROMETER CAVITY DISPLACED FROM THE BEAM AXIS (X-AXIS) USING AN OCTOPOLE ROD FOCUSER.

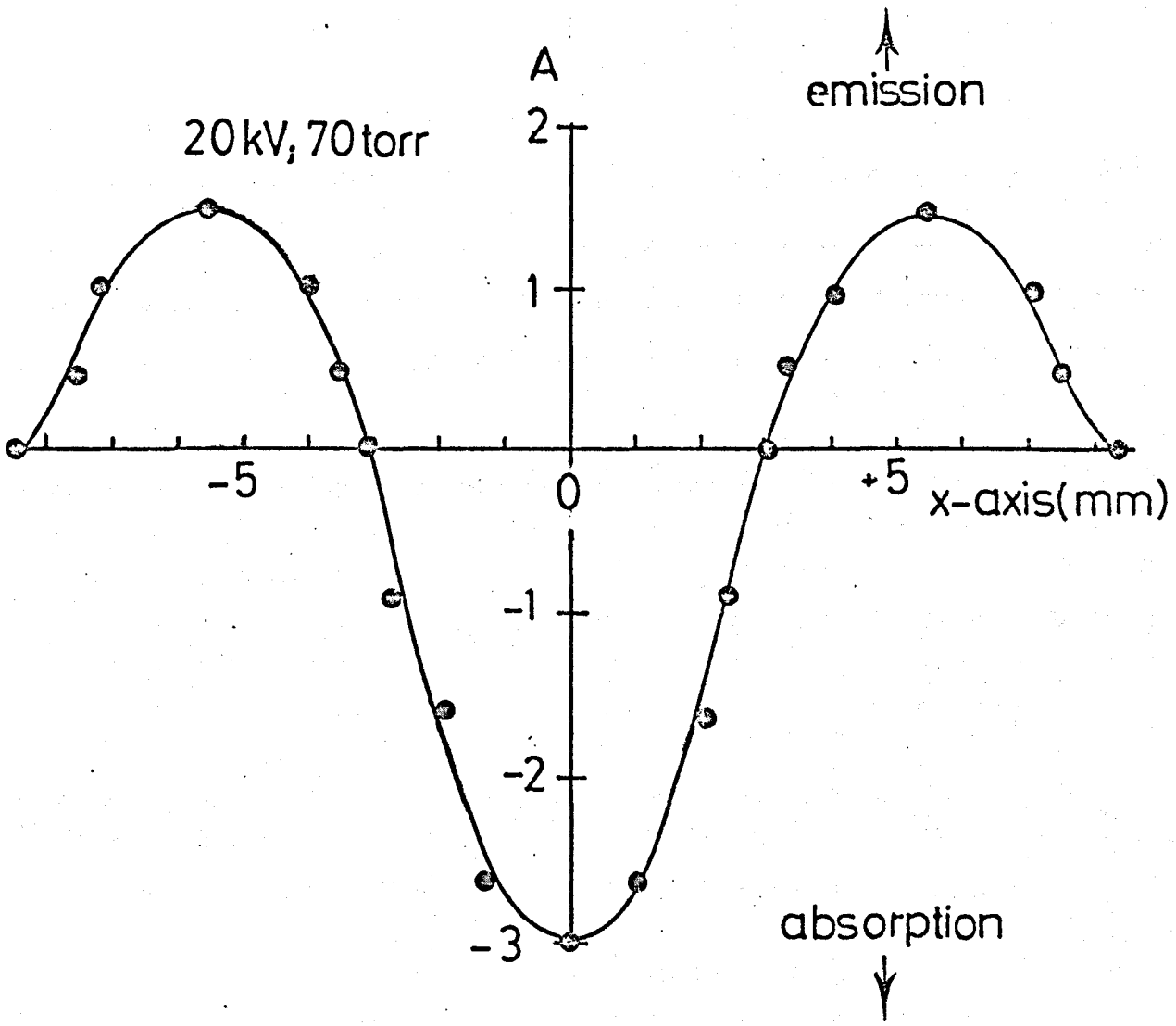

FIGURE(4.6) THE AMPLITUDE OF EMISSION AND ABSORPTION SIGNALS VERSUS TRANSVERSE POSITION OF THE SPECTROMETER CAVITY DISPLACED FROM THE BEAM AXIS (X-AXIS) USING CROSSED-WIRE FOCUSER.

to the beam axis (x-axis), a strong absorption signal on the beam axis was observed and a weak emission signal on either side. This result is in agreement with the theory of the single straight wire focuser discussed in (2.3), as well as the computer results of the trajectory of ammonia molecules described in (4.2) from which it was found that at low voltages applied to the focuser, the majority of molecules entering the on-axis cavity were in the upper energy state, but by increasing the voltage above 10 kV, the lower energy state molecules predominate, and no more upper energy state molecules will enter the cavity, unless the cavity is displaced transversely.

4.2 Enhanced absorption signal by using

a) a crossed-wire focuser

Using the crossed-wire focuser the absorption started to appear when 2.5 kV was applied between focuser electrodes. The amplitude of the absorption signal depended on the position of the focuser inside the vacuum chamber relative to the cavity or the gas source. Evidently the signal depends on the solid angle of the molecules emerging from the nozzle source. In the present investigation the optimum position of the focuser from the cavity was 5 cm, for a maximum level of absorption signal. The optimum pressure behind the multiple hole nozzle (four holes on a PCD of 2 mm) varies with changes in separation of the focuser from the cavity. The amplitude of the enhanced absorption signal plotted as a function of the focuser voltage is shown in fig (4.7). From the graph, it is seen that the amplitude of the absorption signal is enhanced with an increase of the voltage applied to the focuser and the curve passes through the origin. Two focusers (f_1, f_2) were investigated for focusing, and long focuser f_1 was found to be the better one. The optimum pressure behind the multiple hole nozzle was (70-80) torr and (20-30)

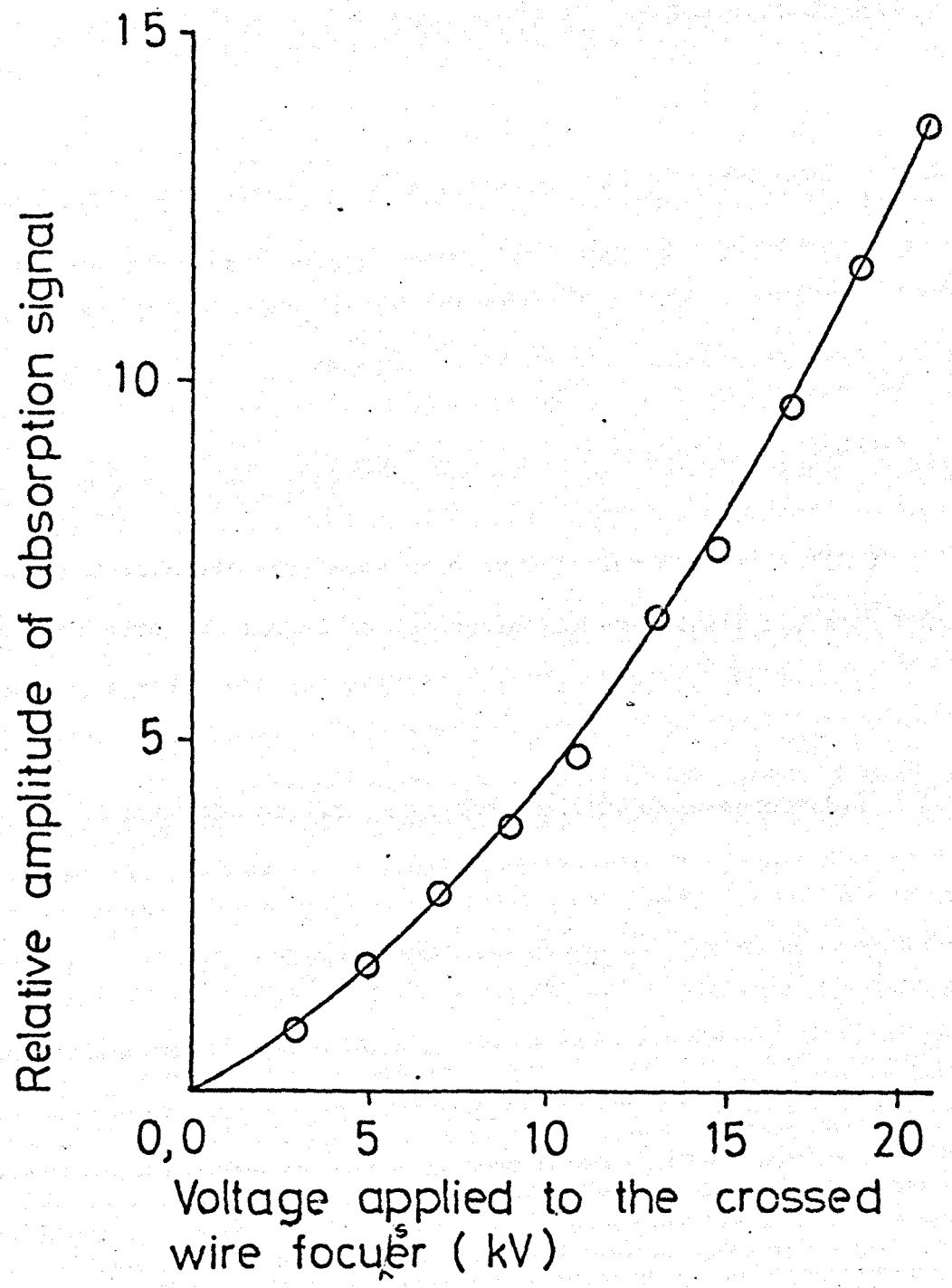

FIGURE(4.7) RELATIVE AMPLITUDE OF ABSORPTION SIGNAL AS A FUNCTION OF THE VOLTAGE APPLIED TO THE CROSSED WIRE FOCUSER.

torr for the focuser f_1, f_2 respectively. Fig (4.8) shows a photograph of the spectroscopic signal enhanced by the crossed-wire focuser.

b) single straight wire focuser

From the spectroscopic point of view, absorptive molecular beams are of interest, since they offer a large number of active molecules which leads to increased sensitivity without the possibility of regenerative narrowing the spectral line (Zeuv & Cheremiskin, 1962).

It was shown in this experiment that an improvement in signal-to-noise ratio can be obtained by using a multiple hole nozzle instead of an effusive source as used by Sweeting and Laine (1972). It was found that the signal has double the amplitude, and a detectable variation of the amplitude with the EHT starts from zero as shown in fig (4.10), compared with Sweeting and Laine (1972) whose result showed that the variation in the amplitude was detectable only from 10 kV. It was also found that the signal was not sensitive to the axial movement of the nozzle pipe. Fig (4.9) shows a photograph taken of the enhanced absorption signal by using single straight wire focuser.

In conclusion it is seen that the experiment results shown in fig (4.10A) are in agreement with the computed result shown in fig (2.5B).

4.3 Oscillation

The maser oscillates if the number of upper energy state molecules in the beam passing through the cavity is increased beyond a certain critical value determined by the losses of the system.

Power P emitted from N excited molecules (total) in the cavity is given by

$$P = N \cdot h\nu \cdot B_{21} \cdot P(\nu) \qquad (4.1)$$

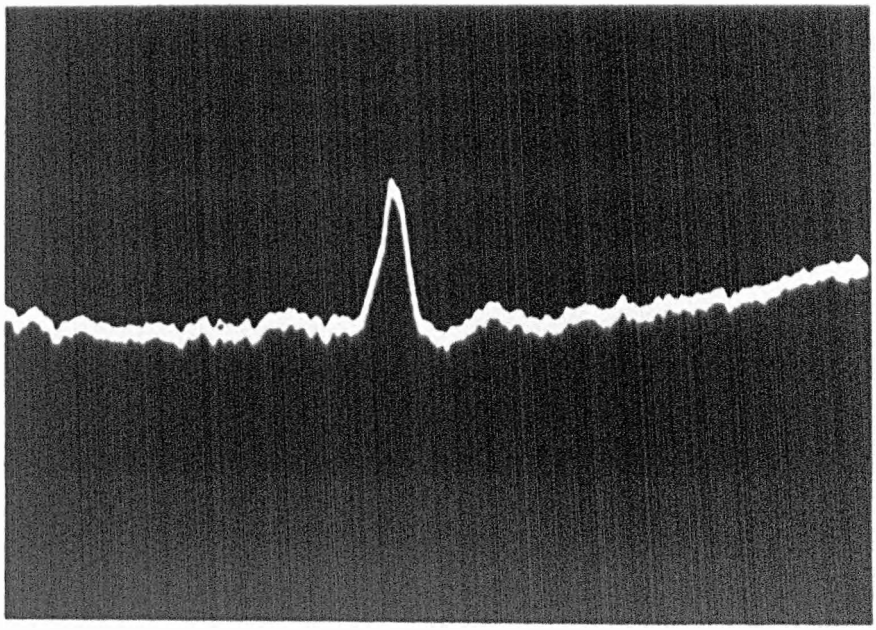

FIGURE (4.8) THE ABSORPTION SPECTRUM OF $^{14}NH_3$ (J=K=3) ENHANCED BY THE CROSSED-WIRE FOCUSER : NOZZLE PRESSURE 80 TORR., STATE SELECTION VOLTAGE 20 kV.

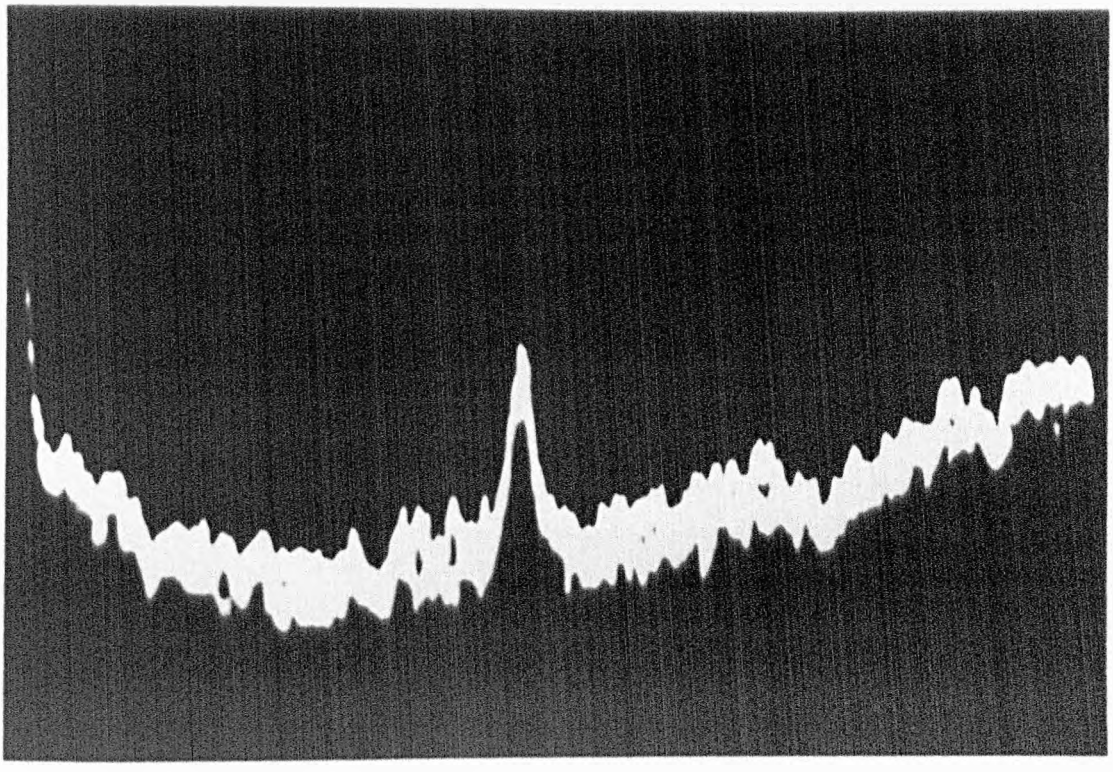

FIGURE (4.9) THE ABSORPTION SIGNAL ENHANCED BY THE SINGLE STRAIGHT WIRE FOCUSER OPERATED AT 30 kV, WITH MULTIPLE NOZZLE GAS PRESSURE OF 100 TORR.

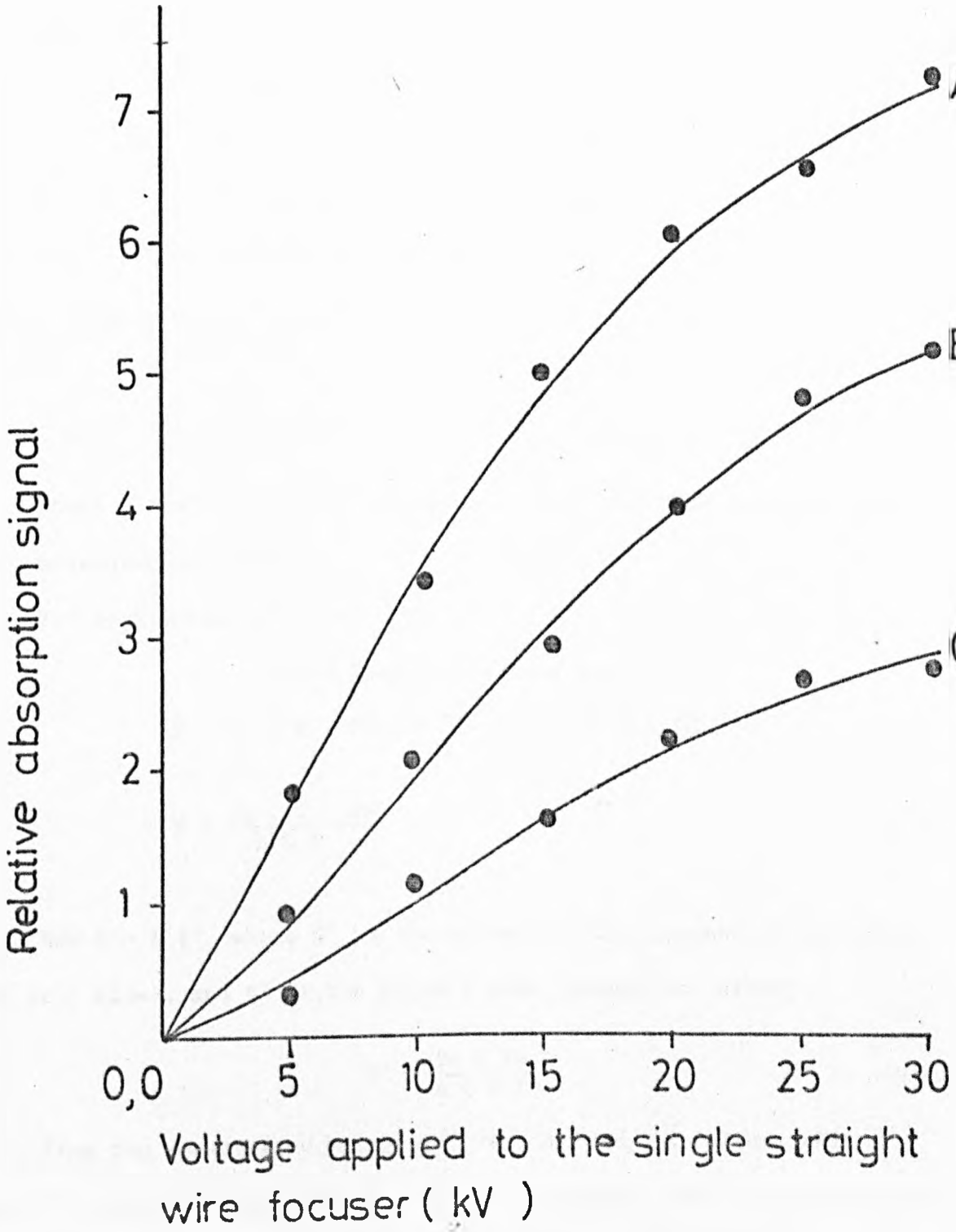

FIGURE (4.10) DEPENDENCE OF THE ABSORPTION ON THE VOLTAGE APPLIED TO THE SINGLE STRAIGHT WIRE FOCUSER. A) REPRESENTS FOCUSER WITH WIRE DIAMETER = 0.28 mm. B) REPRESENTS FOCUSER WITHE WIRE DIAMETER = 0.50mm. C) REPRESENTS FOCUSER WITH WIRE DIA. = 0.57mm.

where $P(\nu)$ is the energy per unit volume per unit bandwidth, at a frequency ν

B_{21} is the probability for a stimulated transition from the upper to lower energy state.

The Q factor is defined as follows

$$Q = \frac{2\pi\nu \cdot \text{Energy stored}}{\text{power lost}}$$

$$Q = \frac{2\pi\nu \cdot V \cdot P(\nu) \cdot \Delta\nu}{\text{power lost}} \tag{4.2}$$

where V = volume of the cavity, $\Delta\nu$ = half the line width of the molecular bandwidth.

For oscillation the condition is

$$\text{Power lost} = \text{Power emitted}$$

$$N \cdot h\nu \cdot B \cdot P(\nu) = \frac{2\pi\nu \cdot V \cdot P(\nu) \cdot \Delta\nu}{Q}$$

$$N = \frac{2\pi \cdot V \cdot \Delta\nu}{h\, Q\, B} \tag{4.3}$$

Now $N = N't'$ where N' is the molecular flux (number of molecules per unit time), and t' is the transit time through the cavity.

$$N' = \frac{2\pi\, N\, \Delta\nu}{h\, Q\, B\, t'} \tag{4.4}$$

From the Uncertainty Principle, $\Delta E \cdot \Delta t = h$, it follows that $\Delta\nu = \frac{v}{L}$, where v is the velocity of the molecules, and L is the length of the cavity. By substituting the value of $\Delta\nu$ and $\Delta t' = \frac{L}{v}$ in the equation (4.4), N' becomes

$$N' = \frac{2\pi \cdot A \cdot v^2}{h \cdot Q \cdot L \cdot B} \tag{4.5}$$

By substituting the value of $B = \frac{8\pi^3\mu^2}{3h^2}$ in equation (4.5), N' becomes

$$N' = \frac{h\nu^{\,2}\, A}{4\pi^2\, \mu_{12}^2\, LQ} \tag{4.6}$$

since $\mu_{12}^{\,2} = \frac{\mu_x^2}{3} + \frac{\mu_y^2}{3} + \frac{\mu_z^2}{3}$; $\mu_x = \mu_y = \mu_z = \mu$

where $\mu_{x,y,z}$ = components of the matrix dipole moment

$$\mu_{12}^2 = \frac{\mu^2}{3} \quad \text{or} \quad \mu_{12} = \frac{\mu}{\sqrt{3}}$$

N' in equation (4.6) represents the minimum number of upper energy state molecules entering the cavity per second to sustain oscillation.

A is the cross sectional area of the cavity,

V is the mean molecular velocity of the molecular beam,

h is the Planck's Constant,

L is the cavity length,

Q is the cavity quality factor,

and μ_{12} is the induced dipole moment.

This result is identical to that obtained by a more rigorous method (Shimoda et al., 1956). By using $v = 7 \times 10^4$ cm/sec, $h = 6.625 \times 10^{-27}$ erg.sec, L = 10.8 cm, Q = 6050, J = K = 3, $M_J = \sqrt{7}$, $\mu_0 = 1.47 \times 10^{-18}$ e.s.u, $\mu_{12} = \mu_0 \frac{M_J K}{J(J+1)} = 9.723 \times 10^{-19}$ e.s.u., and $A = (0.45)^2 \pi = 0.636$ cm^2 where 0.45 cm is the radius of the cavity used in the work described in this thesis.

A typical value for N' for J = K = 3 line NH_3 molecules is 9.7×10^{11} molecules/sec. Since only 3% of the total beam is in the upper energy state of J = K = 3 transition, and the efficiency of state selection is ≈ 1%, then the actual value for N' is only 0.03% of the actual flux required. Thus the total beam flux of the order of 3×10^{15} molecules/sec.

The frequency of oscillation varies as a function of the following principal parameters (Barnes, 1959): a) the nozzle source pressure, b) the voltage applied to the focuser, and c) the cavity tuning.

Because of these and other frequency effects, the molecular beam maser oscillator has been used as a secondary rather than a primary

standard of frequency.

Shimoda et al. (1956) calculated the amplitude of oscillation as a function of the molecular beam intensity and obtained the following expression

$$\frac{N}{N'} = \frac{\theta^2}{\sin^2\theta} \qquad (4.7)$$

where θ is the amplitude of oscillation

N' is the number of molecules required to build up oscillation

and N is the number of molecules entering the cavity per unit time.

If the pressure behind the beam source is kept constant, then the number of molecules entering the cavity is approximately proportional to the square of the voltage applied to the focuser, (Gordon, 1955; Gordon et al., 1955). Experimental results given by Shimoda et al. (1956) shows that the threshold number of molecules N' for the E_{010} mode was smaller by about three times than that for the H_{011} cavity.

By the use of a single beam maser, Shimoda (1958) studied the relation between the oscillation amplitude and the voltage applied to aquadrupole rod type of focuser. This experiment permits an investigation of the focusing properties of the state selector above the threshold oscillation. Studies of the focusing properties of a state selector at voltages too low to sustain an oscillation may be carried out by the use of two head on beams (Shimoda, 1966), one of which is operated normally at high voltage to produce maser oscillation, and the other is operated at low voltages required for the study of its state selection properties.

In this thesis, experiments have been carried out using the maser oscillation sustained by one beam to act as a detector of an absorptive

second beam. Details are given in section (6.2).

Multiple hole nozzles were used in conjunction with the molecular beam maser. The threshold of oscillation using a ring focuser with the parameters given in table (3.2), was dropped by a factor of approximately 1 kV per hole. Fig (4.11) illustrates the experimental results obtained with an increasing number of holes.

It is clear that the drop in the oscillation threshold voltage is due to the increasesin the intensity of the molecular beam with the increased number of holes. Clearly there must be the maximum possible number of holes on the account of scattering.

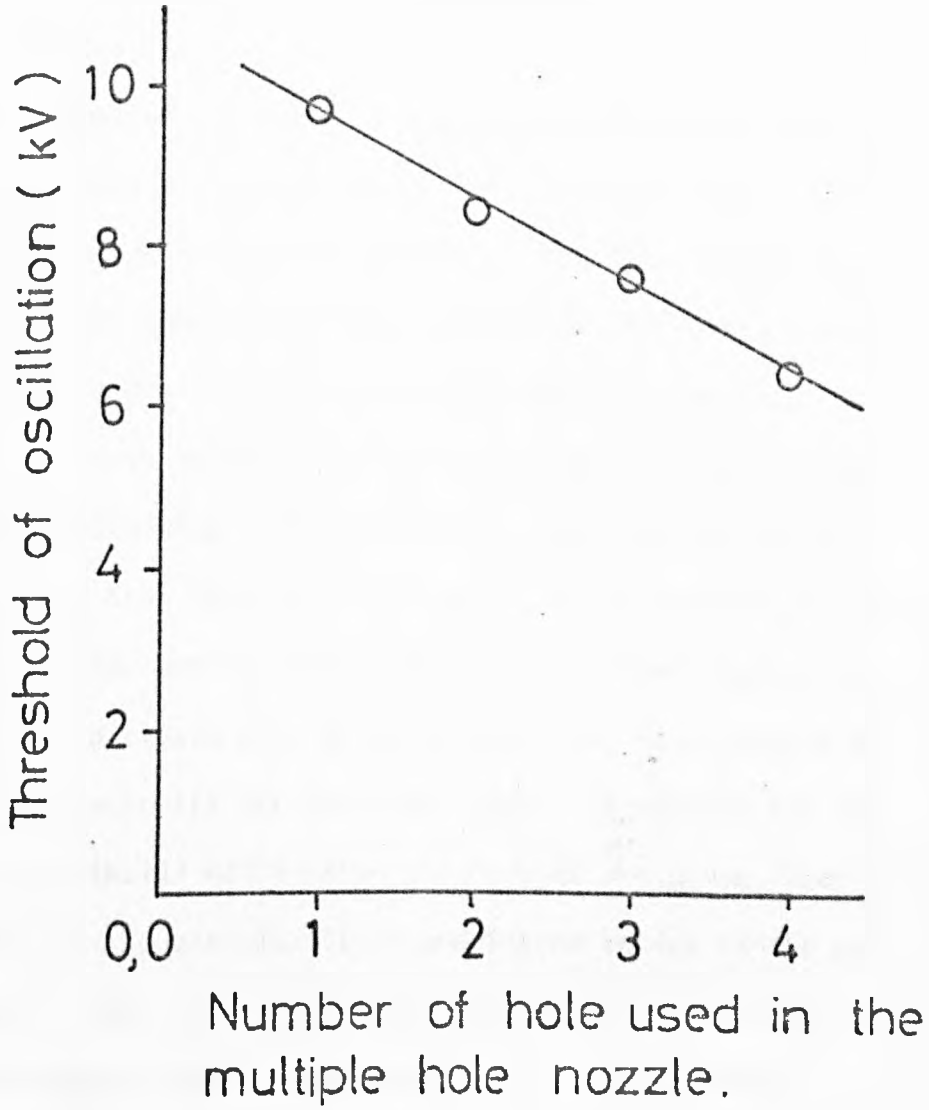

FIGURE (4.11) RELATION BETWEEN THE THRESHOLD OF OSCILLATION AND NOZZLE HOLE NUMBER.

CHAPTER 5

NEW SCHEMES AND METHODS OF STATE SELECTION

5.1 Introduction

In this chapter two types of focuser are discussed theoretically and experimentally in some detail. These are the ring state selector and single wire helix types of focuser. The first of these, the ring focuser, has been recognised to be useful for state selection of molecules with a positive induce dipole moment, in addition to its usual role of state selection of molecules with an induced dipole moment of opposite sign. The potential, the electric field and force equations have been derived from which the trajectories are calculated for the ammonia molecule in the J = K = 3 inversion state.

Secondly, a single wire helix focuser, has been studied experimentally and theoretically for the first time. Equations for the potential both inside and outside the focuser are given, from which the equation of the electric field and forces acting on the molecules are derived. From these results the trajectories of ammonia molecules in the J = K = 3 inversion state are calculated.

5.2 The theory of the negative Stark slope ring focuser

Calculations are given here for the potential outside a ring capacitor used as a focusing system for a molecular beam. The analysis is developed from that given previously by Shcheglov (1961).

The ring capacitor consists of a large number of thin coaxial metallic rings as shown in fig (5.1). Opposite potentials $+\phi_o$ and $-\phi_o$ are carried by neighbouring rings. Since the electrode system has axial symmetry, it is natural to use cylindrical system coordinates(P, Z, θ). The Laplace equation in the cylindrical coordinate system for ($P \geq P_o$) in the presence of axial symmetry has the following form which is valid for all values of P.

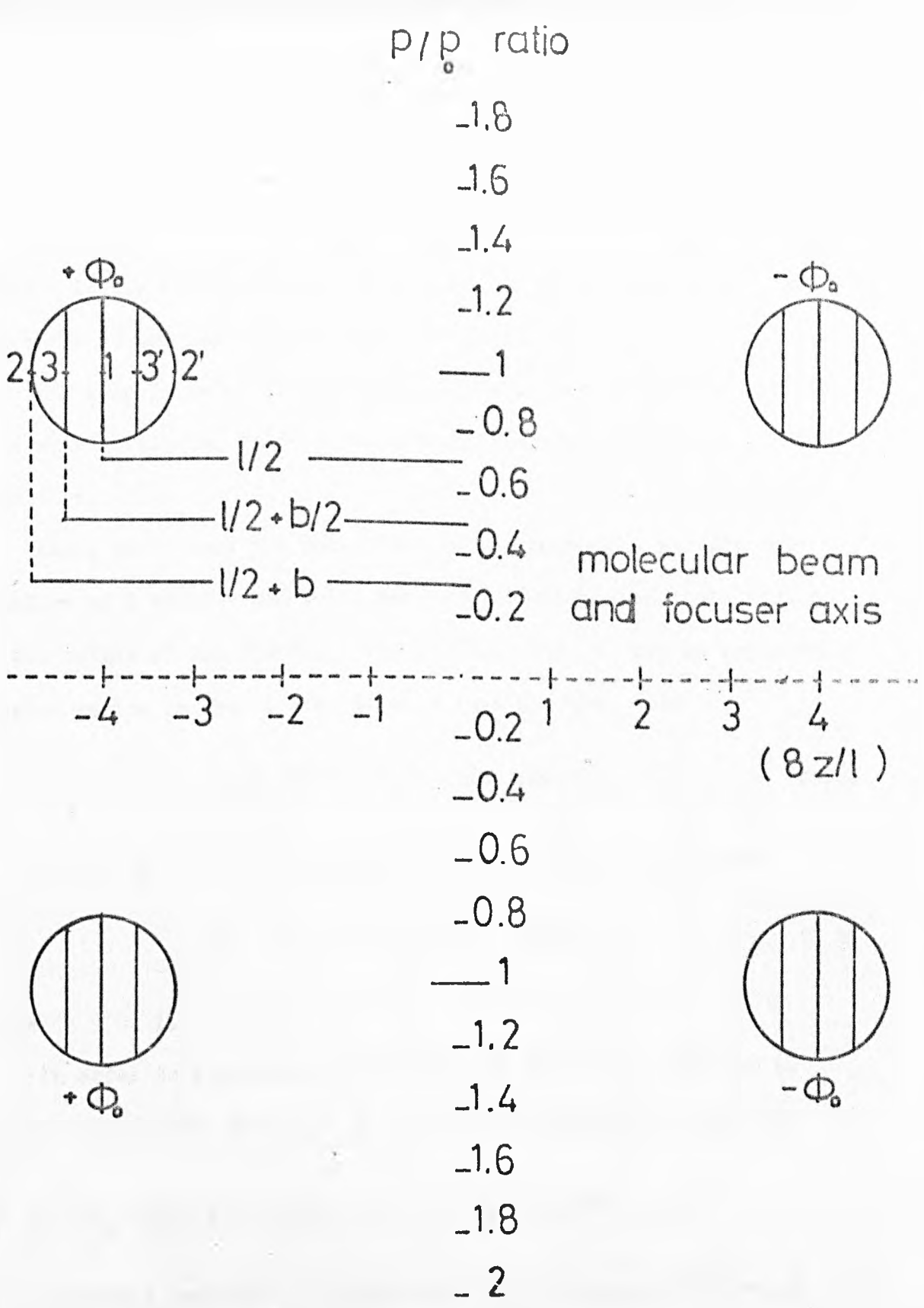

FIGURE (5.1) CROSS SECTION OF ADJACENT ELEMENTS OF A RING FOCUSER IN A PLANE CONTAINING THE FOCUSER AND MOLECULAR BEAM AXIS.

$$\frac{1}{P}\frac{\partial}{\partial P}\left(P\frac{\partial \phi}{\partial P}\right) + \frac{\partial^2 \phi}{\partial Z^2} = 0 \qquad (5.1)$$

where P is the radial distance from the focuser axis, ϕ is the potential at any point at any part in space.

For simplicity of the calculation the number of the rings is to be assumed infinite, in order to neglect the edge effects of the ring capacitor.

Along the Z-axis the potential $\phi(P, Z)$ becomes a periodic odd function of Z about a mid point between two successive rings chosen as the origin of the Z-axis. The function $\phi(P, Z)$ can be expanded as a Fourier series in the Z direction, with sine terms only

$$\phi(P, Z) = \sum_k \phi_k(P) \sin (k\pi Z/l) \qquad (5.2)$$

According to general Fourier theory, equation (5.2) becomes

$$\phi(P) = \frac{2}{l} \int_0^l \phi(P. Z) \sin (k\pi Z/l)\, dz \qquad (5.3)$$

where (k = 0, 1, 2, 3 ...)

In order to determine $\phi_k(P)$, equation (5.1) is multiplied by $\frac{2}{l}$. sin $(k\pi Z/l)$ dz (k = 1, 2, 3 ..) and after integration becomes

$$\frac{2}{l}\int_0^l \frac{1}{P}\frac{\partial}{\partial P}\left(P\frac{\partial \phi}{\partial P}\right) \sin\left(\frac{k\pi Z}{l}\right) dz + \frac{2}{l}\int_0^l \frac{\partial^2 \phi}{\partial Z^2} \sin\left(\frac{k\pi Z}{l}\right) dz = 0 \qquad (5.4)$$

by integrating equation (5.4) successively by parts, and by using the fact the potential function $\phi(P, Z)$ vanishes in the Z plane, where $Z = \pm l_n$ (n = 0, 1, 2, ..) then the modified Bessel function

$$\frac{1}{P}\frac{d}{dP}\left(P\frac{d\phi_k}{dP}\right) - \left(\frac{k\pi}{l}\right)^2 \phi_k = 0 \qquad (k = 1, 2, 3 ..) \qquad (5.5)$$

The general integral of the equation (5.5) given by

$$\phi_k(P) = A_k I_o\left(\frac{k\pi P}{l}\right) + B_k K_o\left(\frac{k\pi P}{l}\right) \qquad (5.6)$$

Here $I_o\left(\frac{k\pi P}{\ell}\right)$ is the Bessel function of zero order of pure imaginary argument, and $K_o\ (k\pi P/\ell)$ is the Bessel function of zero order and pure imaginary argument. If this expression for potential is to be valid outside the electrode ring diameter to ∞ then $A_k\ I_o\ (k\pi P/\ell)$ must be equal to zero since $I_o\ (k\pi P/\ell) \to \infty$ as $P \to \infty$.

The potential $\phi(P, Z)$ must satisfy the boundary condition in which the electric field has only a radial component in the plane $Z = \pm\ (2n + 1)\ \frac{\ell}{2}$ $(n = 0, 1, 2\ ..\ )$ which means that $\frac{\partial \phi}{\partial Z} = 0$. This condition is satisfied if $\cos[\ (2n + 1)\pi/2] = 0$ for any integral, with $K = 2n + 1$ $(n = 0, 1, 2\ ..\ )$. Thus from equation (5.2), the electrostatic potential of a condenser consisting of a large number of rings, $(P > P_o)$ is given by

$$\phi(P.\ Z) = \sum_{n=0}^{\infty} B_n\ K_o\ [\ \frac{(2n+1)\pi P}{\ell}\ ]\ \sin[\frac{2n+1}{\ell}\ \pi Z] \qquad (5.7)$$

where

B_n is the coefficient determined by the boundary conditions and is a rapidly decreasing function of the index n.

Z is the distance along focuser axis

P_o is the radius of the ring

P is the radial distance from the focuser axis

ℓ is the distance between rings

$K_o(x)$ is the Bessel function of zero order and pure imaginary argument.

To determine the coefficients B_n, which satisfy the boundary value problem, the equation (5.7) is used to find an approximate solution. For simplicity the thickness of the ring is assumed to be sufficiently small, for which $2b \ll P$, $2b \ll P_o$, $2b \ll \ell$ ($2b$ = thickness of the ring, ℓ = ring separation, P_o = radius of the ring system, or the radial distance between the ring and the focuser axis (Z axis)). In equation (5.7) if all the terms for which $n > 0$

are neglected, only the first three harmonic terms are used. Then

$$\phi\ (P,\ Z) = \sum_{n=0}^{2} B_n\ K_o\ [\ 2n+1]\ \pi P/l]\ \sin\ [\ (2n+1)\pi Z/l]$$

where n = 0, 1, 2 , then

$$\phi\ (P,\ Z) = B_o\ K_o\ [\ \pi P/l]\ \sin\ (\pi Z/l) + B_1\ K_o\ (3\pi P/l)\ \sin\ (3\pi Z/l)$$

$$+ B_2\ K_o\ [\ 5\pi P/l]\ \sin\ (5\pi Z/l) \qquad (5.8)$$

The potential $+\phi_o$ on the points 1, 2, 3 have the following coordinates (as shown in fig (5.1))

point 1 $\quad Z = \frac{l}{2} \qquad P_1 \geq P_0$

point 2 $\quad Z = \frac{l}{2} + b \qquad P_1 \geq P_0$

point 3 $\quad Z = \frac{l}{2} + \frac{b}{2} \qquad P_1 \geq P_0$

by introducing the following notation

at point 1 $\quad m_0 = B_o K_o\ (\frac{\pi P_1}{l})$

point 2 $\quad m_1 = B_1\ K_0\ \frac{(3\pi P_1)}{l}$

point 3 $\quad m_2 = B_2\ K_0\ (\frac{5\pi P_1}{l})$

Then the following system of equations are obtained:

$$\phi_o = m_o - m_1 + m_2\ ;$$

$$\phi_o = m_o \cos\ (\pi b/l) - m_1 \cos\ (3\pi b/l) + m_2 \cos\ (5\pi b/l)\ , \qquad (5.9)$$

$$\phi_o = m_o \cos\ (\pi b/2l) - m_1 \cos\ (3\pi b/2l) + m_2 \cos\ (5\pi b/2l).$$

The potential automatically assumes the value $+\phi_o$ at the points 2' , 3' with the following coordinates;

point 2' $\quad Z = l/2 - b \qquad P_1 \geq P_0$.

point 3' $\quad Z = l/2 - b/2 \qquad P_1 \geq P_0$.

Substituting in equation (5.9) the cosines by the corresponding Taylor series: $\cos x = 1 - \frac{x^2}{2!} + \frac{x^2}{4!}$ (by neglecting the third term of

the Taylor series), the following values are obtained.

$$m_0 = 1.2\ \phi_0 ,$$

$$m_1 = 0.19\ \phi_0 ,$$

$$m_2 = -0.01\ \phi_0 .$$

Consequently the amplitude of the harmonics have the following values

$$B_0 = \frac{1.2\ \phi_0}{K_0(\pi P_1/\ell)} ,$$

$$B_1 = \frac{0.19\ \phi_0}{K_0(3\pi P_1/\ell)} ,$$

$$B_2 = \frac{-0.01\ \phi_0}{K_0(5\pi P_1/\ell)} ,$$

If the third harmonic term B_2 is neglected because it is small, equation (5.8) becomes

$$\phi(P, Z) = B_0 K_0 [\pi P/\ell] \sin(\pi Z/\ell) + B_1 K_0 (3\pi P/\ell) \sin(3\pi Z/\ell). \quad (5.10)$$

by substituting the value B_0, B_1 and by substituting $\phi_0 = \frac{U_0}{2}$ equation (5.10) becomes

$$\phi(P, Z) = \frac{1.2 \times \frac{U_0}{2}}{K_0(\pi P_1/\ell)} \cdot K_0 (\pi P/\ell) \sin(\pi 2/\ell) + \frac{0.19 \times \frac{U_0}{2}}{K_0(3\pi P_1/\ell)} \cdot$$

$$K_0 (3\pi P/\ell) \sin(3\pi Z/\ell) .$$

or

$$\phi(P, Z) = \frac{0.6\ U_0}{K_0(\pi P_1/\ell)} K_0 (\pi P/\ell) \sin(\pi Z/\ell) + \frac{0.1\ U_0}{K_0(3\pi P_1/\ell)} \cdot$$

$$K_0 (3\pi P/\ell) \sin(3\pi Z/\ell) . \quad (5.11)$$

The modulus of the electric field intensity is determined by

$$E = \left[\left(\frac{\partial\phi}{\partial P}\right)^2 + \left(\frac{\partial\phi}{\partial Z}\right)^2\right]^{\frac{1}{2}}$$

$$E = 0.3\pi \frac{U_0}{l} \left\{ \left[2\frac{K_0(\pi P/l)}{K_0(\pi P_1/l)} \sin\frac{\pi Z}{l} + \frac{K_1(3\pi P/l)}{K_0(3\pi P_1/l)} \sin\frac{3\pi Z}{l}\right]^2 \right.$$

$$\left. + \left[2\frac{K_0(\pi P/l)}{K_0(\pi P_1/l)} \cos\frac{\pi Z}{l} + \frac{K_0(3\pi P/l)}{K_0(3\pi P_1/l)} \cos\frac{3\pi Z}{l}\right]^2 \right\}^{\frac{1}{2}} \qquad (5.12)$$

Fig (5.2) illustrates the computed results and shows the dependence of the modulus of the electric field intensity on the variation of the $Z(x\frac{8}{l})$-coordinate in the range $(-l/2 \leq Z \leq l/2)$, for fixed values of P and for the case when $P_0 = l$. It is seen from the graph that the magnitude of the modulus drops to 1/3 maximum value just when $P = 1.2\ P_0$.

Fig (5.3) shows the computed plot of the dependence of the modulus of the intensity E on the distance from the P axis $(P \geq P_0)$ at fixed values of Z. It is seen that the magnitude of the modulus E drops to a 1/3 maximum value just when $P = 1.45\ P_0$.

The value of the electric field E at $P = P_0 = l$, averaged over the period Z calculated from the fig (5.2), is equal to

$$\bar{E}_m = \tfrac{1}{2}\left[E_{max}(P_0, Z) + E_{min}(P_0, Z)\right]$$

where $E_{min} = 1.16\ U_0/l$ and $E_{max} = 2.82\ U_0/l$ and therefore $\bar{E}_m = 2.08\ U_0/l$.

Trajectory of the ammonia molecules passing outside the ring focuser

The position of molecules at the entrance of the ring focuser may be described by the following equations.

$Z_0 = 0$

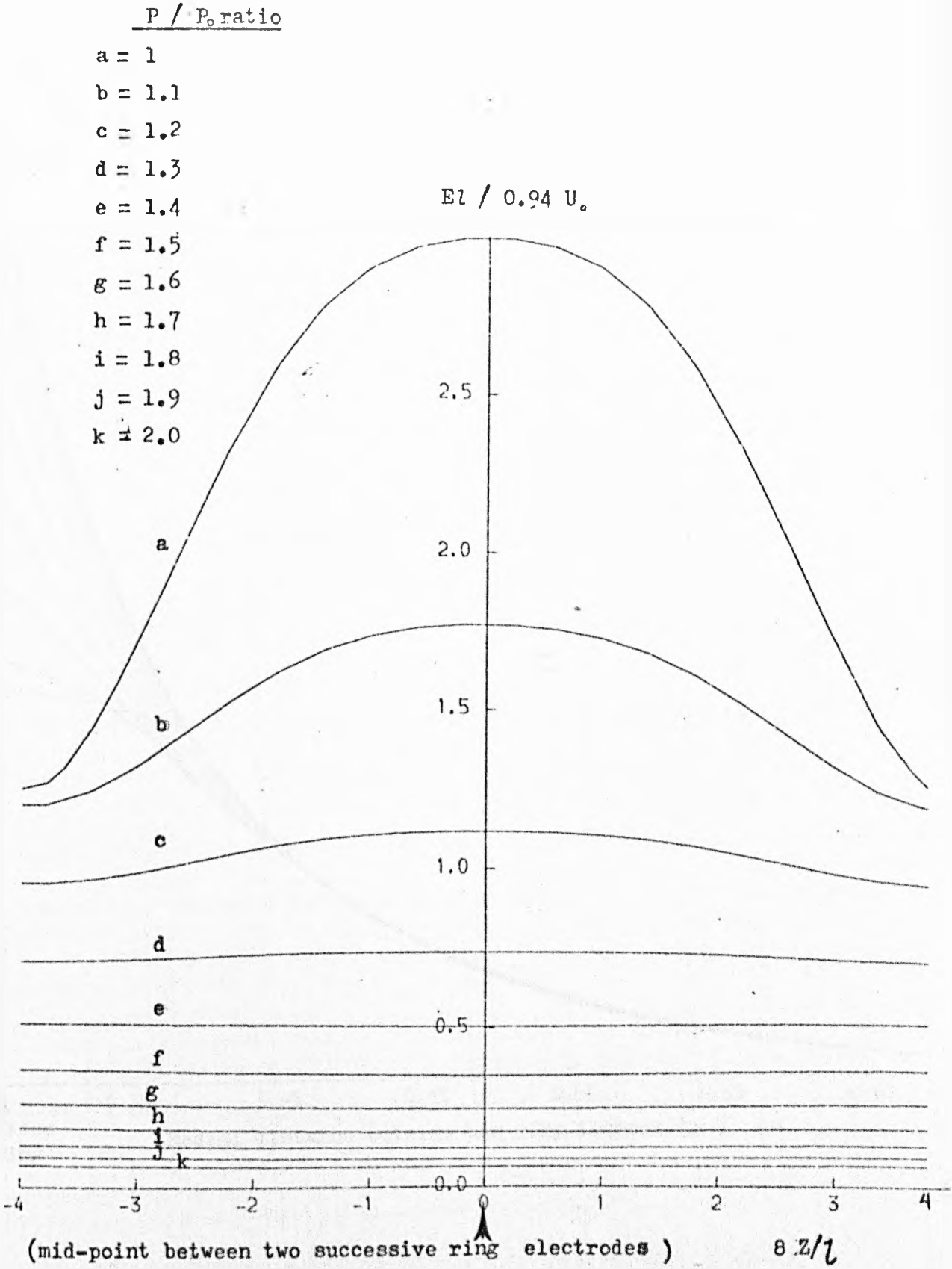

FIGURE(5.2) COMPUTED PLOT SHOWING THE DEPENDENCE OF THE MODULUS OF THE INTENSITY OF THE ELECTRIC FIELD E OUTSIDE A RING FOCUSER ON Z ($-l/2 \leq Z \leq l/2$) FOR FIXED VALUES OF P ($|Z| \leq l/2$, $P_0 = l$). ZERO IN THE ($8\,Z/l$) - AXIS REPRESENTS THE MID - POINT BETWEEN TWO SUCCESSIVE RING ELECTRODES.

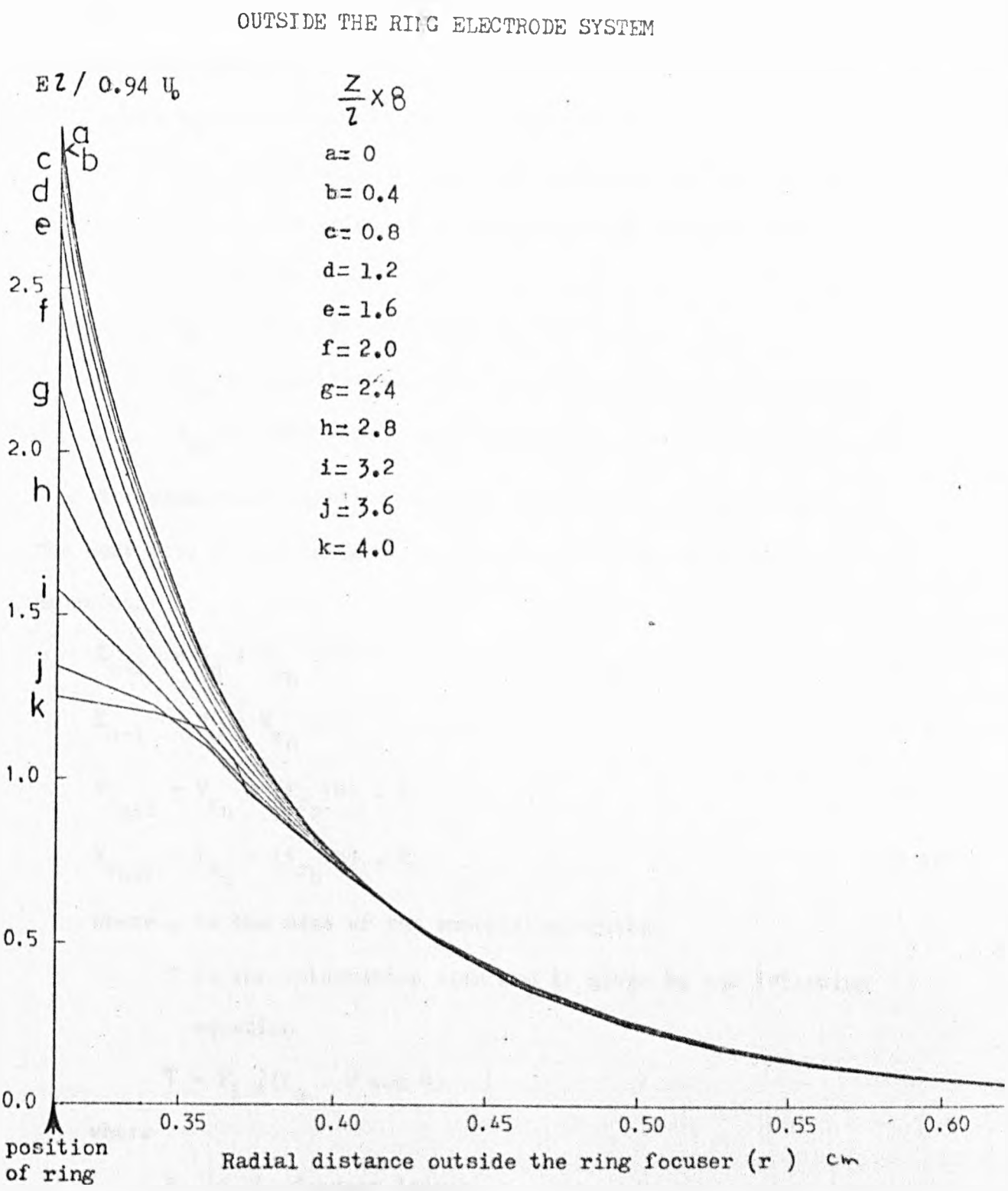

FIGURE (5.3) COMPUTED RESULTS GIVING THE DEPENDANCE OF THE MODULUS OF THE INTENSITY OF THE ELECTRIC FIELD OUTSIDE THE RING FOCUSER ON THE RADIAL DISTANCE r AT A FIXED VALUE OF Z ($P \gg P_o = l$).

$$r_0 = N_F \cdot \tan \beta$$

$$V_{r0} = V \cdot \sin \beta$$

$$V_{z0} = V \cdot \cos \beta$$

where N_F is the nozzle-focuser separation

β is the angle between the molecules and the focuser axis

V is the velocity of the molecules emerging from the nozzle source

Z_0 is the origin of the focuser

V_{r0} is the initial radial molecular velocity component

V_{z0} is the initial axial molecular velocity component

The prediction equations for the position of the molecules at the next step of the integration was described by the following equations

$$Z_{n+1} = Z_n + V_{z_n} \cdot T \tag{5.13}$$

$$R_{n+1} = R_n + V_{r_n} \cdot T \tag{5.14}$$

$$V_{r_{n+1}} = V_{r_n} + (F_{r_n}/m) \cdot T \tag{5.15}$$

$$V_{z_{n+1}} = V_{z_n} + (F_{z_n}/m) \cdot H \tag{5.16}$$

where m is the mass of the ammonia molecules

T is the integration step and is given by the following equation

$$T = F_l / (Z_a \cdot V \cos \beta)$$

where

F_l is the focuser length

Z_a is the number of the integration steps

F_r is the radial component of the electrostatic field

F_z is the axial component of the electrostatic force

The correction equation for the position of the molecules at the next step of integration is given by the following equation

$$Z_{n+1} = Z_n + (V_{z_n} + V_{z_{n+1}}) \cdot \frac{T}{2} \tag{5.17}$$

$$R_{n+1} = R_n + (V_{r_n} + V_{r_{n+1}}) \cdot \frac{T}{2} \tag{5.18}$$

$$V_{r_{n+1}} = V_{r_n} + [(F_{r_n} + F_{r_{n+1}}) / m] \cdot \frac{T}{2} \tag{5.19}$$

$$V_{z_{n+1}} = V_{r_n} + [(F_{r_n} + F_{r_{n+1}}) / m] \cdot \frac{T}{2} \tag{5.20}$$

When the molecules emerge from the focuser it is assumed that no further deflection forces are operative i.e. any force due to fringe field effect are neglected. The following equation shows the radial position of the molecules at the entrance of the cavity x cm away from the ring focuser

$$D_r = r_f + V_{r_f} \cdot \frac{x}{V \cos \beta} \tag{5.21}$$

where r_f is the final radial distance at the end of the ring focuser

V_{r_f} is the final radial component of velocity at the focuser exit.

The force equations, for both components F_r and F_z are given by the following equations

$$F_r = \mp q\,(E) \frac{\partial E^2}{\partial r} \tag{5.22a}$$

$$F_z = \mp q\,(E) \frac{\partial E^2}{\partial z} \tag{5.22b}$$

where $q\,(E) = [\mu_{12}]^2 / \left[\left(\frac{h\nu_0}{2}\right)^2 + (\mu_{12}E)^2\right]^{\frac{1}{2}}$

The negative and positive sign refer to the force effects upper and lower energy state ammonia molecules respectively.

Fig (5.4) shows the computed values of the radial gradient of the square of the electric field $\frac{\partial E^2}{\partial r}$ at fixed values of Z. The step in the graph is due to the sudden variation of the radial gradient as the radial distance increases outwards from the outside

OUTSIDE THE RING ELECTRODE SYSTEM

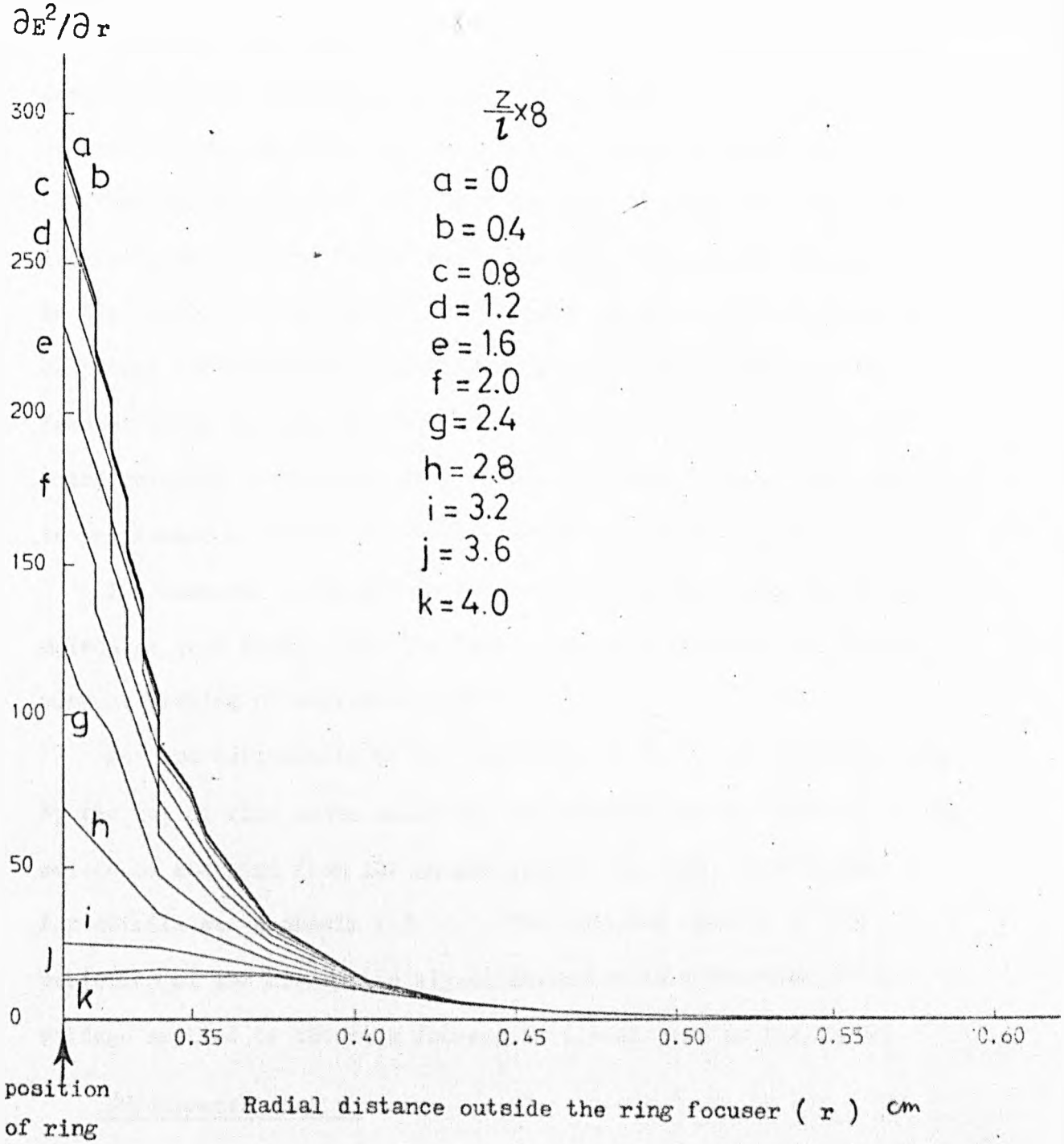

FIGURE (5.4) COMPUTED RESULTS GIVING THE RADIAL GRADIENT OF THE SQUARE OF THE ELECTRIC FIELD $\partial E^2/\partial r$ OUTSIDE THE RING FOCUSER AS A FUNCTION OF THE RADIAL DISTANCE r FOR A FIXED VALUE OF Z ($p \geqslant p_o = l$). THE SUDDEN STEP IN THE GRAPH IS DUE TO THE QUANTIZATION OF THE RADIAL DISTANCE INTO 10 INCREMENT STEPS.

ring electrode.

The first electrode of the ring focuser was filled with a beam stop to prevent the molecules from passing inside the state selector, in order to increase the intensity of the enhanced absorption signal.

The trajectories of the J = K = 3 ammonia molecules that pass initially outside and later inside the ring focuser are sketched in fig (5.8). Consequently the computer programme was adjusted to calculate the molecular trajectories point by point outside the focuser using the outside form of E, F_r, F_z ... etc. If the computed molecular trajectory goes inside the ring focuser, the computer is programmed to switch to the inside formula of E, F_r, F_z ... etc.

The computer programme was adjusted to account only for those molecules that emerge from the focuser and pass through the cavity without hitting or colliding with the walls.

For the calculation of the intensity of the state selected beam by the use of ring state selector, the Maxwellian distribution of the molecules emerging from the nozzle source was taken into account. For details see appendix (5). The computed results of the variation of the absorption signal intensity as a function of the voltage applied to the ring focuser is illustrated in fig (5.9).

Experimental set up

A four-hole nozzle was used as a beam source, in order to give a near approximation to an annular gas source. These nozzles were arranged on a pitch diameter circle of 2 mm, with each hole 0.09 mm diameter in a brass diaphragm 0.1 mm thick. These were supplied with ammonia gas at a pressure of up to 150 torr. The intense ammonia molecular beam so formed passed through an adjustable iris, typically 4 mm in diameter, situated between the nozzle and main chambers respectively. The efficiency of focusing and state selection of lower energy state (J = K = 3 inversion line) NH_3 molecules was

monitored via the microwave power absorption at 23.87 GHz in an E_{010} mode resonant cavity, positioned 16 mm downstream from the ring state selector. Superheterodyne detection was employed using a single klystron in which the exciting signal was one of the two sidebands produced by amplitude modulation at the intermediate frequency, of a portion of the local oscillator power.

Operation of the negative Stark slope ring state selector with an ammonia molecular beam (Al-Amiedy and Lainé, 1978) resulted in the production of a strong molecular absorption signal with associated hyperfine structure of the J = K = 3 inversion transition as shown in fig (5.5). In the absence of focusing, the absorption signal completely disappeared into the background noise of the detection system. If an 'enhancement factor' K is defined as the ratio of signal magnitude with state selection to that without, then even though an observable signal was not obtained in the absence of state selection, a lower limit of K can be given. When a beam stop was used (see fig (3.6)) to prevent molecules entering the ring array and the multiple hole nozzle-focuser separation 293 mm (position A in fig (5.6)) with an EHT of 30 kV, the 'enhancement factor' K was at least 30. Without the beam stop K was reduced to $\sim$ 20. Fig (5.7) shows the relative absorption signal as a function of focuser voltage. This reduction in K was a consequence of opposing radial deflections for molecules in the same inversion state passing inside and outside the system of ring electrodes. Indeed, when this focuser was placed much closer to the gas source without a beam stop, with a nozzle-focuser separation of 50 mm so that a larger fraction of the total beam flux passed through the focuser relative to that sheathing it (position B in fig (5.6)) only stimulated emission was detected in the microwave cavity. Further experiments carried out with the negative Stark ring focuser will be considered in detail in Chapter 6.

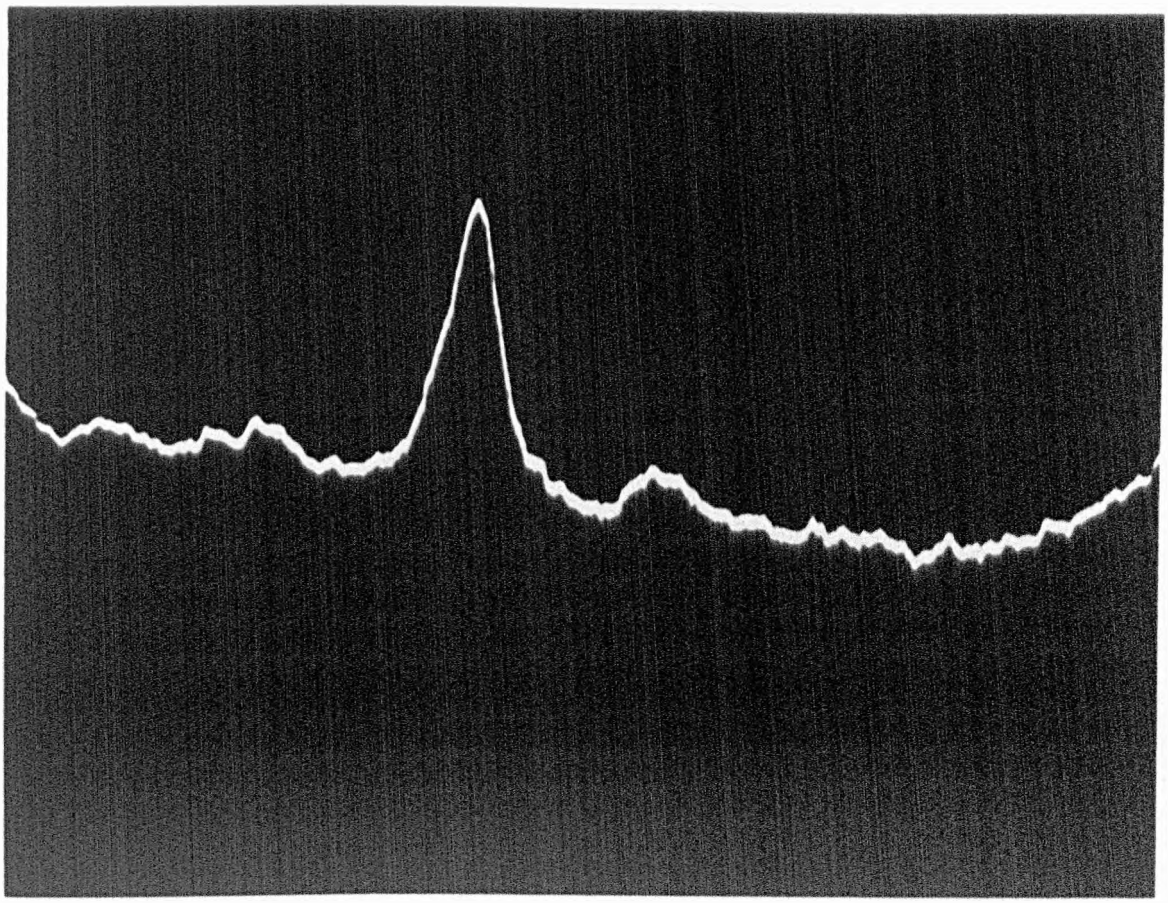

FIGURE (5.5) PHOTOGRAPH OF THE ABSORPTION SIGNAL ENHANCED BY THE RING FOCUSER OPERATED AT 30 kV, WITH MULTIPLE NOZZLE AND GAS PRESSURE OF 100 TORR.

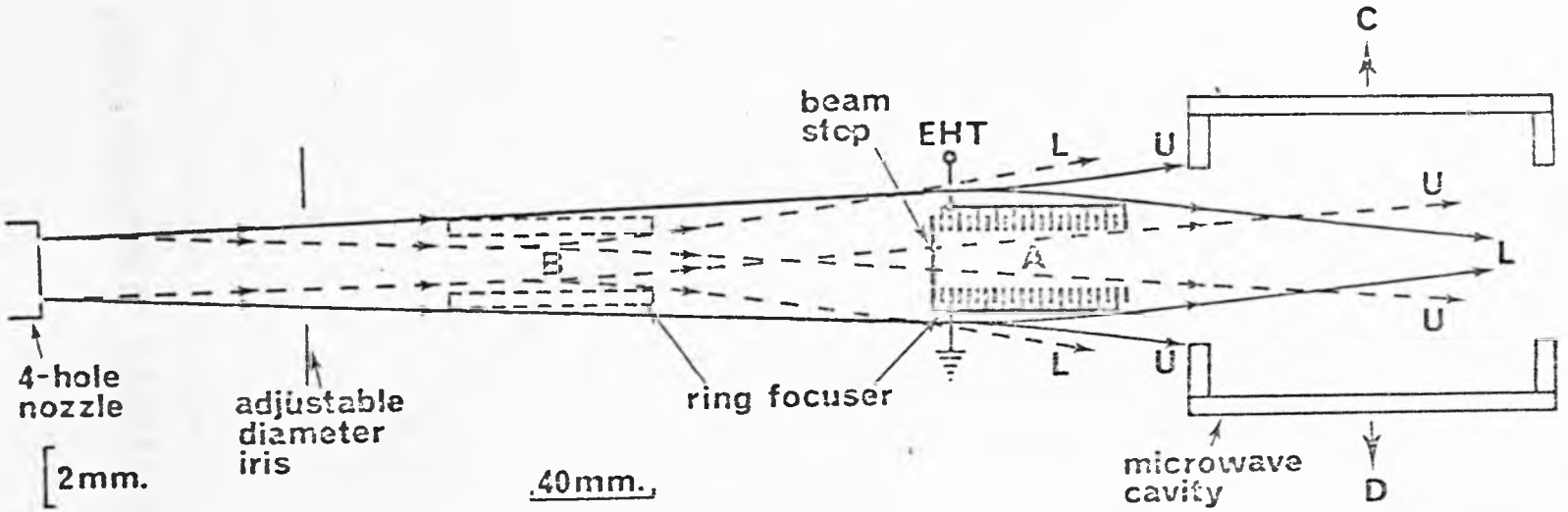

FIGURE(5.6) SCHEMATIC DIAGRAM OF MOLECULAR BEAM SYSTEM. A AND B REPRESENT THE ALTERNATIVE POSITIONS OF THE RING FOCUSER WITH AND WITHOUT BEAM STOP RESPECTIVELY. DEFLECTION TRAJETORIES OF UPPER AND LOWER ENERGY STATES AMMONIA MOLECULES ARE INDICATED AS U AND L RESPECTIVELY.

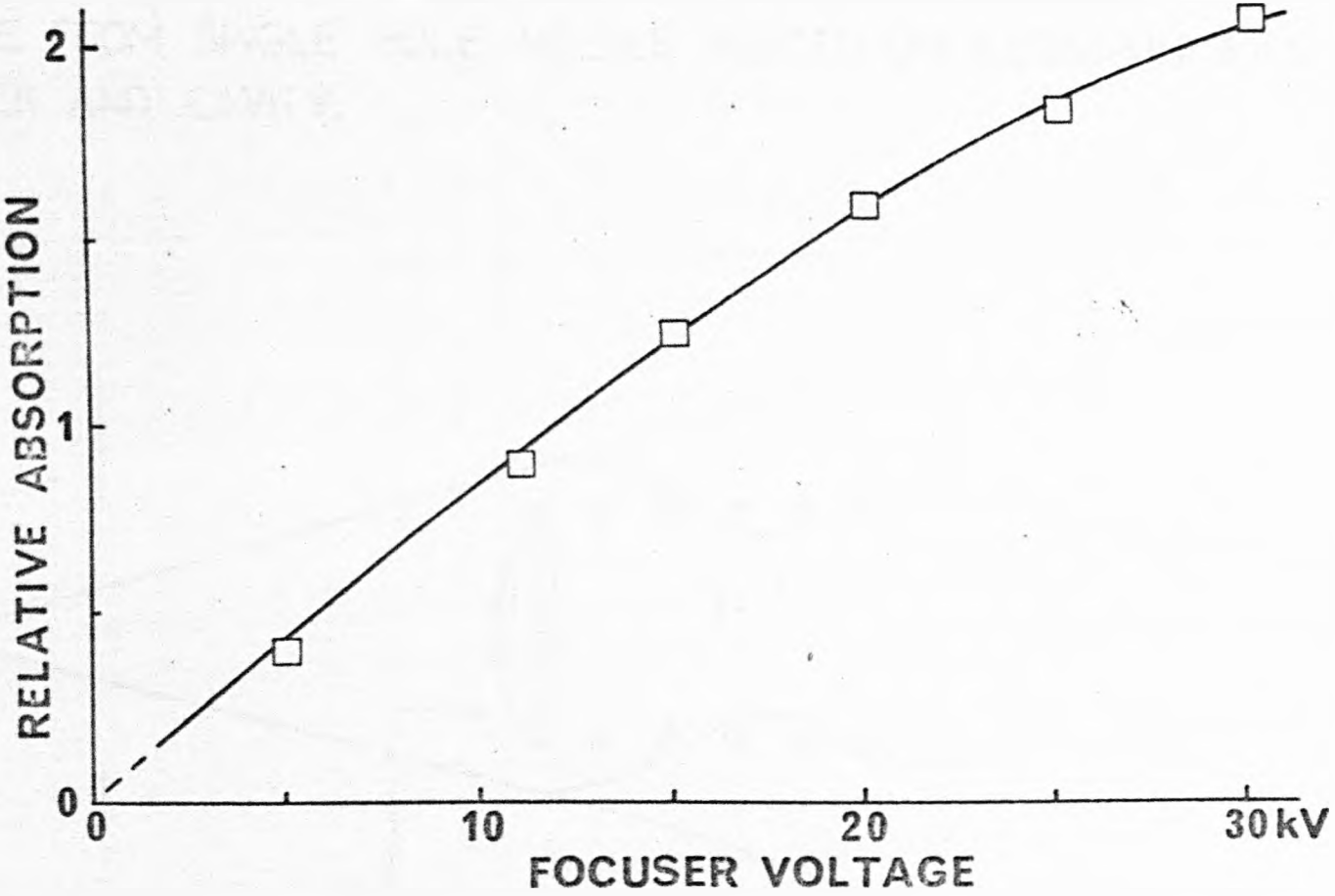

FIGURE (5.7) RELATIVE ABSORPTION SIGNAL AMPLITUDE AS A FUNCTION OF THE VARIATION OF THE VOLTAGE APPLIED TO THE NEGATIVE STARK SLOPE RING FOCUSER.

FIGURE (5.8) SPECIAL CASE TRAJECTORY FOR J=K=3 AMMONIA MOLECULES THAT PASS CLOSE TO THE OUTSIDE THE RING FOCUSER. THE MOLECULES EMERGE FROM SINGLE HOLE NOZZLE PLACED ON A COMMON AXIS WITH FOCUSER AND CAVITY.

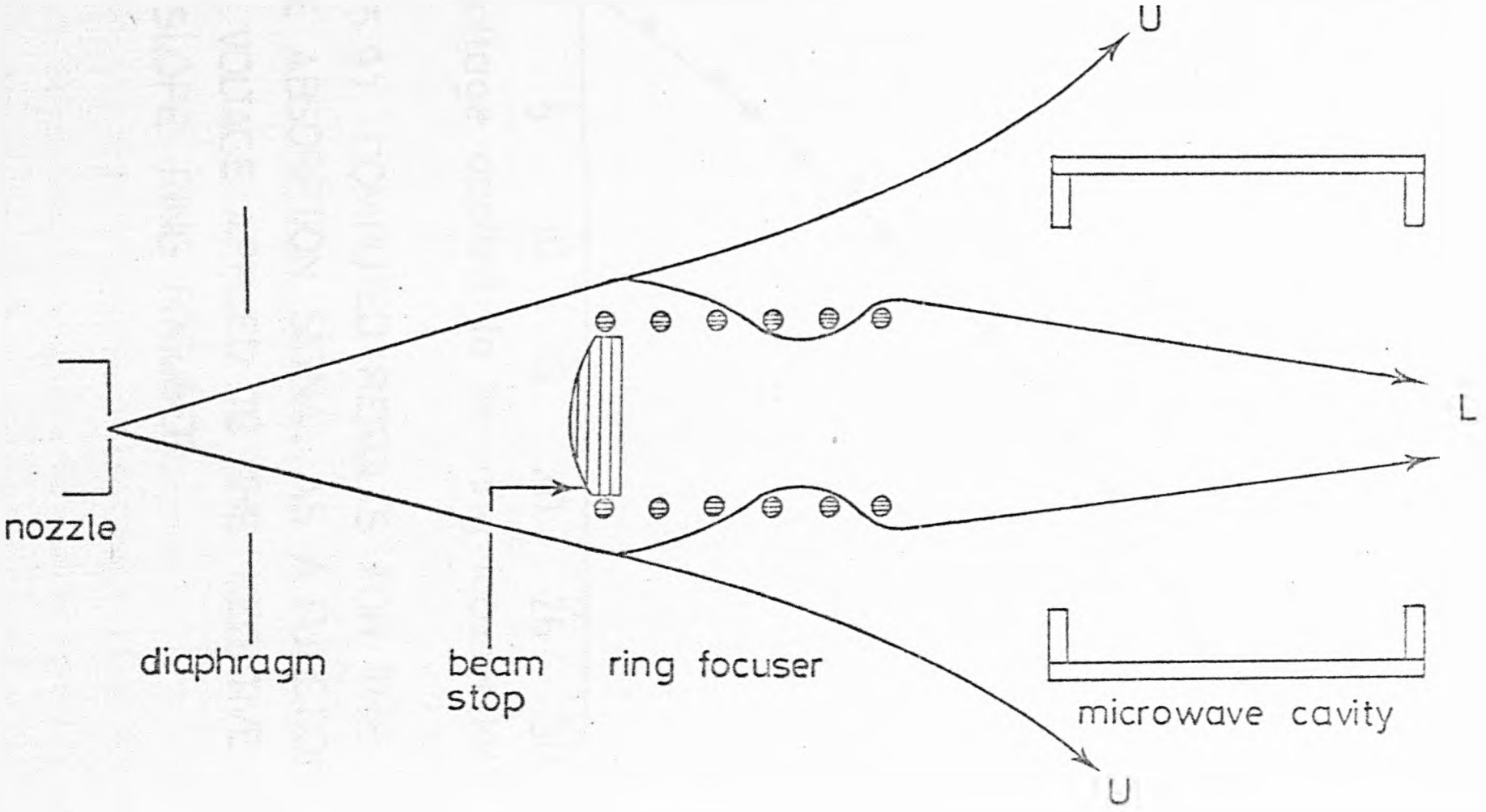

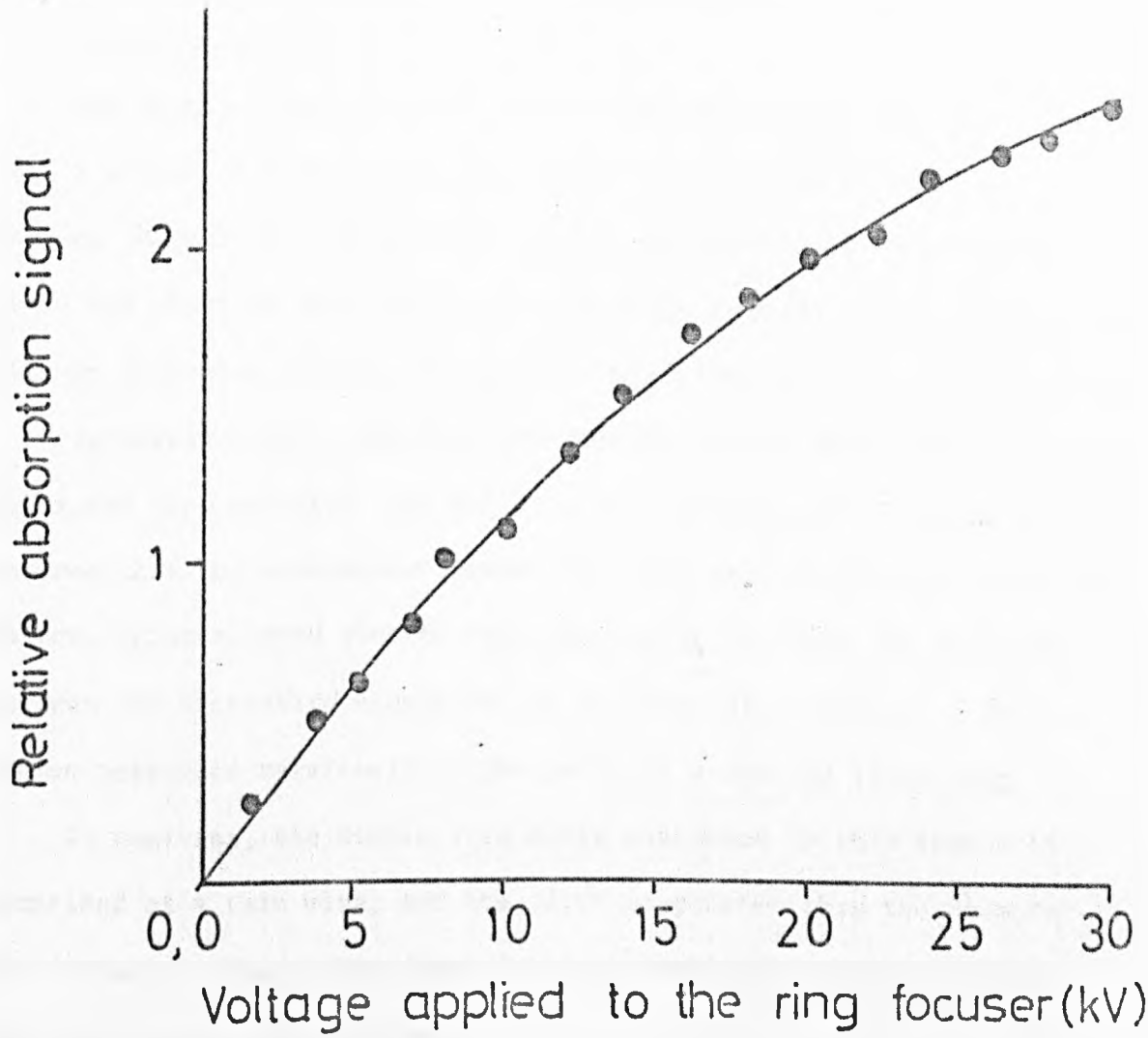

FIGURE(5.9) COMPUTED RESULTS FOR THE RELATIVE ABSORPTION SIGNAL AS A FUNCTION OF THE VOLTAGE APPLIED TO THE NEGATIVE STARK SLOPE RING FOCUSER.

In conclusion it was found that the experimental results in fig. (5.7) followed the same monotonic form as the theoretical results shown in fig (5.9).

5.3 The theory of the single wire helix focuser

Introduction

The single wire helix was used for the first time in conjunction with a molecular beam maser, to produce maser action with a beam passing through it. Anti-maser action (production of an absorptive beam) was obtained when the beam skimmed the outside of the helix only, with no molecules passing through the helix itself.

Igritskii (1961), Mednikov and Parygin (1963) used a tape bifilar helix and tape multipole helix. For the purposes of calculation they assumed that the separation between two successive helix electrodes was narrow, which allowed them to make the assumption that the potential between the successive electrodes has a linear distribution. This system possessed relatively large electrode width and little gap.

In contrast, the single wire helix discussed in this thesis is comprised of a thin wire, and the pitch is greater than the diameter of the focuser. Thus, this form of helix possessed relatively little electrode width and large gap.

The single wire helix, whether of finite or infinite length, has not received any previous theoretical or experimental treatments, in conjunction with space focusing and state selection of molecular beams. Both aspects have been investigated, and the results are presented in this section.

The theory of the single wire helix is developed here to yield the electric field, the force acting on molecules passing through it, and finally, the molecular trajectories.

Theory

In the single wire helix theory presented in this section, it is assumed that the helix is equivalent to a line of charge. The cylindrical coordinate used are defined in fig (5.10). The helix is assumed to extend to infinite length in both direction along the Z-axis. The physical helix would, of course be of limited length and wound with wire of small diameter.

It is convenient for the purpose of discussion to assume the system to be evaluated comprises a line of charge of identical shape to the single wire helix wound on imaginary cylinder surface. Now if the potential at various points on this surface is known, then it is possible to define the potential at a distance r away from the axis within an outer fixed potential coaxial cylindrical electrode.

In the single wire helix, it was assumed that charge was placed on an infinitesimally thin wire. The potential on the wire was then found, and by using Fourier analysis it was possible to calculate the electrostatic potential to a good approximation in the mid region of the length of the helix.

The radial direction from the helix is taken as r and the Z direction as that of the focuser axis. Consider a small length of element of the line charge equal to da at a distance a from the origin, and at a distance $\{l - a\}$ from any general point P as shown in fig (5.10).

The cylindrical coordinate parameters of the system are described as follows

$$Z_a = \frac{L\theta}{2\pi} ,$$

$$X_a = r \cos \theta ,$$

$$Y_a = r \sin \theta$$

where

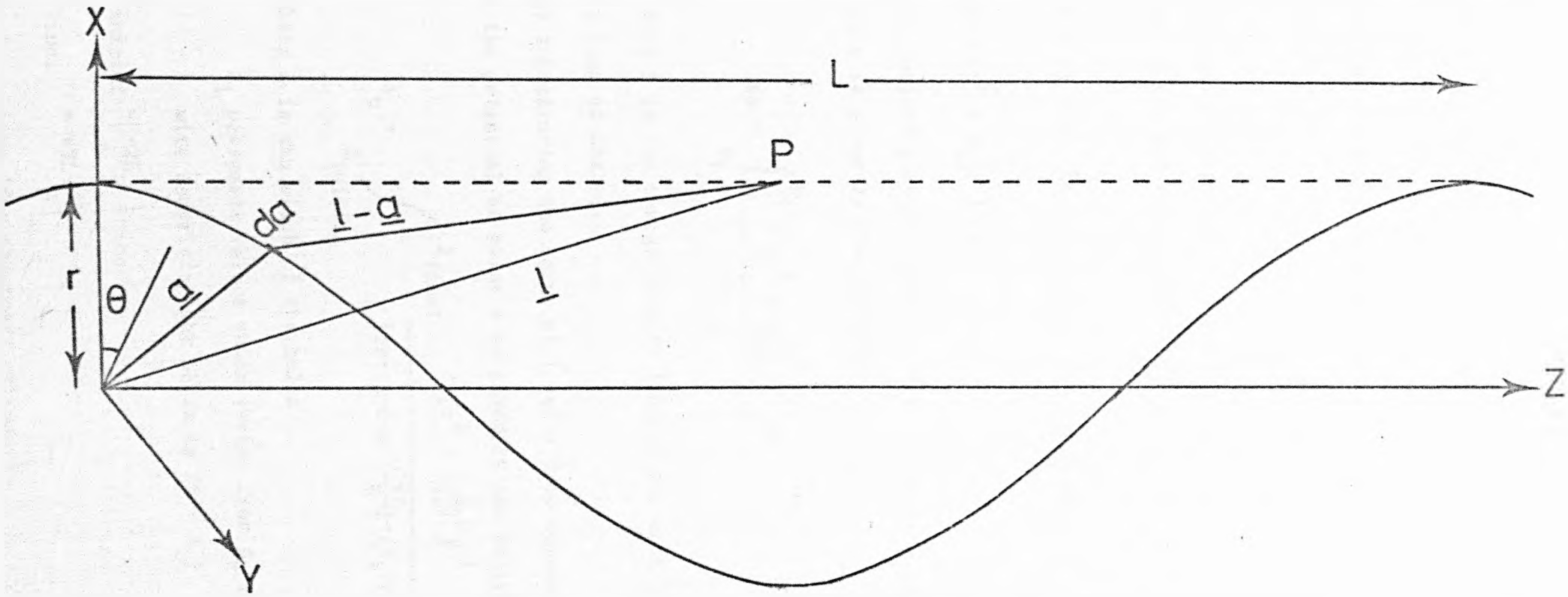

FIGURE (5.10) KEY PARAMETERS OF THE SINGLE WIRE HELIX FOCUSER.

L is the pitch of the helix

θ is the angle between the radial direction r and the x-axis (in the xy plane)

Now the vector ℓ can be written as

$$\ell = ri + zk \tag{5.23}$$

where

ℓ is a vector parallel to the z-axis

$$da = r\cos\theta\, i + r\sin\theta\, j + \frac{L\theta}{2\pi}\, k \tag{5.24}$$

and $$da = -r\sin\theta\, d\theta\, i + r\cos\theta\, d\theta\, j + \frac{1}{2\pi} d\theta\, k \tag{5.25}$$

or $$da = \{r^2 + (\frac{1}{2\pi})^2\}^{\frac{1}{2}}\, d\theta \tag{5.25a}$$

The potential at any general point lying in a line parallel to the z-axis is given by the following formula

$$\phi p = \int_{\theta_1}^{\theta_2} \frac{\delta\, \{r^2 + \frac{1^2}{(2\pi)^2}\}^{\frac{1}{2}}\, d\theta}{\ell - a} \tag{5.26}$$

where δ is the charge density (charge per unit length) of the uniform line of charge.

By substituting the value of ℓ and a from equations (5.23) and (5.24) the potential at point p is given by the following equation

$$\phi_p = \int_{Z_{initial}}^{Z_{final}} \frac{\delta \{r^2 + (\frac{L}{2\pi})^2\}^{\frac{1}{2}}}{\{2r^2(1-\cos(\frac{2\pi Z}{L}) - (Z_1 - Z)^2\}^{\frac{1}{2}}} \tag{5.27}$$

where L is the pitch of the helix

Z_1 possesses values which varies from B_r radius of the wire comprising the helix to $(L - B_r)$

$Z_{initial} = -2L$

$Z_{final} = +3L$

$r = r_1$ (for imaginary cylinder)

An odd number of turns, (in practice 5 is found to be convenient) is taken in order to have a symmetrical value of the potential about the mid region. This was done in order to get the potential for a given pitch. The potential is considered for a single pitch, by taking the contribution of several turns on either side into account.

In practice it was found that two turns on either side was sufficient. Other values of Z were tried, for example a helix consisting of 7 turns ($Z_{initial} = -3L$, $Z_{final} = +4L$). It was found that the potential distribution of the central pitch of this seven turn helix had approximately the same potential distribution of the five turn helix, shown in fig (5.11).

The range of Z is taken to include five turns only. Ideally the integration should run from $-\infty$ to $+\infty$ but for simplicity, only three integration terms for the five helix turns are taken. As a consequence of increasing the value of l, the value of δ decreased, in order to maintain ϕ_p in equation (5.27) equivalent to 1kV.

Equation (5.27) applies to the single wire helix focuser on the assumption that only a finite length of helix was taken into account, and that the helix could be represented by infinitesimally thin line of charge.

By using Simpson's rule (McCracken and Dorn 1964), which is one of the most widely known and used techniques in numerical integration, it is possible to find the coefficients of the potential equation. These will be given later.

The helix used possesses a pitch of 1.5cm. This is divided into 100 smaller intervals in order to integrate the function.

By setting the value of $\delta\{r^2 + (\frac{L}{2\pi})^2\}^{\frac{1}{2}}$ to 1, the function used in this procedure (5.27) becomes

$$f = \frac{1}{\{2r^2\ (1 - \cos\ (\frac{2\pi z}{L})) - (z_1 - z)^2\}^{\frac{1}{2}}} \qquad (5.28)$$

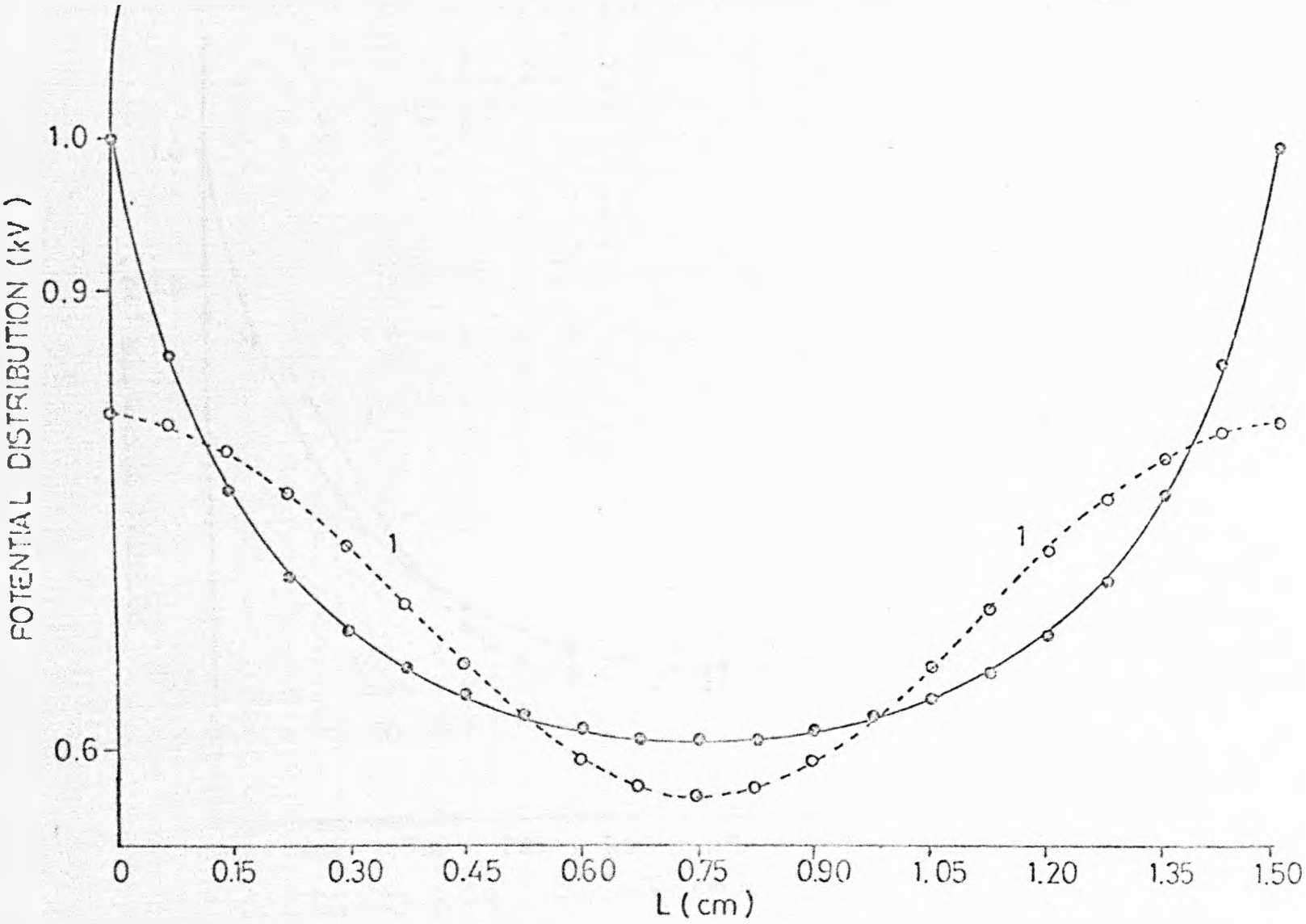

FIGURE(5.11A) REPRESENTATION OF THE POTENTIAL DISTRIBUTION BETWEEN TWO SUCCESSIVE PITCHES, THE DASHED LINE LABELLED 1 IS THE FOURIER COMPONENT OF THE POTENTIAL EQUATION, FOR A FIVE TURN HELIX $Z_{initial} = -2L, Z_{final} = 3L$.

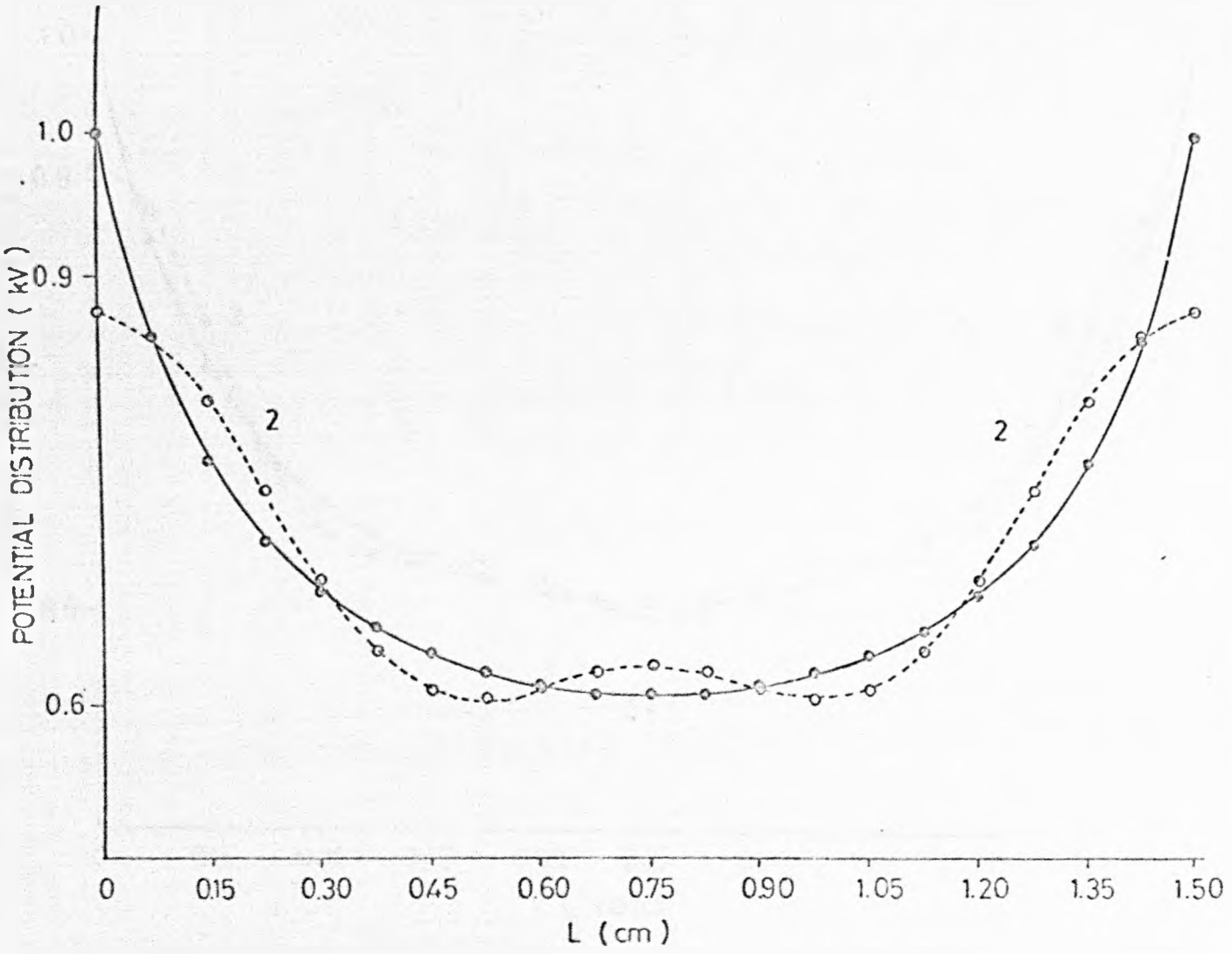

FIGURE(5.11B) REPRESENTATION OF THE POTENTIAL DISTRIBUTION BETWEEN TWO SUCCESSIVE PITCHES, THE DASHED LINE LABELLED 2 IS THE FOURIER COMPONENT OF THE POTENTIAL EQUATION, FOR A FIVE TURN HELIX $Z_{initial}=-2L, Z_{final}=3L$.

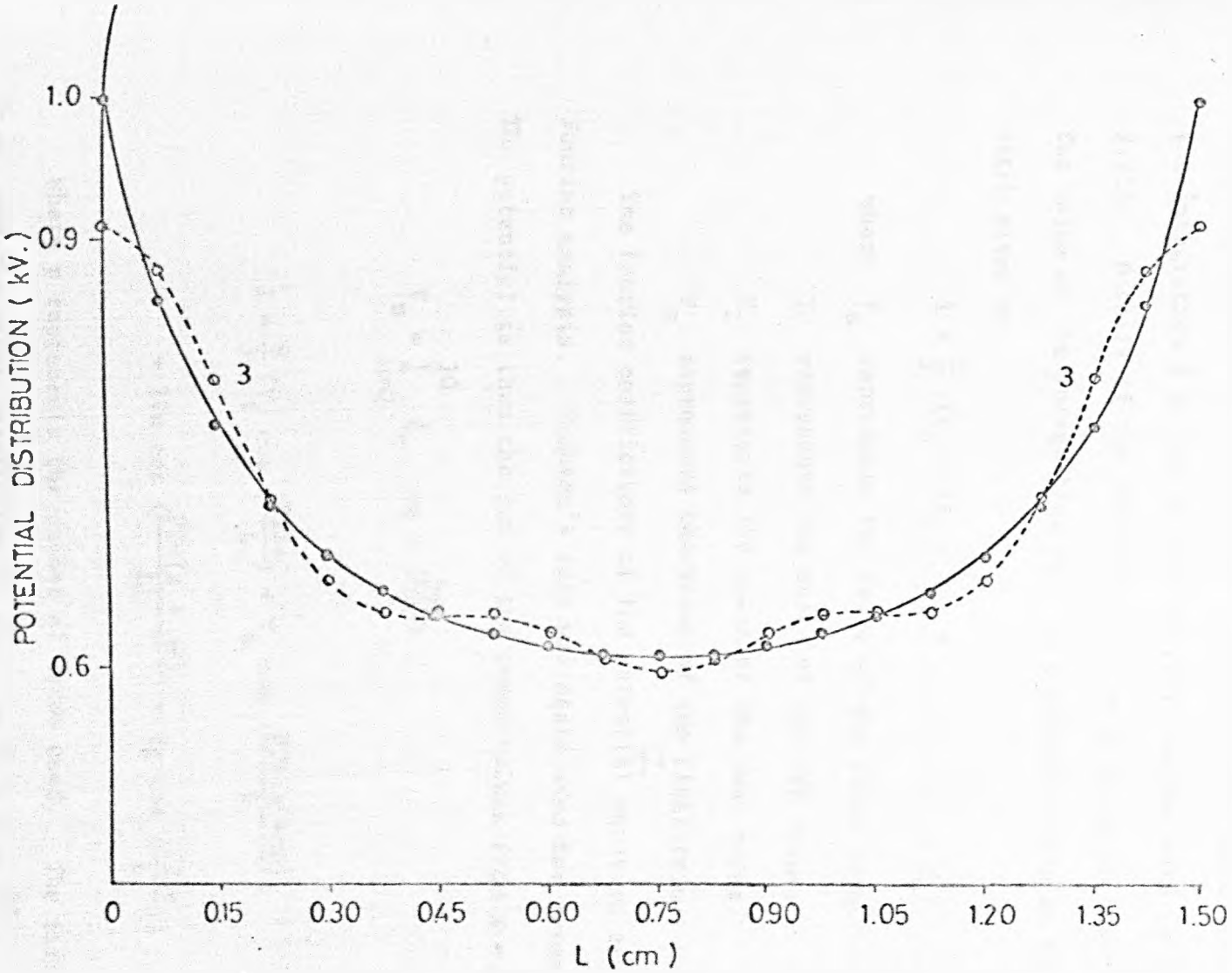

FIGURE(5.11C) REPRESENTATION OF THE POTENTIAL DISTRIBUTION BETWEEN TWO SUCCESSIVE PITCHES, THE DASHED LINE LABELLED 3 IS THE FOURIER COMPONENT OF THE POTENTIAL EQUATION FOR A FIVE TURN HELIX $Z_{initial} = -2L, Z_{final} = 3L$.

By using numerical integration of equation (5.28), it is possible to find the value of the integration I, taking the limits of integration from a = -2L to b = 3L. Dividing the pitch into M = 100 divisions, the number of intervals H in the trapezoidal rule is given by $H = \frac{b-a}{M}$. From the integration of equation (5.28), it was found that the value of the integration I at one particular point on the wire is found to be 9.918. Details of the computer program is given in appendix (The value of the integration fell to a certain value at the middle of a pitch given by

$$I = \frac{H}{3} \left(Y_o + 4Y_1 + 2Y_2 + \ldots\ldots + Y_n\right)$$

where Y_o represents the value of the first term.

Y_1 represents the value of the odd terms.

Y_2 represents the value of the even terms.

Y_n represents the value of the final term.

The Fourier coefficients of the potential equation are found by Fourier analysis. Simpson's rule was again used for terms from 0 to 10. The potential is then the sum of the terms values from N = 0 to N = 10.

$$V_n = \sum_{n=0}^{10} C_n \cos n \left(\frac{2\pi z}{L}\right) \qquad (5.29)$$

$$I = \frac{H}{3} \{V_i \cos \left(\frac{P2\pi a}{L}\right) + V_n \cos \left(\frac{P2\pi(a + nH)}{L}\right)$$

$$+ 2Vn \cos \left(\frac{P2\pi(a + nH)}{L}\right) + V_f \cos \left(\frac{P2\pi b}{L}\right)\} \qquad (5.30)$$

where p represents the number of terms used. The first $C_o = V_i = \frac{I}{L}$, and the other coefficient is equal to $V_n = C_n = \frac{2I}{L}$. Fig (5.11) shows the computed curves, which represent the potential at the helix wire, and the Fourier terms 1, 2, 3, which represent the potential from the integration process. It is found that the values of the coefficients are as follows

$$C_o = 2.318,\ C_1 = 0.4119,\ C_2 = 0.1896,\ C_3 = 0.113.$$

Since the helix has helical symmetry the potential equation inside the helix is given by

$$\phi_{inside} = U_o \{C_o + \sum_{n=1}^{\infty} \frac{C_n\ I_n\ (\frac{2\pi n r}{L})}{I_n\ (\frac{2\pi n r_1}{L})} \cos n\ (\theta - \frac{2\pi z}{L})\} \tag{5.31}$$

where U_o is voltage relative to the normalized voltage (in e.s.u. kV unit)

r_1 is the radius of the helix (or the matching point between the inside and outside helix boundary condition)

$I_n(x)$ is the Bessel function of the first order and imaginary argument

θ is the angle between the radial direction r an x axis in the xy plane

The equation of the electric field is derived from the potential equation in cylindrical coordinates by using

$$E = \{(\sum_{n=1}^{\infty} \frac{\partial\phi}{\partial r})^2 + \frac{1}{r2}\ (\sum_{n=1}^{\infty} (\frac{\partial\phi}{\partial\theta})^2 + (\sum_{n=1}^{\infty} \frac{\partial\phi}{\partial z})^2\ \}^{\frac{1}{2}} \tag{5.32}$$

For the single wire helix this field ($r < r_1$) is as follows:

$$E = U_o \Big\{ \Big[\frac{\pi}{L} \{ \frac{C_1}{I_1(\frac{2\pi r1}{L})}\ I_2(\frac{2\pi r}{L}) + I_0(\frac{2\pi r}{L})\} \cos\theta$$

$$+ \frac{2\pi}{L} \{ \frac{C_2}{I_2(\frac{4\pi r1}{L})}\ I_3(\frac{4\pi r}{L}) + I_1\ (\frac{4\pi r}{L})\} \cos 2\theta$$

$$+ \frac{3\pi}{L} \{ \frac{C_3}{I_3(\frac{6\pi r1}{L})}\ I_4\ (\frac{6\pi r}{L}) + I_2(\frac{6\pi r}{L})\} \cos 3\theta \Big]^2$$

$$+ \frac{1}{r^2} \{C_1 \frac{I_1(\frac{2\pi r}{L})}{I_1(\frac{2\pi r_1}{L})} \sin\theta + 2C_2 \frac{I_2(\frac{4\pi r}{L})}{I_2(\frac{4\pi r_1}{L})} \sin 2\theta$$

$$+ 3C_3 \frac{I_3(\frac{6\pi r}{L})}{I_3(\frac{6\pi r_1}{L})} \sin 3\theta\}^2$$

$$+ \{\frac{2\pi}{L} C_1 \frac{I_1(\frac{2\pi r}{L})}{I_1(\frac{2\pi r_1}{L})} \sin\theta + \frac{4\pi}{L} C_2 \frac{I_2(\frac{4\pi r}{L})}{I_2(\frac{4\pi r_1}{L})} \sin 2\theta$$

$$+ \frac{6\pi}{L} C_3 \frac{I_3(\frac{6\pi r}{L})}{I_3(\frac{6\pi r_1}{L})} \sin 3\theta\}^2 \quad (5.33)$$

where U_o is the voltage applied to the single wire helix focuser, and for the outside case

$$\phi_{outside} = U_o \quad C_o \frac{\ln(\frac{r}{R})}{\ln(\frac{r_1}{R})}$$

$$+ \sum_{n=1}^{\infty} \frac{C_n K_n(\frac{2\pi n r}{L})}{K_n(\frac{2\pi n r_1}{L})} \cos n(\theta - \frac{2\pi z}{L}) \quad (5.34)$$

where R is the radius of the cylinder (the vacuum chamber in the work described in this thesis)

$K_n(x)$ is the bessel function of zero order of pure imaginary argument

The electric field intensity for the external electric field ($r > r_1$) can be derived from equation (5.34) in a similar way to the inside case, from equation (5.32).

It is possible to give an approximate value of the magnitude of the electric field in the xy plane which is perpendicular to the focuser axis. Fig (5.12) shows the computed plot of the absolute

value of the electric field inside the single wire focuser as a function of the radial distance r for different values of θ. From the graph it is seen that the electric field has a finite value (about ¼ of the maximum values at a distance 0.01R away from the focuser axis, where R is the radius of the focuser). As the radial distance increases the electric field gradually rises. However, for such an angle as 120°, the electric field changes with radius in a different way, since it decreases monotonically right out to a point at a distance equal to the radius of the helix, from axis of the device.

Outside the helix, the absolute value of the electric field as shown in fig (5.13) has a maximum value at a point equal to the radius of the helix, for a various values of θ with the exception of a small range of θ near 120° close to the helix. As the radial distance increases away from a point equal to the radius of the helix, the electric field drops gradually.

The focusing properties of the single wire helix could be understood in more detail if the knowledge of the variation of the radial force with the radial distance from the focuser axis were to be obtained. Since the radial force is proportional to $E \frac{\partial E}{\partial r}$ for molecules with a quadratic Stark effect, it is inappropriate to use the data of fig (5.12) for the force constant $E \frac{\partial E}{\partial r}$ which varies with r. Fig (5.14) illustrates the radial gradient of the square of the electric field as a function of the radial distance r away from the helix axis. It is seen from the graph that the radial gradient has a finite value at the focuser axis. As the radial distance increases away from the axis ($r < R/2$), the gradient gradually increases for all angles between 0° and 90°, whereas for angles between 90° and 180° the gradient decreases. When $R > r > R/2$ the gradient becomes positive for all angles except a range of θ around 120°, which has a negative gradient.

Immediately outside the single wire helix focusing system, the

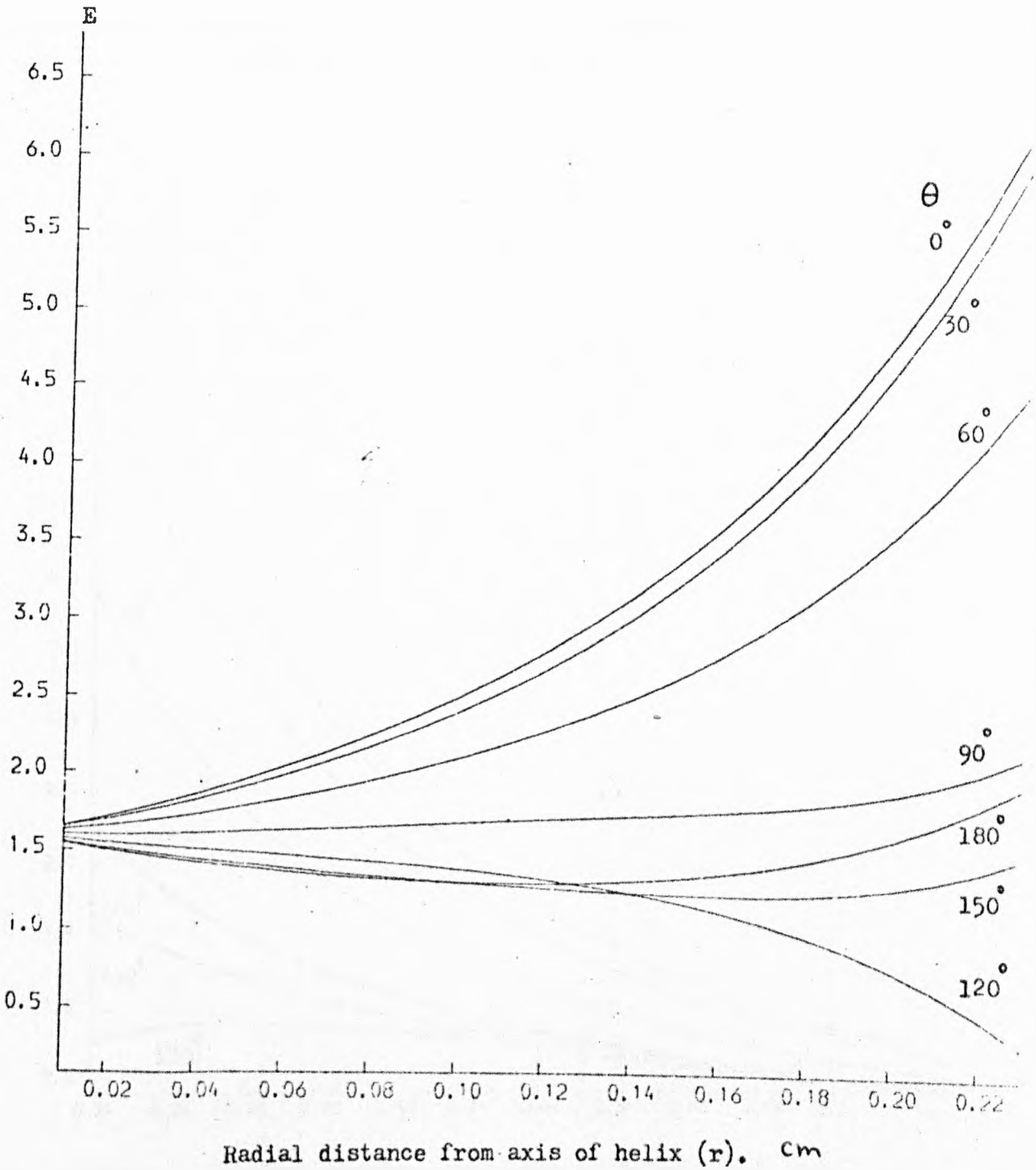

FIGURE (5.12) COMPUTED CURVES SHOWING THE DEPENDENCE OF THE ELECTRIC FIELD INSIDE THE SINGLE WIRE HELIX ON THE RADIAL DISTANCE AWAY FROM THE FOCUSER AXIS FOR DIFFERENT VALUES OF θ .

OUTSIDE THE HELIX ELECTRODE SYSTEM

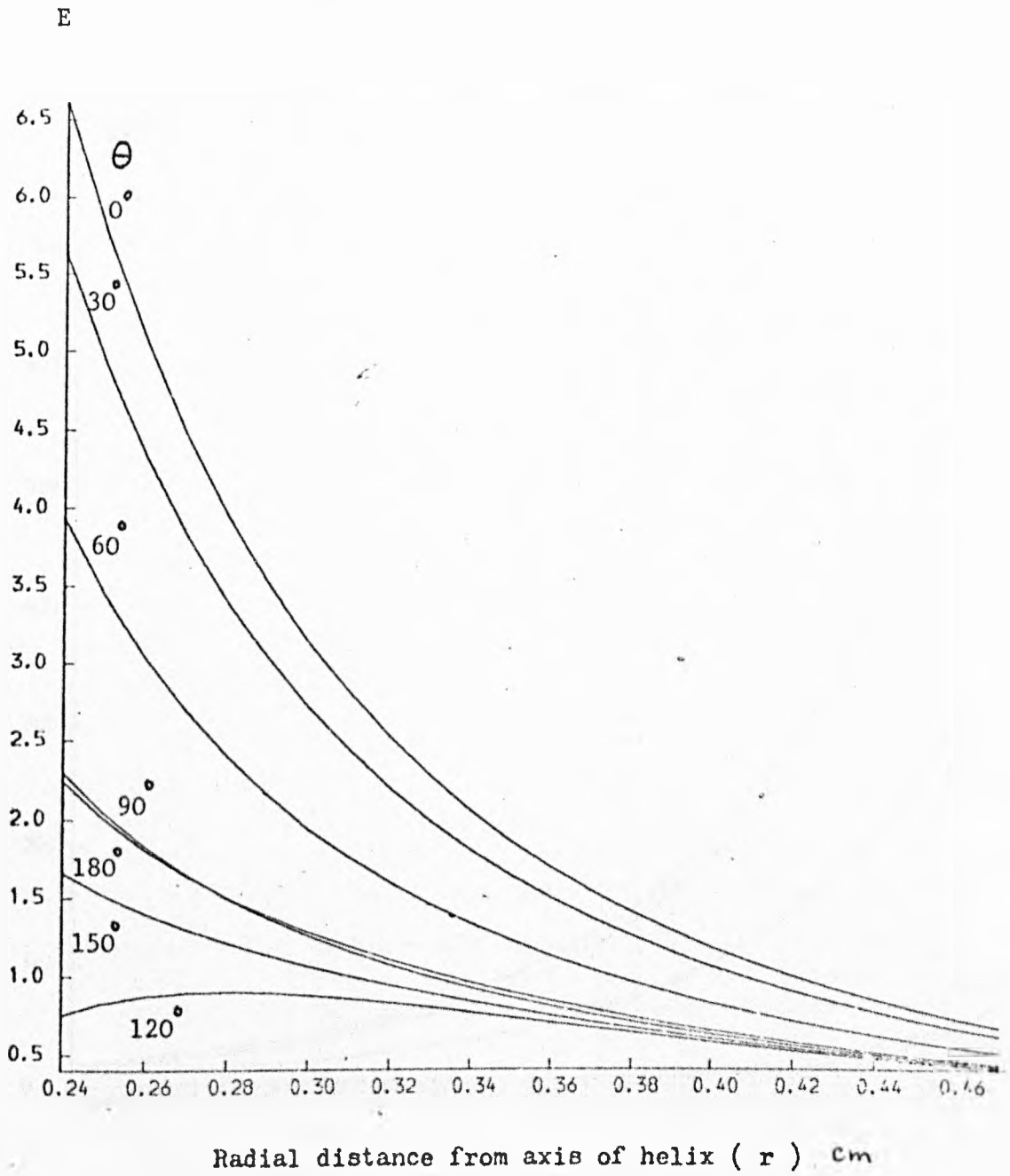

FIGURE (5.13) COMPUTED RESULTS GIVING THE DEPENDENCE OF THE ELECTRIC FIELD INTENSITY OUTSIDE THE SINGLE WIRE HELIX FOCUSER ON THE RADIAL DISTANCE r AWAY FROM THE HELIX ELECTRODE AND FOR A DIFFERENT VALUES OF θ .

INSIDE THE HELIX ELECTRODE SYSTEM

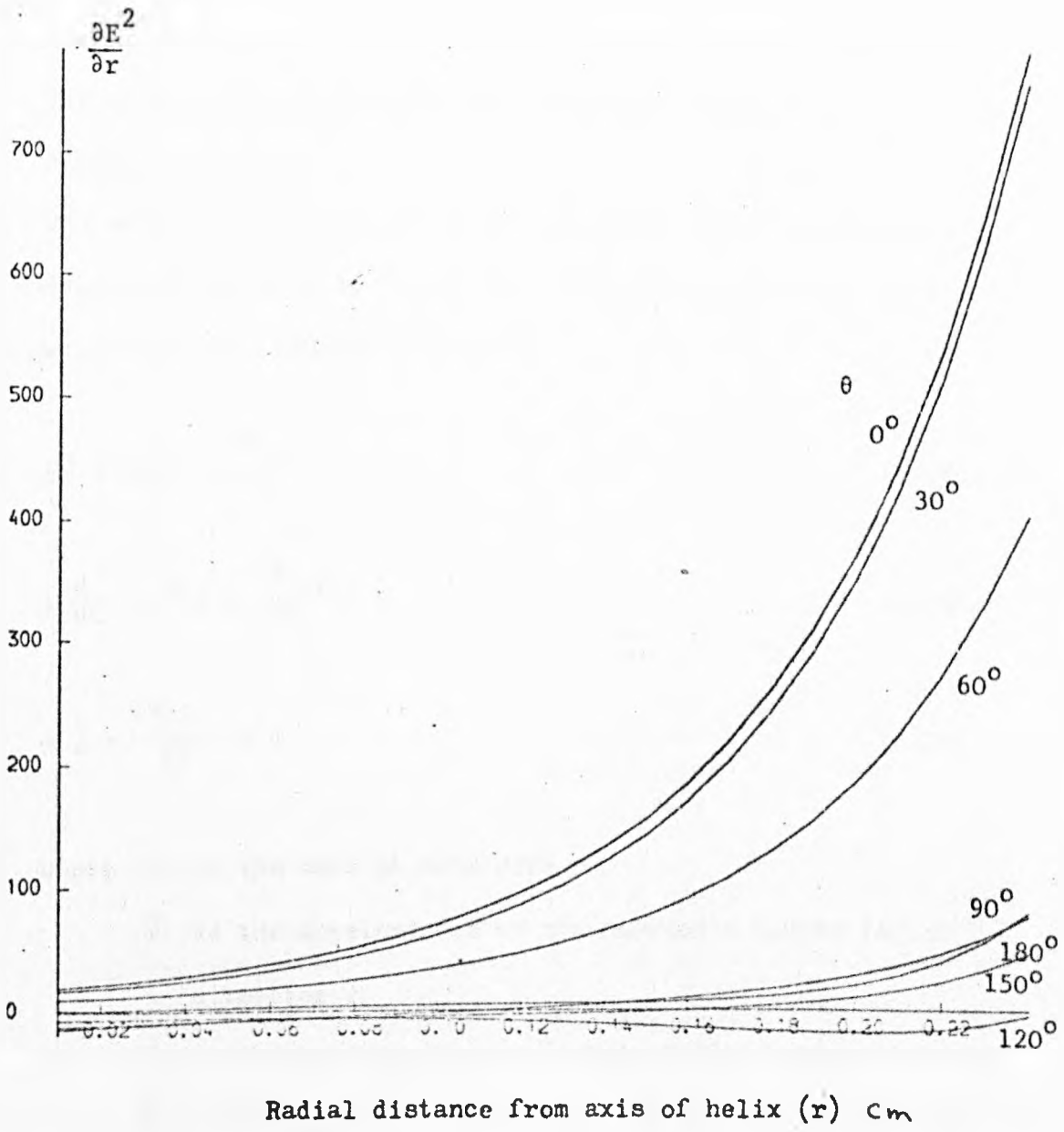

FIGURE (5.14) COMPUTED RESULTS GIVING THE RADIAL GRADIENT OF THE SQUARE OF THE ELECTRIC FIELD INSIDE THE SINGLE WIRE HELIX FOCUSER AS A FUNCTION OF THE RADIAL DISTANCE r, FOR DIFFERENT ANGLES θ

radial gradient of the square of the electric field has a maximum value for all values of θ except a small range around 120° as illustrated in fig (5.15). It is seen from the figure that the radial gradient drops to one-seventh of its maximum value just at a distance 1.3R, where R is the radius of the helix.

Trajectory of ammonia molecules passing through the single wire helix focuser

The equation of motion of upper and lower energy state molecules in cylindrical coordinates for a helical focusing system is given by the following equations (KOSHELKOV, 1973).

$$m\ddot{r} - mr\dot{\theta}^2 + \frac{\partial W_{U,L}}{\partial r} = 0 \qquad (5.35a)$$

$$m\frac{d}{dt}(r^2\dot{\theta}) + \frac{\partial W_{U,L}}{\partial \theta} = 0 \qquad (5.35b)$$

$$m\ddot{z} + \frac{\partial W_{U,L}}{\partial z} = 0 \qquad (5.35c)$$

where m is the mass of molecules

$\ddot{r}$ is the acceleration of the molecules in the radial direction r.

$\dot{\theta}$ is the rate of change of angle θ with respect to time

$\ddot{z}$ is the acceleration of the molecules in the z-direction (focuser axis)

$W_{U,L}$ is the interaction anergy of the upper (U) and lower (L) energy state molecules with the electrostatic field of the focusing system. This is given by the following equation for ammonia:

$$W_{U,L} = \pm \frac{h\nu}{2}\left\{ \left(1 + 4\frac{\mu^2 E^2}{h^2\nu^2}\right)^{\frac{1}{2}} - 1 \right\} \qquad (5.36)$$

OUTSIDE THE HELIX ELECTRODE SYSTEM

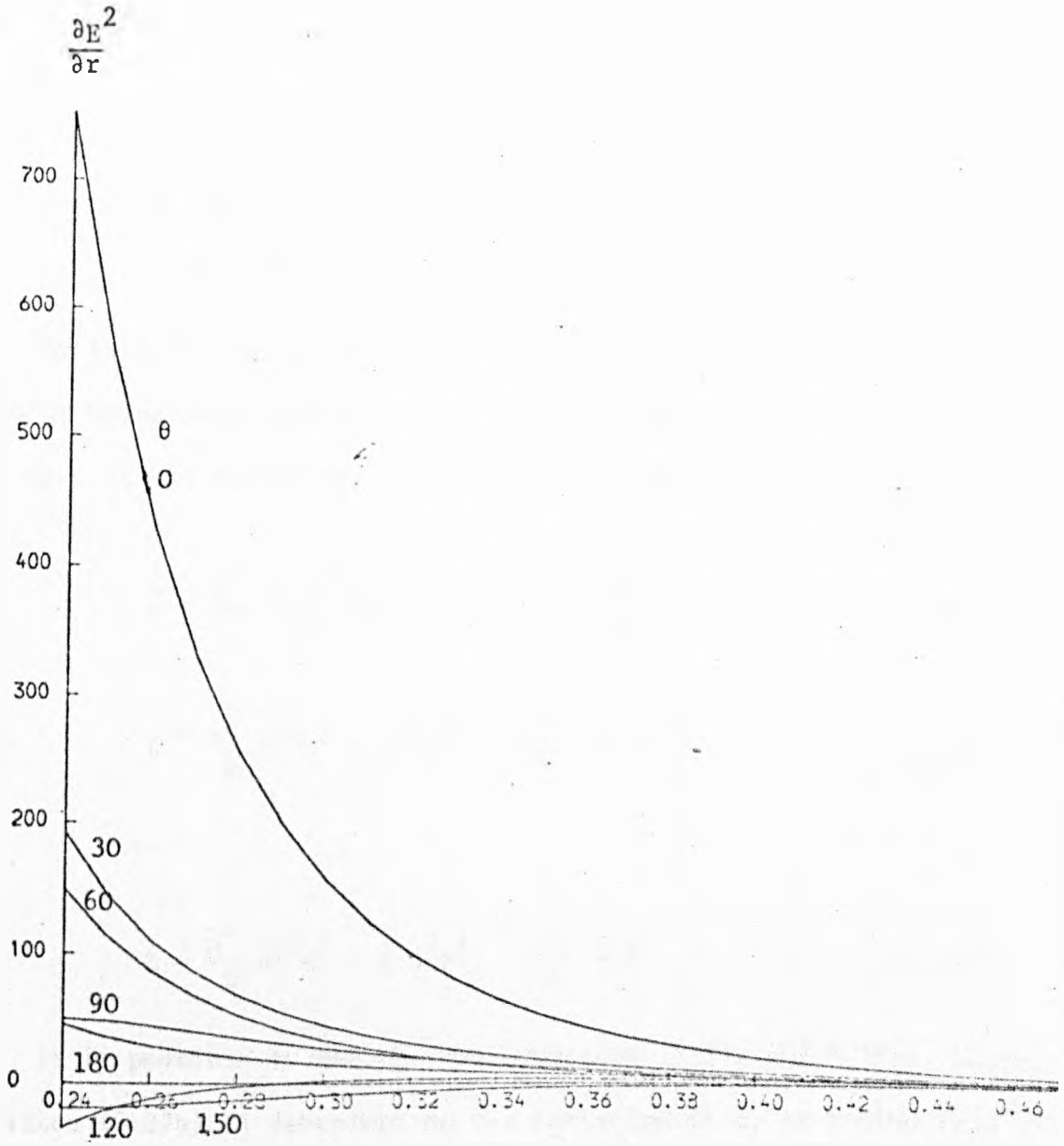

FIGURE (5.15) COMPUTED RESULTS OF THE RADIAL GRADIENT OF THE SQUARE OF THE ELECTRIC FIELD OUTSIDE THE SINGLE WIRE HELIX FOCUSER AS A FUNCTION OF THE RADIAL DISTANCE r, FOR DIFFERENT ANGLES θ

where μ is the matrix element

ν is the frequency of the transition between upper and lower energy state molecules

h is Planck's constant

and E is the electric field intensity of the focuser given by

$$E = \sqrt{f(r_1\theta_1 z)} \quad \text{where} \quad f = f(r,\theta,z) = E_r^2 + E_\theta^2 + E_z^2$$

By introducing the quantity $M = \theta' r^2$, which is related to J the angular momentum of the molecules by the formula $M = J/m$ where m is the mass of the molecules, then equations (5.35) can be written as

$$\ddot{r} - \frac{M^2}{r^3} \pm \frac{\mu^2}{m} (h^2\nu^2 + 4\mu^2E^2)^{-\frac{1}{2}} \frac{\partial E^2}{\partial r} = 0 \qquad (5.37a)$$

$$\dot{M} \pm \frac{\mu^2}{m} (h^2\nu^2 + 4\mu^2E^2)^{-\frac{1}{2}} \frac{\partial E^2}{\partial \theta} = 0 \qquad (5.37b)$$

$$\ddot{z} \pm \frac{\mu^2}{m} (h^2\nu^2 + 4\mu^2E^2)^{-\frac{1}{2}} \frac{\partial E^2}{\partial z} = 0 \qquad (5.37c)$$

It is possible to use the two equations (5.37a and 5.37c), because equation (5.37b) is dependent on the variation of z, as follows from the following equation (Koshelkov, 1973).

$$M = \lambda - \frac{1}{\gamma} z' \qquad (5.38)$$

where $\lambda = M_o + \frac{z'}{\frac{2\pi}{L}}$

and M_o is the initial angular momentum of the molecules with respect to the z-axis, ($M_o = 0$ for an on-axis beam source)

and M is the related to the angular momentum.

The calculation of the trajectory of the ammonia molecules emerging from an on-axis nozzle beam source, and focused by the single wire helix

focuser is carried out as follows.

Assume that the ammonia molecules have the speed V at the entrance of the focuser. Then the initial position of the ammonia molecules is represented by the following equations:

The radial component of the speed $V_r = V \sin(\beta)$,

The axial component of the speed $V_z = V \cos(\beta)$,

The radial position of the molecule $V_o = N_F \tan(\beta)$,

where N_F is the nozzle-focuser separation

and β is the angle between the molecule and the beam axis,

the axial position of the molecule $Z_o = 0$,

the angle between the molecule and the beam axis (or focuser axis in on-axis nozzle source case) is β_2,

the initial angular speed of the molecules $V_\beta = 0$

The minimum angle was normally zero, but for the purpose of computer calculation was set equal to 0.0055 radians to avoid problems associated with the Bessel functions used in the equation of the electric field. The maximum angle β that the molecules possessed at the entrance of the focuser is 0.040 radians. As the molecules passed through the focuser, they interacted with the electric field. In this device, the electric field is more complicated than for other helical electrode systems (bifilar helix, quadrupole helix, etc.) since it has three components in the r, θ, and z directions, i.e. the electric field has an angular component besides the transverse and longitudinal components with respect to the beam axis.

In order to calculate the trajectory and the final values of r and the components V_r, V_θ, V_z) of the molecules emerging from the focuser exit, two equations were set. The first is the prediction equation and the second is the correction equation (McCracken and Dorn 1964).

The prediction equations for the position of the molecules for the next step of integration inside the focuser are:

$$Z_{n+1} = Z_n + Vz_n \cdot T \tag{5.39}$$

$$R_{n+1} = R_n + Vr_n \cdot T \tag{5.40}$$

$$V\theta_n = \left(\frac{Vz_o - Vz_n}{\frac{2\pi}{L}}\right) / R_n^2 \tag{5.41}$$

$$\theta_{n+1} = \theta_n + V\theta_n \cdot T \tag{5.42}$$

$$Vr_{n+1} = Vr_n + (G_R (r_n, \theta_n, z_n)/m + V\theta_n^2 \cdot r_n) \cdot T \tag{5.43}$$

$$Vz_{n+1} = Vz_n + (G_Z (r_n, \theta_n, z_n)/m) \cdot T \tag{5.44}$$

$$V\theta_{n+1} = \left(\frac{Vz_o - Vz_{n+1}}{\frac{2\pi}{L}}\right) / R_{n+1}^2 \tag{5.45}$$

where T represents the integration step, and is equal to

$$T = F_\ell / Z_a \cdot \bar{v} \cos(\beta)$$

F_ℓ is the focuser length

Z_a is the number of the integration step used

$$G_R (\nu, \theta, z) = \pm \mu^2 (h^2 \nu^2 + 4\mu^2 E^2)^{-\frac{1}{2}} \frac{\partial E^2}{\partial r}$$

$$G_Z (r, \theta, z) = \pm \mu^2 (h^2 \nu^2 + 4\mu^2 E^2)^{-\frac{1}{2}} \frac{\partial E^2}{\partial Z}$$

The positive and the negative sign refers to the lower and upper energy states of ammonia respectively.

Then in order to correct these equations, the following equations were used in the next step of integration inside the focuser

$$Z_{n+1} = Z_n + (Vz_n + Vz_{n+1}) \cdot T \cdot 0.5 \ , \tag{5.46}$$

$$r_{n+1} = r_n + (Vr_n + Vr_{n+1}) \cdot T \cdot 0.5 \ , \tag{5.47}$$

$$V\theta_n = \left(\frac{Vz_o - Vz_n}{\frac{2\pi}{L}}\right) / Rn^2 \tag{5.48}$$

$$\theta_{n+1} = \theta_n + (V\theta_n + V\theta_{n+1}) \cdot T \cdot 0.5 \quad , \tag{5.49}$$

$$Vr_{n+1} = Vr_n + (G_R(r_n, \theta_n, z_n)/m) + V\theta_n^2 \cdot r_n \tag{5.50}$$

$$+ (G_R(r_{n+1}, \theta_{n+1}, z_{n+1})/m) + V\theta_{n+1}^2 \, r_{n+1} \cdot T \cdot 0.5 \tag{5.51}$$

$$Vz_{n+1} = Vz_n + (G_Z(r_n, \theta_n, z_n) + G_Z(r_{n+1}, \theta_{n+1}, z_{n+1})) \cdot T \cdot 0.5 \tag{5.52}$$

$$V\theta_{n+1} = \left(\frac{Vz_o - Vz_{n+1}}{\frac{2\pi}{L}}\right) / R_{n+1}^2 \tag{5.53}$$

where Z_{n+1} is the axial distance at the next step of integration

r_{n+1} is the radial distance at the next step of integration

$V\theta_n$ is the angular velocity at the nth step of integration

θ_{n+1} is the angle of the molecules at the next step of integration with respect to a plane passing perpendicularly to the focuser axis

Vr_{n+1} is the radial component of the speed at the next step of integration

Vz_{n+1} is the axial component of the speed at the next step of integration

$V\theta_{n+1}$ is the angular component of the speed at the next step of integration

When the molecules emerge from the focuser, no further forces act, provided that the effect of the fringe field is neglected. The molecules have three final components at the cavity entrance at position A as shown in fig (5.16).

The computer programme was adjusted to calculate the molecular trajectories point by point inside the single wire helix. It was adjusted also to account for only those molecules that emerge from the focuser and pass through the cavity without hitting or colliding with

FIGURE (5.16) DIAGRAM SHOWING COORDINATES OF THE MOLECULES THAT ARE ABOUT TO ENTER THE CAVITY AFTER STATE SELECTION. HERE B REPRESENTS THE BEAM AXIS, A THE POSITION OF THE MOLECULES, AND THE CIRCLE THE CAVITY WALL.

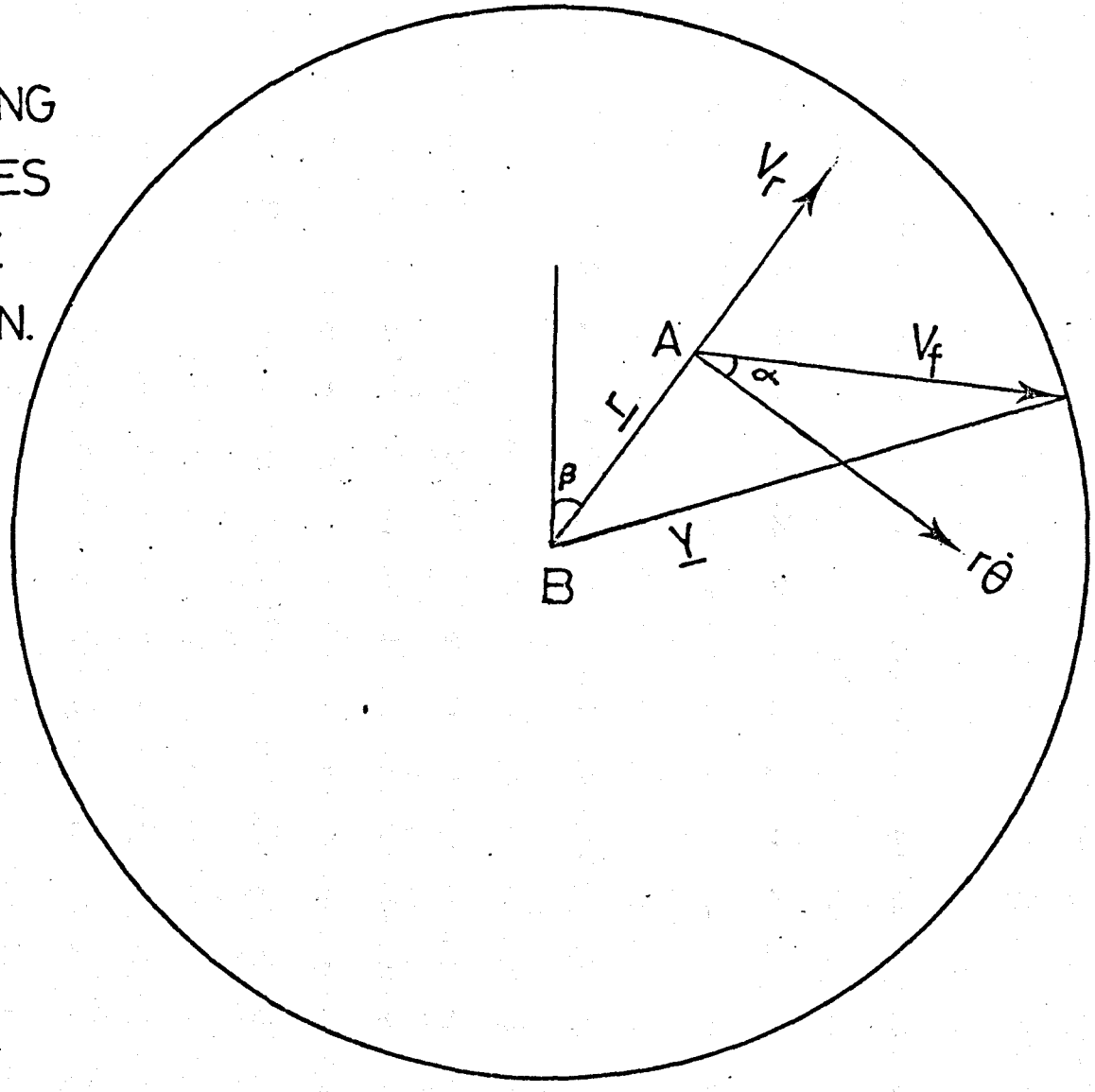

the walls.

For the calculation of the intensity of the state selected beam by the use of the single wire helix focuser, the Maxwellian distribution of molecules emerging from the nozzle source was taken into account. For details see appendix (4). The computed results of the variation of the emission signal intensity as a function of the voltage applied to the single wire helix focuser is illustrated in fig (5.17).

Experimental Set Up

The beam source was either a single hole nozzle for use with the narrowest beams, or a multiple hole nozzle (three or four holes) for broad beam operation. The nozzle holes were 0.09mm diameter, and in case of the multiple hole nozzle, the holes were arranged symmetrically on a pitch diameter circle of 2mm, and drilled in a brass diaphragm 0.1mm thick. A beam of ammonia molecules produced by the nozzle passed through a variable aperture camera-type iris whose diameter could be varied. The iris diameter was typically 4mm. The molecular beam then passed through the single wire helix (section 3.4). At a remote point on the focuser axis, the efficiency of the focusing and state selection of lower or upper energy state (J = K = 3 inversion line) NH_3 molecules was monitored via the microwave power absorbed or emitted at 23.87GHz in an E_{010} mode cylindrical microwave cavity, positioned 50mm downstream from the helix. Single klystron superhetrodyne detection was employed in which the exciting signal was one of the two sidebands produced by amplitude modulation at the intermediate frequency, of a partion of the local oscillation power.

Operation of the single wire helix with a tubular molecular beam of ammonia which sheathed the helix, resulted in the production of a strong absorptive molecular beam of the J = K = 3 inversion transition on the device axis. Fig (5.18) shows the relative absorption signal as a function of the voltage applied to the helix focuser. In contrast,

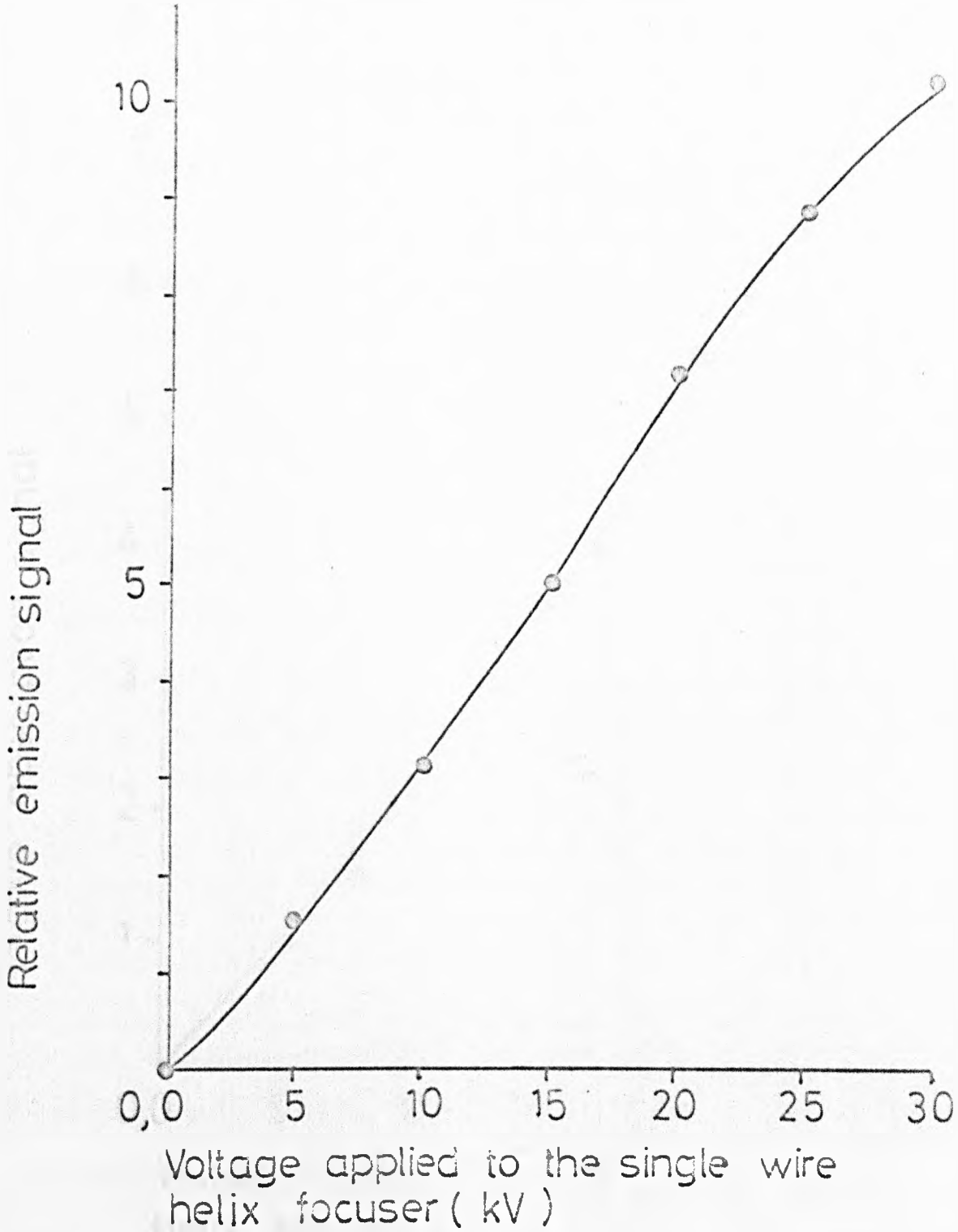

FIGURE(5.17) COMPUTED RESULTS GIVING THE RELATIVE EMISSION INTENSITY AS A FUNCTION OF THE VOLTAGE APPLIED TO THE SINGLE WIRE HELIX FOCUSER.

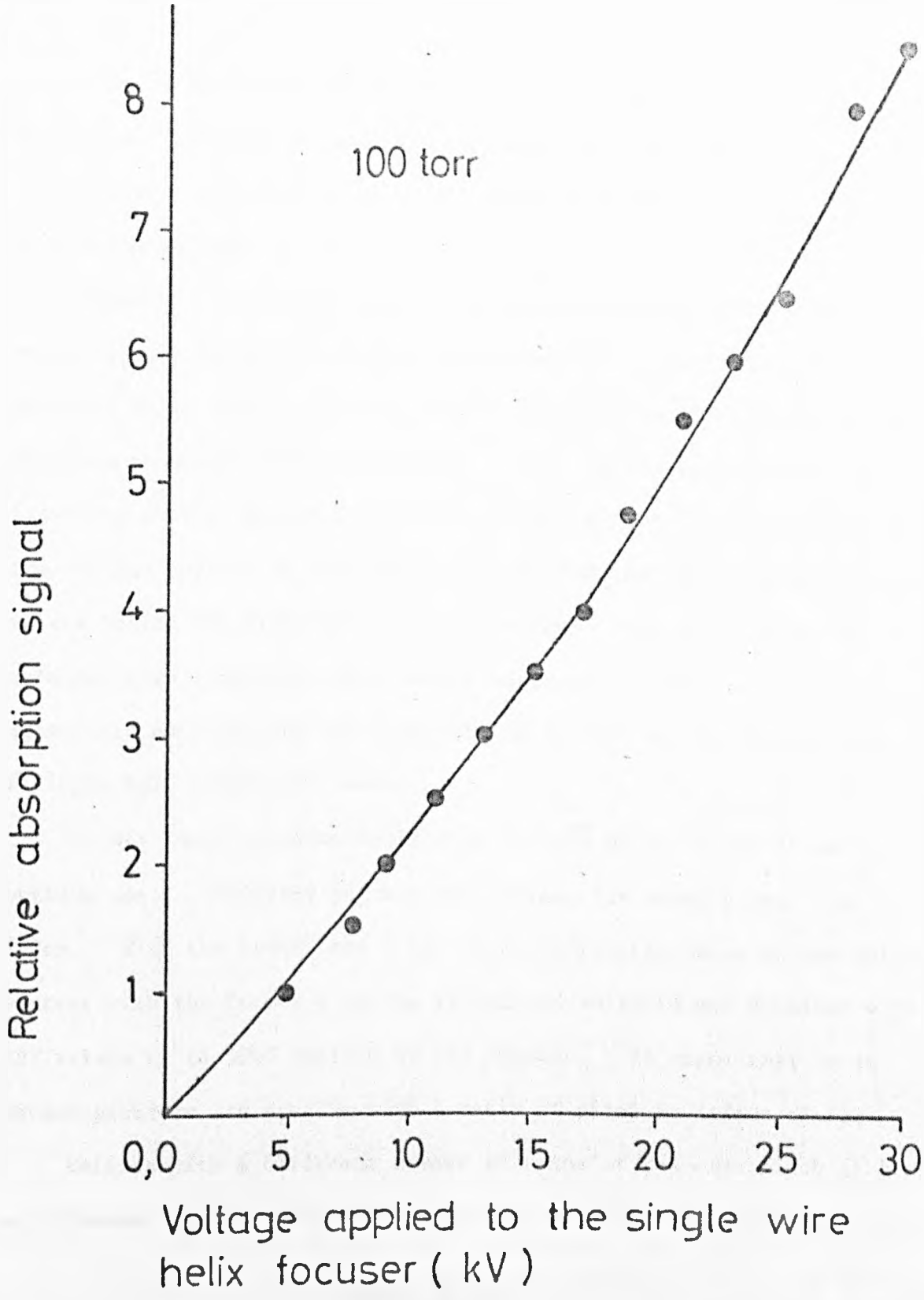

FIGURE (5.18) ABSORPTION SIGNAL AMPLITUDE AS A FUNCTION OF THE FOCUSER VOLTAGE FOR THE CASE OF A BROAD BEAM.

operation of the helix focuser with a narrow beam which passed inside the focuser resulted in an emission signal on the device axis. Fig (5.19) shows the relative emission signal as a function of the single wire helix voltage.

Maser oscillation set in at a focuser potential of 15kV and rose monotonically in amplitude with increasing EHT. No voltage breakdown occurred up to 30kV. Clearly higher levels of oscillation should be possible at higher focuser voltages. Fig. (5.20) illustrates a family of curves representing the oscillation levels as a function of the voltage applied to the focuser for a different fixed pressures values behind the beam source. It was found that oscillation was obtained when a multiple hole nozzle was used, whereas a strong stimulated emission was obtained with up to 30kV on the focuser when a single hole nozzle was used.

It was found experimentally that a pitch of L = 1.5cm is an optimum one. Different pitches were tried, for example 3cm, and 0.2cm. With the latter one a very weak stimulated emission was obtained, whereas with the former a strong stimulated emission was obtained with EHT values up to 30kV applied to the focuser. It seems that it is advantageous to use a helix with a ratio of pitch to radius of ~3.

Helices with a different number of turns of the same pitch (1.5cm), and diameter (0.46cm) were used, and the results are shown in table (5.1)

TABLE (5.1)

Number of turns	Threshold of oscillation (kV)	Pressure behind four hole nozzle (torr)
8	23.3	110
9	21.7	120
12	stimulated emission up to 30kV	130

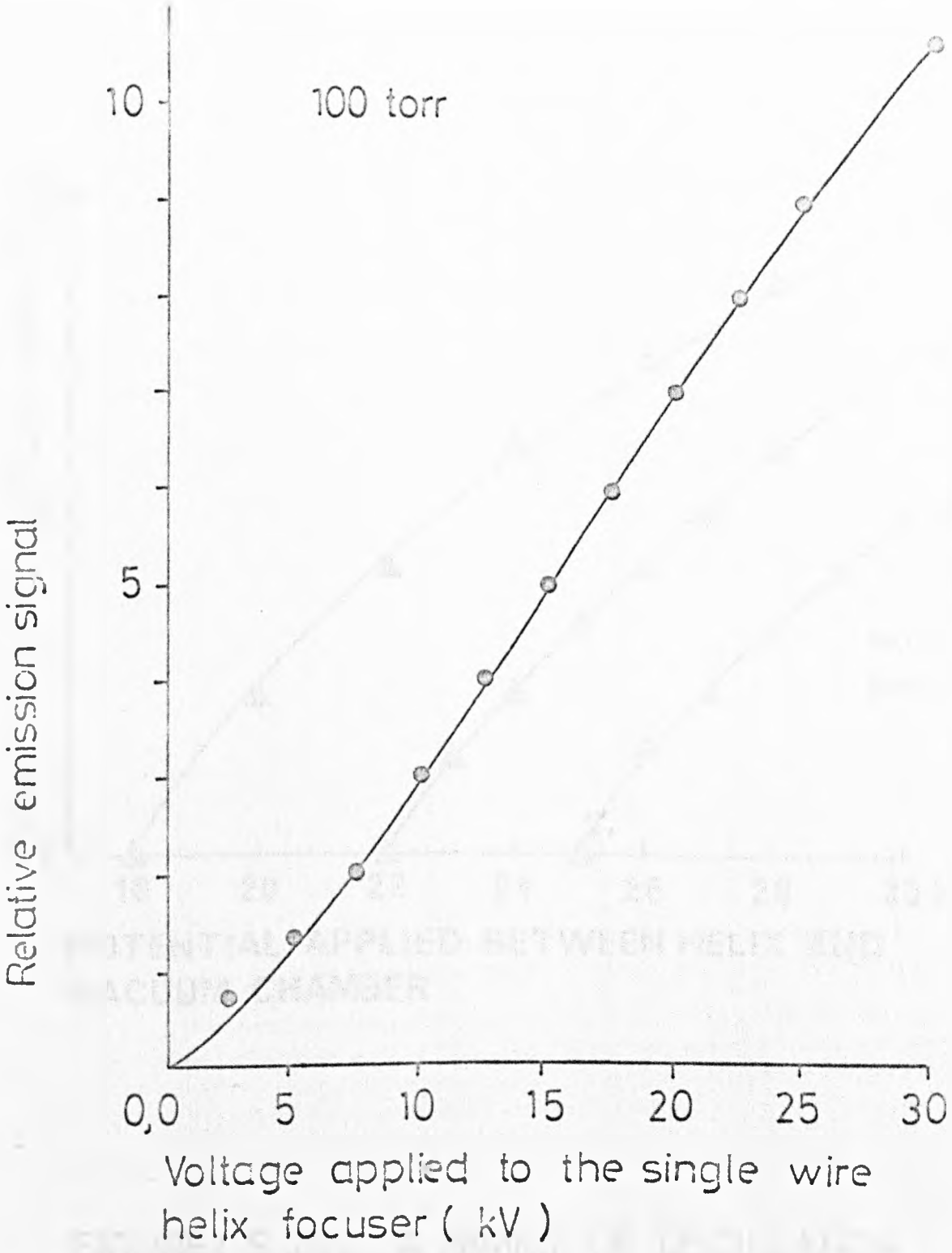

FIGURE (5.19) RELATIVE EMISSION SIGNAL AS A FUNCTION OF THE FOCUSER VOLTAGE FOR THE CASE OF A NARROW BEAM.

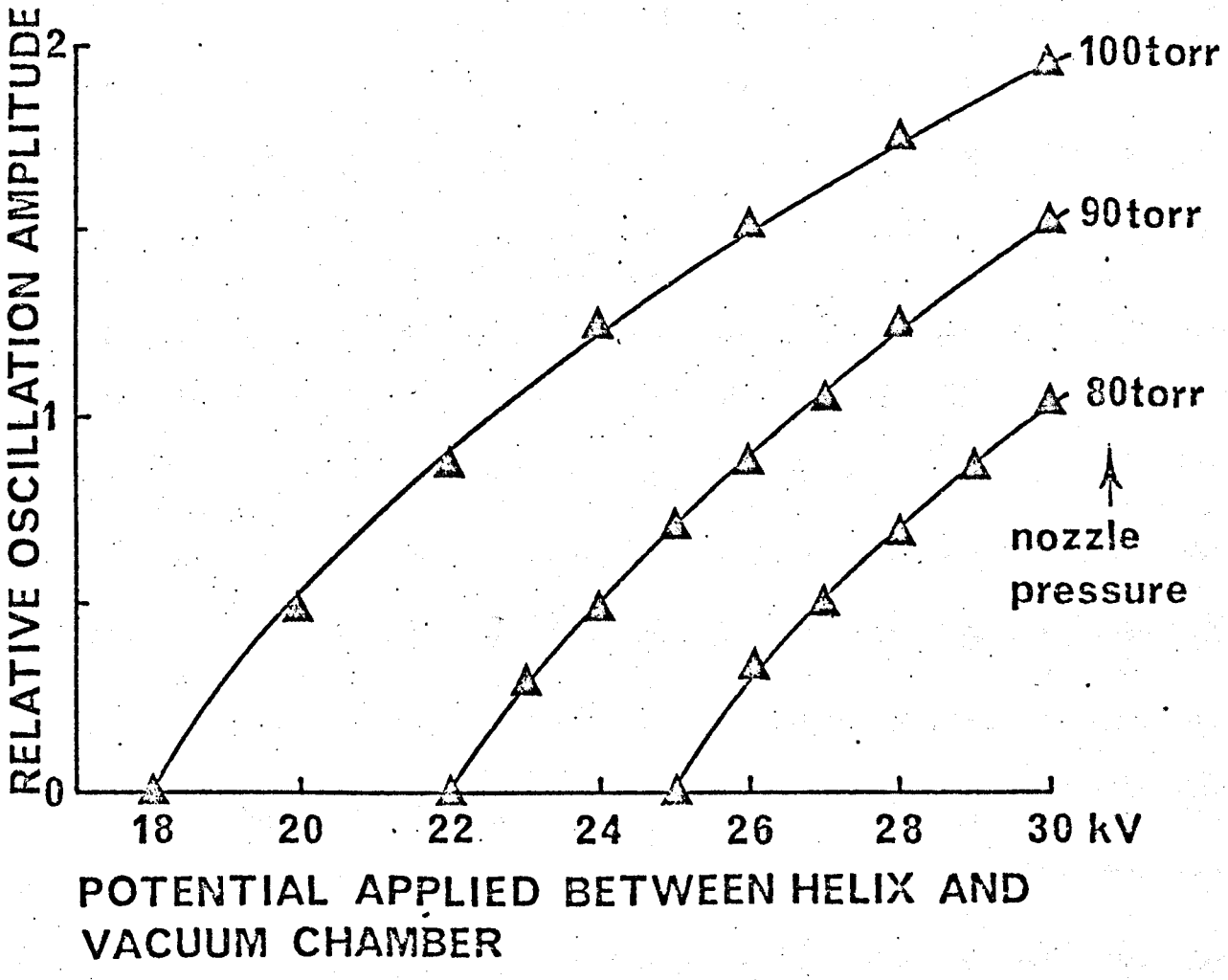

FIGURE (5.20) A FAMILY OF OSCILLATION AMPLITUDE CURVES PLOTTED AS A FUNCTION OF THE VOLTAGE APPLIED TO A SINGLE WIRE HELIX.

A single wire helix with the same pitch of 1.5cm but with a thinner wire diameter 0.027cm has also been used. In this case the maser oscillated with a threshold of 20.3kV applied to the helix with a pressure behind the source of 60 torr, where all other relevant parameters were unchanged. These results suggested that with a helix made with thinner diameter wire more molecules will escape, resulting in a higher oscillation threshold value of EHT.

In conclusion it was found the emission amplitude (fig 5.19) followed the same monotonic form as the theoretical results shown in fig (5.17).

CHAPTER SIX

EXPERIMENTS WITH MULTIPLE STATE SELECTOR USING AN OSCILLATOR MASER

6.1 Studies of the spatial reorientation effect

Introduction

In the beam maser molecules which increase in energy in an applied electric field ($\mu_{eff}<0$) are focused by the influence of the inhomogeneous electric field of the focuser. The spatial reorientation of molecules emerging from the focuser is not isotropic, since the deflection and focusing of active molecules depends upon their quantum state, and in particular on the quantum number M.

The molecules, after emerging from the focuser, pass through the cavity. Inside the cavity, the interaction between the active molecules and the microwave field of the resonator depends upon the spatial orientation of the molecules. For this reason the probability of emission of molecules from the upper to the lower energy state will depend upon any reorientation effects which may occur in the space between the focuser and the resonant cavity.

Basov, Oraevskii et al (1963, 1964) were the first to observe spatial reorientation using a molecular beam maser with weak electric and magnetic fields applied to the maser molecules in the space between the focuser and the resonator.

The spatial reorientation was detected by the change in emission power and oscillation frequency. The theory of the spatial reorientation effect was discussed by Basov, Oraevskii et al (1963, 1964) in the light of their results. It was pointed out that the spatial reorientation effect was due to the reorientation rather than transitions of molecules from upper to lower energy states induced by the weak fields between the focuser and the cavity, since the adiabatic condition applies

$$\frac{h}{W_2 - W_1} \left(\frac{\partial H}{\partial t}\right)_{12} << 1 \qquad (6.1)$$

where W_1 and W_2 are lower and upper energy levels of the maser transition respectively, and $\left(\frac{\partial H}{\partial t}\right)_{12}$ is the matrix element of the time derivative of the Hamiltonian of the interaction of the molecule with an external field.

Mednikov and Parygin (1963) pointed out that operating a focuser which possesses a longitudinal electric field with respect to the molecular beam axis provides a beam of active molecules with the most desirable direction of space quantization for maximum emission of molecules in the E_{010} mode cylindrical microwave cavity, which possesses a longitudinal oscillating electric field with respect to the axis of the molecular beam. This was confirmed by Krupnov and Skvortsov (1965) who concluded that when the fields in the cavity and in the sorting system have the same direction, the probability of emission during the passage of molecules through the cavity will be a maximum. If, on the other hand, the fields are perpendicular, the probability of emission will be zero.

The molecules emerging from the region of the electric field of the sorting system (Krupnov and Skvortsov 1965) does not travel from upper energy level to the lower but rotates in space, following the change in the direction of the electric field existing in the space between the sorting system and the cavity.

Krupnov and Skvortsov (1965) studied the spatial reorientation effect in a molecular oscillator using $1_{01} \rightarrow 0_{00}$ transition of formaldehyde (CH_2O) by means of a weak electric field. The results were similar to that obtained by Basov, Ovarvekii et al (1963) for ammonia no spatial reorientation effect was found with magnetic fields up to 5×10^{-3}T.

Further experiments were carried out by Krupnov and Skvortsov (1966) who investigated the spatial reorientation effect in an ammonia maser

using the J = k = 3 transition of NH_3, using the weak reorientation electric field, between ring focuser and cylindrical cavity. It was pointed out by them that in the case of the ammonia oscillator, the dependence of the excitation parameter on the reorienting-electrode voltages was not very pronounced (~1%) and did not contain a series of oscillations. When a parallel plate capacitor was used as a reorientating electric field, similar to that used by Barov, Oraveskii et al (1963) with ammonia, it was found that the maximum of the excitation parameter* was 20% less than in the case of formaldehyde.

Koshurinov (1969) has investigated in detail the effect of the field symmetry upon spatial reorientation of molecules in the fringe field between quadrupole rod focuser and cylindrical maser cavity. A similar effect was also investigated using an annular sorting system (or ring focuser), but no suggestion was made that the experimental results were in any way different to those that produced by the use of the quadrupole rod focuser.

---

* The excitation parameters (Smart 1973) lies between zero and unity in the amplification region and equal unity at the oscillation threshold of the maser and is defined by the following equation

$$\eta = \frac{2\,Lp}{v}\left(\frac{QN}{Vh}\right)^{\frac{1}{2}}$$

where η is the excitation parameter

L is the length of the region of uniform radiation field

p is the microwave power emitted by the molecules

Q is the quality factor of the cavity

N is the number of upper energy state molecules passing through the region of uniform radiation field in unit time, or more correctly the difference $N_1 - N_2$ of the population in the upper and lower energy states.

v is the velocity of the molecular beam

V is the volume of the cavity

h is Planck's constant

Recently Truman and Lainé (1976) reported an operation of an ammonia maser with a positive Stark slope ring focuser. It was shown that their results were significantly different from those reported by Koshurinov (1969) for a quadrupole rod focusing system.

It is shown experimentally in this section of the thesis that an ammonia molecular beam maser operated with two ring focusers in series has an anomalous behaviour. This phenomenon is attributed to the spatial reorientation of molecules in the weak electric field produced by the external field of a negative Stark slope ring focuser situated between the maser ring focuser and an E_{010} mode cylindrical cavity.

With a single molecular beam operated with a negative Stark slope ring focuser, the amplitude of enhanced absorption signal increases monotonically as the voltage applied to the negative Stark slope ring focuser increases, irrespective of whether the focuser is of negative or positive polarity with respect to the earthed cavity (Al-Amiedy and Lainé 1978).

Beam masers employing a single molecular beam are usually operated with one electrostatic focuser and an earthed cavity. Under normal conditions, the amplitude of the maser signal (emission or oscillation) increases monotonically as the voltage applied to the focuser rises, irrespective whether the focuser is of the longitudinal or transverse field type (Lainé, 1975). The monotonic maser signal behaviour is found not to occur, however, when a negative Stark slope ring focuser is operated in series with the maser-type ring focuser.

Significant effects on the amplitude of maser oscillation amplitude were noticed for a small voltage applied to the negative Stark slope ring focuser. This effect appears irrespective of whether the focuser is of negative or positive polarity with respect to the other focuser, the cavity being earthed.

Experimental set up

The molecular beam was produced in the usual way. The molecular beam then passed through the maser ring focuser, then after travelling a further distance of 7.4cm measured along the beam axis, the state selected beam sheathed the negative Stark slope ring focuser but did not enter it. The focuser parameters are given in tables 3.2a and 3.2c. At a remote point on the focuser axis, the signal resulting from emission from the state selected upper energy state ammonia molecules (J = K = 3 inversion line) was monitored, via stimulated emission in the maser cavity situated 3.5cm downstream from the negative Stark slope ring focuser. The schematic diagram of the experiment is shown in fig (6.1).

Operation of the maser ring focuser with a narrow beam of ammonia resulted in the production of a beam of emissive molecules of sufficient intensity to support oscillation. When the oscillation amplitude was set to a certain level, a voltage in range 0-30kV was applied to the second focuser. Two oscillation dips were observed, the first at 100 volts and the second at 400 volts applied to the second ring focuser. When the voltage applied to the second focuser reached 10kV, the amplitude of oscillation started to decay monotonically with further increases in voltage. A family of curves, illustrating the dependence of the maser oscillating signal on the voltage V_1 applied to the second focuser with the voltage V_2 across the maser ring focuser held constant is shown in fig (6.2). All voltage are relative to earth potential.

It was found experimentally that when the negative Stark slope ring focuser was operated with negative polarity two dips occurred at successively higher voltage, i.e. 120 volts and 420 volts, and then above 10kV, the oscillation level fell smoothly as mentioned above.

The interpretation of this behaviour is complicated because of the

FIGURE (6.1) SCHEMATIC DIAGRAM OF TWO RING FOCUSERS IN SERIES FOR SPATIAL REORIENTATION STUDIES.

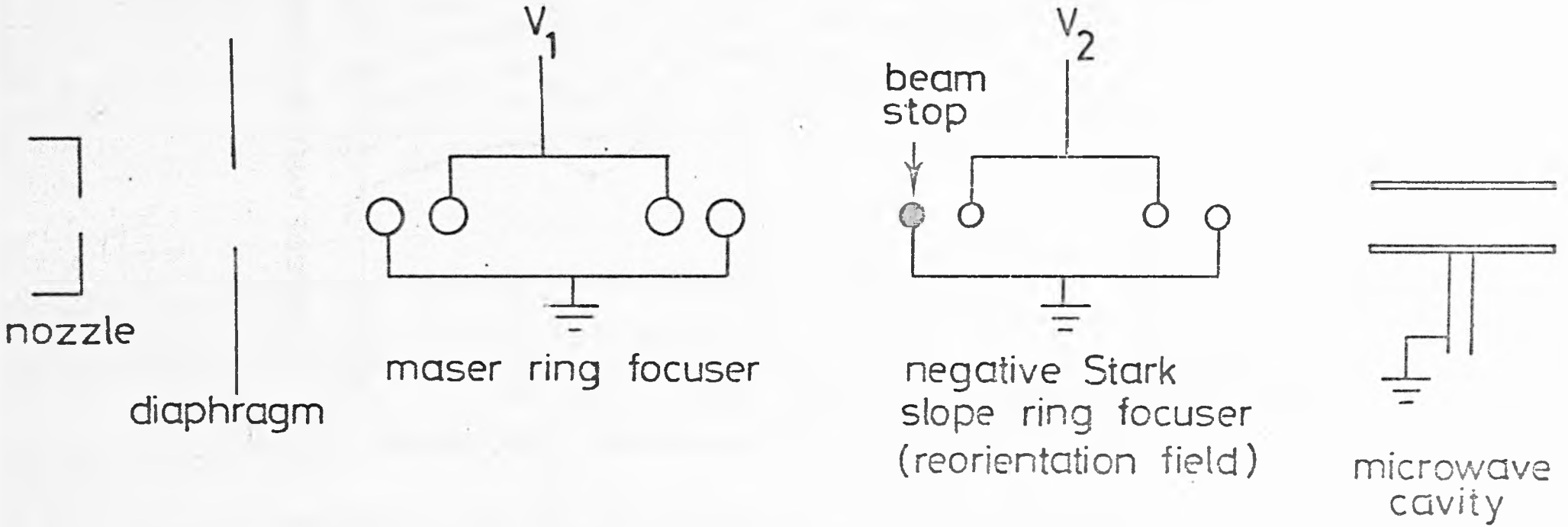

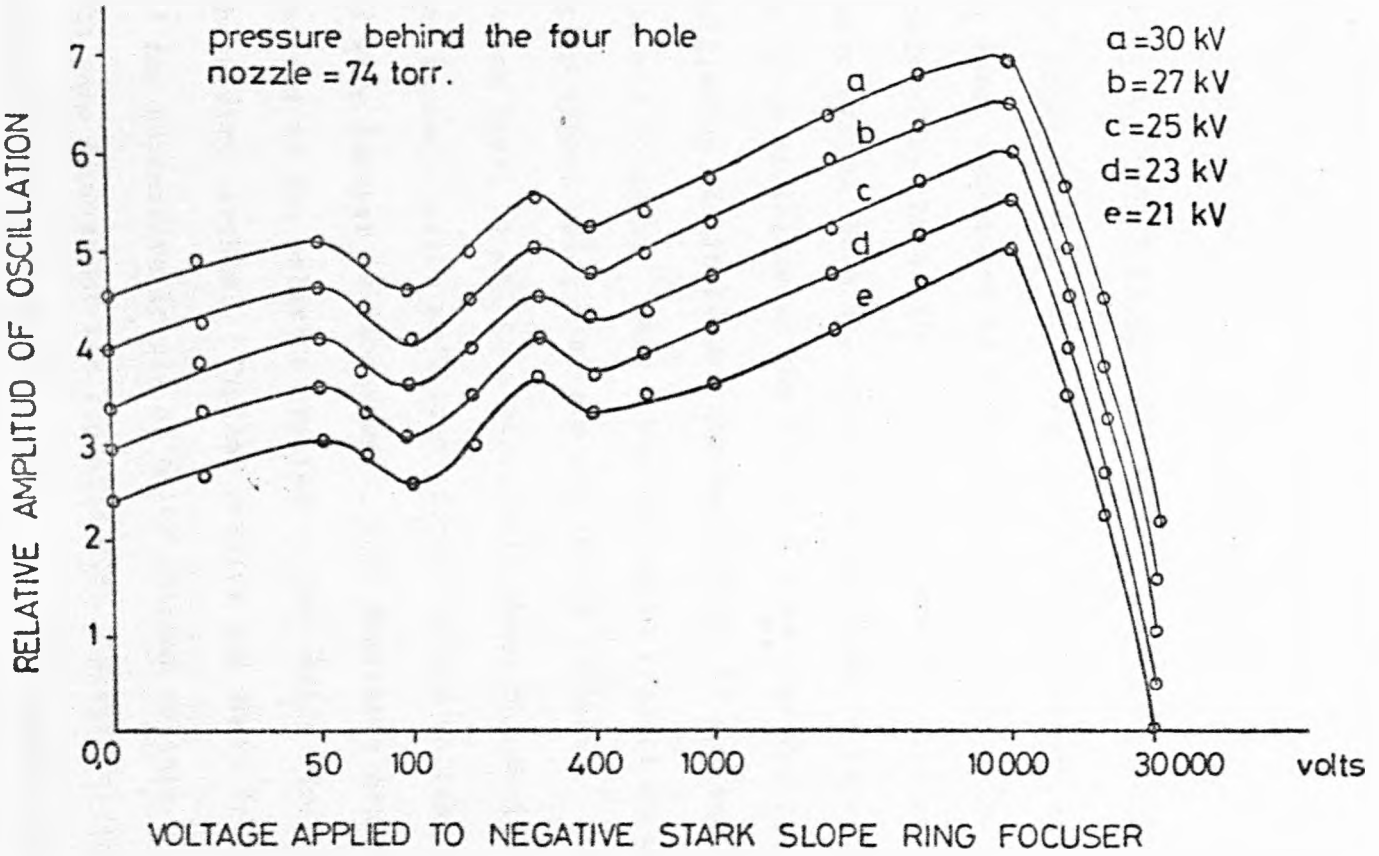

FIGURE(6.2) RELATIONSHIP BETWEEN THE OSCILLATION AMPLITUDE USING A RING FOCUSER AS A FUNCTION OF VOLTAGE APPLIED TO THE NEGATIVE STARK SLOPE RING FOCUSER FOR DIFFERENT SET VALUES OF VOLTAGE ON FIRST FOCUSER.

complex configuration of the electric field outside the negative Stark slope ring focuser, and the unknown spatial distribution or magnitude of the fringe field between the second focuser exit and the earthed cavity. For that reason the precise origin of the two dips is not clear. The smooth decay of the oscillation amplitude for voltages of 10kV and above, applied to the second focuser occurs as a result of cancellation of the focused emission beam by the focuser action of the external field of the second ring focuser.

6.2 Maser oscillator as detector of absorptive molecules

The focusing of lower energy state molecules may be studied by using a maser oscillator as a detector of the absorptive molecular beam produced by the single wire helix focuser. The second molecular beam maser system (beam 2), head on to the beam to be studied (beam 1) was set up to oscillate on the J = 3, K = 3 inversion line of NH_3. The oscillation threshold was reached with 14 kV applied to the octopole rod focuser. Beam 1 was set up to produce an enhanced absorption signal using a single wire helix focuser. When the maser oscillation level is set to a value well above threshold, a smooth decrease in oscillation amplitude occurs, as the voltage applied to the crossed wire focuser is increased. This monotonic decrease occurs irrespective of the polarity applied to the single wire helix focuser, with the cavity earthed. Typical results are shown in fig (6.3) plotted for successive levels of maser focuser voltage.

The same experiment was repeated with a single straight wire, crossed-wire and negative Stark slope focusing systems and similar results were obtained.

6.3 Studies of the amplitude of absorption or emission using two focusers in series

a) Two crossed-wire focusers in series

When two crossed-wire focusers were operated with the parameters

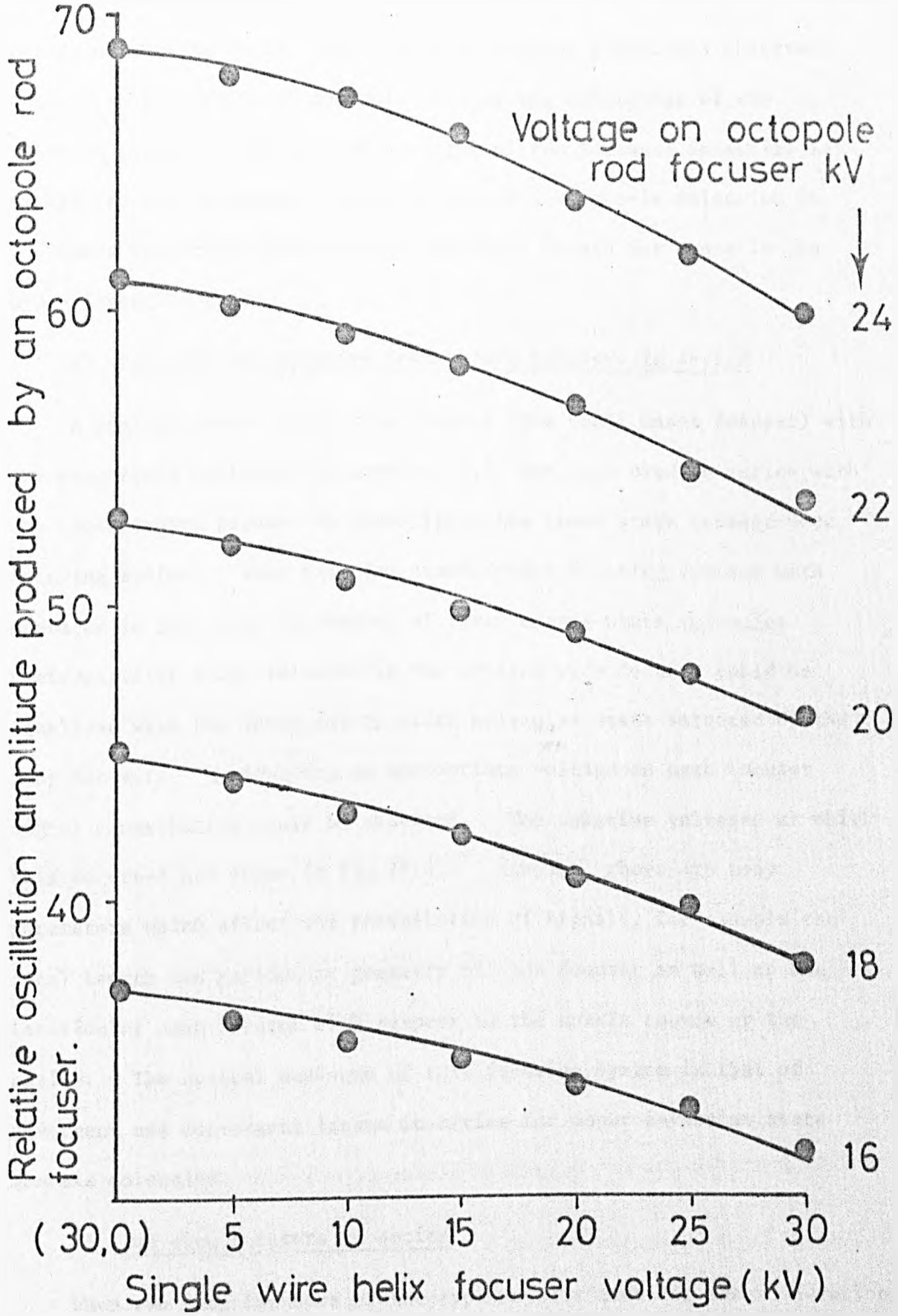

FIGURE (6.3) AMPLITUDE OF MASER OSCILLATION USING BEAM 2 AS A FUNCTION OF THE SINGLE WIRE HELIX FOCUSER VOLTAGE (BEAM 1) PRODUCING AN ENHANCED ABSORPTION.

detailed in table (3.2), only a weak absorption signal was observed, because of scattering of gas molecules by the electrodes of the focusing system. The optical analogue of two focusers in series is similar to two convergent lenses in series for ammonia molecules in the lower inversion state and two divergent lenses for those in the upper inversion state.

b) Positive and negative Stark slope focusers in series

A positive Stark slope ring focuser (the usual maser focuser) with the parameters mentioned in section (3.4) has been used in series with the crossed-wire focuser to investigate the lower state crossed-wire focusing system. When ring and crossed-wire focusing systems were operated in this way, the number of lower energy state molecules preferentially state selected by the crossed-wire focuser could be equalized with the upper energy state molecules state selected by the ring focuser. By applying an appropriate voltage on each focuser signal cancellation could be observed. The relative voltages at which this occurred are shown in fig (6.4). However, there are many parameters which affect the cancellation of signals, for example the focal length and particular geometry of each focuser as well as the location of each focuser with respect to the nozzle source or the cavity. The optical analogue of this focusing system is that of divergent and convergent lenses in series for upper inversion state ammonia molecules.

c) Two ring focusers in series

When two ring focusers of the type usually used for maser operation were operated with the parameters detailed in table (3.3a,b), strong stimulated emission was observed. The amplitude of the emission signal was two to three times that of each ring focuser operated individually as shown in fig (6.5).

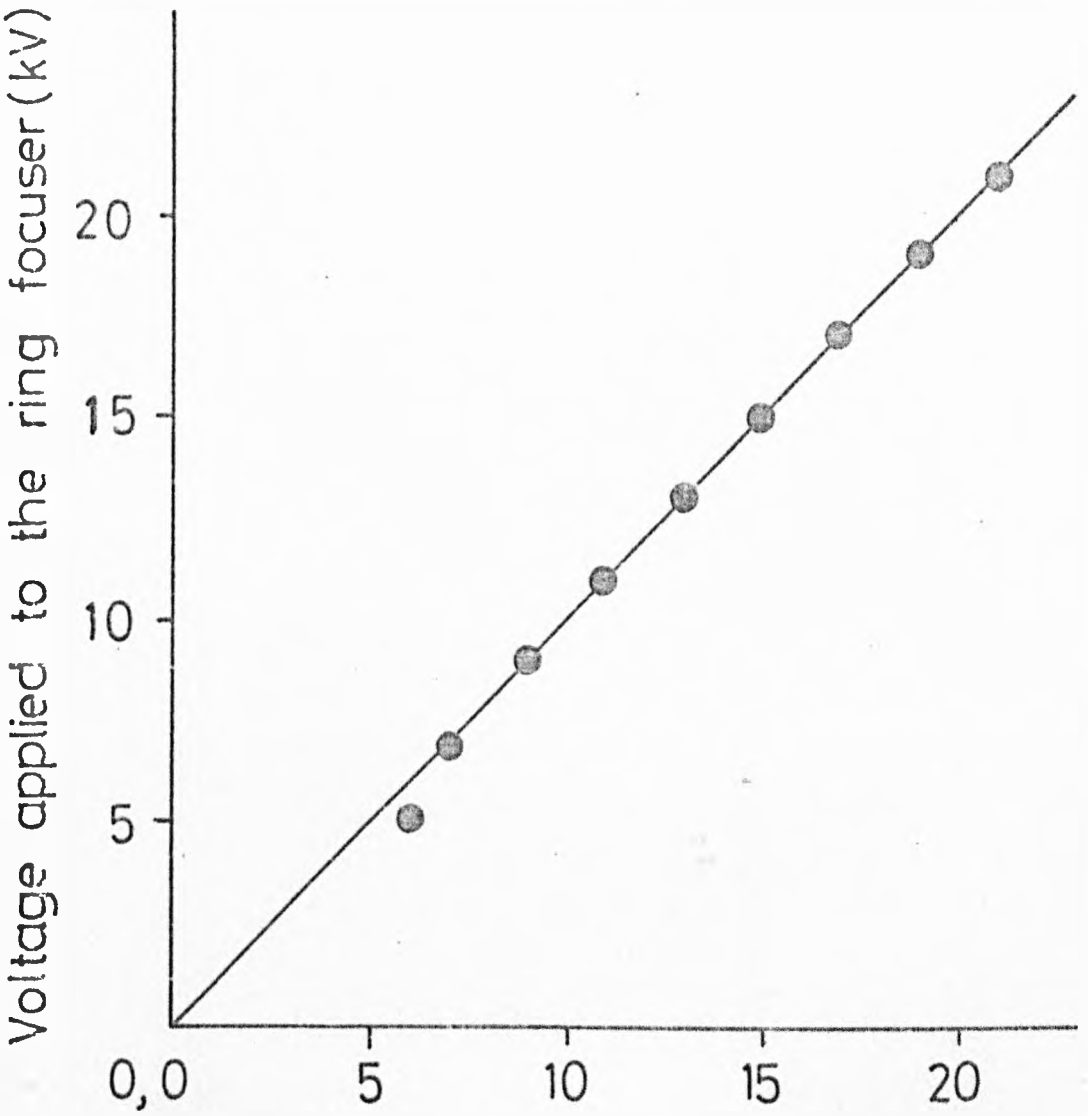

FIGURE (6.4) VOLTAGE RELATIONSHIP FOR RING AND CROSSED WIRE FOCUSER COMBINATION FOR SIGNAL CANCELLATION.

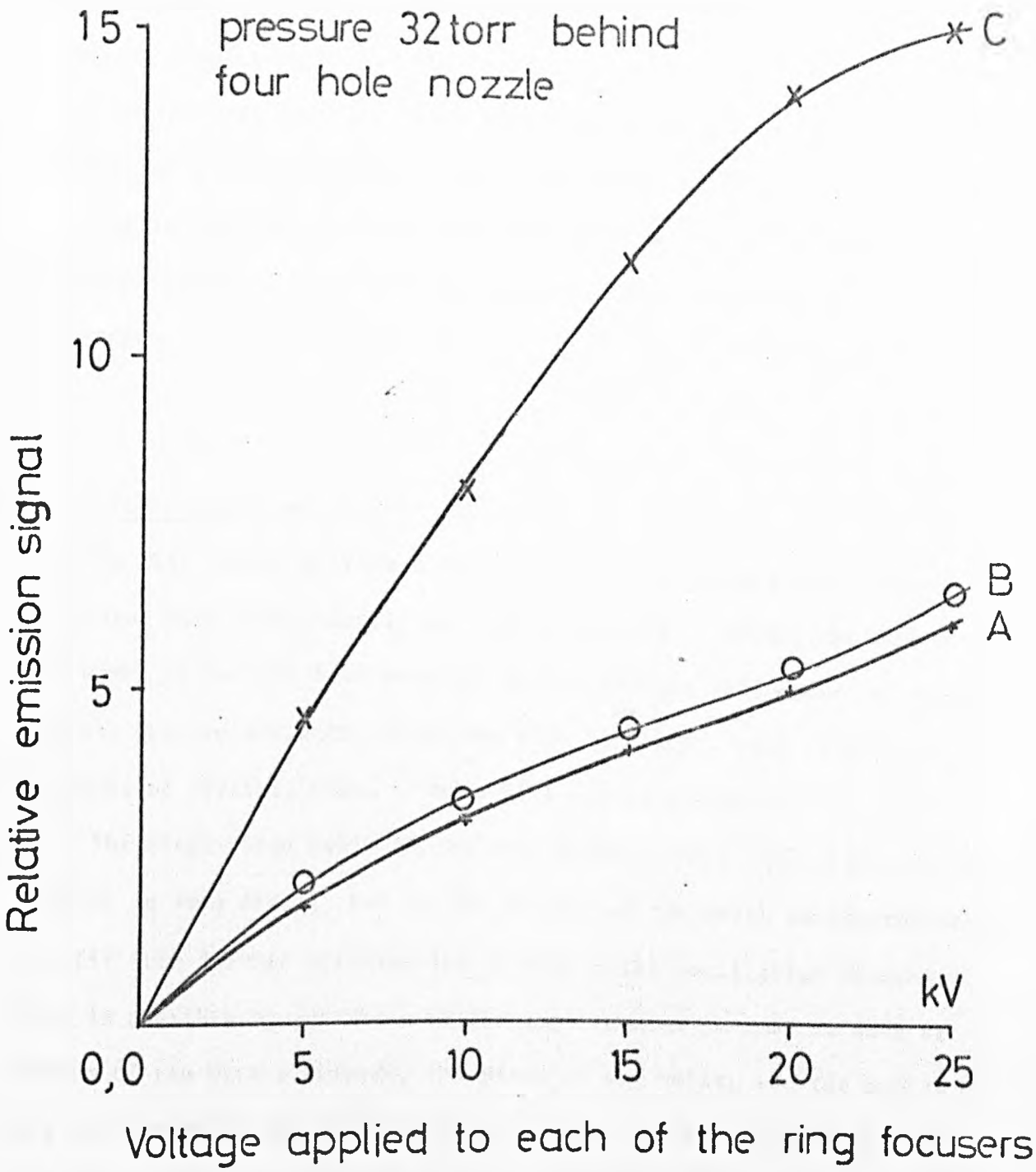

FIGURE(6.5) RELATIONSHIP BETWEEN TWO RING FOCUSERS IN SERIES FOR MAXIMIZING THE EMISSION SIGNAL, A,B REPRESENT THE AMPLITUDE OF THE EMISSION SIGNAL WHEN EACH FOCUSER IS OPERATED INDIVIDUALLY, C REPRESENTS THE EMISSION AMPLITUDE WHEN THE RING FOCUSER ARE OPERATED IN SERIES.

The first ring had a 3mm internal diameter with solid angle of beam capture 0.03 radian, whereas the second ring focuser had a 6mm internal diameter with a solid angle of capture of 0.02 radian.

The optical analogue of two focusers in series is similar to two convergent lenses for the upper inversion state of ammonia molecules.

It is important to point out that there is an improvement in detected signal strength over a single focuser, by using two focusers in series.

6.4 Conclusions and Further Work

In this thesis different types of focusing schemes have been discussed both theoretically and experimentally. During the course of the work, it has not been possible to add all the refinements or carry out all the improvements, which now with hindsight, seem to offer interesting possibilities. These will now be discussed.

The single wire helix (Al-Amiedy, Dugdale and Laine, 1979) has been studied in some detail, but in the context of the maser oscillator could benefit from further optimization to reduce the oscillation threshold. This is possible by variation of the experimental parameters such as radius of the wire electrode, the pitch of the helix, and the number of the helix turns used, in similar way that the multipole longitudinal rod focuser was improved in performance (Helmer et al, 1960).

A further improvement may result by the use of a tapered single wire helix. Like the basic helical focuser, this would be quite easy to construct. Again the helix could be wound with freshly stretched nickel wire of small diameter on a conical former, after which it is removed and extend to the pitch required. The tapered single wire helix is then mounted in a frame whose state selection properties are sufficiently small be ignored.

It would be useful initially to use a tapered helix having the same length as the single wire helix discussed in this thesis in order to compare the relative efficiency of tapered and non-tapered types.

It may also be possible to use the external field of the tapered single wire helix to enhance molecular beam absorption in a similar way to that with a ring focuser, by using a beam stop at the entrance of the focuser.

The use of the electrostatic field outside the ring focuser was a new approach for focusing schemes which state select molecules that possess a positive induced dipole moment. This fact stimulated a re-examination of some of the more common focusing systems both experimentally and theoretically, such as the ring, octopole rod and bifilar helix types which are commonly used for focusing molecules that possess a negative induced dipole moment ($\mu_{eff} < 0$). The recognition of the importance of the external field also opens up a new approach which takes into account molecules which possess a positive induced dipole moment ($\mu_{eff} > 0$) in the calculation of molecular trajectories. Previous investigators such as Shcheglor (1961). Mednikov and Parygin (1963) and others ignored these molecules in their calculations, and assumed that molecules rejected from the focuser were totally lost from the beam.

A new feature of state selection with two ring focusers in series has been obtained in the form of an anomalous behaviour of oscillation amplitude with second focuser voltage. This has been attributed to spatial reorientation of molecules. However, more work needs to be carried out to identify the exact cause of each oscillation dip at low voltages applied to the second ring focuser.

The multipole hole nozzle in the experiments discussed in this thesis was used as a beam source and an improvement of the intensity of the molecular beam was obtained with up to four holes. It is clearly possible to go further and use five or six hole nozzles in conjunction

with the ammonia molecular beam to find an optimum value for the number of holes.

An improvement was made by using the four hole rather than a single hole nozzle as a beam source with the single wire helix from the signal-to-noise point of view. This improvement also benefitted the crossed-wire focuser and single straight focuser in a similar way, for which an axial beam source is clearly not the most appropriate one, since the central portion of the state selecting device acts as a beam stop.

APPENDIX 3

```
  'BEGIN'
     'REAL''ARRAY' V[0:1100];
'REAL''ARRAY' C[0:10] ;
     'REAL' I ;
'REAL' I2;
'REAL'H,A,B,L,Z,Z1,R,TWOPI,BR ;
'INTEGER' P ;
'INTEGER' N,M ;
'REAL' K;
'REAL' 'PROCEDURE' FN(Z   );'VALUE'Z   ;'REAL' Z    ;
     'BEGIN'
     FN   := (1/SQRT(2*R↑2*(1-COS((TWOPI*Z)/L) ) + (Z1-Z)↑2 ) ) ;
'END' OF FN PROCEDURE;
     M := 1000 ;
     L:= 1.5 ;
     TWOPI:= 2*3.14159;
     R:= 0.229 ;
     A := ( - 2*L ) ;
     B :=  3 * L ;
     H := ( (B-A)  / M ) ;
    'FOR' Z1:=0.029'STEP'((L  -2*0.029)/10)'UNTIL'(L  -0.029)'DO'
     'BEGIN'
       I := FN(A) +FN(B) ;
       'FOR' N := 1 'STEP'  2 'UNTIL' ( M-1 ) 'DO'
       I := I + FN ( A+N*H ) * 4 ;
       'FOR' N := 2 'STEP'  2 'UNTIL' ( M-2 ) 'DO'
       I := I + FN ( A+N*H ) * 2 ;
       I := H* I /3 ;
       PRINT(Z1,3,3);SPACE(2);
       PRINT(I,0,3);NEWLINE(2);
     'END';
     'END'
```

```
'BEGIN'
     'COMMENT'
     A IS THE INTIAL VALUE OF THE INTEGRATION .
    BR IS THE RADIUS OF THE WIRE.
     B IS THE FINAL VALUE OF THE INTEGRATION.
  Z1   HAS THE VALUE FROM BR ( RADIUS OF THE WIRE  TO (L-BR) .
      Z= N*L/100 .
   V= SUM FROM N=0 TO N=10 OF AN* COS  N*TWOPI*Z / L .
     H IS THE INTEGRATION STEP.
      M IS EVEN NUMBER ALWAYS;
    'REAL''ARRAY' V[0:1100];
'REAL''ARRAY' C[0:10] ;
'REAL' I2;
'REAL'H,A,B,L,Z,Z1,R,TWOPI,BR ;
'REAL' K;
'INTEGER' P ;
'INTEGER' N,M ;
'REAL' 'PROCEDURE' FN(Z,Z1);'VALUE'Z,Z1;'REAL' Z,Z1 ;
     'BEGIN'
     FN   := (1/SQRT(2*R↑2*(1-COS((TWOPI*Z)/L) ) + (Z1-Z)↑2 ) ) ;
'END' OF FN PROCEDURE;
```

```
'REAL''PROCEDURE' I(Z1);'VALUE'Z1;'REAL' Z1;
'BEGIN'
'INTEGER' N ;
'REAL' A,B,K,H;
     A := ( -2*L) ;
     B:= 3*L ;
     'IF' Z1 < BR 'THEN' I:= 9,918
      'ELSE'  'IF' Z1 > (L-BR) 'THEN' I:= 9,918        'ELSE'
         'BEGIN'
     H:=((B-A) /M  ) ;
    K:=  FN(A,Z1) + FN(B,Z1) ;
     'FOR' N := 1 'STEP' 2 'UNTIL' ( M-1) 'DO'
     K := K +  FN((A + N*H),Z1) * 4 ;
     'FOR' N := 2 'STEP' 2 'UNTIL' ( M-2) 'DO'
     K := K +  FN((A + N*H),Z1) * 2 ;
     I := H * K / 3 ;
'END';
'END' OF SIMPSION RULE INTEGRATION PROCEDURE ;
A:= 0;
M:= 100 ;
     R:= 0,229 ;
BR:= 0,029;
   'BEGIN'
     L := 1,5 ;
      B := L ;
H:= ((B-A)/M) ;
TWOPI:= 2*3,14159;
     'FOR' N:= 0 'STEP' 1 'UNTIL' 100 'DO'
    'BEGIN'
       V[N] := I(( N*L)/ 100 ) * (( 10 ) /( 3*9,918 ) ) ;
PRINT(N,2,2);SPACE(4);
      PRINT( V[N] ,0,3) ;
     SPACE(2);
  PRINT(L,2,2);
'END' OF L  LOOP ;
    'END';
      'FOR' P:= 0 'STEP' 1 'UNTIL'  10 'DO'
'BEGIN'
      I2 := V[0] *COS((P*TWOPI*A) / L )+ V[M]*COS((P*TWOPI*B)/L);
'FOR' N:= 1 'STEP' 2 'UNTIL' ( M- 1) 'DO'
      I2 := I2 + V[N] * COS ( P * TWOPI * ( A+N*H)  /  L  ) * 4 ;
'FOR' N:= 2 'STEP' 2 'UNTIL' ( M- 2) 'DO'
      I2 := I2 + V[N] * COS ( P * TWOPI * ( A+N*H)  /  L  ) * 2 ;
     I2 := H * I2 /3 ;
'IF' P=0 'THEN' C[P] := I2/L
    'ELSE'   C[P]:= I2 * 2 / L ;
PRINT( P,2,2);SPACE(2);
PRINT(C[P],0,3);SPACE(2);
PRINT(I2,0,3);SPACE(2);
PRINT(H,0,3);SPACE(2);
PRINT(V[0],0,3);SPACE(2);
PRINT(V[M],0,3);SPACE(2);
PRINT(V[N],0,3);SPACE(2);
PRINT(N,2,2);SPACE(2);
    NEWLINE(2);
'END' OF  P LOOP ;
```

```
      'FOR' N:= 0 'STEP' 1 'UNTIL'  10 'DO'
'BEGIN'
PRINT(N,2,2);SPACE(4);
   PRINT(C[N],0,3);
   NEWLINE(2);
'END';
'FOR' N:= 0 'STEP' 1 'UNTIL' 100 'DO'
'BEGIN'
V[N]:= 0 ;
    'FOR' P := 0 'STEP'  1 'UNTIL'  1 'DO'
       V[N] := V[N] + C[P] * COS (  ( P*TWOPI*N ) / 100 ) ;
PRINT(N,2,2);SPACE(4);
PRINT(V[N],0,3);SPACE(4);
NEWLINE(2);
'END';
'FOR' N:= 0 'STEP' 1 'UNTIL' 100 'DO'
'BEGIN'
V[N]:= 0 ;
    'FOR' P := 0 'STEP'  1 'UNTIL'  2 'DO'
       V[N] := V[N] + C[P] * COS (  ( P*TWOPI*N ) / 100 ) ;
PRINT(N,2,2);SPACE(4);
PRINT(V[N],0,3);SPACE(4);
NEWLINE(2);
'END';
'FOR' N:= 0 'STEP' 1 'UNTIL' 100 'DO'
'BEGIN'
V[N]:= 0 ;
    'FOR' P := 0 'STEP'  1 'UNTIL'  3 'DO'
       V[N] := V[N] + C[P] * COS (  ( P*TWOPI*N ) / 100 ) ;
PRINT(N,2,2);SPACE(4);
PRINT(V[N],0,3);SPACE(4);
NEWLINE(2);
'END';
'END'
```

APPENDIX 4

```
      'BEGIN'
      'REAL''PROCEDURE'S18AEA(X,IFAIL);'VALUE'X;'REAL'X;'INTEGER'IFAIL;
      'ALGOL';
      'REAL''PROCEDURE'S18AFA(X,IFAIL);'VALUE'X;'REAL'X;'INTEGER'IFAIL;
      'ALGOL';
      'REAL''PROCEDURE'S18ACA(X,IFAIL);'VALUE'X;'REAL'X;'INTEGER'IFAIL;
      'ALGOL';
      'REAL''PROCEDURE'S18ADA(X,IFAIL);'VALUE'X;'REAL'X;'INTEGER'IFAIL;
      'ALGOL';
      'INTEGER' IFAIL ;
      'REAL' RF2,RHS,Y2,RVH,COSAL,ML,DT,OSD;
      'REAL' DE,DZ;
      'REAL' PN,TN,ZN;
      'REAL' DR2,ML2,SINAL;
      'REAL' EL,FRG,FZG;
      'REAL' ANGLEQ2,VFIN,VRS,VHS,PHTHS;
      'REAL' VOL02 ;
      'INTEGER' Q2 ;
      'REAL' LTP,HT ;
      'REAL' I0TPR1 ,I2TPR1 ;
      'REAL''ARRAY' R,Z,TH,VR,VZ,VH[0:800];
       'REAL' BK,NT,KT,ND,DF,NF,FL,FC,CL,Y,M,ZA,VOL0,OMEGAAV,PS,S,
      NS,OMEGA,DA,Q,ANGLE,SINANG,COSANG,TANANG,T;
      'REAL' I3TPRL,I4FPRL, I5SPRL,I1TPR1,THPL2, HTPL2;
      'REAL'HV02,FUE2,HFUE,AM2,AM,UUM;
      'INTEGER' N ;
      'REAL' I2SPR1 ;
'REAL' UE,I2FPR1 ;
      'REAL' ONEPI,TWOPI,THREEPI,FOURPI,SIXPI,R1,TPR1,I0R1,I1R1,I2R1,
      SPR1,        CO,CT,CE,FPR1,        I2FPRL,I0SPRL,PHTH3,PHTH,
      COSTH,COSTWOTH,COSTHREETH,I0TPRL,I2TPRL,        I0FPRL,I1FPRL,
      I1SPRL,I2SPRL,I3SPRL,        PHR1,PHR2,PHR3,PHR,PHRT,PHTH1,PHTH2,
      RPHTH,RPHTH2,PHZ1,PHZ2,PHZ3,PHZ,PHZT,E,MJ,J,K,U0,U,H,V0,HV0,HHV0,
      OPL,TPL,THPL,FPL,SPL,TPRL,FPRL,SINTH,SINTWOTH,SINTHREETH,
      HHV02,U2,UE2,QE, L,  SPRL,THETA,I1TPRL,I3FPRL,I4SPRL,I3SPR1;
      'REAL'OPL2,TPL2,HOPL2,FPL2,HFPL2,SPL2,HSPL2,
      ERR1,ERR2,ERR3,ERR,ETHR1,ETHR2,ETHR3,ETHR,
      EZR1,EZR2,EZR3,EZR,     ERZ1,ERZ2,ERZ3,ERZ,
     ETHZ1,ETHZ2,ETHZ3,ETHZ,EZZ1,EZZ2,EZZ3,
      EZZ,DR ;
'REAL''PROCEDURE' BESI(W,Z);'VALUE'W,Z;'INTEGER' W;'REAL' Z;
 'BEGIN'
    'IF' W<2 'THEN'
                 'BEGIN'
                      'IF'W=0 'THEN'
                     BESI:= S18AEA(Z,IFAIL)  'ELSE'
                     BESI:= S18AFA(Z,IFAIL);
               'END'
       'ELSE'
                BESI:=BESI((W-2),Z)- (2*(W-1) /Z) * BESI((W-1),Z);
              'END' OF I BESSEL FUNCTION PROCEDURE;
'REAL''PROCEDURE' BESK(W,Z);'VALUE' W,Z;'INTEGER' W;'REAL'Z;
    'BEGIN'
        'IF'  W<2 'THEN'
                        'BEGIN'
                             'IF' W=0 'THEN'
                               BESK:= S18ACA(Z,IFAIL)  'ELSE'
                               BESK:= S18ADA(Z,IFAIL) ;
```

```
                    'END'
                'ELSE'
            BESK:=BESK((W-2),Z)+ (2*(W-1) /Z) * BESK((W-1),Z);
  'END' OF K BESSEL FUNCTION  PROCEDURE ;
 'REAL''PROCEDURE' ELE(PN,ZN,TN);'VALUE'PN,ZN,TN;
 'REAL'PN,ZN,TN;
 'BEGIN'
 L := 1.5 ;
 ONEPI:=3.14159;
 TWOPI:=2*ONEPI;
 THREEPI:=3*ONEPI;
 FOURPI:=4*ONEPI;
 SIXPI:=6*ONEPI;
 R1:=0.23;
 TPR1:=((TWOPI*R1)/L);
I0R1:=S18AEA(TPR1,IFAIL);
I1R1:=S18AFA(TPR1,IFAIL);
I2R1:=BESI(2,TPR1);
 FPR1:=2*TPR1;
 I2FPR1:=BESI(2,FPR1);
SPR1:=3*TPR1;
 I3SPR1 := BESI(3,SPR1) ;
 CO:=4.119 &-1;
 CT:=1.896 &-1;
 CE:=1.113 &-1;
 OPL:=ONEPI/L;
 TPL:=TWOPI/L;
 THPL:=THREEPI/L;
 FPL:=FOURPI/L;
 SPL:=SIXPI/L;
 TPRL := (( TWOPI * PN ) / L ) ;
 FPRL := 2 * TPRL ;
 SPRL := 3 * TPRL ;
 THETA:=(TN-((TWOPI*ZN)/L));
 SINTH:=SIN(THETA);
 SINTWOTH:=SIN(2*THETA);
 SINTHREETH:=SIN(3*THETA);
 COSTH:=COS(THETA);
 COSTWOTH:=COS(2*THETA);
 COSTHREETH:=COS(3*THETA);
 I0TPRL:=S18AEA(TPRL,IFAIL);
 I1TPRL:=S18AFA(TPRL,IFAIL);
 I2TPRL:=BESI(2,TPRL);
 I0FPRL:=S18AEA(FPRL,IFAIL);
 I1FPRL:=S18AFA(FPRL,IFAIL);
 I2FPRL:=BESI(2,FPRL);
 I3FPRL:= BESI(3,FPRL) ;
 I0SPRL:=S18AEA(SPRL,IFAIL);
 I1SPRL:=S18AFA(SPRL,IFAIL);
 I2SPRL:=BESI(2,SPRL);
 I3SPRL:=BESI(3,SPRL);
 I4SPRL:=BESI(4,SPRL);
 PHR1:=((OPL*CO*(I2TPRL+I0TPRL)*COSTH)/I1R1);
 PHR2:=((TPL*CT*(I3FPRL+I1FPRL)*COSTWOTH)/I2FPR1);
 PHR3:=((THPL*CE*(I4SPRL+I2SPRL)*COSTHREETH)/I3SPR1);
 PHR:=PHR1+PHR2+PHR3;
 PHRT:=PHR *PHR ;
 PHTH1:=((CO*I1TPRL*SINTH)/I1R1);
 PHTH2:=((2*CT*I2FPRL*SINTWOTH)/I2FPR1);
 PHTH3:=((3*CE*I3SPRL*SINTHREETH)/I3SPR1);
 PHTH:=-(PHTH1+PHTH2+PHTH3);
```

```
RPHTH := ( PHTH / PN ) ;
RPHTH2:=RPHTH*RPHTH;
PHZ1:=((TPL*CO*I1TPRL*SINTH)/I1R1);
PHZ2:=((FPL*CT*I2FPRL*SINTWOTH)/I2FPR1);
PHZ3:=((SPL*CE*I3SPRL*SINTHREETH)/I3SPR1);
PHZ:=PHZ1+PHZ2+PHZ3;
PHZT:=PHZ*PHZ;
ELE := VOL0 * SQRT( PHRT + RPHTH2 + PHZT ) ;
'END' OF ELE  PROCEDURE;
'REAL''PROCEDURE' DE2R(PN,ZN,TN);'VALUE' PN,ZN,TN;
'REAL' PN,ZN,TN;
'BEGIN'
 VOL02 := VOL0*VOL0 ;
L := 1,5 ;
CO:=4,119 &-1;
CT:=1,896 &-1;
CE:=1,113 &-1;
ONEPI:=3,14159;
TWOPI:=2*ONEPI;
THREEPI:=3*ONEPI;
FOURPI:=4*ONEPI;
SIXPI:=6*ONEPI;
R1:=0,23;
TPR1:=((TWOPI*R1)/L);
I0R1:=S18AEA(TPR1,IFAIL);
I0 TPR1 :=  I0 R1 ;
I1R1:=S18AFA(TPR1,IFAIL);
I1 TPR1 :=  I1 R1 ;
I2R1:=BESI(2,TPR1);
I2 TPR1 :=  I2 R1 ;
FPR1:=2*TPR1;
I2FPR1:=BESI(2,FPR1);
SPR1:=3*TPR1;
I3SPR1 := BESI(3,SPR1);
OPL:=ONEPI/L;
OPL2:=OPL*OPL;
HOPL2:=0,5*OPL2;
TPL:=TWOPI/L;
TPL2:=TPL*TPL;
HTPL2 := 0,5 * TPL2 ;
THPL:=THREEPI/L;
THPL2 := THPL *THPL ;
FPL:=FOURPI/L;
FPL2:=FPL*FPL;
HFPL2:=0,5*FPL2;
SPL:=SIXPI/L;
SPL2:=SPL*SPL;
HSPL2:=0,5*SPL2;
TPRL := (( TWOPI * PN ) / L ) ;
FPRL := 2 * TPRL ;
SPRL := 3 * TPRL ;
I0TPRL:=S18AEA(TPRL,IFAIL);
I1TPRL:=S18AFA(TPRL,IFAIL);
I2TPRL:=BESI(2,TPRL);
I3TPRL:=BESI(3,TPRL);
I0FPRL:=S18AEA(FPRL,IFAIL);
I1FPRL:=S18AFA(FPRL,IFAIL);
I2FPRL:=BESI(2,FPRL);
I3FPRL:=BESI(3,FPRL);
I4FPRL:=BESI(4,FPRL);
I0SPRL:=S18AEA(SPRL,IFAIL);
```

```
I1SPRL:=S18AFA(SPRL,IFAIL);
I2SPRL:=BESI(2,SPRL);
I3SPRL:=BESI(3,SPRL);
I4SPRL:=BESI(4,SPRL);
I5SPRL:=BESI(5,SPRL);
THETA:=(TN-((TWOPI*ZN)/L));
SINTH:=SIN(THETA);
SINTWOTH:=SIN(2*THETA);
SINTHREETH:=SIN(3*THETA);
COSTH:=COS(THETA);
COSTWOTH:=COS(2*THETA);
COSTHREETH:=COS(3*THETA);
PHR1:=((OPL*CO*(I2TPRL+I0TPRL)*COSTH)/I1R1);
PHR2:=((TPL*CT*(I3FPRL+I1FPRL)*COSTWOTH)/I2FPR1);
PHR3:=((THPL*CE*(I4SPRL+I2SPRL)*COSTHREETH)/I3SPR1);
PHR := PHR1 + PHR2 + PHR3 ;
PHTH1:=((CO*I1TPRL*SINTH)/I1R1);
PHTH2:=((2*CT*I2FPRL*SINTWOTH)/I2FPR1);
PHTH3:=((3*CE*I3SPRL*SINTHREETH)/I3SPR1);
PHTH := PHTH1 + PHTH2 + PHTH 3 ;
PHTHS := PHTH * PHTH ;
PHZ1 := ((TPL*CO*I1TPRL*SINTH)/I1R1);
PHZ2:=((FPL*CT*I2FPRL*SINTWOTH)/I2FPR1);
PHZ3:=((SPL*CE*I3SPRL*SINTHREETH)/I3SPR1);
PHZ := PHZ1 + PHZ2 + PHZ3 ;
ERR1:=OPL2*(CO/I1TPR1)*((I3TPRL+I1TPRL)+(2*I1TPRL))*COSTH;
ERR2:=TPL2*(CT/I2FPR1)*((I4FPRL+I2FPRL)+
(I2FPRL+I0FPRL))*COSTWOTH;
ERR3:=THPL2*(CE/I3SPR1)*((I5SPRL+I3SPRL)+
(I3SPRL+I1SPRL))*COSTHREETH;
ERR := ERR1 + ERR2 + ERR3 ;
ETHR1:=(CO/I1TPR1)*OPL*(I2TPRL+I0TPRL)*SINTH;
ETHR2:=(CT/I2FPR1)*FPL*(I3FPRL+I1FPRL)*SINTWOTH;
ETHR3:=(3*CE/I3SPR1)*THPL*(I4SPRL+I2SPRL)*SINTHREETH;
ETHR := ETHR1 + ETHR2 + ETHR3 ;
EZR1:=HTPL2*(CO/I1TPR1)*(I2TPRL+I0TPRL)*SINTH;
EZR2:=(HFPL2*(CT/I2FPR1)*(I3FPRL+I1FPRL)*SINTWOTH )  ;
EZR3 :=HSPL2*(CE/I3SPR1)*(I4SPRL+I2SPRL)*SINTHREETH;
EZR:=EZR1+EZR2+EZR3;
DE2R:= VOL02*2*( PHR*ERR+((1/PN↑2)*PHTH*ETHR)-((1/PN↑3)*PHTHS)+
     PHZ*EZR) ;
'END' OF  DE2R  PROCEDURE ;
'REAL''PROCEDURE' DE2Z(PN,ZN,TN);'VALUE' PN,ZN,TN;
'REAL' PN,ZN,TN;
'BEGIN'
L := 1,5 ;
CO:=4,119&-1;
CT:=1,896&-1;
CE:=1,113&-1;
ONEPI:=3,14159;
TWOPI:=2*ONEPI;
THREEPI:=3*ONEPI;
FOURPI:=4*ONEPI;
SIXPI:=6*ONEPI;
OPL:=(ONEPI/L);
OPL2:=OPL*OPL;
HOPL2:=0,5*OPL2;
TPL:=2*OPL;
TPL2:=TPL*TPL;
HTPL2 := 0,5 * TPL2 ;
THPL:=3*OPL;
```

```
THPL2 := THPL *THPL ;
FPL:=4*OPL;
FPL2:=FPL*FPL;
HFPL2:=0.5*FPL2;
SPL:=6*OPL;
SPL2:=SPL*SPL;
HSPL2:=0.5*SPL2;
R1:=0.23;
TPR1:=((TWOPI*R1)/L);
I0R1:=S18AEA(TPR1,IFAIL);
I0 TPR1 :=  I0 R1 ;
I1R1:=S18AFA(TPR1,IFAIL);
I1 TPR1 :=  I1 R1 ;
I2R1:=BESI(2,TPR1);
I2 TPR1 :=  I2 R1 ;
FPR1:=2*TPR1;
I2FPR1:=BESI(2,FPR1);
SPR1:=3*TPR1;
I3SPR1 := BESI(3,SPR1) ;
TPRL:=(TWOPI*PN/L);
FPRL:=2*TPRL;
SPRL:=3*TPRL;
I0TPRL:=S18AEA(TPRL,IFAIL);
I1TPRL:=S18AFA(TPRL,IFAIL);
I2TPRL:=BESI(2,TPRL);
I0FPRL:=S18AEA(FPRL,IFAIL);
I1FPRL:= S18AFA(FPRL,IFAIL);
I2FPRL:=  BESI(2,FPRL);
I3FPRL:=BESI(3,FPRL);
I0SPRL:=S18AEA(SPRL,IFAIL);
I1SPRL:=S18AFA(SPRL,IFAIL);
I2SPRL:=BESI(2,SPRL);
I3SPRL:=BESI(3,SPRL);
I4SPRL:=BESI(4,SPRL);
I5SPRL:=BESI(5,SPRL);
THETA:=(TN-((TWOPI*ZN)/L));
SINTH:=SIN(THETA);
SINTWOTH:=SIN(2*THETA);
SINTHREETH:=SIN(3*THETA);
COSTH:=COS(THETA);
COSTWOTH:=COS(2*THETA);
COSTHREETH:=COS(3*THETA);
PHR1:=((OPL*CO*(I2TPRL+I0TPRL)*COSTH)/I1R1);
PHR2:=((TPL*CT*(I3FPRL+I1FPRL)*COSTWOTH)/I2FPR1);
PHR3:=((THPL*CE*(I4SPRL+I2SPRL)*COSTHREETH)/I3SPR1);
PHR:=PHR1+PHR2+PHR3;
PHTH1:=((CO*I1TPRL*SINTH)/I1R1);
PHTH2:=((2*CT*I2FPRL*SINTWOTH)/I2FPR1);
PHTH3:=((3*CE*I3SPRL*SINTHREETH)/I3SPR1);
PHTH:=-(PHTH1+PHTH2+PHTH3);
PHZ1:=((TPL*CO*I1TPRL*SINTH)/I1R1);
PHZ2:=((FPL*CT*I2FPRL*SINTWOTH)/I2FPR1);
PHZ3:=((SPL*CE*I3SPRL*SINTHREETH)/I3SPR1);
PHZ:=PHZ1+PHZ2+PHZ3;
ERZ1:=OPL*(CO/I1TPR1)*(I2TPRL+I0TPRL)*SINTH * TPL ;
ERZ2:=FPL*(CT/I2FPR1)*(I3FPRL+I1FPRL)*SINTWOTH * FPL ;
ERZ3:=3*THPL*(CE/I3SPR1)*(I4SPRL+I2SPRL)*SINTHREETH * SPL ;
ERZ:=ERZ1+ERZ2+ERZ3;
ETHZ1:=(CO/I1TPR1)*I1 TPRL *COSTH;
ETHZ2:=4*(CT/I2FPR1)*I2FPRL*COSTWOTH;
ETHZ3:=9*(CE/I3SPR1)*I3SPRL*COSTHREETH;
```

```
    ETHZ:=ETHZ1+ETHZ2+ETHZ3;
    EZZ1:=TPL*(CO/I1TPR1)*I1TPRL*COSTH * TPL ;
 EZZ2:=2*FPL*(CT/I2FPR1)*I2FPRL*COSTWOTH   * FPL ;
    EZZ3:=3*SPL*(CE/I3SPR1)*I3SPRL*COSTHREETH * SPL ;
    EZZ:=EZZ1+EZZ2+EZZ3;
  DE2Z:= (2*PHR*(-1)*ERZ+2*(PHTH/PN↑2)*ETHZ+2*PHZ*EZZ )*VOL0↑2     ;
    'END' OF  DE2Z  PROCEDURE ;
    'REAL''PROCEDURE' GZ(PN,ZN,TN);'VALUE'PN,ZN,TN;
     'REAL' PN,ZN,TN;
    'BEGIN'
    M := 28,22 & - 24 ;
    H:= 6,6 & -27;
    VO := 2,4 & 10 ;
    HVO := H* VO ;
    HVO2:=HVO*HVO;
    HVO2 := ( HVO2 / 4 ) ;
    MJ:= SQRT(7) ;
    J:= 3;
    K:= 3;
    UO:= 1,47 & -18 ;
    U := (( UO*MJ*K)/(J* (J+1)));
      U2 := U*U ;
    UE := U * ELE(PN,ZN,TN) ;
      UE2 := UE *UE ;
    FUE2:=4*UE2;
    HFUE:=(HVO2+  UE 2);
  GZ:= (U2 *(1/SQRT(HFUE))*DE2Z(PN,ZN,TN) / M    ) ;
    'END' OF GZ PROCEDUER ;
    'REAL''PROCEDURE' GR(PN,ZN,TN);'VALUE'PN,ZN,TN;
     'REAL' PN,ZN,TN;
    'BEGIN'
    M := 28,22 & - 24 ;
    H:= 6,6 & -27;
    VO := 2,4 & 10 ;
    HVO := H* VO ;
    HVO2:=HVO*HVO;
    HVO2 := ( HVO2 / 4 ) ;
    MJ:= SQRT(7) ;
    J:= 3;
    K:= 3;
    UO:= 1,47 & -18 ;
    U := (( UO*MJ*K)/(J* (J+1)));
      U2 := U*U ;
    UE := U * ELE(PN,ZN,TN) ;
      UE2 := UE *UE ;
    FUE2:=4*UE2;
    HFUE:=(HVO2+  UE 2);
  GR:= (U2 *(1/SQRT(HFUE))*DE2R(PN,ZN,TN) / M    ) ;
    'END' OF GR PROCEDUER ;
    ONEPI:=3,14159;
    TWOPI := 2 * ONEPI ;
    THREEPI:=3*ONEPI;
    FOURPI:=4*ONEPI;
    SIXPI:=6*ONEPI;
    L:= 1,5 ;
    LTP := ( L / TWOPI ) ;
    BK:= 1,38 &-16;
    NT:= 240;
    KT:= BK*NT;
```

```
      ND:= 5;
      DF:= 5 ;
       NF:= ND+DF;
      FL := 7,5 ;
      FC := 5,5 ;
      CL:= 10,8;
      Y:= 0,45 ;
      Y2 := Y * Y ;
      M:= 28,22 & -24 ;


      ZA:= 80;



      VOL0 := 30 ;

      'BEGIN'
       OMEGAAV := 0;
      PS := 14 ;
      'BEGIN'
      S:=PS*0,5& 4;
NS:= FOURPI*S    * (M/(TWOPI*KT) )↑1,5 * EXP( -M*S↑2 /(2*KT) ) ;
      OMEGA:=0;
      DA := 20 ;
       'FOR' Q := 60 'STEP' DA 'UNTIL' 220 'DO'
      'BEGIN'
      ANGLE:=(Q/&4);
      SINANG:=SIN(ANGLE);
      COSANG:= COS(ANGLE);
      TANANG:= SIN(ANGLE)/COS(ANGLE);
      OSD := ((  ONEPI * SINANG * DA ) / & 4 ) ;
      T:=(FL/(ZA*S*COSANG));
      HT := T * 0,5 ;
      'FOR' Q2 := 0 'STEP' 1 'UNTIL' 10 'DO'
      'BEGIN'
      ANGLEQ2 :=  (TWOPI*Q2 )/ 10 ;
      R[0] := NF * TANANG ;
      Z[0] := 0 ;
      TH[0] := ANGLEQ2 ;
      VR[0] := S * SINANG ;
      VZ[0] := S * COSANG ;
      'FOR' N:= 0 ,N+1 'WHILE' Z[N] < FL 'DO'
      'BEGIN'
        'IF' R[N]  < 0 'THEN'
                              'BEGIN'
                                    R[N] := - R[N] ;
                                   VR[N] := - VR[N];
                              'END';
      'IF' R[N] > 0,229 'THEN' 'GOTO' X;
      Z[N+1] := Z[N] + VZ[N] * T ;
      R[N+1] := R[N] + VR[N] * T ;
      VH[N] := (  (  VZ[0] - VZ[N] ) * LTP          ) / R[N] ↑ 2 ;
      TH[N+1] := TH[N] + VH[N] * T ;
      VR[N+1] :=VR[N]+ (( VH[N]↑2*R[N]) - GR(R[N],Z[N],TH[N])    )*T;
      VZ[N+1] := VZ[N] + ( GZ(R[N],Z[N],TH[N] )   ) * T ;
      VH[N+1] := (  ( VZ[0] - VZ[N+1] )*LTP         ) / R[N+1] ↑2 ;
```

```
Z[N+1]:=Z[N]+(VZ[N]+VZ[N+1])*HT ;
R[N+1] := R[N] + ( VR[N] + VR[N+1] ) * HT ;
VH[N] := (  ( VZ[0] - VZ[N] ) * LTP          ) / R[N] ↑ 2 ;
TH[N+1] := TH[N] + ( VH[N] + VH[N+1] ) * HT ;
VR[N+1]:= VR[N]+ (( VH[N]↑2*R[N]  - GR(R[N],Z[N],TH[N])    ) +
(  VH[N+1] ↑2 * R[N+1]- GR(R[N+1],Z[N+1],TH[N+1] )   )  ) *HT ;
VZ[N+1]:=VZ[N]+(GZ(R[N],Z[N],TH[N])
+GZ(R[N+1],Z[N+1],TH[N+1]))* HT ;
VH[N+1] := (  ( VZ[0] - VZ[N+1] )*LTP          ) / R[N+1] ↑2 ;
'END' OF N LOOP;
VRS := VR[N-1] * VR[N-1] ;
VHS := VH[N-1] * VH[N-1] ;
RF2 := R[N-1] * R[N-1] ;
RHS := VHS * RF2 ;
RVH := R[N-1] * VH[N-1] ;
VFIN := SQRT ( VRS + RHS );
SINAL := ( VR[N-1] / VFIN ) ;
ML := VFIN * ( FC / VZ[N-1] ) ;
ML2 := ML * ML ;
DR2 := RF2+ML2 + 2*R[N-1]*ML*SINAL ;
'IF' DR2 < Y2 'THEN'
'BEGIN'
ML := VFIN *(( FC+CL) / VZ[N-1]  ) ;
ML2 := ML * ML ;
DR2 := RF2+ML2 + 2*R[N-1]*ML*SINAL ;
'IF' DR2 < Y2 'THEN'
'BEGIN'
OMEGA := OMEGA+OSD ;
'END' OF D LOOP AT THE EXIT OF THE CAVITY;
          'END' OF D LOOP AT THE ENTRANCE OF THE CAVITY;
X;
'END' OF   Q2  LOOP ;
'END' OF Q ANGLE LOOP;
OMEGAAV:=OMEGAAV+OMEGA*NS* 1·&4;
'END' OF PS SPEED LOOP ;
PRINT(VOL0     ,2,2); SPACE(3);
PRINT(OMEGA,0,3); SPACE(3);
PRINT(OMEGAAV,0,3);
NEWLINE(2);
'END' OF VOLTAGE LOOP;
'END'
```

APPENDIX 5

```
      'BEGIN'
      'INTEGER'Q2;
      'REAL'  I0THPL, I1 THPL ;
      'REAL'RS,RS2,NTAN,ANT,TF1,TF12,TF2,TF22,
      RNT,VAR,VAR2,SVAR,VTO,AM,AM2,M2;
      'REAL' SSIN,ANGLEQ2,VTF,VTF2;
'REAL' I0THP0L,I1THP0L,I0P0L,I1P0L,I2PL,I2THPL,I0PL,I1PL;
     'REAL''PROCEDURE'S18ADA(X,IFAIL);'VALUE'X;'REAL'X;'INTEGER'IFAIL;
     'ALGOL';
     'REAL''PROCEDURE' S18ACA(X,IFAIL);'VALUE'X;'REAL'X;'INTEGER' IFAIL;
     'ALGOL';
     'REAL''PROCEDURE'S18AEA(X,IFAIL);'VALUE'X;'REAL'X;'INTEGER'IFAIL;
'ALGOL';
     'REAL''PROCEDURE'S18AFA(X,IFAIL);'VALUE'X;'REAL'X;'INTEGER'IFAIL;
'ALGOL';
      'REAL''ARRAY' P,Z,R,VR,VZ[0:800];
      'REAL' EL,FRG,FZG;
     'REAL' K0P0L,VOL0,K2THP0L,PVL2;
      'REAL' HHV02,Q,ZNL,XY,ST,PS,ZA,W,DR,Y,BK,NT,KT,ND,DF,NF,P0,FL,FC,
      CL,CR,M,V,OMEGA,S,T,OMEGAAV,NS,ONEPI,TWOPI,THREEPI,FOURPI,DA,ANGLE,
      SINANG,COS ANG,TANANG,K0THP0L,K1THP0L,OPL,UO,H,VO,HVO,HHVO,MJ,J,K,
            K1P0L,K2P0L,K0THPL,K1THPL,K1PL,K0PL,K2PL,K2THPL,PZL,THPZL,
      PVL,PUL2,PL,THPL,P0L,THP0L,L,U,U2,ZUL,UE,UE2,QE;
      'INTEGER'N,IFAIL;
'REAL''PROCEDURE' BESI(W,Z);'VALUE'W,Z;'INTEGER' W;'REAL' Z;
 'BEGIN'
     'IF' W<2 'THEN'
                  'BEGIN'
                        'IF'W=0 'THEN'
                     BESI:= S18AEA(Z,IFAIL)  'ELSE'
                     BESI:= S18AFA(Z,IFAIL);
                'END'
        'ELSE'
                   BESI:=BESI((W-2),Z)- (2*(W-1) /Z) * BESI((W-1),Z);
                 'END' OF I BESSEL FUNCTION PROCEDURE;
'REAL''PROCEDURE' BESK(W,Z);'VALUE' W,Z;'INTEGER' W;'REAL'Z;
     'BEGIN'
        'IF'  W<2 'THEN'
                        'BEGIN'
                              'IF' W=0 'THEN'
                                BESK:= S18ACA(Z,IFAIL)  'ELSE'
                                BESK:= S18ADA(Z,IFAIL) ;
                        'END'
                    'ELSE'
                   BESK:=BESK((W-2),Z)+ (2*(W-1) /Z) * BESK((W-1),Z);
      'END' OF K BESSEL FUNCTION  PROCEDURE ;
'REAL''PROCEDURE' OLE(PN,ZNL);'VALUE'PN,ZNL;'REAL'PN,ZNL;
      'BEGIN'
      ONEPI:=3,14159;
      TWOPI:=2*ONEPI;
      THREEPI:=3*ONEPI;
      FOURPI:=4*ONEPI;
      OPL:=(ONEPI/L);
      MJ:=SQRT(7);
      J:=3;
      K:=3;
```

```
      UO:=1,47&-18;
      U:=((UO*MJ*K)/(J*(J+1)));
      U2:=U*U;
      H:=6,6&-27;
      VO:=2,4&10;
      HVO:=H*VO;
      HHVO := HVO * 0,5;
      HHVØ2 := HHVO * HHVO;
        PØ := L ;
      PØL:=  ( ONEPI * PØ / L ) ;
      THPØL :=  3 * PØL ;
      KØPØL := S18ACA (PØL,IFAIL);
      K1PØL := S18ADA(PØL,IFAIL);
      KØTHPØL := S18ACA(THPØL,IFAIL);
      K1THPØL := S18ADA(THPØL,IFAIL);
      PL := (ONEPI * PN / L);
      KØPL := S18ACA(PL,IFAIL);
      K1PL := S18ADA(PL,IFAIL);
      K2PL := BESK(2,PL);
      THPL := (THREEPI * PN/L);
      KØTHPL := S18ACA(THPL,IFAIL);
      K1THPL := S18ADA(THPL,IFAIL);
      K2THPL := BESK(2,THPL);
      ZUL := (ZNL /L);
      PZL := ONEPI * ZUL;
      THPZL := THREEPI * ZUL;
      PVL := Ø,3 * ONEPI * VOLØ /L;
        OLE:=  PVL * SQRT(
      (2*(K1PL/KØPØL)*SIN(PZL)+(K1THPL/KØTHPØL)*SIN(THPZL))↑2+
      (2*(KØPL/KØPØL)*COS(PZL)+(KØTHPL/KØTHPØL)*COS(THPZL))↑2);
         'END' OF  OLE  PROCEDURE ;
'REAL''PROCEDURE' ILE(PN,ZNL);'VALUE'PN,ZNL;'REAL'PN,ZNL;
         'BEGIN'
      PØ := L ;
ONEPI := 3,14159 ;
TWOPI := 2 * 3,14159 ;
      THREEPI:= 3*3,14159;
FOURPI := 4 * 3,14159 ;
      OPL:=  ( ONEPI / L  );
      MJ:= SQRT(7) ;
     J:=3;
     K:=3;
     UO:=1,47&-18;
      U:=  (  ( UO*MJ*K)  /  ( J* ( J+1 )  )    ) ;
     U2:=U*U;
     H:=6,6 &-27;
     VO:=2,4 &10;
     HVO:= H* VO ;
     HHVO:=HVO*0,5;
       HHVØ2 :=  HHVO * HHVO ;
     PØL:=ONEPI*PØ/L;
     IØPØL:=S18AEA(PØL,IFAIL);
     I1PØL:=S18AFA(PØL,IFAIL);
     THPØL:=THREEPI*PØ/L;
     IØTHPØL:=S18AEA(THPØL,IFAIL);
     I1THPØL:=S18AFA(THPØL,IFAIL);
        PL := ( ONEPI * PN /  L  );
     IØ PL:=S18AEA(PL,IFAIL);
     I1 PL:=S18AFA(PL,IFAIL);
     I2PL:=IØPL-(2/PL)*I1PL;
       THPL :=  ( THREEPI * PN  /  L  );
```

```
    I0THPL:=S18AEA(THPL,IFAIL);
    I1THPL:=S18AFA(THPL,IFAIL);
    I2THPL:=I0THPL-(2/THPL)*I1THPL;
     ZUL := ZNL  / L  ;
    PZL:=ONEPI*ZUL;
    THPZL:=THREEPI*ZUL;
    PVL:=0.3*ONEPI*VOL0/L;
       ILE:=  PVL * SQRT(
        (2*(I1PL/I0P0L)*SIN(PZL)+(I1THPL/I0THP0L)*SIN(THPZL)) ↑2  +
        (2*(I0PL/I0P0L)*COS(PZL)+(I0THPL/I0THP0L)*COS(THPZL)) ↑2  ) ;
        'END' OF  ILE  PROCEDURE ;
'REAL''PROCEDURE'OFR(PN,ZNL);'VALUE' PN,ZNL;'REAL' PN,ZNL;
    'BEGIN'
    ONEPI := 3.14159;
    TWOPI := 2*ONEPI;
    THREEPI := 3*ONEPI;
    FOURPI := 4 * ONEPI;
    OPL := (ONEPI/L);
    MJ := SQRT(7);
    J:=3;
    K:=3;
    U0:=1.47&-18;
    U:=((U0*MJ*K)/(J*(J+1)));
    H:=6.6&-27;
    V0:=2.4&10;
    HV0:=H*V0;
    HHV0:=HV0*0.5;
    HHV02:=HHV0*HHV0;
    PVL:=0.3*ONEPI*VOL0/L;
    PVL2:=PVL*PVL;
    PL:=(ONEPI*PN/L);
    K0PL:=S18ACA(PL,IFAIL);
    K1PL:=S18ADA(PL,IFAIL);
    K2PL:=BESK(2,PL);
    THPL:=(THREEPI*PN/L);
    K0THPL:=S18ACA(THPL,IFAIL);
    K1THPL:=S18ADA(THPL,IFAIL);
    K2THPL:=BESK(2,THPL);
      P0 := L ;
    P0L:=  ( ONEPI * P0 / L ) ;
    K0P0L:=S18ACA(P0L,IFAIL);
    K1P0L:=S18ADA(P0L,IFAIL);
    K2P0L:=BESK(2,P0L);
    THP0L :=  3 * P0L ;
    K0THP0L:=S18ACA(THP0L,IFAIL);
    K1THP0L:=S18ADA(THP0L,IFAIL);
    U2:=U*U;
    UE:= U * OLE(PN,ZNL);
    UE2:=UE*UE;
    QE:=((U2)/(SQRT(HHV02+UE2)));
    ZUL:=ZNL/L;
    PZL:=ONEPI*ZUL;
    THPZL:=THREEPI*ZUL;
   OFR:= (  QE*2*OPL*PVL2* (
    (2*(K1PL/K0P0L)*SIN(PZL)+(K1THPL/K0THP0L)*SIN(THPZL))*
    (((K2PL+K0PL)/K0P0L)*SIN(PZL)+
    1.5*((K2THPL+K0THPL)/K0THP0L)*SIN(THPZL) )   +
    (2*(K0PL/K0P0L)*COS(PZL)+(K0THPL/K0THP0L)*COS(THPZL))*
    ((2*K1PL/K0P0L)*COS(PZL)+3*(K1THPL/K0THP0L)*COS(THPZL))));
'END' OF PROCEDURE  OFR ;
```

```
 'REAL''PROCEDURE'IFR(PN,ZNL);'VALUE' PN,ZNL;'REAL' PN,ZNL;
'BEGIN'
ONEPI := 3.14159 ;
TWOPI := 2 * 3.14159 ;
     THREEPI:= 3*3.14159;
FOURPI := 4 * 3.14159 ;
     OPL:=  ( ONEPI / L  );
     MJ:= SQRT(7) ;
    J:=3;
    K:=3;
    U0:=1.47&-18;
     U:=  (  ( U0*MJ*K)  /  ( J* ( J+1 )  )    ) ;
    H:=6.6 &-27;
    V0:=2.4 &10;
    HV0:= H* V0 ;
    HHV0:=HV0*0.5;
     HHV02 :=  HHV0 * HHV0 ;
    PVL:=0.3*ONEPI*VOL0/L;
     PVL2 := PVL * PVL ;
       PL := ( ONEPI * PN /  L  );
    I0 PL:=S18AEA(PL,IFAIL);
    I1 PL:=S18AFA(PL,IFAIL);
    I2PL:=I0PL-(2/PL)*I1PL;
      THPL :=  ( THREEPI * PN  /  L  );
    I0THPL:=S18AEA(THPL,IFAIL);
    I1THPL:=S18AFA(THPL,IFAIL);
    I2THPL:=I0THPL-(2/THPL)*I1THPL;
       P0 := L ;
    P0L:=ONEPI*P0/L;
    I0P0L:=S18AEA(P0L,IFAIL);
    I1P0L:=S18AFA(P0L,IFAIL);
    THP0L:=THREEPI*P0/L;
    I0THP0L:=S18AEA(THP0L,IFAIL);
    I1THP0L:=S18AFA(THP0L,IFAIL);
    U2:=U*U;
     UE:= U * ILE(PN,ZNL);
    UE2:=UE*UE;
      QE := ((  U2) / ( SQRT( HHV02 + UE2 )  )    ) ;
     ZUL := ZNL  / L  ;
    PZL:=ONEPI*ZUL;
    THPZL:=THREEPI*ZUL;
    IFR:= (  QE*2*OPL*PVL2* (
        (2*(I1PL/I0P0L)*SIN(PZL)+(I1THPL/I0THP0L)*SIN(THPZL)) *
        (((I2PL+I0PL)/I0P0L)*SIN(PZL)+
         1.5 *((I2THPL + I0THPL) / I0 THP0L) *SIN(THPZL))  +
        (2*(I0PL/I0P0L)*COS(PZL)+(I0THPL/I0THP0L)*COS(THPZL)) *
        ((2*I1PL/I0P0L)*COS(PZL)+3*(I1THPL/I0THP0L)*COS(THPZL)) ) ) ;
'END' OF PROCEDURE  IFR ;
 'REAL''PROCEDURE'OFZ(PN,ZNL);'VALUE' PN,ZNL;'REAL' PN,ZNL;
     'BEGIN'
     ONEPI:=3.14159;
     TWOPI:=2*ONEPI;
     THREEPI:=3*ONEPI;
     FOURPI:=4*ONEPI;
     OPL:=(ONEPI/L);
     MJ:=SQRT(7);
     J:=3;
     K:=3;
     U0:=1.47&-18;
     U:=((U0*MJ*K)/(J*(J+1)));
     H:=6.6&-27;
```

```
      V0:=2,4&10;
      HV0:=H*V0;
      HHV0:= HV0 * 0,5 ;
      HHV02:=HHV0*HHV0;
      PL:=(ONEPI*PN/L);
      K0PL:=S18ACA(PL,IFAIL);
      K1PL:=S18ADA(PL,IFAIL);
      K2PL:=BESK(2,PL);
      THPL:=(THREEPI*PN/L);
      K0THPL:=S18ACA(THPL,IFAIL);
      K1THPL:=S18ADA(THPL,IFAIL);
      K2THPL:=BESK(2,THPL);
        P0 := L ;
      P0L:=  ( ONEPI * P0 / L ) ;
      THP0L :=  3 * P0L ;
      K0P0L:=S18ACA(P0L,IFAIL);
      K1P0L:=S18ADA(P0L,IFAIL);
      K2P0L:=BESK(2,P0L);
      K0THP0L := S18ACA(THP0L,IFAIL);
      K1THP0L := S18ADA(THP0L,IFAIL);
      K2THP0L := BESK(2,THP0L);
      U2 := U*U;
      UE := U * OLE(PN,ZNL);
      UE2 := UE*UE;
      QE := ((U2)/(SQRT(HHV02 + UE2 )  )  ) ;
      ZUL:=ZNL/L;
      PZL := ONEPI*ZUL;
      THPZL := THREEPI * ZUL ;
      PVL := 0,3*ONEPI*VOL0/L;
      PVL2 := PVL * PVL;
     OFZ:= (  QE*2*OPL*PVL2* (
      (2*(K1PL/K0P0L)*SIN(PZL)+(K1THPL/K0THP0L)*SIN(THPZL))*
      (2*(K1PL/K0P0L)*COS(PZL)+(K1THPL/K0THP0L)*COS(THPZL)*3)-
      (2*(K0PL/K0P0L)*COS(PZL)+(K0THPL/K0THP0L)*COS(THPZL))*
      (2*(K0PL/K0P0L)*SIN(PZL)+(K0THPL/K0THP0L)*SIN(THPZL)*3)));
'END' OF PROCEDURE  OFZ ;
 'REAL''PROCEDURE'IFZ(PN,ZNL);'VALUE' PN,ZNL;'REAL' PN,ZNL;
'BEGIN'
ONEPI := 3,14159 ;
TWOPI := 2 * 3,14159 ;
      THREEPI:= 3*3,14159;
FOURPI := 4 * 3,14159 ;
      OPL:=  ( ONEPI / L  );
      MJ:= SQRT(7) ;
     J:=3;
     K:=3;
     U0:=1,47&-18;
      U:=  (  ( U0*MJ*K)  /  ( J* ( J+1 )  )    )  ;
     H:=6,6 &-27;
     V0:=2,4 &10;
     HV0:= H* V0 ;
     HHV0:=HV0*0,5;
       HHV02 :=  HHV0 * HHV0 ;
        PL := ( ONEPI * PN /  L  );
     I0 PL:=S18AEA(PL,IFAIL);
     I1 PL:=S18AFA(PL,IFAIL);
     I2PL:=I0PL-(2/PL)*I1PL;
       THPL :=  ( THREEPI * PN  /  L  );
     I0THPL:=S18AEA(THPL,IFAIL);
     I1THPL:=S18AFA(THPL,IFAIL);
     I2THPL:=I0THPL-(2/THPL)*I1THPL;
```

```
      P0 := L ;
    P0L:=ONEPI*P0/L;
    I0P0L:=S18AEA(P0L,IFAIL);
    I1P0L:=S18AFA(P0L,IFAIL);
    THP0L:=THREEPI*P0/L;
    I0THP0L:=S18AEA(THP0L,IFAIL);
    I1THP0L:=S18AFA(THP0L,IFAIL);
    U2:=U*U;
     UE := U * ILE(PN,ZNL);
    UE2:=UE*UE;
      QE := ((  U2) / ( SQRT( HHV02 + UE2 )  )    ) ;
     ZUL := ZNL  / L  ;
    PZL:=ONEPI*ZUL;
    THPZL:=THREEPI*ZUL;
    PVL:=0.3*ONEPI*VOL0/L;
     PVL2 := PVL * PVL ;
    IFZ:= (  QE*2*OPL*PVL2* (
        (2*(I1PL/I0P0L)*SIN(PZL)+(I1THPL/I0THP0L)*SIN(THPZL)) *
        (2*(I1PL/I0P0L)*COS(PZL)+(I1THPL/I0THP0L)*COS(THPZL)* 3) -
        (2*(I0PL/I0P0L)*COS(PZL)+(I0THPL/I0THP0L)*COS(THPZL)) *
        (2*(I0PL/I0P0L)*SIN(PZL)+(I0THPL/I0THP0L)*SIN(THPZL)* 3 ) ) );
'END' OF PROCEDURE  IFZ ;
     'REAL''PROCEDURE' FR(PN,ZNL); 'VALUE' PN,ZNL; 'REAL'PN,ZNL;
     'BEGIN'
     'IF'  PN < 0.16 'THEN'
     FR :=  IFR(PN,ZNL )
     'ELSE'
         FR := OFR(PN,ZNL) ;
     'END' OF PROCEDURE FR;
 'REAL''PROCEDURE' FZ(PN,ZNL);'VALUE' PN,ZNL;'REAL' PN,ZNL;
     'BEGIN'
     'IF'  PN < 0.16 'THEN'
     FZ :=  IFZ(PN,ZNL )
     'ELSE'
         FZ := OFZ(PN,ZNL) ;
'END' OF PROCEDURE FZ ;
      L := 0.16 ;
     TWOPI:=2*3.14159;
     FOURPI:=4*3.14159;
     BK:=1.38&-16;
     NT:=240;
     KT:=BK*NT;
     ND:=5;
     DF:=10.5;
      NF:= 29.3 ;
     FL := 7.7 ;
     FC:=3;
       CL:= 10.8 ;
     Y:=0.45;
     M:=28.22&-24;
     ZA:=40;

     'FOR' VOL0:= 20/3'STEP'20/3'UNTIL' 310 / 3 'DO'

     'BEGIN'
     OMEGAAV :=  0 ;
       'FOR' PS:= 2 'STEP'  2  'UNTIL'  30 'DO'
     'BEGIN'
     S:=PS*0.5& 4;
NS:= FOURPI*S   * (M/(TWOPI*KT) )↑1.5 * EXP( -M*S↑2 /(2*KT) ) ;
```

```
OMEGA:=0;
DA:= 40 ;
'FOR' Q :=  55 'STEP' DA 'UNTIL' 160 'DO'
'BEGIN'
ANGLE:=(Q/&4);
SINANG:=SIN(ANGLE);
COSANG:= COS(ANGLE);
TANANG:= SIN(ANGLE)/COS(ANGLE);
T:=(FL/(ZA*S*COSANG));
Z[0]:=0;
R[0]:=NF*(SINANG/COSANG);
VR[0]:=S*SINANG;
VZ[0]:=S*COSANG;
'FOR' N:= 0 , N+1  'WHILE'  Z[N] < FL  'DO'
'BEGIN'
'IF'R[N]<0'THEN'
'BEGIN'
R[N]:=-R[N];
VR[N]:=-VR[N];
'END';
Z[N+1] := Z[N] + VZ[N] * T;
R[N+1] := R[N] + VR[N] * T;
'IF' R[N+1]  < 0 'THEN'
                          'BEGIN'
                                  R[N+1] := - R[N+1] ;
                                 VR[N+1] := -VR[N+1] ;
                          'END';
VR[N+1] := VR[N] + (FR(R[N],Z[N])/M)*T;
VZ[N+1] :=VZ[N]+(FZ(R[N],Z[N])/M)*T;
Z[N+1]:=Z[N]+ (VZ[N] + VZ[N+1])*T*0.5;
R[N+1]:=R[N]+ (VR[N]+VR[N+1])*T*0.5;
VR[N+1] := VR[N]+(FR(R[N],Z[N])+
FR(R[N+1],Z[N+1]))*T*0.5/M;
VZ[N+1]:=VZ[N]+(FZ(R[N],Z[N])+
FZ(R[N+1],Z[N+1]))*T*0.5/M;
'END' OF N LOOP;
DR:=R[N-1] + VR[N-1]*(FC/VZ[N-1]);
'IF' DR↑2 < Y↑2 'THEN'
'BEGIN'
DR := R[N-1]+VR[N-1]*((FC+CL)/VZ[N-1]);
'IF' DR↑2 < Y↑2 'THEN'
'BEGIN'
OMEGA := OMEGA+ONEPI*SINANG*DA/&4;
'END' OF D LOOP AT THE EXIT OF THE CAVITY;
'END' OF D LOOP AT THE ENTRANCE OF THE CAVITY;
X;
'END' OF Q ANGLE LOOP;
OMEGAAV:=OMEGAAV+OMEGA*NS* 1 &4;
'END' OF PS SPEED LOOP ;
PRINT(VOL0*3/10,2,2); SPACE(3);
PRINT(OMEGA,0,3); SPACE(3);
PRINT(OMEGAAV,0,3);SPACE(2);
NEWLINE(2);
'END' OF VOLTAGE LOOP;
'END'
```

APPENDIX 6

```
      'BEGIN'
      'INTEGER'Q2;
      'REAL'  I0THPL, I1 THPL ;
      'REAL'RS,RS2,NTAN,ANT,TF1,TF12,TF2,TF22,
      RNT,VAR,VAR2,SVAR,VTO,AM,AM2,M2;
      'REAL' SSIN,ANGLEQ2,VTF,VTF2;
'REAL' I0THP0L,I1THP0L,I0P0L,I1P0L,I2PL,I2THPL,I0PL,I1PL;
     'REAL''PROCEDURE'S18ADA(X,IFAIL);'VALUE'X;'REAL'X;'INTEGER'IFAIL;
    'ALGOL';
     'REAL''PROCEDURE' S18ACA(X,IFAIL);'VALUE'X;'REAL'X;'INTEGER' IFAIL;
     'ALGOL';
     'REAL''PROCEDURE'S18AEA(X,IFAIL);'VALUE'X;'REAL'X;'INTEGER'IFAIL;
'ALGOL';
     'REAL''PROCEDURE'S18AFA(X,IFAIL);'VALUE'X;'REAL'X;'INTEGER'IFAIL;
'ALGOL';
      'REAL''ARRAY' P,Z,R,VR,VZ[0:800];
      'REAL' EL,FRG,FZG;
     'REAL' K0P0L,VOL0,K2THP0L,PVL2;
      'REAL' HHV02,Q,ZNL,XY,ST,PS,ZA,W,DR,Y,BK,NT,KT,ND,DF,NF,P0,FL,FC,
      CL,CR,M,V,OMEGA,S,T,OMEGAAV,NS,ONEPI,TWOPI,THREEPI,FOURPI,DA,ANGLE,
      SINANG,COS ANG,TANANG,K0THP0L,K1THP0L,OPL,UO,H,VO,HVO,HHVO,MJ,J,K,
            K1P0L,K2P0L,K0THPL,K1THPL,K1PL,K0PL,K2PL,K2THPL,PZL,THPZL,
      PVL,PUL2,PL,THPL,P0L,THP0L,L,U,U2,ZUL,UE,UE2,QE;
      'INTEGER'N,IFAIL;
'REAL''PROCEDURE' BESI(W,Z);'VALUE'W,Z;'INTEGER' W;'REAL' Z;
 'BEGIN'
    'IF' W<2 'THEN'
                'BEGIN'
                      'IF'W=0 'THEN'
                    BESI:= S18AEA(Z,IFAIL)  'ELSE'
                    BESI:= S18AFA(Z,IFAIL);
              'END'
       'ELSE'
                BESI:=BESI((W-2),Z)- (2*(W-1) /Z) * BESI((W-1),Z);
              'END' OF I BESSEL FUNCTION PROCEDURE;
'REAL''PROCEDURE' BESK(W,Z);'VALUE' W,Z;'INTEGER' W;'REAL'Z;
    'BEGIN'
       'IF'  W<2 'THEN'
                     'BEGIN'
                           'IF' W=0 'THEN'
                             BESK:= S18ACA(Z,IFAIL)  'ELSE'
                             BESK:= S18ADA(Z,IFAIL) ;
                     'END'
                  'ELSE'
                BESK:=BESK((W-2),Z)+ (2*(W-1) /Z) * BESK((W-1),Z);
      'END' OF K BESSEL FUNCTION  PROCEDURE ;
'REAL''PROCEDURE' OLE(PN,ZNL);'VALUE'PN,ZNL;'REAL'PN,ZNL;
     'BEGIN'
     ONEPI:=3,14159;
     TWOPI:=2*ONEPI;
     THREEPI:=3*ONEPI;
     FOURPI:=4*ONEPI;
     OPL:=(ONEPI/L);
     MJ:=SQRT(7);
     J:=3;
     K:=3;
```

```
      U0:=1,47&-18;
      U:=((U0*MJ*K)/(J*(J+1)));
      U2:=U*U;
      H:=6,6&-27;
      V0:=2,4&10;
      HV0:=H*V0;
      HHV0 := HV0 * 0,5;
      HHV02 := HHV0 * HHV0;
        P0 := L ;
      P0L:=  ( ONEPI * P0 / L ) ;
      THP0L :=  3 * P0L ;
      K0P0L := S18ACA (P0L,IFAIL);
      K1P0L := S18ADA(P0L,IFAIL);
      K0THP0L := S18ACA(THP0L,IFAIL);
      K1THP0L := S18ADA(THP0L,IFAIL);
      PL := (ONEPI * PN / L);
      K0PL := S18ACA(PL,IFAIL);
      K1PL := S18ADA(PL,IFAIL);
      K2PL := BESK(2,PL);
      THPL := (THREEPI * PN/L);
      K0THPL := S18ACA(THPL,IFAIL);
      K1THPL := S18ADA(THPL,IFAIL);
      K2THPL := BESK(2,THPL);
      ZUL := (ZNL /L);
      PZL := ONEPI * ZUL;
      THPZL := THREEPI * ZUL;
      PVL := 0,3 * ONEPI * VOL0 /L;
        OLE:=  PVL * SQRT(
      (2*(K1PL/K0P0L)*SIN(PZL)+(K1THPL/K0THP0L)*SIN(THPZL))↑2+
      (2*(K0PL/K0P0L)*COS(PZL)+(K0THPL/K0THP0L)*COS(THPZL))↑2);
         'END' OF  OLE  PROCEDURE ;
'REAL''PROCEDURE' ILE(PN,ZNL);'VALUE'PN,ZNL;'REAL'PN,ZNL;
        'BEGIN'
ONEPI := 3,14159 ;
TWOPI := 2 * 3,14159 ;
     THREEPI:= 3*3,14159;
FOURPI := 4 * 3,14159 ;
     OPL:=  ( ONEPI / L  );
     MJ:= SQRT(7) ;
    J:=3;
    K:=3;
    U0:=1,47&-18;
     U:=  (  ( U0*MJ*K)  /  ( J* ( J+1 )  )    ) ;
    U2:=U*U;
    H:=6,6 &-27;
    V0:=2,4 &10;
    HV0:= H* V0 ;
    HHV0:=HV0*0,5;
      HHV02 :=  HHV0 * HHV0 ;
    P0L:=ONEPI*P0/L;
    I0P0L:=S18AEA(P0L,IFAIL);
    I1P0L:=S18AFA(P0L,IFAIL);
    THP0L:=THREEPI*P0/L;
    I0THP0L:=S18AEA(THP0L,IFAIL);
    I1THP0L:=S18AFA(THP0L,IFAIL);
       PL := ( ONEPI * PN /  L );
    I0 PL:=S18AEA(PL,IFAIL);
    I1 PL:=S18AFA(PL,IFAIL);
    I2PL:=I0PL-(2/PL)*I1PL;
      THPL :=  ( THREEPI * PN  /  L  );
```

```
    I0THPL:=S18AEA(THPL,IFAIL);
    I1THPL:=S18AFA(THPL,IFAIL);
    I2THPL:=I0THPL-(2/THPL)*I1THPL;
     ZUL := ZNL  / L  ;
    PZL:=ONEPI*ZUL;
    THPZL:=THREEPI*ZUL;
    PVL:=0,3*ONEPI*VOL0/L;
       ILE:=  PVL * SQRT(
        (2*(I1PL/I0P0L)*SIN(PZL)+(I1THPL/I0THP0L)*SIN(THPZL)) ↑2  +
        (2*(I0PL/I0P0L)*COS(PZL)+(I0THPL/I0THP0L)*COS(THPZL)) ↑2  ) ;
        'END' OF  ILE  PROCEDURE ;
'REAL''PROCEDURE'OFR(PN,ZNL);'VALUE' PN,ZNL;'REAL' PN,ZNL;
    'BEGIN'
    ONEPI := 3,14159;
    TWOPI := 2*ONEPI;
    THREEPI := 3*ONEPI;
    FOURPI := 4 * ONEPI;
    OPL := (ONEPI/L);
    MJ := SQRT(7);
    J:=3;
    K:=3;
    U0:=1,47&-18;
    U:=((U0*MJ*K)/(J*(J+1)));
    H:=6,6&-27;
    V0:=2,4&10;
    HV0:=H*V0;
    HHV0:=HV0*0,5;
    HHV02:=HHV0*HHV0;
    PVL:=0,3*ONEPI*VOL0/L;
    PVL2:=PVL*PVL;
    PL:=(ONEPI*PN/L);
    K0PL:=S18ACA(PL,IFAIL);
    K1PL:=S18ADA(PL,IFAIL);
    K2PL:=BESK(2,PL);
    THPL:=(THREEPI*PN/L);
    K0THPL:=S18ACA(THPL,IFAIL);
    K1THPL:=S18ADA(THPL,IFAIL);
    K2THPL:=BESK(2,THPL);
      P0 := L ;
    P0L:=  ( ONEPI * P0 / L ) ;
    K0P0L:=S18ACA(P0L,IFAIL);
    K1P0L:=S18ADA(P0L,IFAIL);
    K2P0L:=BESK(2,P0L);
    THP0L :=  3 * P0L ;
    K0THP0L:=S18ACA(THP0L,IFAIL);
    K1THP0L:=S18ADA(THP0L,IFAIL);
    U2:=U*U;
    UE:= U * OLE(PN,ZNL);
    UE2:=UE*UE;
    QE:=((U2)/(SQRT(HHV02+UE2)));
    ZUL:=ZNL/L;
    PZL:=ONEPI*ZUL;
    THPZL:=THREEPI*ZUL;
   OFR:=-(  QE*2*OPL*PVL2* (
    (2*(K1PL/K0P0L)*SIN(PZL)+(K1THPL/K0THP0L)*SIN(THPZL))*
    (((K2PL+K0PL)/K0P0L)*SIN(PZL)+
    1,5*((K2THPL+K0THPL)/K0THP0L)*SIN(THPZL) )   +
    (2*(K0PL/K0P0L)*COS(PZL)+(K0THPL/K0THP0L)*COS(THPZL))*
    ((2*K1PL/K0P0L)*COS(PZL)+3*(K1THPL/K0THP0L)*COS(THPZL))));
'END' OF PROCEDURE  OFR ;
```

```
 'REAL''PROCEDURE'IFR(PN,ZNL);'VALUE' PN,ZNL;'REAL' PN,ZNL;
'BEGIN'
ONEPI := 3,14159 ;
TWOPI := 2 * 3,14159 ;
     THREEPI:= 3*3,14159;
FOURPI := 4 * 3,14159 ;
      OPL:=  ( ONEPI / L  );
      MJ:= SQRT(7) ;
     J:=3;
     K:=3;
     U0:=1,47&-18;
      U:=  (  ( U0*MJ*K)  /  ( J* ( J+1 )  )    ) ;
     H:=6,6 &-27;
     V0:=2,4 &10;
     HV0:= H* V0 ;
     HHV0:=HV0*0,5;
       HHV02 :=  HHV0 * HHV0 ;
     PVL:=0,3*ONEPI*VOL0/L;
      PVL2 := PVL * PVL ;
        PL := ( ONEPI * PN /  L  );
     I0 PL:=S18AEA(PL,IFAIL);
     I1 PL:=S18AFA(PL,IFAIL);
     I2PL:=I0PL-(2/PL)*I1PL;
       THPL :=  ( THREEPI * PN  /  L  );
     I0THPL:=S18AEA(THPL,IFAIL);
     I1THPL:=S18AFA(THPL,IFAIL);
     I2THPL:=I0THPL-(2/THPL)*I1THPL;
        P0 := L ;
     P0L:=ONEPI*P0/L;
     I0P0L:=S18AEA(P0L,IFAIL);
     I1P0L:=S18AFA(P0L,IFAIL);
     THP0L:=THREEPI*P0/L;
     I0THP0L:=S18AEA(THP0L,IFAIL);
     I1THP0L:=S18AFA(THP0L,IFAIL);
     U2:=U*U;
      UE:= U * ILE(PN,ZNL);
     UE2:=UE*UE;
       QE := ((  U2) / ( SQRT( HHV02 + UE2 )  )    ) ;
      ZUL := ZNL  / L  ;
     PZL:=ONEPI*ZUL;
     THPZL:=THREEPI*ZUL;
     IFR:=-(  QE*2*OPL*PVL2* (
         (2*(I1PL/I0P0L)*SIN(PZL)+(I1THPL/I0THP0L)*SIN(THPZL)) *
         (((I2PL+I0PL)/I0P0L)*SIN(PZL)+
          1,5 *((I2THPL + I0THPL) / I0 THP0L) *SIN(THPZL))  +
         (2*(I0PL/I0P0L)*COS(PZL)+(I0THPL/I0THP0L)*COS(THPZL)) *
         ((2*I1PL/I0P0L)*COS(PZL)+3*(I1THPL/I0THP0L)*COS(THPZL)) ) ) ;
'END' OF PROCEDURE  IFR ;
 'REAL''PROCEDURE'OFZ(PN,ZNL);'VALUE' PN,ZNL;'REAL' PN,ZNL;
      'BEGIN'
      ONEPI:=3,14159;
      TWOPI:=2*ONEPI;
      THREEPI:=3*ONEPI;
      FOURPI:=4*ONEPI;
      OPL:=(ONEPI/L);
      MJ:=SQRT(7);
      J:=3;
      K:=3;
      U0:=1,47&-18;
      U:=((U0*MJ*K)/(J*(J+1)));
      H:=6,6&-27;
```

```
      V0:=2,4&10;
      HV0:=H*V0;
      HHV0:= HV0 * 0,5 ;
      HHV02:=HHV0*HHV0;
      PL:=(ONEPI*PN/L);
      K0PL:=S18ACA(PL,IFAIL);
      K1PL:=S18ADA(PL,IFAIL);
      K2PL:=BESK(2,PL);
      THPL:=(THREEPI*PN/L);
      K0THPL:=S18ACA(THPL,IFAIL);
      K1THPL:=S18ADA(THPL,IFAIL);
      K2THPL:=BESK(2,THPL);
        P0 := L ;
      P0L:=  ( ONEPI * P0 / L ) ;
      THP0L :=  3 * P0L ;
      K0P0L:=S18ACA(P0L,IFAIL);
      K1P0L:=S18ADA(P0L,IFAIL);
      K2P0L:=BESK(2,P0L);
      K0THP0L := S18ACA(THP0L,IFAIL);
      K1THP0L := S18ADA(THP0L,IFAIL);
      K2THP0L := BESK(2,THP0L);
      U2 := U*U;
      UE := U * OLE(PN,ZNL);
      UE2 := UE*UE;
      QE := ((U2)/(SQRT(HHV02 + UE2 )  )  ) ;
      ZUL:=ZNL/L;
      PZL := ONEPI*ZUL;
      THPZL := THREEPI * ZUL ;
      PVL := 0,3*ONEPI*VOL0/L;
      PVL2 := PVL * PVL;
     OFZ:=-(  QE*2*OPL*PVL2* (
      (2*(K1PL/K0P0L)*SIN(PZL)+(K1THPL/K0THP0L)*SIN(THPZL))*
      (2*(K1PL/K0P0L)*COS(PZL)+(K1THPL/K0THP0L)*COS(THPZL)*3)-
      (2*(K0PL/K0P0L)*COS(PZL)+(K0THPL/K0THP0L)*COS(THPZL))*
      (2*(K0PL/K0P0L)*SIN(PZL)+(K0THPL/K0THP0L)*SIN(THPZL)*3)));
'END' OF PROCEDURE  OFZ ;
 'REAL''PROCEDURE'IFZ(PN,ZNL);'VALUE' PN,ZNL;'REAL' PN,ZNL;
'BEGIN'
ONEPI := 3,14159 ;
TWOPI := 2 * 3,14159 ;
      THREEPI:= 3*3,14159;
FOURPI := 4 * 3,14159 ;
      OPL:=  ( ONEPI / L  );
      MJ:= SQRT(7) ;
     J:=3;
     K:=3;
     U0:=1,47&-18;
      U:=  (  ( U0*MJ*K)  /  ( J* ( J+1 )  )    )  ;
     H:=6,6 &-27;
     V0:=2,4 &10;
     HV0:= H* V0 ;
     HHV0:=HV0*0,5;
       HHV02 :=  HHV0 * HHV0 ;
        PL := ( ONEPI * PN /  L  );
     I0 PL:=S18AEA(PL,IFAIL);
     I1 PL:=S18AFA(PL,IFAIL);
     I2PL:=I0PL-(2/PL)*I1PL;
       THPL :=  ( THREEPI * PN  /  L  );
     I0THPL:=S18AEA(THPL,IFAIL);
     I1THPL:=S18AFA(THPL,IFAIL);
     I2THPL:=I0THPL-(2/THPL)*I1THPL;
```

```
      P0 := L ;
    P0L:=ONEPI*P0/L;
    I0P0L:=S18AEA(P0L,IFAIL);
    I1P0L:=S18AFA(P0L,IFAIL);
    THP0L:=THREEPI*P0/L;
    I0THP0L:=S18AEA(THP0L,IFAIL);
    I1THP0L:=S18AFA(THP0L,IFAIL);
    U2:=U*U;
     UE := U * ILE(PN,ZNL);
    UE2:=UE*UE;
      QE := ((  U2) / ( SQRT( HHV02 + UE2 )  )     )  ;
     ZUL := ZNL  / L  ;
    PZL:=ONEPI*ZUL;
    THPZL:=THREEPI*ZUL;
    PVL:=0.3*ONEPI*VOL0/L;
     PVL2 := PVL * PVL ;
    IFZ:=-(  QE*2*OPL*PVL2* (
        (2*(I1PL/I0P0L)*SIN(PZL)+(I1THPL/I0THP0L)*SIN(THPZL)) *
        (2*(I1PL/I0P0L)*COS(PZL)+(I1THPL/I0THP0L)*COS(THPZL)* 3) -
        (2*(I0PL/I0P0L)*COS(PZL)+(I0THPL/I0THP0L)*COS(THPZL)) *
        (2*(I0PL/I0P0L)*SIN(PZL)+(I0THPL/I0THP0L)*SIN(THPZL)* 3 ) ) );
'END' OF PROCEDURE  IFZ ;
     'REAL''PROCEDURE' FR(PN,ZNL); 'VALUE' PN,ZNL; 'REAL'PN,ZNL;
     'BEGIN'
     'IF' PN < 0.31 'THEN'
     FR :=  IFR(PN,ZNL )
     'ELSE'
         FR := OFR(PN,ZNL) ;
     'END' OF PROCEDURE FR;
 'REAL''PROCEDURE' FZ(PN,ZNL);'VALUE' PN,ZNL;'REAL' PN,ZNL;
     'BEGIN'
     'IF' PN < 0.31 'THEN'
     FZ :=  IFZ(PN,ZNL )
     'ELSE'
         FZ := OFZ(PN,ZNL) ;
'END' OF PROCEDURE FZ ;
     L:= 0.31 ;
    BK:=1.38&-16;
    NT:= 240 ;
    KT:=BK*NT;
    ND:=5;
    DF:=2.5;
    NF:=ND+DF;
    FL:=8.5;
    FC:=8;
    CL:=10.8;
    CR:=0.45;
     Y:= 0.45 ;
    M:=28.22&-24;
     ZA:= 40 ;
     'FOR' VOL0 := 260/3 'STEP' 20/3 'UNTIL' 310/3 'DO'
        'BEGIN'
    TWOPI:= 2*3.14159 ;
     FOURPI:= 4 * 3.14159 ;
    OMEGAAV:=0;
       'FOR' PS:= 2 'STEP'  2  'UNTIL'  30 'DO'
    'BEGIN'
     S:= PS * 0.5 &4 ;
NS:= FOURPI*S   * (M/(TWOPI*KT) )↑1.5 * EXP( -M*S↑2 /(2*KT) ) ;
```

```
    OMEGA:= 0;
    DA:=20;
     'FOR' Q := 40'STEP' DA 'UNTIL' 400 'DO'
    'BEGIN'
    ANGLE:= Q/&4;
    SINANG:=SIN(ANGLE);
    COSANG:=COS(ANGLE);
    TANANG:=SIN(ANGLE)/ COS(ANGLE);
      T:=  ( FL / ( ZA* S * COSANG )  ) ;
    Z[0] := 0 ;
    R[0] := NF * ( SIN(ANGLE) / COS(ANGLE) ) ;
    VR[0] := S * SIN(ANGLE) ;
    VZ[0] := S * COS (ANGLE) ;
     'FOR'  N:= 0  ,N+1 'WHILE'  Z[N] < FL 'DO'
     'BEGIN'
       'IF'  R[N]  <  0  'THEN'
'BEGIN'
            R[N] :=  - R[N] ;
            VR[N] :=  - VR[N] ;
      'END';
     Z[N+1] := Z[N] + VZ[N] * T ;
     R[N+1] := R[N] + VR[N] * T ;
    VR[N+1] := VR[N] +(FR(R[N],Z[N])/M)*T;
    VZ[N+1] := VZ[N] +(FZ(R[N],Z[N])/M)*T;
     Z[N+1] := Z[N] +  (VZ[N] + VZ[N+1] ) * T * 0.5 ;
     R[N+1] := R[N] +  (VR[N] + VR[N+1] ) * T * 0.5 ;
     VR[N+1] :=  VR[N] + ( FR(R[N],Z[N])     +
            FR(R[N+1],Z[N+1])  ) * T * 0.5  / M ;
     VZ[N+1] :=  VZ[N] + ( FZ(R[N],Z[N] ) +
            FZ(R[N+1],Z[N+1] )  ) *T  *0.5 / M ;
     'END' OF  N  LOOP ;
     DR:= R[N-1] + VR[N-1] * ( FC / VZ[N-1]  ) ;
       'IF'  DR ↑2 < Y↑2 'THEN'
       'BEGIN'
     DR:= R[N-1] + VR[N-1] * ( ( FC+CL )  / VZ[N-1]  ) ;
       'IF'  DR ↑2 < Y↑2 'THEN'
           'BEGIN'
    OMEGA:=OMEGA+ONEPI *SINANG* DA/ &4;
     'END' OF  D  LOOP AT THE  EXIT OF THE CAVITY ;
     'END' OF  D  LOOP AT THE  ENTRANCE OF THE CAVITY ;
      'END' OF  Q ANGLE  LOOP ;
    OMEGAAV:=OMEGAAV+OMEGA* NS*  1 &4;
      'END' OF PS  SPEED  LOOP ;
    PRINT(VOL0 * 3/10,2,2);SPACE(3);
    PRINT(OMEGA,0,3);
SPACE(3);
PRINT(OMEGAAV,0,3);SPACE(2);
NEWLINE(2);
    'COMMENT'
THIS PROGRAM IS CALCULATED THE TRAJECTORY OF J=3,K=3, AMMONIA MOLECULES
    BK=BOLTZMAN CONSTANT.
OMEGA SOLID ANGLE ;
      'END' OF VOLTAGE   LOOP ;
'END'
```

APPENDIX 7

A) ON - AXIS NOZZLE SOURCE .

```
'BEGIN'
'REAL' KT ;
'REAL' L,Z,S,C,H,ANGLE,M,D,X,Y,DA,ONEGA,OMEGAAV,K,T,NS,VO,U,PC,E,
R1,R2,VOL,CONST1,CONST2,CONST3,C1,E1,J,ANGLEQ2,A,NF,   VTO,CONST,VTF,
TF1,TF2,LNR21,H5,H5M,NS54,A2,NTAN,ANT,RNT,SSIN,SCONST,UE2,PCVO,M2,J2,
VTF2,SDA,TF22,TF12 ,UE12                    ;
'REAL' 'ARRAY' R [0:20] , V[0:20] ;
'INTEGER' N,P,Q,Q2;
A:= 0,1016;
A2:= A↑2;
NF:= 8,5 ;
     R1:=0,029;
R2 := 5 ;
LNR21:= LN(R2/R1) ;
VO := 2,4 & 10;
PC := 6,6 & - 27 ;
PCVO:= ( PC*VO*0,5) ↑ 2;
U:= 9,723 & - 19 ;
K:=  1,38 & - 16 ;
T:= 240;
X:= 9,5 ;
Y :=0,45 ;
M:= 28,22 & - 24;
M2:=M↑2;
DA:= 20;
'FOR' VOL := 10/3 'STEP' 10/3 'UNTIL' 100/3 ,150/3 'STEP' 50/3 'UNTIL
350/3  'DO'
'BEGIN'
L:= 8;
OMEGAAV :=0;
Z := 40 ;
'FOR' P := 1 'STEP' 1 'UNTIL' 30 'DO'
'BEGIN'
S := P * 0,5&4 ;
OMEGA := 0;
'FOR' Q:= 15 'STEP' DA 'UNTIL' 330 'DO'
'BEGIN'
'REAL' COSANG,SINANG,TANANG,TWOPI,FOURPI,ONEPI;
ANGLE := Q / &4 ;
ONEPI := 3,14159 ;
TWOPI :=2*3,14159;
FOURPI :=4*3,14159;
     KT := K*T ;
NS:= FOURPI*S   * (M/(TWOPI*KT) )↑1,5 * EXP( -M*S↑2 /(2*KT) ) ;
NS54:= NS*0,5*& 4;
COSANG :=COS(ANGLE);
SINANG :=SIN(ANGLE);
SSIN:= S* SINANG;
TANANG := 8,5 * SIN(ANGLE) / COS(ANGLE) ;
 NTAN:= ( NF*TANANG)↑2;
ANT:= 2* A* NF*TANANG ;
SDA:= SINANG * DA / & 4;
TF1 := X / ( S* COSANG) ;
TF12:= TF1↑2;
```

```
TF2 := ( X+ 10.8 ) / ( S* COSANG );
TF22:= TF2↑2;
CONST 2 :=      ( U*VOL / LNR21 ) ↑ 2 ;
H:= L /(Z*S*COSANG);
H5:= H* 0.5;
H5M:= H*0.5 / M ;
      Q2:= 0;
'BEGIN'
ANGLEQ2 := ( TWOPI*Q2 ) / 10 ;
R[0]:= ( A2+  NTAN - ANT*COS(ANGLEQ2)) ↑ 0.5 ;
RNT:= 2* R[0] * NF* TANANG ;
CONST:= ( R[0]↑2 + NTAN-A2 ) / RNT ;
SCONST:= ( 1-CONST ↑2+ & -7 ) ↑ 0.5 ;
V[0]:= SSIN* CONST ;
VTO:= SSIN * SCONST ;
    J :=0;
J2:= J↑2;
'FOR' N:= 0 'STEP' 1 'UNTIL' 19 'DO'
'BEGIN'
E:= VOL / ( LNR21 * R[N] ) ;
UE2:= ( U*E) ↑2;
CONST  1 :=  ( PCVO + UE2 ) ↑ ( - 0.5) ;
C:= CONST 1 * CONST 2 ;
R[N+1] := R[N] + V[N] * H;
V[N+1] := V[N] - C*H / (M*R[N] ↑3) + ( J 2 / ( M 2 * R[N] ↑3 ) ) * H;
 E1 := VOL / ( LNR21 * R[N+1] );
UE12 := ( U*E1 ) ↑2 ;
CONST 3 := ( PCVO + UE12 ) ↑0.5 ;
C1 := CONST 2 * CONST 3 ;
R[N+1] := R[N] + ( V[N] + V[N+1] ) * H5 ;
V[N+1] := V[N] - C*H / (M*R[N] ↑3) + ( J 2 / ( M 2 * R[N] ↑3 ) ) * H;
E1:= VOL / ( LNR21 * R[N+1] );
UE12:= ( U*E1) ↑2;
CONST 3:= ( PCVO+UE12) ↑ 0.5;
R[N+1] := R[N] + ( V[N] + V[N+1] ) *H5 ;
V[N+1] := V[N] - ( C / R[N] ↑ 3 + C1 / R[N+1] ↑ 3 ) * H5M +
  (J2 / ( M2*R[N] ↑3 ))*H5 + ( J2 / ( M2*R[N+1] ↑3 ))*H5 ;
'END';
 VTF:= ( R[0]*VTO) / R[20] ;
VTF2:= VTF↑2;
D:= (R[20]↑2+(V[20]↑2+VTF2)*TF12+2*R[20]*V[20]*TF1 ) ↑0.5;
'IF' D↑2 <Y↑2 'THEN'
'BEGIN'
D:= (R[20]↑2+(V[20]↑2+VTF2)*TF22+2*R[20]*V[20]*TF2 ) ↑0.5;
'IF' D↑2 < Y↑2 'THEN'
'BEGIN'
OMEGA:= OMEGA + ONEPI*SDA ;
'END' ;
'END';
'END' OF Q2 LOOP;
'END';
OMEGAAV := OMEGAAV + OMEGA * NS54 ;
'END' OF  P LOOP ;
  PRINT( VOL* 3/10,2,2) ;
  SPACE(4);
 PRINT(OMEGAAV,0,3) ;
      NEWLINE(2);
 'END';
 'END'
```

B) OFF - AXIS NOZZLE SOURCE .

```
'BEGIN'
'REAL' KT ;
'REAL' L,Z,S,C,H,ANGLE,M,D,X,Y,DA,OMEGA,OMEGAAV,K,T,NS,VO,U,PC,E,
R1,R2,VOL,CONST1,CONST2,CONST3,C1,E1,J,ANGLEQ2,A,NF,   VTO,CONST,VTF,
TF1,TF2,LNR21,H5,H5M,NS54,A2,NTAN,ANT,RNT,SSIN,SCONST,UE2,PCVO,M2,J2,
VTF2,SDA,TF22,TF12 ,UE12                ;
'REAL' 'ARRAY' R [0:20] , V[0:20] ;
'INTEGER' N,P,Q,Q2;
A:= 0,1016;
A2:= A↑2;
NF:= 8,5 ;
     R1:=0,029;
R2 := 5 ;
LNR21:= LN(R2/R1) ;
VO:= 2,4 & 10;
PC:= 6,6 & - 27 ;
PCVO:= ( PC*VO*0,5) ↑ 2;
U:= 9,723 & - 19 ;
K:=  1,38 & - 16 ;
T:= 240;
X:= 9,5 ;
Y :=0,45 ;
M:= 28,22 & - 24;
M2:=M↑2;
DA:= 20;
'FOR' VOL := 10/3 'STEP' 10/3 'UNTIL' 100/3 ,150/3 'STEP' 50/3 'UNTIL
350/3  'DO'
'BEGIN'
L:= 8;
OMEGAAV :=0;
Z := 40 ;
'FOR' P := 1 'STEP' 1 'UNTIL' 30 'DO'
'BEGIN'
S := P * 0,5&4 ;
OMEGA := 0;
'FOR' Q:= 15 'STEP' DA 'UNTIL' 330 'DO'
'BEGIN'
'REAL' COSANG,SINANG,TANANG,TWOPI,FOURPI,ONEPI;
ANGLE := Q / &4 ;
TWOPI :=2*3,14159;
FOURPI :=4*3,14159;
ONEPI := 3,14159 ;
     KT := K*T ;
NS:= FOURPI*S   * (M/(TWOPI*KT) )↑1,5 * EXP( -M*S↑2 /(2*KT) ) ;
NS54:= NS*0,5*& 4;
COSANG :=COS(ANGLE);
SINANG :=SIN(ANGLE);
SSIN:= S* SINANG;
TANANG :=8,5 * SIN(ANGLE) / COS ( ANGLE) ;
 NTAN:= ( NF*TANANG)↑2;
ANT:= 2* A* NF*TANANG ;
SDA:= SINANG * DA / & 4;
TF1 := X / ( S* COSANG) ;
TF12:= TF1↑2;
TF2 := ( X+ 10,8 ) / ( S* COSANG );
TF22:= TF2 ↑ 2 ;
CONST 2 :=   - ( U*VOL / LNR21 ) ↑ 2 ;
```

```
H:= L /(Z*S*COSANG);
H5:= H* 0,5;
H5M:= H*0,5 / M ;
'FOR' Q2:= 0 'STEP' 1 'UNTIL' 9 ' DO'
'BEGIN'
ANGLEQ2 := ( TWOPI*Q2 ) / 10 ;
R[0]:= ( A2+  NTAN - ANT*COS(ANGLEQ2)) ↑ 0,5 ;
RNT:= 2* R[0] * NF* TANANG ;
CONST:= ( R[0]↑2 + NTAN-A2 ) / RNT ;
SCONST:= ( 1-CONST ↑2+ &'-7 ) ↑ 0,5 ;
V[0]:= SSIN* CONST ;
VTO:= SSIN * SCONST ;
    J :=  M * R[0] * VTO ;
J2:= J↑2;
'FOR' N:= 0 'STEP' 1 'UNTIL' 19 'DO'
'BEGIN'
E:= VOL / ( LNR21 * R[N] ) ;
UE2:= ( U*E) ↑2;
CONST  1 :=  ( PCVO + UE2 ) ↑ ( - 0,5) ;
C:= CONST 1 * CONST 2 ;
R[N+1] := R[N] + V[N] * H;
V[N+1] := V[N] - C*H / (M*R[N] ↑3) + ( J 2 / ( M 2 * R[N] ↑3 ) ) * H
 E1 := VOL / ( LNR21 * R[N+1] );
UE12 := ( U*E1 ) ↑2 ;
CONST 3 := ( PCVO + UE12 ) ↑0,5 ;
C1 := CONST 2 * CONST 3 ;
R[N+1] := R[N] + ( V[N] + V[N+1] ) * H5 ;
V[N+1] := V[N] - ( C / R[N] ↑ 3 + C1 / R[N+1] ↑ 3 ) * H5M +
  (J2 / ( M2*R[N] ↑3 ))*H5 + ( J2 / ( M2*R[N+1] ↑3 ))*H5 ;
'END';
 VTF:= ( R[0]*VTO) / R[20] ;
VTF2:= VTF↑2;
D:= (R[20]↑2+(V[20]↑2+VTF2)*TF12+2*R[20]*V[20]*TF1 ) ↑0,5;
'IF' D↑2 <Y↑2 'THEN'
'BEGIN'
D:= (R[20]↑2+(V[20]↑2+VTF2)*TF22+2*R[20]*V[20]*TF2 ) ↑0,5;
'IF' D↑2 < Y↑2 'THEN'
'BEGIN'
OMEGA:= OMEGA + ONEPI*SDA ;
'END' ;
'END';
'END' OF Q2 LOOP;
'END';
OMEGAAV := OMEGAAV + OMEGA * NS54 ;
'END' OF  P LOOP ;
PRINT( VOL* 3/10,2,2) ;
SPACE(4);
PRINT( C,0,3);
SPACE (4);
PRINT( E,0,4 );
SPACE (4);
PRINT( C1,0,3);
SPACE(4);
PRINT(E1,0,3) ;
     SPACE(4)  ;
PRINT(OMEGAAV,0,3) ;
     NEWLINE(2);
'END';
'END'
```

REFERENCES

AL-AMIEDY,D.H.H., DUGDALE,D.E. and LAINE,D.C. (1979) Book of Abstracts (to be published) " 7th International Syomposium on Molecular Beams, Trento, Italy. May 28 - June 1.

AL-AMIEDY,D.H.H. and LAINE,D.C. (1978). Phys. lett. 66A, 94 -6.

ANDERSON,J.B., ANDERS,R.P. and FENN,J.B. (1965). Adv. Mol. Phys.,1,345.

ANDERSON,J.B., ANDERS,R.P. and FENN,J.B. (1966). Adv. Mol. Phys.,10,275.

ANDERSON,J.B.,(1968). Intermediate Energy Molecular Beams from Free Jets of Mixed Gases, Project Squid O.N.R. Tech Rept PR 166P.

AUERBACH,D., BROMBERG,E.A.and WHARTON,L. (1966). J.Chem. Phys.,45,2160.

BARDO,W.S. and LAINE,D.C. (1971) J. of Phys E(Scient. Inst), 4 , 595 - 7.

BARNES,F.S. (1959). Proc. IRE., 47 ,

BASOV,N.G., ORAVESKII,A.N., STRAKHOVSKII,G.M. and TATARENKOV,V.M. (1964) Quantum Electronics III, Ed.P.Grivet and N. Blombergen (New York : Columbia University Press). pp 377 - 92.

BASOV,N.G., ORAEVSKII,A.N., STRAKHOVSKII,G.M. and TATARENKOV,V.M. (1963) Zh.Eksper.Teor.Fiz.,45,1768 - 77 (Eng. transl. 1964, Sov. Phys. - JETP., 18 , 1211 - 17) .

BASOV,N.G., ZUEV,V.S. and SVIDINSKII,K.K. (1963) Trudy Fiz Inst. P.N. Lebedev, 21 , 176 - 99 (Eng transl. 1964, Soviet Maser Research, New York: Consultants Bureau, pp. 149 - 67).

BECKER,G. (1961) Z. angew Phys., 13 , 59 - 64 .

BECKER,G. (1963) Z. angew Phys., 15 , 13 - 20.

BECKER,G. (1963) Z. angew Phys., 15 , 281 - 5 .

BECKER,E.W. and BIER,K. (1954). Z. Naturforsch, 9A , 975 .

BENNEWITZ,H.G., PAUL,W. and SCHLIER,C. (1955). Z.Physik, 141 , 6 .

BIER,K. and HAGENA,O. (1963) Rarefied Gas Dynamics, 1 , 478. Academic Press, New York.

BIER,K. and HAGENA,O.F. (1966) Rarefied Gas Dynamics, 4th Symposium, Vol 2, pp 260 - 278 .

BIER,K. and SCHMIDT,B. (1961). Z.angew Phys., 1 3 , 493.

BOBBIO S.M. CHIOU,C.T., GREENE,E.F. and LAMBROPOULOS,H.D. (1975) J.Chem. Phys., 62 , 190 - 6.

BOSSEL,U. (1968). University of California, Report No. AS - 68-6.

BOSSEL,U. (1969). Entropie, No 30, pp 11 - 15.

BOSSEL,U. (1971). Entropie, No 42, pp 12 - 17.

CAMPARGUE,R. (1969) Entropie, No 30, 15 - 21.

CENTRY,W.R. and GLESE,C.F. (1975) Rev. sci. Instrum., 46 , 104.

CLEETON,C.E. and WILLIAMS,N.H. (1934) Phys. Rev., 45 , 234.

DE LUCIA,F. and GORDY,W. (1969) Phys. Rev., 187 , 58.

DYMANUS,A. (1976) MTP (Med. Tech. Publ. Co.) Int. Rev. Sci. :Phys. Chem., Ser. Two, 3 , Ed. D.A.Ramsey, Butterworths, London.

ENGLISH,T.C. and ZORN,J.C. (1974). In " Methods of Experimental Physics " (D.Williams,ed), 2nd ed., Vol. 3, Part B, p.669. Academic Press, New York.

FENN,J.B. and DECKERS,J. (1963). Rarefied Gas Dynamics, 1 , Academic Press, New York.

FLUENDY,M.A.D. and LAWLEY,K.P. (1973). " Chemical Applications of Molecular Beam Scattering " Chapman & Hall - London.

FRIEDBURG,H. and PAUL,W. (1951). Naturwissenchaften, 38 , 159.

GORDON,J.P. (1955). Phys. Rev., 99 , 1253 - 63 .

GORDON,J.P., ZEIGER,H.J. and TOWNES,C.H. (1955). Phys. Rev.,99, 1264 - 74.

GUNTHER,F. and SCHUGERL,K. (1972). Z. Phys. Chem., 80 , 155.

HAGENA,O. (1963). Z. angew Phys., 16 , 183.

HELMER,J.C. (1956) " Maser Oscillator " M.L.Report No. 327, U.S. Army, Signal corps Engineering Laboratories, Fort Monmouth, New Jersey.

HELMER,J.C. (1956). "Theory of a Molecular Oscillator" M.L.Report No.311. U.S.Army signal corps Engineering Laboratories, Fort Monmouth, N.J.

HELMER,J.C. (1957). Phys, Rev. 107 , 902 - 3.

HELMER,J.C., JACOBUS,F.B. and STURROCK,P.A. (1960). J. Appl. Phys.,31,458-63.

HERRMANN,J. and BONANOMI,J. (1956). Helv. Phys. Acta, 29 , 448.

HIGA,W.H. (1957). Rev. Sci. Inst., 28 , 726 - 7.

HILL,R.M. and GALLAGHER,T.F. (1975). Physical. Review A, 12 , 451 - 9.

HIRONO,M. (1959). J. Radio. Res. Lab., 6 , 515 - 32.

HOPE,S. (1979). M.Sc. Thesis, Keele University, (Unpublished).

HUGHES,H.K. (1947). Phys. Rev., 76 , 614 - 25.

IGRIITSKII,A.L. (1961). Radiotekhnika i Electronika, 6 , 4 , 613.

INGRAM,D.J.E. (1955). " Spectroscopy at radio and microwave frequencies" Butterworths, London.

KAKATI,D. and LAINÉ,D.C. (1967). Phys. Lett., 24A , 676.

KAKATI,D. and LAINÉ,D.C. (1971). J.Phys.E (Sci. Inst.), 4 , 269 - 273.

KANTROWITZ,A. and GREY,J. (1951). Rev. Sci. Instr., 22 , 328.

KAZACHOK,V.S. (1965). Zh. Tekh. Fiz., 35 , 1145 - 9 (Eng. transl. 1965, Soviet. Phys. Tech. Phys., 10 , 882 - 5).

KOSHEL'KOV,V.A. (1973). Radio. Engng. Electron. Physics., 18 , 1242 - 8 .

KOSHEL'KOV,V.A. (1975). Radio. Engng. Electron. Physics., 20 , 145 - 6 .

KOSHEL'KOV,V.A. and KROCHIK,G.M. (1972). Radio. Engng. Electron. Physics, 17 , 854 - 7.

KOSHURINOV,E.I. (1969). Radio. Engng. Electron. Physics., 14 , 1589 - 91 .

KRUPNOV,A.F. (1959). Izv. Vyssh. Uch. Zav. Radiofiz., 2 , 658 - 9 .

KRUPNOV,A.F. and SKVORTSOV,V.A. (1965). Prib. Tekh. Eksp., 1 , 128 - 32 (Eng. transl. 1965, Instrum. Exper. Tech., 1 , 126 - 9).

KRUPNOV,A.F. and SKVORTSOV,V.A., 1966, Izv. Vyssh. Uch. Zav. Radiofiz.,9, 827 - 8 (Eng. transl.1966, Sov. Radiophys., 9 , 488 - 9).

KUSH,P. and HUGHES, V.W. (1959) in "Handbook of Physics" (S. Flugge, ed). Vol 37, Part 1, p.1. Springer, Berlin.

LAINÉ,D.C. (1970). Rep. Progr. Phys., 33 , 1001.

LAINÉ,D.C. (1975). Advances in Electronic and Electron Physics,Vol 39, 183-251, Academic Press,New York, San Francisco, London.

LAINÉ,D.C. and SMART,G.D.S. (1971). J. Phys. D , 4 , L 23.

LAINÉ,D.C. and SWEETING,R.C. (1971). Phys. Lett., 34A, 144 - 5 .

MARCUSE,D. (1962). IRE. Trans. Inst., 1 - 11 , 187.

Mc COLM,D. (1966). Rev. Sci. Instrum., 37 , 1115 .

Mc CRACKEN,D.D. and DORN,W.S. (1964). " Numerical Methods and Fortran Programming " John Wiley and Sons, Inc., New York. London. Sydney.

Mc MICHAEL,G.E. and FRENCH,J.B. (1966). Physics of Fluids., Vol 9 . No. 7 , 1419 - 20 .

MEDNIKOV,O.I. and PARYGIN, V.H. (1963). Radiotekh. i Elektron., 8 , 653-8 (Eng. transl. 1963, Radio. Engng. Electron. Phys., 8 , 685 - 90 .

ter MEULEN,J.J. (1974). Quarterly Report No. 34, Katholieke Universiteit, (werkgroep voor Atoom - en Molekuulfysika). pp 153 - 166 .

MONTGOMERY,C.G. (1947). " Technique of Microwave Measurements ", MIT Radiation Laboratory Series, Vol 11, (Board Editors, Ridenour,L.N. & Collins,G.B.). Mc Graw - Hill Book Company,Inc. New York and London.

MORAN,J.P. (1970). AIAA Journal, Vol 8 , NO. 3 , 539 -44.

MULLER,M. (1956) J. Brit. Instn. Radio. Engng., 16 , 83 - 94 .

ORAEVSKII,A.N. (1964). Molecular Generators (Moscow:Nauka).

PARKER,H.M., KUHLTHAU,A.R., ZAPATA,R.N. and SCOTT,J.E.Jr. (1960). Rarefied Gas Dynamics, (Devienne,F.M.,Ed.) Pergamon Press,New York, pp 69 - 79.

PAULY,H. and TOENNIES,J.P. (1965). Adv. At. Mol. Phys., 1 , 201 .

PETER,M. and STRANDBERG,M.W.P. (1957). J. Chem. Phys., 26 , 1657 - 9 .

PIERCE,J.R.(1949). "Theory and Design of Electron Beams " Van Nstrand, N.Y.

RAMSEY, N. F., (1956)."Molecular Beams" (London:Oxford University Press).

REUSS,J. and NELISSEN,L. (1967). Phys. Lett., 25A , 626 .

SHCHEGLOV,V.A.,(1961). Izv. Vyssh. Uch. Zav. Radiofiz., 4 , 648 - 55 .

SHIMODA,K. (1957). J. Phys. Soc. Jap., 12 , 1006 - 1015 .

SHIMODA,K. (1958).JJ.Phys. Soc. Japan., 13 , 939 - 47 .

SHIMODA,K. (1960). Rendiconti della Scuola Internationale di Fisica " enrico Fermi ",XVII Corso, 1 .(New York : Academic Press).

SHIMODA,K. WANG,T.C. and TOWNES,C.H. (1956). Phys. Rev., 102 , 1308 - 21 .

SHIRLEY,J.H. (1963). J. Chem. Phys., 38 , 2896 .

SMART,G.D.S. (1973). Ph.D. Thesis, University of Keele, Unpublished.

SMITH,A.L.S. (1966). Ph.D.Thesis, University of Keele, Unpublished.

STRAKHOVSKII,G.M. and TATARENKOV,V.M. (1964) Izv. Vuz. Radiofizika, Vol. 7 , No. 5 , pp 994 - 5 .

STRASHKEVICH,A.M. (1965). Radiotekhnika i Electronika, 10 , 2 , 285 - 91 .

STRAUGHAN,B.P. and WALKER,S. (1976). " Spectroscopy " Chapman & Hall,London.

SWEETING,R.C. (1971). Ph.D.Thesis, University of Keele, Unpublished.

THADDEUS,P. and KRISHER,L.C. (1961). Rev. Sci. Instrum., 32 , 1083 .

TORREY,H.C., and WHITMER,C.A. (1948). " Crystal Rectifiers ", MIT Radiation Lab. Series, Vol 15 , Mc Graw-Hill Book Company Inc, New York.

TROTSYUK,N.I. (1969). Soviet. Phys.-Tech. Phys., 13 , 944 - 9 .

TRUMAN,M.J. and LAINE,D.C. (1976). J.Phys. D. (Applied Physics), 9 , L 175-8.

TOWNES , C.H. (1953). J.Instn. Elect. Commun. Engr. (Japan), 36 , 650 - 4.

TOWNES,C.H. and SCHAWLOW,A.L. (1955). " Microwave Spectroscopy " (New York : McGraw - Hill).

VALLEAU,J.B. and DECKERS,J.M. (1964). Can. J. Chem., 42 , S.225 - 245 .

VALLEAU,J.B. and DECKERS, J.M. (1965). Can. J. Chem., 43 , S.6 - 17 .

VAN MIERLO,G.W.M. (1974). Quarterly Report 40 ,werkgroep voor Atoom -en Molekuulfysika, University of Nijmegen, The Netherlands.

VONBUN,F.O. (1957). " A multiple separator for maser ", Engineering Report NRE -1203, U.S.Army Signal Crops Engineering Laboratories. Fort Monmouth, New Jersey.

VONBUN,F.O. (1958). J.Appl. Phys., 29 , 632 - 6 .

WAECH,T.G., KRAMER,K.H. and BERNSTEIN,R.B. (1968). J.Chem. Phys., 48 , 3978.

ZAPATA,R.N. (1961). Rarefied Gas Dynamic, 2nd Symposium, Vol 1,pp 67 - 81.

ZINCHENKO,N.S (1967). Ukrainskii. Fizicheskii. Zhurnal.,Vol 12,NO.11,1828-38.

ZINCHENKO,N.S. and SAEKO,V.I. (1963). Zhurnal. Tekhnicheskoi. Fiziki,Vol 33, No.2, pp 154 - 163. (eng.transl. 1963 Soviet. Physics - Technical. Physics., 8 , 111 - 6 .

ZORN,J.C. and ENGLISH,T.C. (1973). In "Advances in Atomic and Molecular Physics",(bates,D.R,& Estermann,I .eds),Vol 19 ,pp 243 - 321.

Academic Press, New York. London.

ZUEV,V.S. and CHERMISKIN,I.V. (1962). Radiotekh i Elektron., 7 , 918 - 19.

(Eng transl. 1962, Radio. engng. Electron. Phys., 7 , 869 70 .